UAB
Universitat Autònoma de Barcelona

Horizontal transfer to Salmonella of bacteriophage defence systems in the broiler intestinal tract and role of the plasmid-encoded ibfA gene as a defence mechanism

Júlia López Pérez

ADVERTIMENT. L'accés als continguts d'aquesta tesi queda condicionat a l'acceptació de les condicions d'ús establertes per la següent llicència Creative Commons: https://creativecommons.org/licenses/?lang=ca

ADVERTENCIA. El acceso a los contenidos de esta tesis queda condicionado a la aceptación de las condiciones de uso establecidas por la siguiente licencia Creative Commons: https://creativecommons.org/licenses/?lang=es

WARNING. The access to the contents of this doctoral thesis it is limited to the acceptance of the use conditions set by the following Creative Commons license: https://creativecommons.org/licenses/?lang=en

Universitat Autònoma de Barcelona

Horizontal transfer to *Salmonella* of bacteriophage defence systems in the broiler intestinal tract and role of the plasmid-encoded *ibfA* gene as a defence mechanism

PhD Thesis

Júlia López Pérez

Thesis directors: Dr Montserrat Llagostera Casas, Dr María Pilar Cortés Garmendia and Dr Ivan Erill Sagalés

Thesis tutor: Dr María Pilar Cortés Garmendia

Genetics and Microbiology Department

Bellaterra, 2024

UAB
Universitat Autònoma de Barcelona

Horizontal transfer to *Salmonella* of bacteriophage defence systems in the broiler intestinal tract and role of the plasmid-encoded *ibfA* gene as a defence mechanism

PhD Thesis to obtain the **PhD degree in Microbiology** from the Autonomous University of Barcelona

Júlia López Pérez

With the blessing of the thesis directors

Dr Montserrat Llagostera Casas	Dr María Pilar Cortés Garmendia	Dr Ivan Erill Sagalés
Director	Director and tutor	Director

SUMMARY

Antibiotic resistance is becoming an increasingly worrying global threat, with predictions foreseeing up to 10 million deaths by 2050 (Sugden *et al*., 2016). Therefore, investigating innovative treatment options against bacterial infections and devising alternative strategies to overcome antibiotic-resistant bacteria is imperative. Phage therapy emerges as a promising solution, yet understanding the emergence of bacteriophage resistance and their underlying molecular mechanisms is crucial to pre-empt potential hurdles in their application.

Our group has previously performed studies focused on the emergence of bacteriophage resistance in broilers infected with the *Salmonella enterica* serovar Typhimurium ATCC14028 strain resistant to rifampicin (Rif^R) and subjected to oral phage therapy using a cocktail comprising three bacteriophages: UAB_Phi20, UAB_Phi78, and UAB_Phi87, belonging to the genera *Lederbergvirus*, *Zindervirus*, and *Felixounavirus*, respectively (Otero J, 2019). Variants of ATCC14028 Rif^R were isolated from ceca samples of both untreated and treated animals, and an initial susceptibility testing was conducted against phage UAB_Phi78 due to its receptor location within the lipopolysaccharide (LPS) core. Variants displaying reduced susceptibility to this phage were further evaluated against UAB_Phi20 and UAB_Phi87 phages. Seven of these *Salmonella* variants exhibiting reduced susceptibility to either all three bacteriophages or specifically only to UAB_Phi78 and UAB_Phi87 were chosen for further studies, which ruled out changes in phage receptors as the cause of the lower susceptibility detected (Otero J, 2019).

Building upon these findings, this thesis aims to elucidate the causes of the reduced susceptibility to the bacteriophages of the cocktail observed in the seven *Salmonella* variants. First, the adsorption constant (*K*) of the bacteriophages was determined. No significant differences were found in the *K* values of UAB_Phi20 and UAB_Phi78 phages when infecting both the parental strain and the seven variants, while the UAB_Phi87 phage exhibited a compromised adsorption onto the variants. Further characterization through determination of efficiency of plating (EOP), efficiency of centres of infection (ECOI), and burst size, elucidated the interference phenotype of the *Salmonella* variants. Combining these results with prior infection kinetics analysis (Otero J, 2019), we inferred that the observed interference against the UAB_Phi20, UAB_Phi78, and UAB_Phi87 phages was compatible with an abortive infection.

On the other hand, analysis of unmapped Illumina reads demonstrated that all seven variants carried a large conjugative plasmid [~96-100 kilobases (Kb)] from the I1α incompatibility group (IncI1α). Furthermore, some of these variants carried additional plasmids of smaller sizes belonging to other incompatibility groups. We hypothesized that these plasmids were acquired through lateral transfer from the commensal microbiota of the broilers' digestive tract. The presence of the large conjugative plasmids in all seven variants suggested that they could encode genes involved in interference with the phages. Conjugative experiments and plasmid curation confirmed that these plasmids were fully

responsible for the observed interference with the multiplicative cycle of UAB_Phi20 and UAB_Phi78, and partially responsible for interference with UAB_Phi87, highlighting their role as carriers of defence mechanisms against bacteriophages.

A detailed examination of the genes encoded within the large IncI1α conjugative plasmids revealed a highly variable region. Previous studies had suggested that variable regions often carry genes associated with phage defence mechanisms (Chevallereau and Westra, 2022; Rousset *et al*., 2022; Hochhauser *et al*., 2023). Thus, we focused our investigation on this region to uncover potential defence mechanisms encoded within these IncI1α plasmids. Notably, one such plasmid, pUA1135, harboured by variant IC5, contained the *ibfA* gene within its variable region, which was part of a transcriptional unit but with its own promoter. This gene shared homology with the *ibfA* gene of the R64 plasmid, also within the same incompatibility group, which had been previously linked to interference against coliphages BF23, PhiI and λ, as well as *S*. Typhimurium phages P22 and St (Anderson and Lewis, 1965; Hughes and Meynell, 1977; Furuichi *et al*., 1984), although its mechanism of action remained undescribed. Through deletion and complementation assays of *ibfA*, we confirmed its role in the interference with UAB_Phi20 in the IC5 variant, prompting further exploration of the molecular mechanism underlying *ibfA*'s interference with this bacteriophage. Given the close similarity between the virulent phage UAB_Phi20 and the temperate phage P22, we hypothesized that the lytic cycle regulatory pathways of UAB_Phi20 would be similar to those described for P22. Furthermore, examination of IbfA's domains revealed it was a two-domain protein, composed of an ATPase and a topoisomerase-primase (TOPRIM) domain. However, contrary to the defence system described by Rousset *et al*., 2023, a luciferin/luciferase assay demonstrated that the interference performed by IbfA did not involve adenosine triphosphate (ATP) depletion attributable to its ATPase domain.

Our analysis of several infection parameters, including EOP, ECOI, infection kinetics, and burst size, revealed that *ibfA* induces a reduction in UAB_Phi20 productivity, accompanied by a decline in cellular viability without observable cell lysis, confirming that this gene gives rise to an abortive infection of UAB_Phi20 phage in *Salmonella*. Using transmission electron microscopy (TEM) on cellular cross sections of infected cells we corroborated that there was a reduction in UAB_Phi20 viral particles being formed inside *ibfA*$^+$ cells and observed a delay in cell lysis. Subsequently, we assessed the effects of *ibfA* on UAB_Phi20 replication and transcription. While *ibfA* exhibited no influence on the replication of UAB_Phi20 genome, a significant dysregulation of UAB_Phi20 gene expression was observed in *ibfA*$^+$ cells. Specifically, the expression of early genes (*gp74*, *int* and *gp3*), as well as those of the *immC* (*cro*, *c2* and *c1*) and *immI* (*arc*, *ant* and *sar*) regions of UAB_Phi20, was significantly higher in those cells, except for the early gene *gp14*, that encodes the late antiterminator, and which exhibited reduced expression due to the elevated C1 expression (Ho *et al*., 1992). Consequently, antitermination of the late transcript was diminished, leading to

significant underexpression of late genes encoding structural proteins and those associated with cell lysis, thereby hindering UAB_Phi20's virion production and cellular lysis. Furthermore, we propose that IbfA, directly or indirectly, disrupts the control of the expression of the antirepressor *ant*, responsible for the inhibition of the C2 repressor of the lytic cycle (Susskind and Botstein, 1978), leading to the sequestering of the C2 protein present in the cell. The resulting imbalance in Cro/C2 concentration, crucial for the control of the lysis/lysogeny decision, prompts the elevated early gene expression levels, akin to the phenotype of the Arc^- mutants observed by Susskind, 1980.

In summary, this thesis presents, to our knowledge, the first documentation that the reduced susceptibility to a three-phage cocktail observed in *Salmonella* variants isolated from an oral phage therapy study in broilers can be attributed to the acquisition by horizontal transfer of large IncI1α conjugative plasmids from the broilers' microbiota. Furthermore, we disclose the previously unreported molecular mechanism behind P22-like phage defence mediated by the gene *ibfA*. By affecting the control of the expression from P_{ANT}, this gene ultimately causes a decrease in the expression of phage genes related to virion structure and cellular lysis, resulting in a decline in UAB_Phi20 progeny and abortive infection. Finally, we uncover the wide distribution of *ibfA* among prokaryotic genomes and plasmids, indicating that it might confer additional advantages to bacterial cells.

INDEX

Page

Summary 5

Index 9

Figure Index 12

Table Index 15

1. Introduction 17

1.1 *Salmonella* and salmonellosis 18

1.1.1 The genus *Salmonella* 18

1.1.2 *Salmonella* pathogenicity 18

1.1.3 Incidence and epidemiology of *Salmonella* 21

1.1.3.1 Incidence of *Salmonella* in humans in the European Union between 2018 and 2022 21

1.1.3.2 Incidence of *Salmonella* in *Gallus gallus* in the European Union between 2018 and 2022 24

1.2 Bacteriophages 26

1.2.1 Phage structure and classification 27

1.2.2 Phage life cycle 28

1.2.3 Bacteriophage therapy 29

1.2.3.1 Advantages and disadvantages of the use of phage therapy 30

1.2.4 Bacterial defence against phage infection 31

1.2.5 *Salmonella* bacteriophages UAB_Phi20, UAB_Phi78 and UAB_Phi87 35

1.2.5.1 Transcriptional regulation of the P22 bacteriophage 36

2. Objectives 41

3. Chapter I 43

Summary 44

3.1 Introduction 46

3.2 Materials and methods 46

3.3 Results 50

3.4 Discussion 57

References 61

Supplementary materials 63

4. Chapter II 71

Summary 72

4.1 Introduction 74

4.2 Materials and methods 75

4.3 Results 83

4.4 Discussion 100

References 104

Supplementary materials 110

5. Discussion 119

6. Conclusions 129

7. References 133

Annex 151

Annex 1. Materials and methods used in this work 152

Acknowledgements 175

Figure Index

Figure 1.1 Schematic representation of the routes of infection of *Salmonella* in the intestinal epithelium. 20

Figure 1.2 Occurrence of antibiotic resistance in human cases of *Salmonella* serovars important to public health in 2022 in the European Union. 23

Figure 1.3 Occurrence of antibiotic resistance in *Salmonella* serovars isolated from broilers and laying hens in 2021 in the European Union. 26

Figure 1.4 Morphotypes of bacteriophages. 27

Figure 1.5 The three different morphologies of tailed bacteriophages. 28

Figure 1.6 Schematic representation of the four types of a bacteriophage life cycle. 29

Figure 1.7 Known antiphage defence systems found in bacteria. 32

Figure 1.8 Representation of the LPS molecule and the points where the three receptors of the cocktail phages were found. 36

Figure 1.9 Regulation of expression of P22. 39

Figure 1.10 Schematic representation of the region regulating the expression of promoters P_R, P_L and P_{RM}, along with the affinities of binding of C2 repressor and Cro to the operators at these sites. 40

Figure 3.1 Scheme of *S.* Typhimurium LPS and detail of the infective capacity of bacteriophages UAB_Phi20, UAB_Phi78 and UAB_Phi87 against different LPS mutants of *S.* Typhimurium LT2. 50

Figure 3.2 LPS electrophoretic profiles of the variants isolated from LAB, FOOD, and LPS mutants of *S.* Typhimurium LT2 strain. 53

Figure 3.3 Deletion found in the *rfc* gene in variants HT1 and HT4 isolated from FOOD. 54

Figure 3.4 Procedures for curing plasmids pUA1135, pUA1136 and pUA1139 from IC5, IC6, and IT2 variants, respectively. 57

Figure S3.1 Growth kinetics, measured as absorbance (A_{550} nm) and viable count of cultures of the parental strain ATCC14028 Rif^R and the variants IC10 and IT2 as examples of those isolated from PT, non-infected and infected with UAB_Phi78 bacteriophage. 63

Figure S3.2 LPS electrophoretic profiles of the sixteen ATCC14028 Rif^R variants isolated from PT. 64

Figure 4.1 Frequency distribution of the fraction of shared COGs in pairwise comparisons of the variable region and the rest of pUA1135 plasmid sequence. 83

Figure 4.2 Schematic representation of the variable region of pUA1135 plasmid. Annotations of each gene correspond to their predicted protein product. 85

Figure 4.3 Schematic representation of the transcriptional unit containing *pUA1135_00003*, *ibfA*, *ydeA* and *ydfA* genes. RT-PCR analysis was conducted on the intergenic regions between *pUA1135_00003* and *ibfA*, *ibfA* and *ydeA*, and *ydeA* and *ydfA* and resolved by agarose gel electrophoresis of the products. 85

Figure 4.4 Growth kinetics of ATCC14028 Rif^R/pBAD33, and ATCC14028 Rif^R/pBAD33::*ibfA* strains. 87

Figure 4.5 Doermann and one-step growth curves of UAB_Phi20 when infecting the ATCC14028 Rif^R/pBAD33 and ATCC14028 Rif^R/pBAD33::*ibfA* strains. 88

Figure 4.6 Infection kinetics of ATCC14028 Rif^R/pBAD33 and ATCC14028 Rif^R/pBAD33::*ibfA* strains by the UAB_Phi20 bacteriophage. 89

Figure 4.7 Expression of the *ibfA* gene in uninfected and UAB_Phi20-infected cultures of the ATCC14028 Rif^R/pBAD33::*ibfA* strain at different times after phage adsorption. 90

Figure 4.8 ATP concentration in ATCC14028 Rif^R/pBAD33 and ATCC14028 Rif^R/pBAD33:*ibfA* strains, uninfected and infected with the bacteriophage UAB_Phi20. 91

Figure 4.9 Genome replication of the UAB_Phi20 phage in ATCC14028 Rif^R/pBAD33 and ATCC14028 Rif^R/pBAD33::*ibfA* strains. 92

Figure 4.10 Expression levels of early UAB_Phi20 genes in the absence of *ibfA* and in the presence of this gene after phage adsorption. 94

Figure 4.11 Expression of UAB_Phi20 *immC* region genes in absence of *ibfA* and in the presence of this gene after phage adsorption. 95

Figure 4.12 Expression of UAB_Phi20 *immI* region genes in absence of *ibfA* and in presence of this gene after phage adsorption. 96

Figure 4.13 Expression levels of late UAB_Phi20 genes in absence of *ibfA* and in the presence of this gene after phage adsorption. 97

Figure 4.14 Transmission electron micrographs of ultrathin sections from ATCC14028 Rif^R/pBAD33 and ATCC14028 Rif^R/pBAD33::*ibfA* cells after infection with UAB_Phi20 phage at different times. 98

Figure 4.15 Phylogenetic tree of IbfA homologues in bacterial and archaeal complete plasmids or chromosomes. 99

Figure S4.1 Schematic representation of the genome of UAB_Phi20 phage. Enlargement of the early genes controlled by P_L and P_R, whose transcription was studied through RT-qPCR. 110

Figure S4.2 Schematic representation of the genome of UAB_Phi20 phage. Enlargement of the *immC* and of the *immI* regions, whose transcription was studied through RT-qPCR. 111

Figure S4.3 Schematic representation of the genome of UAB_Phi20 phage. Enlargement of the late genes controlled by P_{LATE}, whose transcription was studied through RT-qPCR. 112

Figure 5.1. Graphic representation of the model on the molecular mechanism of *ibfA*-mediated interference in the phage lytic cycle. 127

Figure A1. Sample of plotted results of the production of phage during the time course of a single infection cycle. 154

Figure A2. Example of a one-step growth curve. 156

Table Index

Table 1.1 Number of confirmed human non-typhoidal salmonellosis cases and notification rate per 100,000 population from 2018 to 2022. 21

Table 1.2 Number and percentage of confirmed cases of human salmonellosis in the EU, from 2018 to 2022, for those serovars with more than 1,000 confirmed cases. 22

Table 1.3 Serotyped *Salmonella*-positive sampling units in *Gallus gallus* and derived products (2018-2022), and percentage relative to total *Salmonella*-positive sampling units across animal and food sources analyzed. 25

Table 1.4 Number of *Salmonella*-positive sampling units by serotype in *Gallus gallus* and products thereof in the year 2022. 26

Table 3.1 *S.* Typhimurium ATCC 14028 Rif^R variants with reduced UAB_Phi78-susceptibility isolated from uninfected and phage infected bacterial cultures (LAB). 51

Table 3.2 *S.* Typhimurium ATCC 14028 Rif^R variants with reduced UAB_Phi78-susceptibility isolated from untreated, and phage treated cooked ham slices (FOOD). 51

Table 3.3 *S.* Typhimurium ATCC 14028 Rif^R variants with reduced UAB_Phi78-susceptibility isolated from untreated, and phage treated broiler chickens (PT). 52

Table 3.4 Selected reduced UAB_Phi78-susceptibility *S.* Typhimurium ATCC 14028 Rif^R variants isolated from LAB and FOOD for further characterization. 53

Table 3.5 Mutations identified in the *rfc* and *rfaJ* genes of selected *S.* Typhimurium ATCC 14028 Rif^R variants isolated from LAB and FOOD. 54

Table 3.6 Selected reduced UAB_Phi78-susceptibility *S.* Typhimurium ATCC 14028 Rif^R variants isolated from PT. 55

Table 3.7 Parameters of phages UAB_Phi78 and UAB_Phi20 on reduced phage-susceptibility variants isolated from PT. 55

Table 3.8 Characteristics of plasmids identified in reduced phage-susceptibility variants isolated from PT. 56

Table 3.9 Values of EOP and ECOI of UAB_Phi78, UAB_Phi20 and UAB_Phi87 phages on both donor and transconjugants. 56

Table S3.1 Strains and plasmids used in this study. 65

Table S3.2 Oligonucleotides used in this work. 66

Table S3.3 Point mutations identified in the genomes of all the *Salmonella* variants and the parental strain sequenced with respect to the genome of the NCBI reference strain ATCC14028s (GenBank CP001363.1). 69

Table 4.1 EOP values of the UAB_Phi20 bacteriophage for deletion mutants of the IC5 strain. 86

Table 4.2 EOP values of the UAB_Phi20 bacteriophage for complementation of deletion mutants of the IC5 strain. 86

Table 4.3 Mean of virions per cell section and percentage of cell sections with virions in the presence and absence of the *ibfA* gene. 95

Table S4.1 Strains and plasmids used in this study. 113

Table S4.2 Primers used in this work. 114

Table S4.3 List of COGs from the variable region of homologues of the pUA1135 plasmid 117

Table A.1 Strains and plasmids used in this work. 169

Table A.2 Primers used in this work. 170

1. INTRODUCTION

1.1 *Salmonella* and salmonellosis

1.1.1 The genus *Salmonella*

Salmonella is a genus of Gram-negative rod-shaped bacteria with a diameter of 0.7 to 1.5 μm and a length of 2 to 5 μm. Most *Salmonella* species are motile microorganisms thanks to their peritrichous flagella. The optimal growth conditions for *Salmonella* are 37ºC with a pH of 6.5-7.5, although growth has been recorded at temperatures ranging from 4ºC to 54ºC and pH from 3.8 to 9.5 (Ryan *et al*., 2017). These microorganisms are oxidase negative, catalase positive and non-spore forming. They have a chemoorganotrophic metabolism, whereby they obtain energy from the oxidation of organic compounds, and they are facultative anaerobes, being able to use oxygen if present, but swapping to fermentation or anaerobic respiration when oxygen is not present (Popoff and Le Minor, 2015).

Salmonella belongs to the *Enterobacteriaceae* family, *Enterobacteriales* order, *Gammaproteobacteria* class and *Proteobacteria* phylum. Its taxonomy and nomenclature have changed many times over the years. Initially, *Salmonella* species described the disease they caused, however, in 2005 the Judicial Commission of the International Committee for Systematics of Prokaryotes concluded in the Judicial Opinion 80 (Judicial Commission Of The International Committee On Systematics Of Prokaryotes, 2005) that there are two species inside the *Salmonella* genus: *S. enterica* and *S. bongori*, and six subspecies of *S. enterica*: *S. enterica* subsp. *enterica*, *S. enterica* subsp. *salamae*, *S. enterica* subsp. *arizonae*, *S. enterica* subsp. *diarizonae*, *S. enterica* subsp. *houtenae* and *S. enterica* subsp. *indica* (Tindall *et al*., 2005; Ryan *et al*., 2017). Furthermore, within the *Salmonella* genus there are more than 2,600 serovars that are classified according to the LPS O-antigen, the flagellar H-antigen and the capsular Vi-antigen (Popoff *et al*., 2001; Tindall *et al*., 2005; Ryan *et al*., 2017).

1.1.2 *Salmonella* pathogenicity

S. enterica is a facultative zoonotic intracellular pathogen of global concern for human and animal health, as it is in the top three causes of death due to diarrhoeal disease according to the World Health Organization (WHO) (World Health Organization, 2015), with its highest mortality rates in developing countries and in children under the age of five years. It is also the second most important cause of food-transmitted disease in the European Union (EU) (EFSA and ECDC, 2023). The main hosts of this pathogen are warm-blooded animals in the case of *S. enterica* subsp. *enterica* and cold-blooded animals for all other *S. enterica* subspecies and *S. bongori* (Ellermeier and Slauch, 2006), and it resides in the intestinal tract of these animals. Different *Salmonella* serovars have different host ranges. For example, the *S. enterica* serovar Typhi is specific to humans and serovar Gallinarum is specific to poultry, but the serovar Typhimurium has a much wider host range, being able to cause disease in several species of birds and mammals (Silva *et al*., 2014). Although these animals are the

primary host in which *Salmonella* causes disease, insects and other birds have been found to act as an asymptomatic reservoir for *Salmonella* too (Winfield and Groisman, 2003). Furthermore, *Salmonella* has been found to not only be capable of adhering to the surface of plants, but in some cases also infect plant cells (Silva *et al*., 2014). Transmission to humans and other mammals usually takes place through contaminated food or water, as this bacterium can survive in the environment for prolonged periods of time (Winfield and Groisman, 2003). In fact, *Salmonella* is known to withstand the limiting conditions of a wide range of environments that are thought to act as a secondary habitat, such as water, soil, plants, and even household surfaces (Winfield and Groisman, 2003).

Depending on the symptoms caused to humans, *Salmonella* can be divided into typhoidal and nontyphoidal. *Salmonella enterica* ser. Typhi and *Salmonella enterica* ser. Paratyphi cause typhoid and paratyphoid fever in humans, respectively, both characterized by fever, diarrhoea, vomiting, cramping and headaches, that can last up to a month, although paratyphoid fever presents milder symptoms. Between one to four percent of patients that suffer typhoid fever will develop a chronic carrier state, whereby bacteria are found in the stool of a person that has suffered typhoid fever for up to a year after infection by *Salmonella* (Ellermeier and Slauch, 2006). Other *Salmonella* serovars, such as Typhimurium or Enteritidis, cause nontyphoidal salmonellosis, characterized by a self-limiting gastroenteritis that usually resolves within 10 days. Nontyphoid *Salmonella* can also enter the bloodstream resulting in bacteriemia in children younger than one, the elderly and the immunocompromised (Ellermeier and Slauch, 2006).

Upon ingestion, *Salmonella* faces the acidic environment of the stomach, prompting the activation of the *Salmonella* acid tolerance response to survive the low pH conditions (Ohl and Miller, 2001). When *Salmonella* reaches the small intestine, it first must adhere to the intestinal cells. This adhesion is a two-step process (a first reversible adhesion followed by an irreversible attachment) mediated by fimbriae or other types of adhesins (Figure 1.1a) (Wiedemann *et al*., 2015). One of the particularities of *Salmonella enterica* is that when it reaches the small intestine it can traverse the intestinal epithelium through several mechanisms and virulence factors (dos Santos *et al*., 2018). One of the mechanisms is bacterial-mediated endocytosis of non-phagocytic (enterocytes) cells via the type III secretion system (T3SS) encoded in the *Salmonella* pathogenicity island 1 (SPI1) (Haraga *et al*., 2008). This system is responsible for the translocation of bacterial proteins (effectors) across the host cellular membrane, which induce the formation of membrane "ruffles" (Figure 1.1b), leading to the engulfment of the bacterium in vesicles (Ohl and Miller, 2001; Wiedemann *et al*., 2015). These effectors further stimulate pro-inflammatory cytokine production resulting in polymorphonuclear leukocyte infiltration into the intestinal lumen and subsequent diarrhoea (Haraga *et al*., 2008). Two other mechanisms that *Salmonella* can use to translocate through the epithelium include entry into the phagocytic microfold (M) cells through pinocytosis (Figure 1.1c) or uptake by CD18-positive cells (Figure 1.1d). It is thought that these two mechanisms could enable typhoidal *Salmonella* to

enter the intestinal epithelium without perturbing it (Haraga *et al*., 2008), and therefore not causing an inflammatory response, which is one of the main differences with non-typhoidal salmonellosis (Gal-Mor *et al*., 2014). In all scenarios, the bacterium will end up in a spacious phagosome, which will shrink and finally form the *Salmonella*-containing vacuole (SCV) (Figure 1.1e) (Haraga *et al*., 2008). Intracellular replication will happen inside the SCV, and although this can occur in many cell types, *Salmonella* preferably replicates in macrophages (Figure 1.1f) (Haraga *et al*., 2008). Activation of SPI2 during this phase promotes *Salmonella* replication and survival inside the SCV (Haraga *et al*., 2008; LaRock *et al*., 2015). In the case of typhoidal salmonellosis, the bacterium is able to infect deeper intestinal tissues, reaching underlying lymphoid tissues and disseminating to other organs such as the liver, spleen, and bone marrow (Figure 1.1g) (Gal-Mor *et al*., 2014). Finally, the host's immune response is necessary for the clearing of *Salmonella*, and differential inflammatory pathways are speculated to activate in typhoid and non-typhoid salmonellosis (Gal-Mor *et al*., 2014).

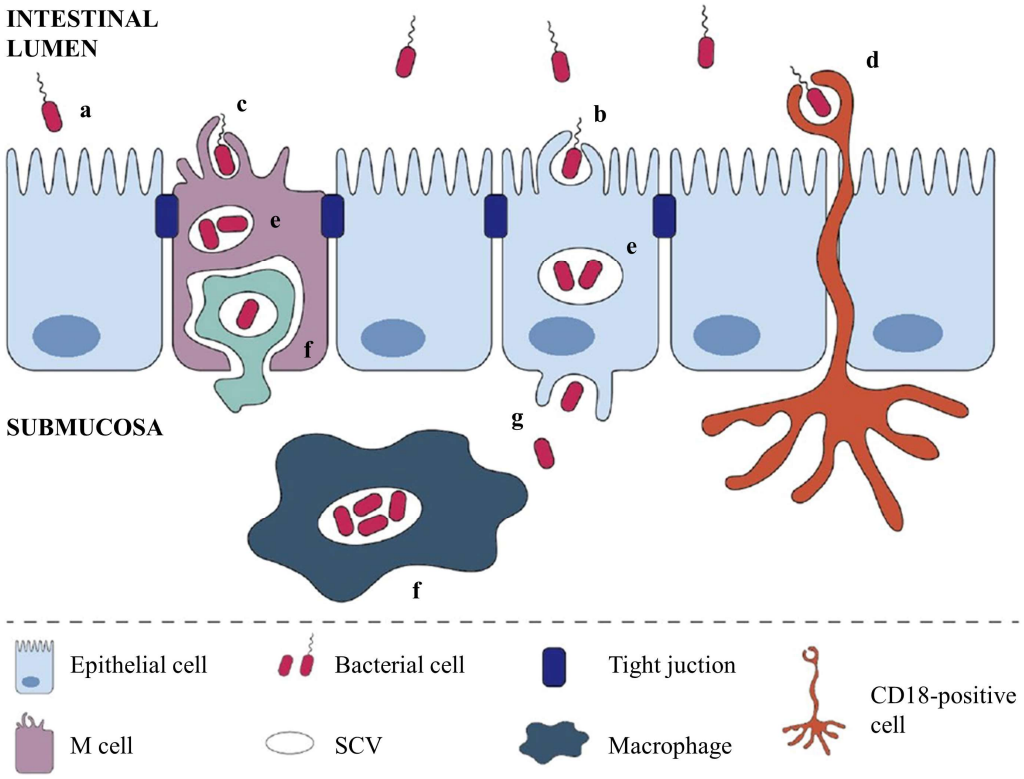


Figure 1.1 Schematic representation of the routes of infection of *Salmonella* in the intestinal epithelium (Figure modified from dos Santos *et al*., 2018). Steps a-g are described in the main text.

1.1.3 Incidence and epidemiology of *Salmonella*

1.1.3.1 Incidence of *Salmonella* in humans in the European Union between 2018 and 2022

The European Union One Health 2022 Zoonoses Report from the European Food Safety Authority (EFSA) and European Centre for Disease Prevention and Control (ECDC) reported 65,208 cases (15.3 cases per 100,000 people) of salmonellosis in the EU (EFSA and ECDC, 2023). While there was a decline in cases in 2020 due to the COVID-19 pandemic, there was a 14% increase in reports in 2021 that remained stable in 2022. Nevertheless, the recorded cases are still lower than those observed in the 2018-2019 period (Table 1.1). Enteritidis, Typhimurium, monophasic Typhimurium (1,4,[5],12:i:-), and Infantis emerged as the four most frequently reported *Salmonella* serovars in 2022 (Table 1.2). Notably, the first three serovars accounted for 77.1% of cases with available serovar information. Bulgaria and Spain are excluded from this analysis due to the absence of serovar data. The ranking of these serovars has remained stable from 2020 to 2022 (EFSA and ECDC, 2023).

Table 1.1 Number of confirmed human non-typhoidal salmonellosis cases and notification rate per 100,000 people from 2018 to 2022.

	2018	**2019**	**2020**	**2021**	**2022**
Number of confirmed human cases	91,858	87,907	52,690	60,169	65,208
Notification rate per 100,000 people	17.6	17.5	12.1	15.3	15.3

Data obtained from EFSA and ECDC (2023).

Table 1.2 Number and percentage of confirmed cases of human salmonellosis in the EU, from 2018 to 2022, for those serovars with more than 1,000 confirmed cases.

Serovar	2018		2019		2020		2021		2022	
	N. cases	%	N. cases	%	N. cases	%	N. cases	%	N. cases	%
Enteritidis	39,516	50.0	39,451	50.4	24,008	56.1	28,045	58.0	25,737	54.6
Typhimurium	10,297	13.0	9,288	11.9	5,337	12.5	5,841	12.1	5,694	12.1
Monophasic Typhimurium 1,4,[5],12:i:-	6,374	8.1	6,432	8.2	4,697	11.0	4,802	9.9	4,906	10.4
Infantis	1,852	2.3	1,912	2.4	1,064	2.5	1,071	2.2	1,093	2.3

Data obtained from EFSA and ECDC (2022 and 2023). N., number.

Antibiotic resistance in *Salmonella* is a significant concern, prompting annual monitoring in the EU. Data is collected from human isolates of *Salmonella* spp. and their resistance to the most commonly used antibiotics in human and/or veterinary medicine (ampicillin, sulphonamides, tetracyclines, ciprofloxacin and third generation cephalosporins) is recorded. Reports from 2022 (EFSA and ECDC, 2024) revealed that although isolation of *Salmonella* spp. with resistance to ampicillin and tetracyclines from human cases was declining in some EU countries, the percentage of isolates with resistance to these antibiotics remained high in 2021: 25.2% for ampicillin and 25.1% for tetracyclines. Sulphonamide resistance also remained high at 25.6%. By serovar, monophasic *S.* Typhimurium (1,4,[5],12:i:-) and *S.* Kentucky showed the most critical resistance levels to these antibiotics, ranging from 77.3% to 86.7% of isolates, and 59.2% to 67.1% of isolates (Figure 1.2), respectively. In contrast, *S.* Enteritidis had the lowest percentages of resistance to these antibiotics (Figure 1.2). Ciprofloxacin and third generation cephalosporins, such as cefotaxime, are classified as critically important antimicrobials (CIA) by the WHO. Although the occurrence of resistance to ciprofloxacin in *Salmonella* spp. was moderate (18.7% of isolates), its notably high prevalence in *S.* Kentucky was cause of concern (Figure 1.2). Resistance to third generation cephalosporins, such as cefotaxime, was found at much lower levels across all serovars (Figure 1.2). Furthermore, multidrug resistance was identified in 22.1% of isolates from human cases (EFSA and ECDC, 2024).

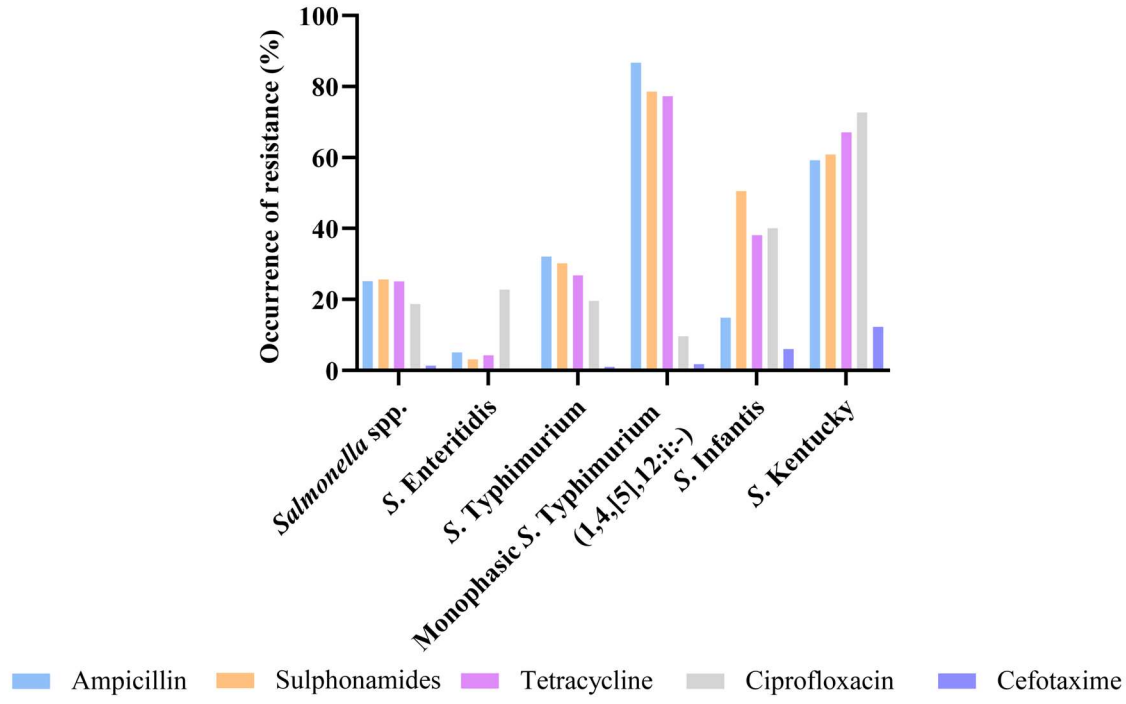


Figure 1.2 Occurrence of antibiotic resistance in human cases of *Salmonella* serovars important to public health in 2022 in the European Union. Data obtained from EFSA and ECDC, 2024.

1.1.3.2 Incidence of *Salmonella* in *Gallus gallus* in the European Union between 2018 and 2022

Animal-based foods represent the most common sources of human salmonellosis. Key reservoirs for *Salmonella* are laying hens and broiler flocks of *Gallus gallus* along with their derived products, such as broiler meat and eggs. Notably, broilers and broiler meat emerged as the two leading categories with the highest percentage of serotyped *Salmonella*-positive sampling units from 2018 to 2022 (Table 1.3). Consequently, the imperative to control *Salmonella* in these animals and their food products is underscored as a priority. Although eggs and egg products yielded the lowest number of positive sampling units, they were identified as the leading cause of salmonellosis outbreaks in the EU in 2022 (EFSA and ECDC, 2023). Analysing specific serovars isolated from these animals and foods, it becomes apparent that the four serovars with the highest reports of human salmonellosis in 2022 were also the most prevalent in these sources. Indeed, reports from 2022 indicated that *S.* Enteritidis and *S.* Typhimurium were the most commonly isolated serovars in laying hens and eggs (44.3% of isolates, Table 1.4). For broilers and broiler meat, *S.* Infantis emerged as the most frequently isolated, followed by *S.* Enteritidis (Table 1.4). These data clearly demonstrate the inadequacy of existing programs aimed at eradicating *Salmonella* in poultry, highlighting the need for novel measures in both farms and the meat processing industry to effectively address this public health concern.

Antibiotic resistance to the most used antibiotics in veterinary medicine (ampicillin, sulfamethoxazole and tetracycline) were documented for *Salmonella* isolates obtained from animals (EFSA and ECDC, 2024). In human medicine, ampicillin holds the classification of a CIA by the WHO, while sulfamethoxazole and tetracycline are considered highly important antimicrobials. In 2022, resistance to tetracycline and sulfamethoxazole were found at high levels in broilers and at comparatively lower levels in laying hens (Figure 1.3). Conversely, ampicillin resistance levels in both animal groups were noted to be low to moderate (Figure 1.3). Antibiotics categorized as CIAs in human medicine, and crucial for treating invasive salmonellosis, were also reported for *Salmonella* isolates obtained from animals and are categorized as highest-priority critically important antimicrobials (hpCIA). These are fluoroquinolones (mostly ciprofloxacin) and third generation cephalosporins (cefotaxime and ceftazidime). Notably, ciprofloxacin resistance was observed at very high levels and high levels in broilers and laying hens, respectively, but resistance to cefotaxime and ceftazidime was either very low or undetectable.

Table 1.3 Serotyped *Salmonella*-positive sampling units in *Gallus gallus* and derived products (2018-2022), and percentage relative to total *Salmonella*-positive sampling units across animal and food sources analyzed.

	2018		2019		2020		2021		2022	
	N. units	**%**	**N. units**	**%**	**N. units**	**%**	**N. units**	**%**	**N. units**	**%**
Broilers	10,093	61.4	10,632	61.9	8,972	50.2	11,143	55.7	9,028	50.6
Broiler meat	1,989	12.1	1,820	10.6	3,379	18.9	3,206	16.0	4,046	22.7
Eggs and egg products	50	0.3	10	0.1	45	0.3	36	0.2	46	0.3

Data obtained from EFSA and ECDC (2022 and 2023). N., number.

Table 1.4 Number of *Salmonella*-positive sampling units by serotype in *Gallus gallus* and products thereof in the year 2022.

	Laying hens and eggs		Broilers and broiler meat	
	N. units	**%**	**N. units**	**%**
Enteritidis	349	34.1	1,009	7.7
Typhimurium	104	10.2	296	2.3
Monophasic Typhimurium 1,4,[5],12:i:-	14	1.4	85	0.65
Infantis	98	9.6	6,540	50.1

Data obtained from EFSA and ECDC (2023). N., number.

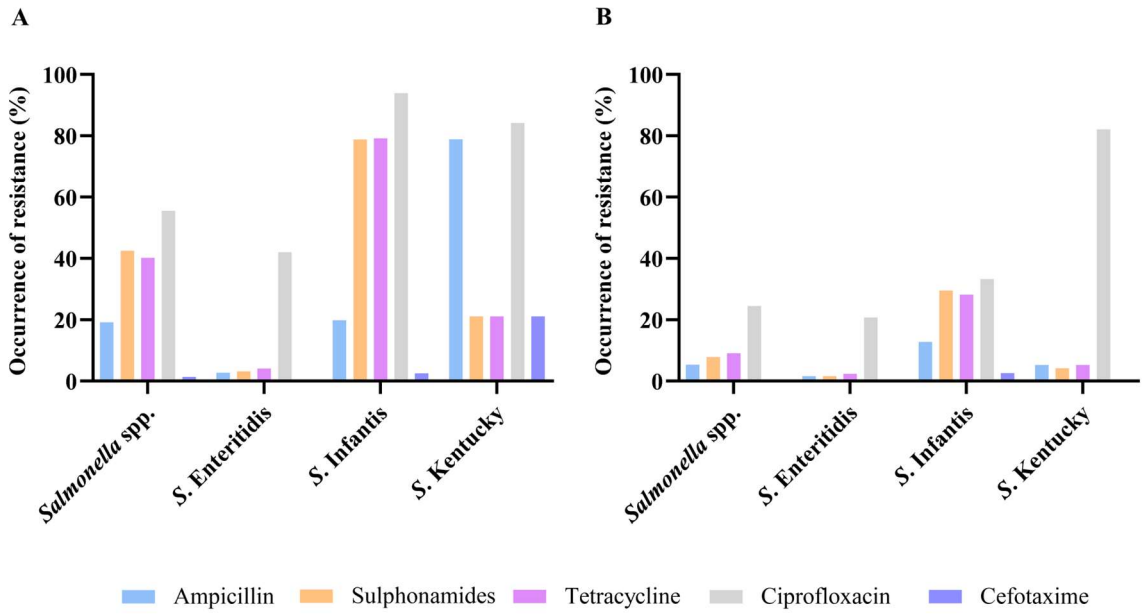


Figure 1.3 Occurrence of antibiotic resistance in *Salmonella* serovars isolated from broilers (A) and laying hens (B) in 2021 in the European Union. Data obtained from EFSA and ECDC, 2024.

1.2 Bacteriophages

Bacteriophages (or phages) are viruses that specifically infect bacteria. They were discovered in 1915 and reported by Frederick Twort and Felix d'Hérelle in 1915 and 1917, respectively (Twort, 1915; D'Hérelle, 1917). Phages stand out as the most abundant and diverse biological entities on Earth (Comeau *et al*., 2008), and are ubiquitously present in all environments inhabited by bacteria (Sharma *et al*., 2017). Initially perceived as highly host-specific, often restricted to individual bacterial species, recent studies suggest that phages can exhibit a broader host range (de Jonge *et al*., 2019). Furthermore, they play crucial roles in bacterial evolution and global environmental processes, since it is believed that they are responsible for lysing 15% to 40% of oceanic bacteria every day (Keen, 2014).

1.2.1 Phage structure and classification

The phage particle is composed of a protein structure termed capsid that contains the phage's genome, which may be single-stranded deoxyribonucleic acid (ssDNA), double-stranded DNA (dsDNA), single-stranded ribonucleic acid (ssRNA) or double-stranded RNA (dsRNA). Phage genomes exhibit a high degree of mosaicism, with variable sizes ranging from a few kilobases to nearly 500 Kb (Keen, 2014). In most cases, the phage capsid is attached to a protein tail; these are known as tailed phages (Figure 1.4). In these phages, the main role of the tail is to recognize the phage receptor on the bacterial surface. Phage receptors encompass bacterial LPS molecules, teichoic acids, flagella, and other bacterial surface proteins (Bertozzi Silva *et al*., 2016). Phage attachment to the receptor is specific and dependant on the environmental conditions. After attachment, the bacteriophage will eventually inject its genome into the bacterial cytoplasm, initiating its multiplicative life cycle. Less frequent phage morphologies are cubic, filamentous, and pleomorphic (Figure 1.4) which are not as widely studied as tailed phages.

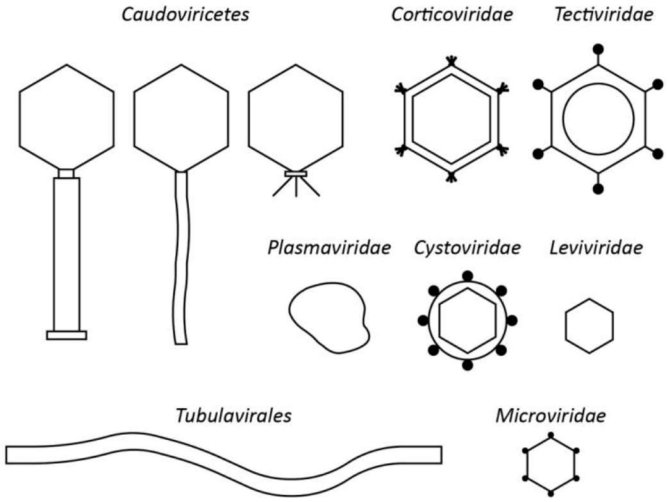


Figure 1.4 Morphotypes of bacteriophages (obtained from Turner *et al*., 2021). *Caudoviricetes* corresponds to a phage class encompassing tailed phages, *Tubulavirales* is a phage order which includes filamentous phages, *Plasmaviridae* is a phage family of pleomorphic phages, and *Corticoviridae*, *Tectiviridae*, *Cystoviridae*, *Levivirudae* and *Microviridae* are phage families of cubic phages.

The International Committee on Taxonomy of Viruses (ICTV) holds the responsibility for phage classification. Historically, phages were classified according to morphology, host range, their genome type and size, and resistance to organic solvents (Sharma *et al*., 2017). In 2023 the ICTV discontinued the morphology-based classification of tailed phages and replaced the *Caudovirales* order with the *Caudoviricetes* class. All former *Caudovirales* phages have been included under this class, with the creation of new orders and families underway (Zhu *et al*., 2022; Turner *et al*., 2023). While the terms "myovirus", "siphovirus" and "podovirus" are no longer taxonomically recognized, they are still used as morphological identifiers for tailed phages (Figure 1.5), depicting contractile long-tailed, non-contractile long-tailed and short-tailed phages, respectively.

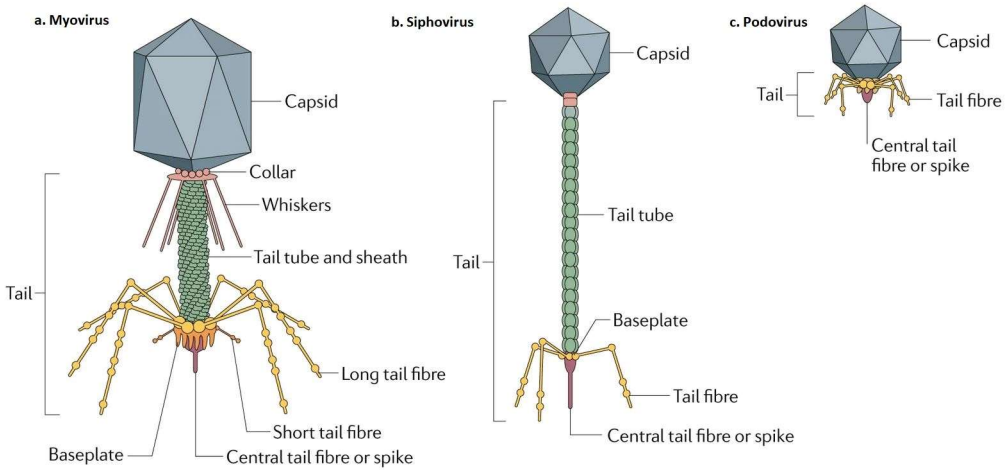


Figure 1.5 The three different morphologies of tailed bacteriophages (adapted from Nobrega *et al*., 2018).

1.2.2 Phage life cycle

Bacteriophages exhibit four distinct life cycles: i) lytic, ii) lysogenic, iii) chronic, or iv) pseudolysogenic (Figure 1.6) (Naureen *et al*., 2020; Venturini *et al*., 2022). The lytic life cycle is typically performed by virulent phages, although temperate and pseudolysogenic phages also complete it, but to a lesser extent. In lytic infections (Figure 1.6a), right after phage adsorption and genome injection, the phage takes over the cellular machinery to allow the production of new phage particles. This involves genome replication and the synthesis of all necessary proteins for both virion formation and bacterial cell lysis. The cycle ends with the lysis of the host cell, releasing the phage progeny which will start a new cycle. In contrast, the lysogenic cycle (Figure 1.6b), characteristic of temperate phages, involves the integration of the phage genome into the bacterial chromosome right after genome injection, constituting what is called a prophage. This prophage will replicate together with the bacterial genome and will segregate into daughter cells as a prophage during cell division. Under stressful conditions, the prophage excision from the bacterial genome will start a lytic cycle which will result in the formation of new phage particles and progeny release by host cell lysis. Chronic infections (Figure 1.6c) are characteristic of filamentous phages. In this cycle, the phage uses the cellular machinery to produce new phage progeny continuously, however virion release is not produced by cell lysis, but via membrane budding or release through pores. A distinguishing feature of chronic infections is the reduction of the bacterial population due to a decrease in the cellular metabolic activity rather than cell death. Finally, in pseudolysogenic cycles (Figure 1.6d), when conditions for phage replication are suboptimal, the phage genome does neither start a lytic cycle nor integrate into the bacterial chromosome, but it remains inactive in the bacterial cytoplasm without undergoing replication or formation of phage particles. Due to the absence of phage genome replication, asymmetrical segregation occurs upon bacterial cell division, leading to the loss of phage

genomes in one daughter cell and retention in the other. Upon restoration of favourable conditions, the phage may re-enter either a lytic or lysogenic cycle.

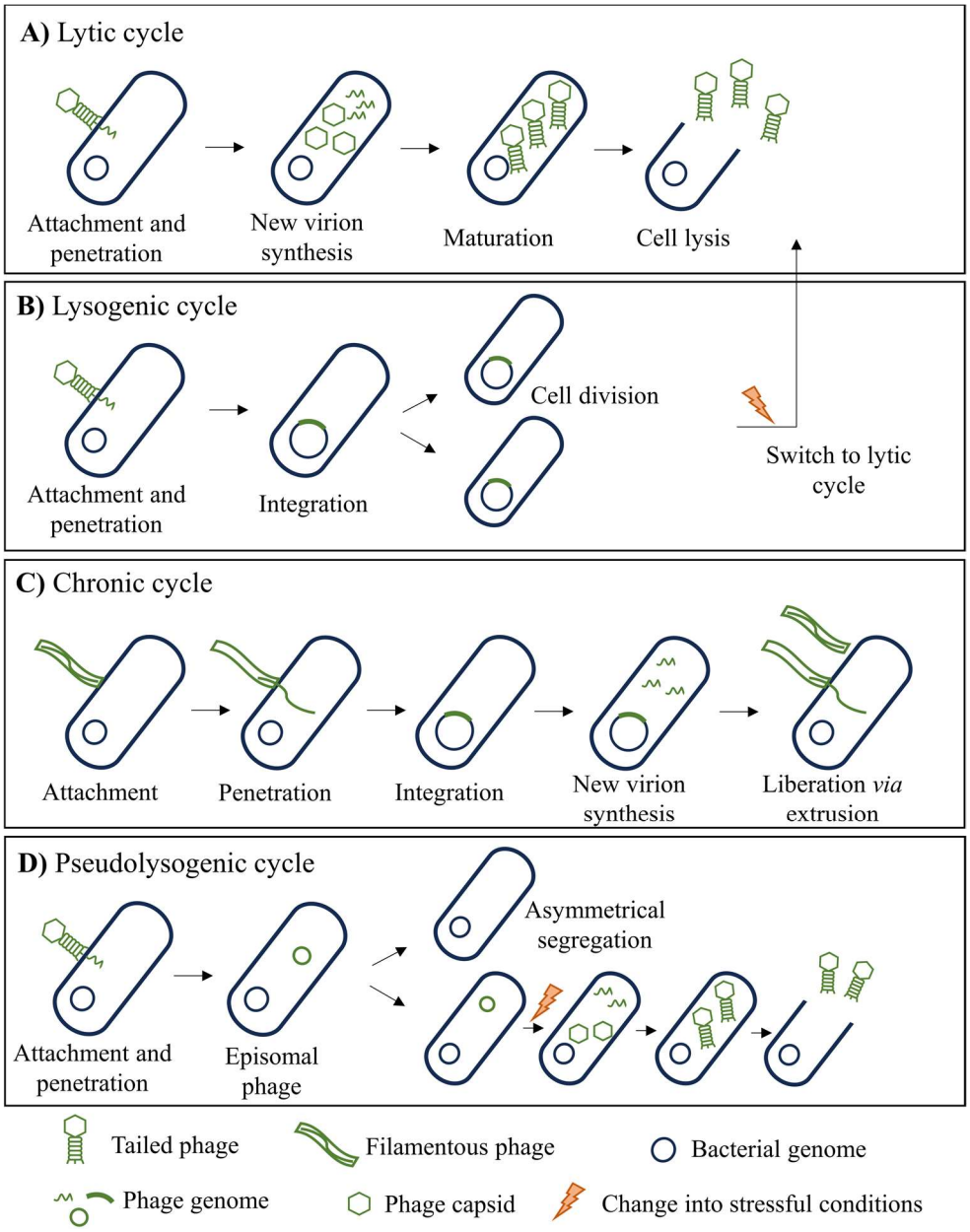


Figure 1.6 Schematic representation of the four types of a bacteriophage life cycle. Adapted from Venturini *et al*., 2022.

1.2.3 Bacteriophage therapy

The first application of bacteriophages to combat bacterial infections was proposed by Felix d'Hérelle to treat patients with dysentery (D'Hérelle, 1917), and phages were subsequently employed as a therapeutic tool against some infectious diseases by different countries, notably by those of the Soviet Union during World War II. However, phage therapy in Western medicine experienced a decline between the 1920s and 1940s, influenced by both scientific and political factors. Biologically,

bacteriophages were controversial, as they were not classified as either living organisms or simple chemicals (Newman, 1937). Furthermore, their biology was poorly understood, and the application of phage preparations often resulted in non-reproducible outcomes due to the inclusion of preservatives (Summers, 2012) that inactivated them before application or because phages were ineffective against the bacteria causing the infections. In addition, the rise of the pharmaceutical industry in countries such as the United States of America and Germany among others, with advancements in methods for scaling up bacterial cultures under sterile conditions, and refining methods for compound separation and purification, facilitated the industrial-level production of previously discovered antibiotics, such as penicillin. All of this, together with the advent of stable pharmaceutical formulations for antibiotics, coupled with their high effectiveness and low toxicity in comparison to other antibacterial compounds, ended the use of phages to combat bacterial infections in the Western world. Despite this, in certain former Soviet Union countries, such as Georgia or Russia, phages continued to be used as antibacterials, a practice that persists today (Chanishvili, 2012). Nevertheless, the acceptance of phages as antibacterials in Western countries encounters several major obstacles, such as the lack of randomized controlled clinical trials confirming the efficacy of phage therapy to regulatory agencies, the requirements of safety, stability, and quality of phage preparations, and the development of strategies that interfere with phage infection, among others (Chanishvili, 2012).

1.2.3.1 Advantages and disadvantages of the use of phage therapy

Bacteriophages offer many advantages that make them a highly effective solution for the treatment of bacterial infections, but they also present some disadvantages (Loc-Carrillo and Abedon, 2011; Loponte *et al*., 2021). One of the most important advantages of phages is their biological nature, enabling auto-replication within their host. This allows for the use of low or even single doses, with phage density increasing *in situ* if the host is present. Additionally, cross-infection between phage infected and non-phage infected subjects has been demonstrated (Smith *et al*., 1987), proving advantageous in agricultural settings and for the treatment of large numbers of animals. Nevertheless, the fact that phages are biological entities can also be a drawback, as the general population tends to be wary of viruses as a treatment option.

Another advantage of phages is that, generally, they are specific to the bacteria they infect, sparing the surrounding microbiota. This limits development of resistance to the few bacterial species which are susceptible to infection (Loc-Carrillo and Abedon, 2011). However, recent reports have shown that phage specificity can, in some cases, be broader (de Jonge *et al*., 2019), underscoring the importance of studying host range when selecting phages for phage therapy. It is also important to note that the host specificity of narrow-range phages may hinder the isolation of phages against bacteria that are difficult to culture in the laboratory.

Resistance to bacteriophages can emerge in the target bacteria, but this can be mitigated by using multiple phages in a cocktail, each targeting the same host bacteria but attaching to different receptors. Notably, resistance mechanisms to phages are distinct from those conferring resistance to antibiotics, making phages valuable for treating infections caused by antibiotic resistant bacteria.

Phages used in phage therapy are always virulent, inducing bacterial lysis and exhibiting a bactericidal effect, and reducing the likelihood of development of resistance compared to bacteriostatic antibiotics (e.g., tetracycline) (Loc-Carrillo and Abedon, 2011). This is one of the main reasons why characterization of phages, primarily through genome sequencing and analysis, is crucial for therapy as temperate phages may confer phage insensitivity to the bacteria carrying them via superinfection exclusion (Sie) or may facilitate acquisition of virulence factors that can be transmitted between bacteria during the recombination-excision process performed during lysogeny. Furthermore, highly virulent phages are preferred for therapy due to their enhanced pathogen elimination potential (Loc-Carrillo and Abedon, 2011).

In terms of environmental impact, phages differ significantly from antibiotics. Comprising mostly proteins and nucleic acids, phages have a lower environmental impact as they cannot survive without their host bacteria and are sensitive to high temperatures or desiccation (Loc-Carrillo and Abedon, 2011). Finally, bacteriophages exhibit high versatility in application, being administered through various routes and forms (liquids, creams, etc.), and allowing for their incorporation into cocktails or even with antibiotics.

1.2.4 Bacterial defence against phage infection

Bacteriophages play a pivotal role in controlling microbial populations, making them a key player in many ecosystems (Rodriguez-Valera *et al*., 2009). The Red Queen or evolutionary arms-race hypothesis (Mueller, 2020) states that continuous phage attacks have driven bacteria to develop a wide range of strategies to fight against phage infections (Figure 1.7) and phages to develop novel strategies to counteract bacterial defences. This means that both phage and bacteria are in constant coevolution (Stern and Sorek, 2011). Understanding these bacterial defence strategies is imperative for the safe implementation of phage therapy. The number of described phage defence strategies has grown exponentially over the last few years, and they can be classified depending on the phase of the phage infection cycle they act at (Georjon and Bernheim, 2023) (Figure 1.7).

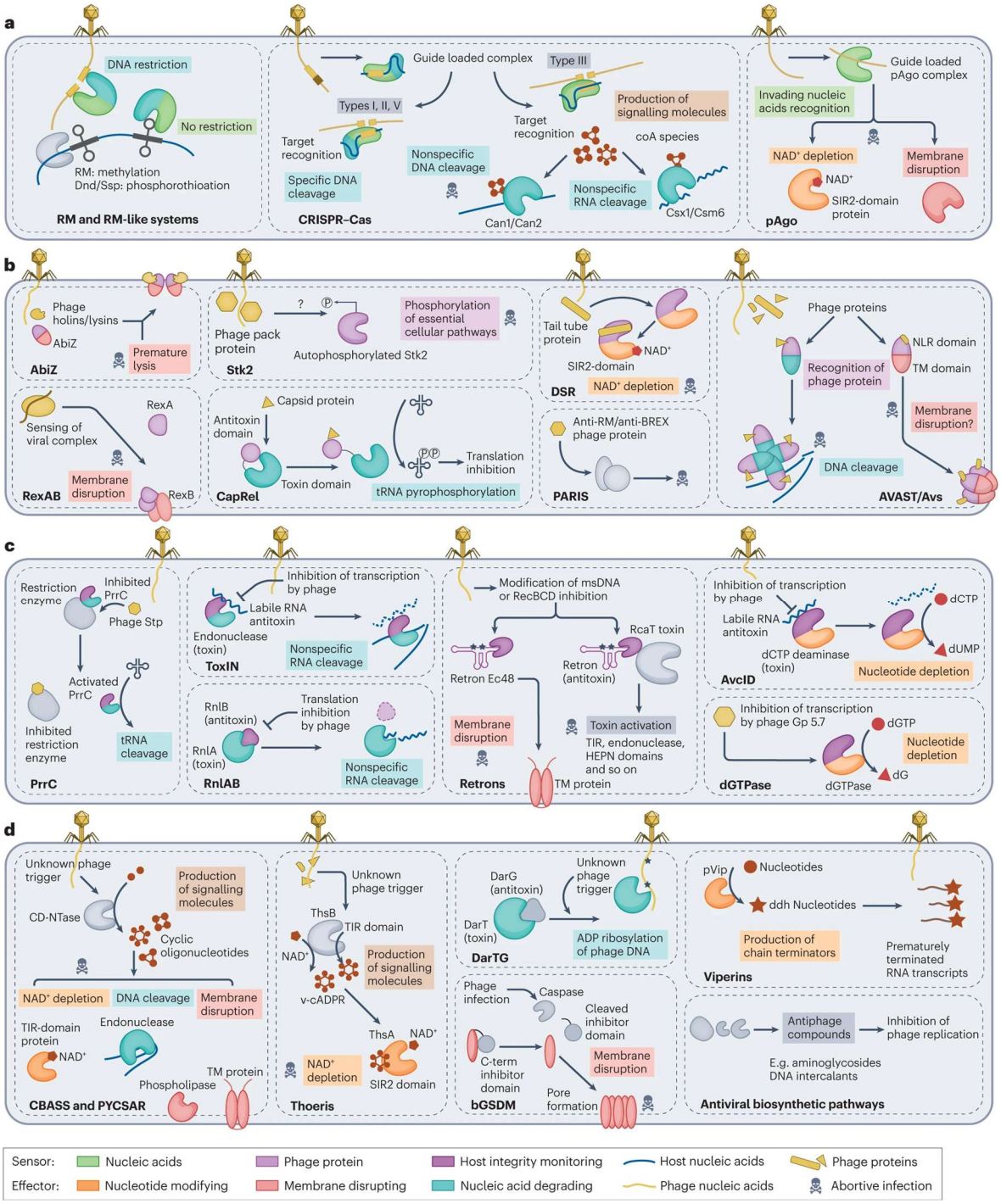


Figure 1.7 Known antiphage defence systems found in bacteria (obtained from Georjon and Bernheim, 2023). (a) Nucleic acid sensing systems, (b) Phage protein sensing systems, (c) Systems monitoring the integrity of the host, and (d) Other mechanisms.

Before the bacterial defence systems can act, resistance mechanisms are the first barrier against phage infection, which involve the prevention of adsorption to their receptors. Bacteria accomplish this through different methods. One is the alteration or loss of the receptor due to mutations or gene deletions, sometimes resulting in a reduction of bacterial virulence (Wang *et al.*, 2023). Another strategy is the masking of the receptors with extracellular polymeric substances or using outer

membrane vesicles as decoys (Bertozzi Silva *et al*., 2016). Subsequent to phage adsorption, mechanisms such as Sie, primarily found in temperate phages, impede the entry of phage DNA identical or very similar to their own DNA (Bondy-Denomy *et al*., 2016; Rousset *et al*., 2022).

Once phage DNA is found inside the cell, several defence mechanisms hinder different stages of the phage cycle. Firstly, the cleavage of injected DNA to interfere with phage replication is achieved through innate immune systems such as restriction-modification (RM) (Tock and Dryden, 2005), phage growth limitation (PgI) (Chinenova *et al*., 1982), bacteriophage exclusion (BREX) (Goldfarb *et al*., 2015), defence island associated with RM (DISARM) (Ofir *et al*., 2018), prokaryotic argonautes (pAgos) (Makarova *et al*., 2009), or clustered regularly interspaces short palindromic repeats and associated proteins (CRISPR-Cas) adaptive immune systems (Hille *et al*., 2018). Classical restriction-modification systems involve a methylase that methylates a specific sequence in the bacterial DNA and a restriction endonuclease that cleaves the sequence when unmethylated, such as an invading phage. Other systems such as PgI, BREX and DISARM use methylation differently. PgI methylates phage DNA upon entry, allowing the phage to complete its cycle, but progeny phages are cleaved when infecting subsequent cells. BREX can recognize self-DNA from invader DNA through different methylation patterns. DISARM also marks self-DNA with methylation, however, this methylation is not sufficient to prevent restriction of phages by an unknown mechanism. pAgos use small single-strand guides obtained from cleavage or degradation of invader genomes at entry, which are used by the pAgos protein to recognize and block the invader genome. CRISPR-Cas systems are the only adaptive immune systems known in bacteria. These can store short sequences of past infections in CRISPR arrays, using them to recognize and cleave the DNA of new infections by the same phage. Another mechanism of interference with phage genome replication, known as RADAR (acronym of phage restriction by an adenosine deaminase acting on RNA), is a process by which bacteria may alter their own transcriptome to resist bacteriophage. RADAR proteins assemble into massive molecular complexes, but two different models about how these assemblies obstruct phage have been recently proposed (Gao *et al*., 2023, Wiryaman and MacRae, 2023).

Transcription of phage DNA, essential for the synthesis of proteins necessary for the formation of the viral capsid, can also be the target of bacterial defences. For example, prokaryotic viperins (pVips) (Bernheim *et al*., 2021) produce several modified ribonucleotides that act as RNA chain terminators, inhibiting phage transcription.

On the other hand, the Abortive infection (Abi) systems cause cell death before phages have completed their life cycle, avoiding the spread of the infection in the population. These systems typically target replication, transcription, or translation, exhibiting diverse mechanisms. Abi systems were initially described in *Lactococcus lactis* (twenty-three systems have been described in more or

less detail, from AbiA to AbiZ) (Sing and Klaenhammer, 1990; Forde and Fitzgerald, 1999; Chopin *et al*., 2005; Barrangou and Horvath 2011) and *Escherichia coli* (for example, PrrC and Lit) (Cooley *et al*., 1979; Tyndall *et al*., 1994). One of the classical Abi strategies are the toxin-antitoxin (TA) systems (Dy *et al*., 2014; Lopatina *et al*., 2020), where a toxin induces cell toxicity counteracted by an antitoxin. TA systems were first described as systems that maintain plasmids through post-segregational killing, but they can also provide defence against phages, e.g., the Hok/Sok system, the ToxIN system, and the AbiEi/AbiEii system (Garvey *et al*., 1995; Pecota and Wood, 1996; Fineran *et al*., 2009). In general terms, when phage infection takes place, the levels of antitoxin are reduced, causing bacteriostasis or cell death by the toxin. Abortive infection mediated by TA systems are one of the most commonly reported plasmid-encoded phage interference mechanisms (Bouchard *et al*., 2002; Chopin *et al*., 2005; Samson *et al*., 2013).

Other more recently described Abi systems include cyclic-oligonucleotide-based antiphage signalling systems (CBASS) (Cohen *et al*., 2019) and Thoeris (Doron *et al*., 2018; Ofir *et al*., 2021). In both systems, recognition of infection stimulates the production of cellular signals that activate effectors which will cause cell death. Bacterial gasdermins (Johnson *et al*., 2022) cause abortive infection through the formation of membrane pores when phage infection is detected. Non-catalytic pAgos (Koopal *et al*., 2022) can also lead to abortive infection by associating their guide-mediated nucleic acid function with effectors that cause cell death. Retrons (Millman *et al*., 2020) use a reverse transcriptase to form RNA-DNA hybrids from non-coding RNAs, which become activated in response to phage infection, signalling effector proteins that will cause abortive infection.

Phage inducible chromosomal islands (PICI) (Fillol-Salom *et al*., 2018) represent a very different phage defence strategy. These systems consist of mobile genetic elements (MGEs) that can encapsulate themselves in a helper phage capsid, interfering with the mature phage virions. To do so, PICIs can alter the production of the viral capsid, resulting in smaller capsids that can only encapsulate the smaller PICI genome (Ram *et al*., 2012). They can also interfere with the small terminase, inhibiting the encapsulation of the phage genome (Ram *et al*., 2012). Finally, it has also been found that PICIs can inhibit late gene expression by binding to the phage's transcription factors (Ram *et al*., 2014). Although they have a similar genomic organization to prophages, PICIs have attachment sites in the bacterial chromosome that are never occupied by prophages, and they do not code for genes related to the lytic cycle or virion morphogenesis (Martínez-Rubio *et al*., 2017). Thus, PICIs offer protection from subsequent infections, as most released viral particles contain a PICI and do not initiate an infectious cycle (Ibarra-Chávez *et al*., 2022). Furthermore, it has been recently reported that PICIs can carry other types of phage defence systems within their sequence (Fillol-Salom *et al*., 2022).

Beyond the mentioned defence systems, numerous mechanisms with unknown functions continue to be discovered, contributing to the interference with the phage cycle (Georjon and Bernheim, 2023).

1.2.5 *Salmonella* bacteriophages UAB_Phi20, UAB_Phi78 and UAB_Phi87

The *Salmonella* bacteriophages UAB_Phi20, UAB_Phi78, and UAB_Phi87 are virulent phages that infect different *S. enterica* subsp. *enterica* serovars, such as Typhimurium and Enteritidis. UAB_Phi20 and UAB_Phi87 phages were isolated from chicken faeces, while UAB_Phi78 phage was obtained from pig faeces (Bardina *et al*., 2012; Spricigo *et al*., 2013). All three phages belong to the *Caudoviricetes* class and have been used in cocktail form in several studies conducted by our research group, including food biocontrol studies (Spricigo *et al*., 2013) and oral phage therapy in broilers (Bardina *et al*., 2012; Colom *et al*., 2015; Colom *et al*., 2017).

Salmonella phage UAB_Phi20 belongs to the *Lederbergvirus* genus. It has an icosahedral head of 60 ± 1.5 nm and a noncontractile short tail (13 ± 0.7 nm) (Bardina *et al*., 2012). Its genome is a linear dsDNA molecule of 41,809 base pairs (bp) in length (Bardina *et al*., 2016). UAB_Phi20 genome shares a high genomic similarity (99.01% sequence identity) with *Salmonella* phage P22, and they share 72% of their proteins (Bardina *et al*., 2016). Despite encoding all the components necessary for a lysogenic cycle, UAB_Phi20 is a virulent phage. This virulent behaviour was attributed to the absence of recognition sites for the C1 protein in the P_{RE} promoter and the lack of an *attP* site, which would avert its integration in the *attB* site of the *Salmonella* chromosome, preventing the phage from lysogenizing (Bardina *et al*., 2016).

UAB_Phi78 belongs to the *Autographiviridae* family and *Zindervirus* genus. Its icosahedral head measures 66 ± 1.7 nm and it has a noncontractile short tail of 14 ± 0.7 nm (Bardina *et al*., 2012). The linear dsDNA genome of UAB_Phi78 is 44,110 bp in length and exhibits high similarity (93.19% sequence identity) to phage SP6 (Bardina *et al*., 2016).

UAB_Phi87 has an icosahedral head of 68 ± 2.7 nm and a long contractile tail of 114 ± 4.3 nm (Bardina *et al*., 2012). Classified under the *Ounavirinae* subfamily and the *Felixounavirus* genus, this phage has a larger genome than the other two phages, with a length of 87,669 bp (Bardina *et al*., 2016). UAB_Phi87 has a percentage sequence identity of 96.63% with phage Felix O1 (Bardina *et al*., 2016).

The receptor of the three phages UAB_Phi20, UAB_Phi78 and UAB_Phi87 is the LPS molecule (Figure 1.8). UAB_Phi20 binds to the α-rhamnosyl 1-3 galactose linkage of the O-chain (Otero J, 2019) similarly to P22 phage (Iwashita and Kanegasaki, 1973). UAB_Phi78 binds to the first glucose of the LPS core, and its tail spike proteins may also interact with the O-antigen before binding to the core (Otero J, 2019) as it was described for SP6 phage (Tu *et al*., 2017). Finally, the N-

acetylglucosamine found bound to the last glucose of the LPS core is the receptor of UAB_Phi87 (Otero J, 2019).

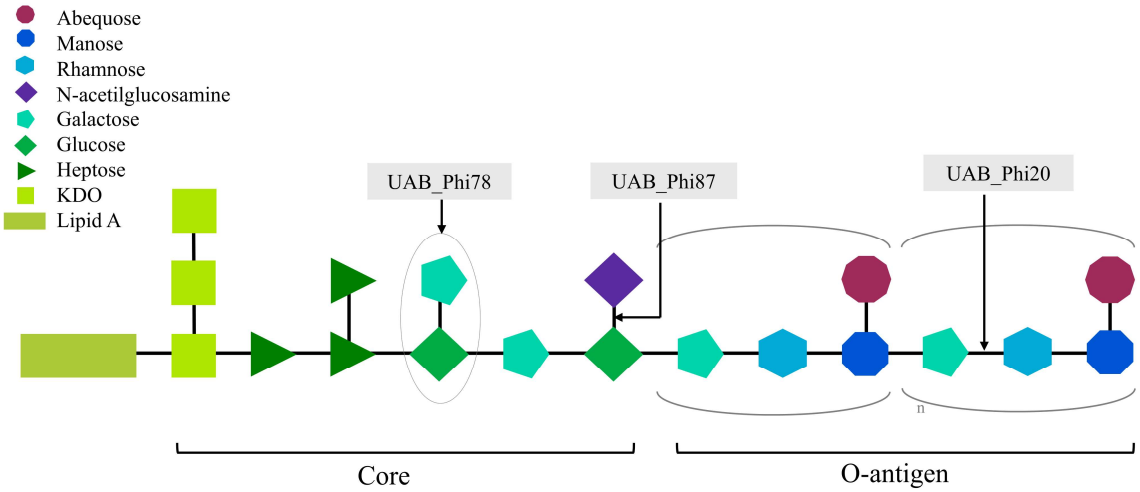


Figure 1.8 Representation of the LPS molecule and the points where the three receptors of the cocktail phages are found (adapted from Otero J, 2019).

1.2.5.1 Transcriptional regulation of the P22 bacteriophage

As previously mentioned, the UAB_Phi20 phage exhibits high similarity to the P22 phage and shares the same regulatory genes. Therefore, we presume that the regulation of its lytic cycle functions similarly to that of the P22 phage. Specifically, P22 phage controls its decision between the lytic or lysogenic cycle through its *immC* immunity region (Figure 1.9), which is analogous to the control mechanism employed by bacteriophage λ (Susskind and Botstein, 1978). The key players in this region are the C2 and Cro repressors. The former inhibits transcription from the of P_R and P_L early gene promoters during lysogeny (Botstein *et al.*, 1975), while the latter shuts down early gene expression from the same two promoters at later stages of the lytic cycle (Winston and Botstein, 1981).

Upon infection, the P22 phage will express immediate early genes *cro* and *24*, from P_R and P_L, respectively. The *24* gene encodes the early antitermination protein, which acts in the points marked in green in Figure 1.9; for P_L at the tL1 point, and for P_R at the tR1 and tR2 points (Figure 1.9). Antitermination at tR1 and tL1 prompts the expression of *c1* and *c3* genes. The C1 protein, stabilized by the C3 protein, will activate expression from P_{RE}, the promoter for repressor establishment, allowing *c2* transcription (Ho *et al.*, 1992), resulting in the production of C2 protein as early as three minutes after infection (Harvey *et al.*, 1981). At this stage, C2 and Cro will compete for the control of promoters P_R and P_L. Is important to notice that each one of these promoters contains three operators, and that C2 and Cro exhibit different affinities for each of them (Figure 1.10). If the lytic cycle is prompted, Cro will bind at O_{R3} first, blocking expression of *c2* from the P_{RM} promoter,

consequently increasing early gene transcription (Poteete and Ptashne, 1982). Early protein synthesis occurs in infected cells between 0 and 20 minutes after infection. However, synthesis is asynchronous, with some proteins observed as early as 0 minutes and others appearing later (Lew and Casjens, 1975). This will result in an increase in Cro concentration within the cell as the cycle progresses to its later stages, causing Cro to bind to operators 1 and 2 from promoters P_R and P_L and repress early gene expression (Winston and Botstein, 1981). Then, late genes will be transcribed from the P_{LATE} promoter, which is antiterminated by the product of the early expressed gene *23* (Susskind and Botstein, 1978) (Figure 1.9). Late protein synthesis happens at around 20 minutes after infection, with all late proteins synthesized simultaneously (Lew and Casjens, 1975). Although gene *23* is transcribed from the P_R promoter, its expression is also negatively regulated by a small antisense RNA transcribed from the P_{A23} promoter, activated by C1 (Ho *et al*., 1992), resulting in this antiterminator being active only during the later stages of the lytic cycle. It is not fully understood whether the regulation by the small RNA occurs at a transcriptional or translational level.

On the other hand, if synthesis of C2 repressor from P_{RE} is high, this protein will occupy operators 1 and 2 from promoters P_R and P_L (Figure 1.10), blocking early gene transcription and inducing a lysogenic cycle (Poteete and Ptashne, 1982). Since *c1* expression will also be blocked, C2 controls its own expression during lysogeny through the P_{RM} promoter, blocking O_{R3} and repressing its own transcription as C2 levels increase or freeing this operator if C2 levels decrease. The concentration of C2 depends on a wide range of environmental and genetic factors, such as the multiplicity of infection (Levine, 1957) or the activity of several phage and host genes. At this point, the integrase and recombinase proteins produced during the lysis/lysogeny decision stages will aide in the integration of the P22 genome into the bacterial chromosome by recombination between the phage *attP* and the bacterial *attB* sites (Leong *et al*., 1985). Because the UAB_Phi20 phage is virulent, the lytic cycle must be initiated immediately after infection (Bardina *et al*., 2016).

Unlike bacteriophage λ, the P22 phage has another immunity region, *immI,* which comprises three protein coding regions (*mnt*, *arc* and *ant*) and a small antisense regulatory RNA (*sar*) (Liao *et al*., 1987; Wu *et al*., 1987) (Figure 1.9). The primary function of this region is the expression of *ant*, an antirepressor protein responsible for inhibiting the C2 repressor. Ant binds to C2 noncovalently, preventing its binding to operators of both P_R and P_L promoters, thereby causing prophage induction and loss of superinfection immunity in lysogens (Susskind and Botstein, 1975). However, the Ant protein is not essential for lytic cycle maintenance (Botstein *et al*., 1975; Levine *et al*., 1975), and does not interfere with establishment of lysogeny (Gough, 1977). The *ant* gene is transcribed from a strong and early rightward promoter P_{ANT}, which is self-repressed by the Arc protein during the lytic cycle (Wu *et al*., 1987) and by the Mnt protein during lysogeny (Wu *et al*., 1987). One would expect that *ant* and *arc* expression would be highest at the beginning of the lytic cycle, declining as the cycle progresses. This dynamic is known for Ant protein synthesis; however, *ant* and *arc* mRNA levels

have never been studied throughout the phage cycle. On the other hand, *ant* and *arc* mRNA are also transcribed from the P_{LATE} promoter (Susskind and Youderian, 1982). The lack of Ant protein synthesis from the P_{LATE} has been demonstrated (Susskind and Youderian, 1982), but whether it applies to Arc has not been thoroughly investigated. Later, it was proved that the small RNA *sar* is responsible for inhibiting the translation of *ant* from the P_{LATE} transcript (Liao *et al*., 1987; Wu *et al*., 1987; Schaefer and McClure, 1997). Finally, Susskind, 1980 discovered that Arc^- mutants have a lethal phenotype, with an overproduction of Ant. The author proposes that *ant* overexpression out-competes other genes for expression, resulting in early genes not being shut-off at later stages of the phage cycle and late proteins are being underproduced.

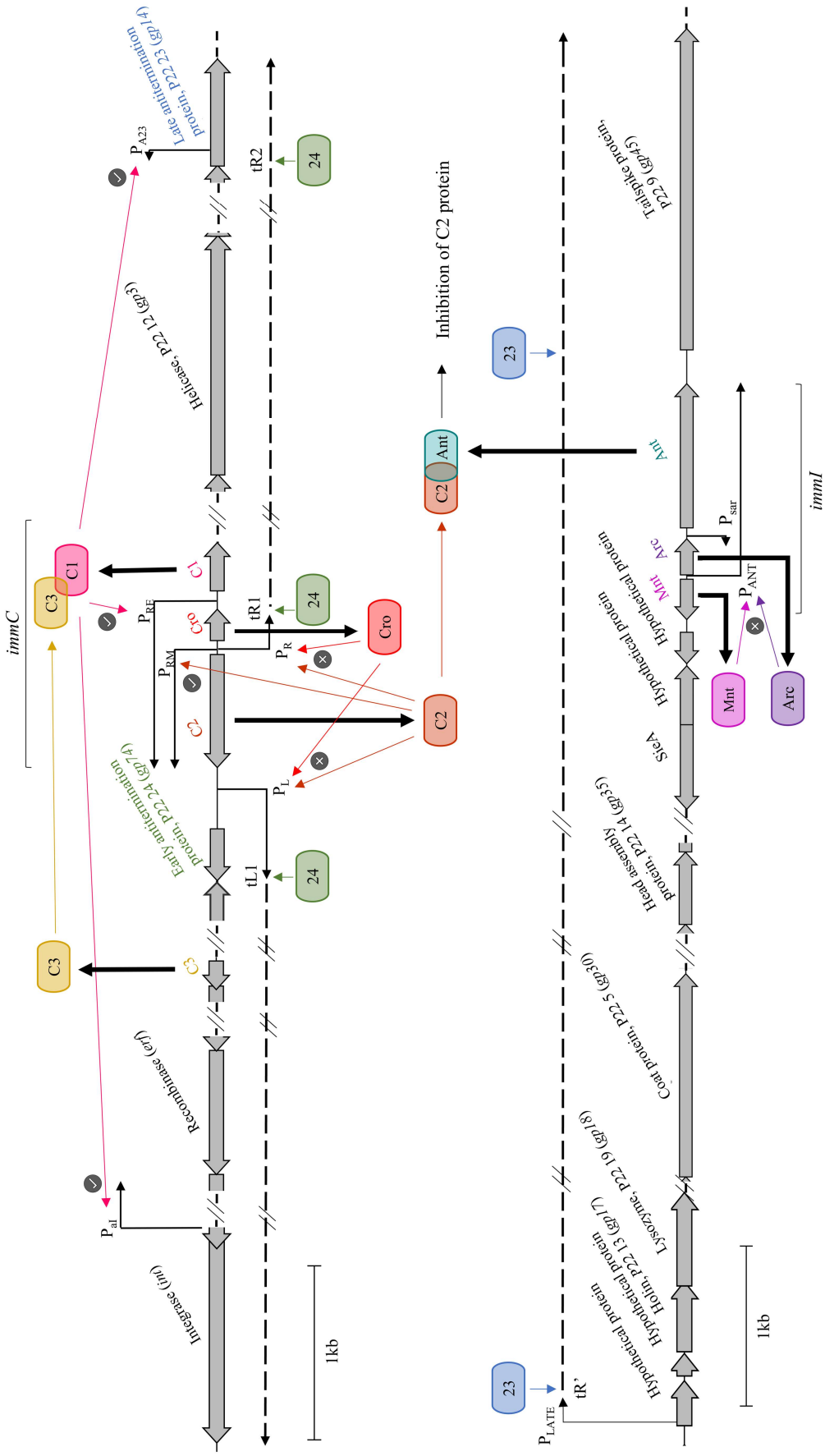
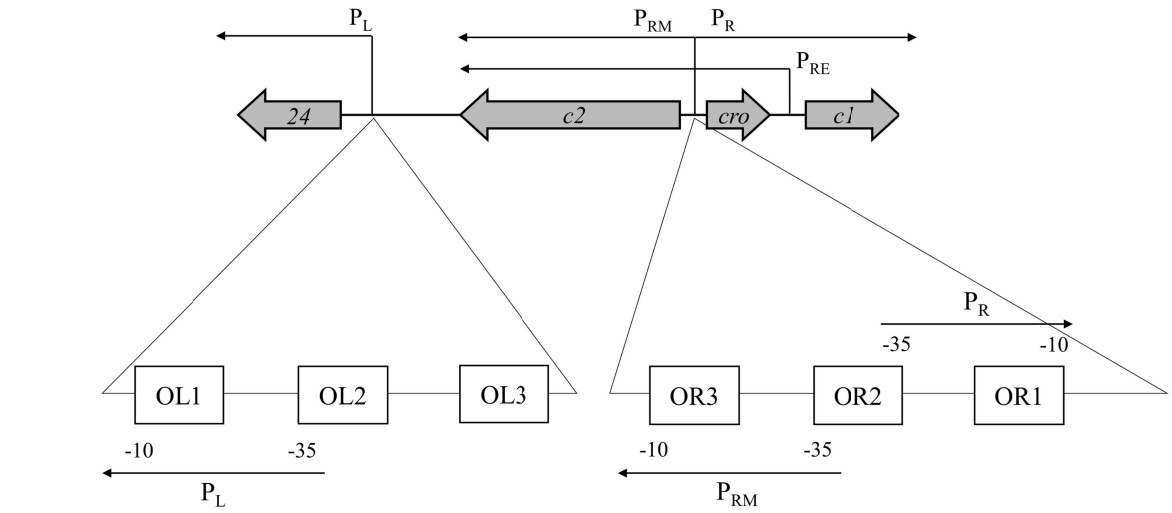


Figure 1.9 Regulation of expression of P22. ⊗ Represents repression of transcription and ◑ represents activation of transcription. Coloured arrows indicate the site of action of the protein with the same colour. Thick black lines indicate protein production. Names of the genes in parentheses correspond to UAB_Phi20.



Affinity for:	OL1	OL2	OL3	OR3	OR2	OR1
C2 repressor	High	High	Low	Low	High	High
Cro	Low	Low	High	High	Low	Low

Figure 1.10 Schematic representation of the region regulating the expression of promoters P_R, P_L and P_{RM}, along with the affinities of binding of C2 repressor and Cro to the operators at these sites.

2. OBJECTIVES

The use of phage therapy as an alternative to antibiotics is becoming increasingly relevant, as evidenced by the growing number of studies examining its efficacy against a wide range of bacterial infections. However, one of the main obstacles to the global adoption of phage therapy lies in the emergence of resistance and/or lytic cycle interference mechanisms that could hinder its effectiveness. In the last few years, there has been an increase in the number of reports describing the various mechanisms employed by bacteria to evade phage infection. Nevertheless, most of these studies have been performed *in vitro*. Furthermore, *in vivo* studies have often attributed resistance to receptor mutations or have inadequately elucidated the underlying mechanism of observed resistance or interference with the multiplicative of bacteriophages.

To address this gap, our research group conducted an extensive study on the emergence of bacterial variants exhibiting reduced phage-susceptibility to phages. This study encompassed three different scenarios: a) laboratory conditions, b) *Salmonella* contaminated cooked ham slices, and c) broilers, using the model organism *S.* Typhimurium ATCC14028 Rif^R and a bacteriophage cocktail integrated by the UAB_Phi20, UAB_Phi78 and UAB_Phi87 phages. Our findings revealed that the *Salmonella* variants with reduced phage susceptibility isolated from *Salmonella* laboratory cultures infected with the phage cocktail, or from ham slices contaminated with *Salmonella* and treated with the cocktail, exhibited phage resistance attributable to mutations in bacterial phage receptors (Otero J, 2019). Conversely, those variants from the farm animal scenario did not display changes on their receptors. In light of these observations, the hypothesis of this thesis posits that *Salmonella* variants with reduced phage susceptibility isolated from broilers may harbour mechanisms that interfere with the multiplicative cycle of phages. Consequently, the objective of this thesis has been to validate this hypothesis and to identify potential mechanisms responsible for the observed reduced susceptibility to phages exhibited by *Salmonella* variants isolated from broilers during oral phage therapy.

To accomplish this main goal, the specific objectives were defined as follows:

1. Characterize the phenotype of *Salmonella* variants isolated from broilers exhibiting reduced susceptibility to the phages of the cocktail used in the study.
2. Identify the biological factors underlying the emergence of interference mechanisms with the phage multiplicative cycle in *Salmonella* variants isolated from broilers, and to evaluate their impact on the efficacy of oral phage therapy.
3. Identify the gene involved in interference of the UAB_Phi20 phage cycle and characterize this mechanism at the molecular level.

3. CHAPTER I

Summary

The research presented in this chapter was undertaken to address the initial two specific objectives:

- Characterize the phenotype of *Salmonella* variants isolated from broilers exhibiting reduced susceptibility to the phages of the cocktail used in the study.
- Identify the biological factors underlying the emergence of interference mechanisms with the phage multiplicative cycle in *Salmonella* variants isolated from broilers, and to evaluate their impact on the efficacy of oral phage therapy.

To achieve these objectives, several parameters of the UAB_Phi20, UAB_Phi78 and UAB_Phi87 bacteriophages were studied, including the EOP, ECOI, the adsorption constant and the burst size. Furthermore, the unmapped Illumina reads obtained from genome sequencing of seven *Salmonella* variants were analysed, revealing the presence of several large size plasmids. To demonstrate that these large plasmids of the I1α incompatibility group encoded genes responsible for the observed interference, conjugation assays and plasmid curing were performed.

The results obtained demonstrate that the reduced susceptibility of seven *Salmonella* variants isolated from broilers to both UAB_Phi20 and UAB_Phi78 bacteriophages is entirely attributable to the presence of the IncI1α plasmids. Furthermore, these plasmids are also partially responsible for the reduced susceptibility that these variants present towards the UAB_Phi87 bacteriophage.

frontiers | Frontiers in Cellular and Infection Microbiology

TYPE Original Research
PUBLISHED 28 September 2023
DOI 10.3389/fcimb.2023.1266685

Check for updates

OPEN ACCESS

EDITED BY
Alicja Wegrzyn,
Polish Academy of Sciences, Poland

REVIEWED BY
Derek Lin,
Veterans Health Administration,
United States Department of Veterans Affairs, United States
Jumpei Fujiki,
University of California San Diego,
United States

*CORRESPONDENCE
Pilar Cortés
mariapilar.cortes@uab.cat
Montserrat Llagostera
montserrat.llagostera@uab.cat

†These authors have contributed equally to this work

RECEIVED 25 July 2023
ACCEPTED 12 September 2023
PUBLISHED 28 September 2023

CITATION
López-Pérez J, Otero J, Sánchez-Osuna M, Erill I, Cortés P and Llagostera M (2023) Impact of mutagenesis and lateral gene transfer processes in bacterial susceptibility to phage in food biocontrol and phage therapy. *Front. Cell. Infect. Microbiol.* 13:1266685. doi: 10.3389/fcimb.2023.1266685

COPYRIGHT
© 2023 López-Pérez, Otero, Sánchez-Osuna, Erill, Cortés and Llagostera. This is an open-access article distributed under the terms of the Creative Commons Attribution License (CC BY). The use, distribution or reproduction in other forums is permitted, provided the original author(s) and the copyright owner(s) are credited and that the original publication in this journal is cited, in accordance with accepted academic practice. No use, distribution or reproduction is permitted which does not comply with these terms.

Impact of mutagenesis and lateral gene transfer processes in bacterial susceptibility to phage in food biocontrol and phage therapy

Júlia López-Pérez[1†], Jennifer Otero[1,2†], Miquel Sánchez-Osuna[1], Ivan Erill[3,4], Pilar Cortés[1*] and Montserrat Llagostera[1*]

[1]Departament de Genètica i de Microbiologia, Universitat Autònoma de Barcelona, Cerdanyola del Vallès, Spain, [2]SK8 Biotech, Parc Científic de Barcelona, Barcelona, Spain, [3]Department of Biological Sciences, University of Maryland, Baltimore, MD, United States, [4]Departament Enginyeria de la Informació i de les Comunicacions, Universitat Autònoma de Barcelona, Cerdanyola del Vallès, Spain

Introduction: The emergence of resistance and interference mechanisms to phage infection can hinder the success of bacteriophage-based applications, but the significance of these mechanisms in phage therapy has not been determined. This work studies the emergence of *Salmonella* isolates with reduced susceptibility to a cocktail of three phages under three scenarios: i) *Salmonella* cultures (LAB), ii) biocontrol of cooked ham slices as a model of food safety (FOOD), and iii) oral phage therapy in broilers (PT).

Methods: *S.* Typhimurium ATCC 14028 RifR variants with reduced phage susceptibility were isolated from the three scenarios and conventional and molecular microbiology techniques were applied to study them.

Results and discussion: In LAB, 92% of *Salmonella* isolates lost susceptibility to all three phages 24 h after phage infection. This percentage was lower in FOOD, with 4.3% of isolates not susceptible to at least two of the three phages after seven days at 4°C following phage treatment. In PT, 9.7% and 3.3 % of isolates from untreated and treated broilers, respectively, displayed some mechanism of interference with the life cycle of some of the phages. In LAB and FOOD scenarios, resistant variants carrying mutations in *rfc* and *rfaJ* genes involved in lipopolysaccharide synthesis (phage receptor) were identified. However, in PT, the significant decrease of EOP, ECOI, and burst size observed in isolates was prompted by lateral gene transfer of large IncI1 plasmids, which may encode phage defense mechanisms. These data indicate that the acquisition of specific conjugative plasmids has a stronger impact than mutagenesis on the emergence of reduced phage-susceptibility bacteria in certain environments. In spite of this, neither mechanism seems to significantly impair the success of *Salmonella* biocontrol and oral phage therapy.

KEYWORDS

mutations, phage resistance, lateral gene transfer, phage interference, IncI1 plasmids, phage biocontrol, phage therapy

10.3389/fcimb.2023.1266685

1 Introduction

The misuse and overuse of antibiotics in animal husbandry, human health care and agriculture have contributed to a substantial increase in antibiotic resistance rates worldwide. The spread of antimicrobial genes is achieved mainly by lateral gene transfer (LGT) events, not only among clinical pathogens but stemming also from commensal and environmental bacteria (von Wintersdorff et al., 2016; Sánchez-Osuna et al., 2019). The emergence of multi-drug resistant bacteria poses serious treatment limitations for a growing list of infectious diseases, increasing mortality rates as well as treatment costs, and urging the development of alternative therapies (European Antimicrobial Resistance Collaborators, 2022).

Bacteriophages have the potential to fulfill this need owing to several advantages when compared to antibiotics. For instance, phages self-replicate in a localized manner and can display a host range from broad to narrow, minimizing effects on commensal microbiota or tissues (de Jonge et al., 2019; Gordillo Altamirano and Barr, 2019). However, there are still some challenges that bacteriophages must overcome before being effectively and widely harnessed as antimicrobials (Górski et al., 2018). Primary among these hurdles is the unfolding of a broad range of anti-phage defense systems by bacteria, which could thwart the success of phage therapy approaches (Isaev et al., 2021a; Isaev et al., 2021b; Egido et al., 2022). These microbial strategies target different stages of the phage cycle: i) prevention of phage adsorption by masking/mutating surface receptors or secreting exopolysaccharides that hinder the access of phages to the surface of the host cell (Bertozzi Silva et al., 2016); ii) prevention of DNA injection by superinfection exclusion mechanisms (Bondy-Denomy et al., 2016; Rousset et al., 2022); iii) targeting the phage genome through mechanisms like restriction-modification systems (Tock and Dryden, 2005), bacteriophage exclusion (BREX) (Goldfarb et al., 2015), defense island associated mechanisms (DISARM) (Ofir et al., 2018) or prokaryotic Argonaute proteins (pAgos) (Makarova et al., 2009), as well as the adaptive immunity by CRISPR-Cas (clustered regularly interspaced palindromic repeats and CRISPR-associated proteins) system (Hille et al., 2018); iv) impairing cellular processes to block phage replication, transcription or translation via toxin-antitoxin, abortive infection systems (Dy et al., 2014; Lopatina et al., 2020) or broad-range anti-phage related systems based on retrons (Millman et al., 2020); and v) a plethora of putative defense systems identified recently and still not fully characterized (Doron et al., 2018; Millman et al., 2022).

Emergence of phage resistance against individual phages or phage cocktails has been reported *in vitro* (Pereira et al., 2016; Oechslin et al., 2017; Bai et al., 2019; Wright et al., 2019), where it is mediated mainly by mutations on genes encoding phage receptors. Similarly, phage resistance has been evidenced *in vivo* (Maura and Debarbieux, 2012; Schooley et al., 2017; Oechslin, 2018; De Sordi et al., 2019; Hernandez and Koskella, 2019; McCallin and Oechslin, 2019; Salazar et al., 2021) and although receptor mutations were also described as mechanism involved in some of them (Schooley et al., 2017), the mechanisms involved in the rest of studies have not been thoroughly investigated.

This study provides insights on the emergence of bacterial resistance and interference mechanisms against bacteriophages using *Salmonella enterica* serovar Typhimurium when exposed to a cocktail of three bacteriophages (UAB_Phi20, UAB_Phi78, and UAB_Phi87). Experiments were performed in three different scenarios: i) phage-infected *Salmonella* cultures (LAB); ii) biocontrol with the phage cocktail on cooked ham experimentally contaminated with *Salmonella*, as model of food matrices (FOOD), and iii) oral phage therapy applied to broilers infected with *Salmonella* in experimental farms (PT) (Colom et al., 2017). Our data reveal that the emergence of bacterial resistance to phages in LAB and FOOD was due to mutations in phage receptors, while acquisition of large plasmids encoding interference mechanisms of the multiplicative phage cycle drove bacterial resistance to phages in oral phage therapy. However, the emergence of bacterial resistance in food biocontrol and oral therapy settings did not significantly impair the success of phage treatments.

2 Materials and methods

2.1 Bacterial strains

Salmonella enterica serovar Typhimurium LB5000 (SGSC181; University of Calgary) was used to propagate and quantify the virulent bacteriophages used in this study and for mating studies. A *S.* Typhimurium ATCC 14028 spontaneous mutant resistant to rifampicin (Rif^R), obtained by us, was used for the studies of the emergence of reduced phage-susceptibility of bacteria. Moreover, *S.* Typhimurium LT2 wild-type strain (University of Calgary), TA1537 strain (Dr. Bruce Ames, University of California, Berkeley), and a collection of lipopolysaccharide (LPS) mutants of *S.* Typhimurium LT2 (University of Calgary) were used to identify the possible receptors of phages UAB_Phi20, UAB_Phi78, and UAB_Phi87. Finally, the strain *Escherichia coli* DH5α was used for mutagenesis strategies (Clontech, Takara Bio, France) (Supplementary Table S1). The *S.* Typhimurium ATCC 14028 Rif^R strain and derived variants were cultured on Luria-Bertani (LB) or XLD Agar (Xylose-Lysine-Desoxycholate Agar; Becton Dickinson) media supplemented with Rifampicin (75 μg/mL). All the other bacterial strains were grown in LB broth or agar plates. In all cases, plates were incubated for 18 h at 37°C.

2.2 Bacteriophage propagation and titration

The bacteriophages studied belong to *Lederbergvirus* (UAB_Phi20, accession number: NC_031019), *Zendervirus* (UAB_Phi78, accession number: NC_020414) and *Felixounavirus* (UAB_Phi87, accession number: NC_027360) genera. These phages have been fully characterized and their genomes have been sequenced in previous studies (Bardina et al., 2012; Bardina et al., 2016).

Phage lysates were prepared following a previously described method (Colom et al., 2015) and filtered through 0.45 μm pore-size

10.3389/fcimb.2023.1266685

polyethersulfone (PES) membranes (Millex®-HP). The phage cocktail was prepared by mixing the UAB_Phi20, UAB_Phi78, and UAB_Phi87 bacteriophages with a ratio of 1:1:1, each phage at a titer of 3.3 log_{10} PFU/mL. The phage cocktail was further diluted with $MgSO_4$ 10 mM to reach the desired concentration of experiments. Individual phages or phage cocktail titration was performed by plating ten-fold serial dilutions onto ATCC 14028 Rif^R LB plates using the double agar method (Kutter, 2009).

2.3 Isolation of *S.* Typhimurium ATCC 14028 Rif^R variants with reduced phage susceptibility

Detection of ATCC 14028 Rif^R isolates with reduced susceptibility to bacteriophages was studied in three different experimental conditions: i) *Salmonella* cultures infected with the phage cocktail (LAB), ii) cooked ham slices previously contaminated with *Salmonella* and treated with the phage cocktail (FOOD), and iii) oral phage therapy applied to broilers experimentally infected with *Salmonella* in experimental farms (PT) (Colom et al., 2017).

Infection of *Salmonella in vitro* cultures was performed as follows. A culture of ATCC 14028 Rif^R strain grown in LB medium at 37°C until an optical density at 550 nm (OD_{550}) of 0.2 was infected with the phage cocktail (MOI of 1 PFU/CFU) and incubated for 24 h at 37°C. An uninfected culture was included as a control. Samples of both cultures were taken at 0, 4.5, 6.5, and 24 h, and appropriate ten-fold serial dilutions were plated on XLD-Rif (75 µg/mL). After 18 h of incubation at 37°C, around 50 colonies were randomly isolated on LB plates per time and type of culture for further studies.

For FOOD experiments, slices of packed cooked ham were purchased in a local supermarket, and the absence of *Salmonella* and bacteriophages capable of infecting the parental strain used in this study was verified through enrichment methods (Guttman et al., 2005). All the processes related to *Salmonella* contamination, phage treatment and drying of the ham slices were carried out in a level II biological safety cabinet (Telstar ™ Bio II Advance 4, Telstar Technologies S.L.). Firstly, slices of cooked ham were cut into 49 cm^2 pieces using sterile material. To remove the remains of preservatives to ensure an efficient contamination with ATCC 14028 Rif^R strain, ham pieces were immersed in 0.9% NaCl (300 mL NaCl 0.9% for every 25 slices) and shaken at 50 r.p.m. for 5 min. Pieces of cooked ham were placed in trays covered with aluminum foil (previously disinfected with 70% ethanol and ultraviolet light for 15 min on each side) and dried in the cabin for 5 min (each side). One side of ham slices was contaminated with ATCC 14028 Rif^R strain by spraying a suspension in 0.9% NaCl [6.1 mL; 1 x 10^7 colony-forming units (CFU)/mL] using an airbrush coupled to a compressor (Ventus Air-23) at a pressure of 1.5 bar. After 15 min of drying, pieces were treated by spraying with the phage cocktail in $MgSO_4$ 10 mM (6.1 mL; 1 x 10^9 PFU/mL). Control samples, untreated, were sprayed with the same volume of $MgSO_4$ 10 mM. After an additional 15 min of drying, each slice of cooked ham was individually stored in Whirl-Pak filter bags (Nasco, Fort Atkinson, WI) at 4°C for 7 days. On days 0, 3, and 7, five pieces were taken, and 50 mL of buffered peptone water (BPW, Merck) was added to each bag. The contents were homogenized with a Bagmixer (Interscience) at maximum speed for 60 s. Determination of *Salmonella* concentration was done as previously described in XLD-Rif (75 µg/mL) (Colom et al., 2015). Finally, 240, 232, and 214 colonies from the plates of the control group on days 0, 3, and 7, respectively, were isolated on LB plates for further studies. Similarly, 235, 198, and 232 colonies were isolated at the same days from the treated group.

Concerning the PT experiment, *Salmonella* isolates came from a previous *in vivo* oral phage therapy study of *Salmonella* ATCC 14028 Rif^R-infected commercial broilers and treated with the phage cocktail (Colom et al., 2017). Before infection, broilers were *Salmonella* and ATCC 14028 Rif^R-specific phage free (Colom et al., 2017). Briefly, twenty-four cecum samples were collected on days 1, 8, and 15 after *Salmonella* infection from phage-treated and untreated group, respectively. After processing of samples (Colom et al., 2015), a total of 720 colonies were isolated from the control group (240 colonies per period) and 630 colonies from the bacteriophage-treated group (166 colonies on day 1, 225 on day 8, and 240 on day 15).

Randomly selected colonies were streaked on LB-Rif (75 µg/mL) and incubated for 18 h at 37°C. Afterwards, they were streaked on green plates (Chan et al., 1972) by three consecutive subcultures to ensure the absence of concomitant bacteriophages with the bacterial cells.

To determine the susceptibility to UAB_Phi78 phage, the isolates were grown in LB liquid medium in 96-well microtiter microplates (Sterilin™, Thermo Fisher Scientific, Massachusetts, USA) by incubation at 37°C with orbital shaking at 500 r.p.m (Kline; K3E model, Ovan, Barcelona, Spain) up to an absorbance at 550 nm (A_{550}) of 0.12-0.15 (equivalent to 1 x 10^7 CFU/mL). Then, cultures were infected with the phage at a MOI of 0.1. The plates were incubated at 37°C with shaking at 500 r.p.m, and growth was monitored by measuring the A_{550} every hour until 3 h, using the plate reader Sunrise (Tecan Trading AG, Switzerland). Moreover, uninfected clones were included as controls. Those isolates whose A_{550} increased over time in a similar way to the uninfected culture were considered to show reduced phage-susceptibility. In contrast, those whose A_{550} decreased over time were categorized as sensitive to phage. Strains ATCC 14028 Rif^R (sensitive to the three bacteriophages) and TA1537 (resistant to the three bacteriophages) were used as controls.

2.4 Spot assays

The sensitivity to UAB_Phi20 and UAB_Phi87 bacteriophages of all isolates showing reduced UAB_Phi78-susceptibility was determined by spot assay. Briefly, 10 µL of the bacteriophage lysate (1 x 10^6 PFU/mL) were dropped onto the double layers of each isolate in LB agar plates and incubated at 37°C overnight (Kutter, 2009). Strains ATCC 14028 Rif^R (sensitive to the three bacteriophages) and TA1537 (resistant to the three bacteriophages) were used as controls.

10.3389/fcimb.2023.1266685

2.5 Effect of phage infection on the bacterial growth kinetics

When necessary, the effect of phage infection on bacterial growth kinetics of the ATCC 14028 Rif^R variants was checked on liquid LB cultures as above described monitoring the A_{550} at 30-min or 1-h intervals after infection till 3.5 h, using the spectrophotometer Genesys 10S UV-Vis (Thermo Fisher Scientific, Massachusetts, USA). In addition, the concentration of viable cells (CFU/mL) was determined each time. Non-infected cultures of the studied strains were included as a control.

2.6 Efficiency of plating

Assessment of the efficiency of plating (EOP) was tested under the stationary phase of both target (ATCC 14028 Rif^R variants) and host (*S.* Typhimurium ATCC 14028 Rif^R) strains. For this, the bacteria were cultured at 37°C for 18 h in LB medium, and 0.1 mL of the cultures were mixed with 0.1 mL of ten-fold serial dilutions of the appropriate phage lysate in LB molten agar (0.7%) and plated in LB agar by the double layer method. The plates were incubated at 37°C for 18 h and the number of PFU was counted. The EOP was calculated as described previously (Khan Mirzaei and Nilsson, 2015): average PFU on target bacteria/average PFU on host bacteria, and the standard deviation was also calculated for a minimum of three assays. For each phage, and according to the EOP value obtained, the variants were considered as high (EOP ≥0.5), medium (EOP < 0.5 but ≥0.1), low (EOP between 0.001 and 0.1) efficiency, and inefficient (<0.0001) (Khan Mirzaei and Nilsson, 2015).

2.7 Phage adsorption, burst size and efficiency of centre of infection

Phage adsorption to target bacteria and burst size of phages was determined as described previously (Kropinski, 2009; Kropinski, 2018). Likewise, center of infection (COI) and ECOI were determined as described previously (Moineau et al., 1993).

2.8 Characterization of *Salmonella* LPS profiles

The bacterial LPS was extracted following a protocol previously designed and kindly provided by Dr. J. Casadesús (Universidad de Sevilla) (Buendía-Clavería et al., 2003). The gels were digitally photographed with the Gel Doc XR system (Bio-Rad Laboratories, S.A).

2.9 Sequencing and analysis of *Salmonella* genomes

Total DNA was prepared using the Easy-DNA^{TM} kit (Invitrogen), following the manufacturer's instructions. Sequencing was performed by Sistemas Genómicos S.L. (Sistemas Genómicos S.L, Valencia, Spain). The pool of the libraries was sequenced by paired-end sequencing (100 x 2) in an Illumina Hiseq 2500 sequencer. The sequencing resulted in around 9 million 101-nt long paired-end reads for each sample, with a mean Phred quality score > 30.

To find the putative mutations responsible for phage reduced susceptibility, the trimmed paired-end reads were aligned against the chromosome and pSLT plasmid sequences of *S.* Typhimurium ATCC 14028s (Genbank accession numbers: CP001363.1 and CP001362.1, respectively) using Geneious Prime 2020.0.4 (https://www.geneious.com) with up to 5 fine-tuning iterations. Single nucleotide polymorphisms (SNPs) calling was performed using the Geneious Prime software while larger insertions/deletions (≥ 5bp) were determined using Mauve Contig Mover (MCM) (Darling et al., 2010). Only insertions/deletions that were not found at the ends of the contigs (more than 20 bp away from the ends) and were absent in *S.* Typhimurium ATCC 14028 Rif^R parental strain were retained.

The existence of unused reads resulting from mapping assemblies revealed the presence of exogenous DNA to the *S.* Typhimurium ATCC 14028s chromosome or pSLT plasmid. To further investigate this acquired DNA, trimmed paired-end reads were re-assembled *de novo* using SPAdes v3.11.1 (with 'careful -k 21,33,55,77' settings) (Bankevich et al., 2012), and the scaffolds matching the genome or plasmid of *S.* Typhimurium 14028s through BLASTn (coverage>75%, e-value<1E-10) (Altschul et al., 1997) were removed from further analysis. To obtain the complete sequences of the acquired DNA, the retained scaffolds were combined with PLACNETw assemblies (Vielva et al., 2017) using Velvet (Zerbino, 2010) through Geneious Prime. Finally, complete plasmid assemblies were annotated using Prokka version 1.12 (Seemann, 2014) against the COG (Tatusov et al., 2000), HAMAP (Pedruzzi et al., 2015) and Pfam (Finn et al., 2016) databases and using their three best BLASTn complete plasmids hits as reference. The replicon sequences of each plasmid were determined using the PlasmidFinder 2.1 web-tool (Carattoli et al., 2014).

2.10 Construction of complemented strains

Construction of plasmids for complementation of mutations of target genes of *Salmonella* genomes was carried out by amplification of each wild-type gene of interest by PCR from the chromosome of ATCC 14028Rif^R using the appropriate primers (Supplementary Table S2). The primers carried homology for appropriate cloning at the 5'-end of the sequence and the PCR was done using the Phusion High-Fidelity DNA Polymerase (Thermo Scientific^{TM}). The resulting PCR products were purified with NzyGelpure kit (NZYTech, Lisboa, Portugal) and cloned into a previously linearized and dephosphorylated pUA1108 vector (Supplementary Table S1) via double digestion with NdeI and BamHI enzymes, as previously described (Mayola et al., 2014). The resulting ligation was used to transform competent *E. coli* DH5α cells by electroporation. Transformants were selected by growth on 50 μg/mL ampicillin plates. Plasmid DNA was extracted with a Plasmid DNA purification kit (NZYTech, Lisboa, Portugal) and the gene sequences were confirmed by sequencing (Macrogen).

10.3389/fcimb.2023.1266685

The confirmed recombinant plasmids were introduced by electroporation in target *Salmonella* electrocompetent cells. Following selection of the transformants, the presence of cloned products was confirmed again by PCR and sequencing (Macrogen). As a control, the empty pUA1108 vector was transformed into the target bacteria under the same conditions.

2.11 Conjugative mating assays

Transference of phage interference mechanisms codified in acquired plasmids of PT variants was assessed by mating assays on a solid surface by adapting the method previously described (García-Quintanilla et al., 2008). *S.* Typhimurium LB5000 Str^R was used as recipient strain. The number of CFUs was recorded and the conjugation frequencies were calculated.

The susceptibility to the phages of the cocktail of four transconjugants of each matting experiment was assayed by spot assay, as described before (Kutter, 2009). Furthermore, the presence of acquired plasmids in such transconjugants was confirmed by conventional PCR using appropriate primers for sequences specific to each plasmid (Supplementary Table S2).

2.12 Introduction of kanamycin cassette on plasmids

Insertion of a kanamycin resistance cassette in the pUA1139 plasmid was performed using a λ-Red recombinase strategy (Datsenko and Wanner, 2000). Briefly, the kanamycin resistance cassette from pKD4 (Supplementary Table S1) was amplified by PCR using the primers with homology with the desired regions (Supplementary Table S2). The resulting linear PCR products were purified with NzyGelpure kit (NZYTech, Lisboa, Portugal), and were introduced by electroporation in the target bacteria carrying the plasmid pKOBEGA (Ap^R; Supplementary Table S1). Transformant clones were selected in LB agar plates supplemented with kanamycin (50μg/mL). The kanamycin cassette insertion was confirmed by PCR and sequencing using the appropriate primers (Supplementary Table S2).

2.13 Plasmid curing methods

The CRISPR/Cas9-based genome editing method (Chen et al., 2018) was adapted to inactivate pUA1135 and pUA1136 plasmids identified in *S.* Typhimurium variants. The pCasPA plasmid encoding the Cas9 protein and the λ-Red recombination system and the pACRISPR plasmid with the BsaI site for cloning the spacers were used. First, the *bla* gene that codifies the beta-lactamase in the pACRISRPR plasmid was replaced by a spectinomycin (*spt*) gene obtained from pSET4s plasmid (Takamatsu et al., 2001). The resulting plasmid was named pUA1148 (Supplementary Table S2). The *spt* gene and pACRISPR (without the *bla* gene) were amplified by PCR using the Phusion polymerase (ThermoFisher Scientific) with appropriate primers (Supplementary Table S2). Then, the PCR products were assembled using the NEBuilder® HiFi DNA Assembly Master Mix (New England Biolabs, Inc) and transformed by electroporation in DH5α competent cells. The transformants were selected on LB agar plates supplemented with spectinomycin (100 μg/mL) and checked by conventional PCR.

The 20 nt sequence (spacer) targeting the *repA* gene of target plasmids was selected using the Find CRISPR Sites tool of the Geneious Prime software. For each CRISPR site identified, off-target binding sites in the *S.* Typhimurium genome or pSLT plasmid were also searched. The spacer with the highest activity and specificity scores was selected. The phosphorylated and annealed primers containing the spacer sequences were designed as described (Chen et al., 2018), and cloned into the pUA1148 using the NEB® Golden Gate Assembly Kit (BsaI-HF®v2; New England Biolabs, Inc) following the manufacturer's instructions. The assembled product pUA1148+gRNA48 (Supplementary Table S2) was transformed by electroporation in DH5α competent cells and transformants were selected on LB agar plates supplemented with spectinomycin (100 μg/mL) and checked by PCR and sequencing (Supplementary Table S2). Afterwards, 1 μg of pCasPA plasmid was transformed by electroporation in *Salmonella* variants and the colonies were selected on LB agar plates supplemented with tetracycline (Tet; 17 μg/mL). Then, 100 ng of pUA1148+gRNA48 were transformed by electroporation into those *Salmonella* electrocompetent cells and the colonies containing pCasPA and pUA1148+gRNA48 were selected on LB agar plates with tetracycline (17 μg/mL) and spectinomycin (200 μg/mL). The elimination of the target plasmid was checked by PCR with suitable primers (Supplementary Table S2). Finally, the pCasPA and pUA1148+gRNA48 were cured by sucrose counter-selection (Chen et al., 2018).

To eliminate the pUA1139 plasmid, the curing method based on λ-Red mutagenesis and I-*Sce*I nuclease (de Moraes and Teplitski, 2015) was applied using the appropriate plasmids and primers (Supplementary Tables S1, S2). Briefly, one-step inactivation (Chaveroche et al., 2000; Datsenko and Wanner, 2000) was used to introduce the kanamycin resistance cassette (obtained from pKD4) and the restriction site for I-*Sce*I deleting gene *pUA1139_00007* from pUA1139 plasmid. At the same time, pUA1165 plasmid was constructed by removing the genes related to the λ-Red system from pKD46 and cloning the I-*Sce*I nuclease controlled by the tetracycline inducible promoter (P_{tetA}) (synthesized at ATG:biosynthetics GmbH, Germany) into the NcoI restriction site using NEBuilder® HiFi DNA Assembly Master Mix (New England Biolabs, Inc) and transformed by electroporation in DH5α competent cells. The transformants were selected on LB agar plates supplemented with ampicillin (100 μg/mL) and checked by conventional PCR. Afterwards, 100 ng of pUA1165 were transformed by electroporation into the *Salmonella* IT2 variant containing the previously modified pUA1139 and made electrocompetent. Induction of I-*Sce*I nuclease was done using anhydrotetracycline (AHT) as described previously (de Moraes and Teplitski, 2015), and clones that were kanamycin sensitive were checked by PCR with suitable primers. Finally, pUA1165 was cured by temperature.

10.3389/fcimb.2023.1266685

3 Results

3.1 Isolation of *S.* Typhimurium ATCC14028 Rif^R variants with reduced UAB_Phi78-susceptibility

To study the emergence of bacterial resistance to phages in different settings, we isolated *S.* Typhimurium ATCC14028 Rif^R clones from the LAB, FOOD and PT experiments, and first identified variants that exhibited reduced susceptibility to UAB_Phi78 by monitoring absorbance at A_{550} of cultures infected with this phage. UAB_Phi78 was used for the initial screening due its fast multiplicate cycle (Bardina et al., 2012) and its ability to infect both smooth and rough *Salmonella* strains (Figure 1) (Bardina et al., 2016). From the LAB scenario, 200 and 197 isolates were randomly selected from uninfected and infected cultures, respectively, at different times after infection with the bacteriophage cocktail. All isolates from the uninfected cultures were sensitive to the UAB_Phi78 phage. However, 92% of isolates from the cocktail-infected culture displayed UAB_Phi78-reduced sensitivity 24 h after phage infection (Table 1).

In the FOOD scenario, 686 and 665 isolates were obtained from 15 untreated and 15 treated cooked ham slices, respectively (Table 2). All isolates from the untreated cooked ham slices were sensitive to UAB_Phi78 phage, whereas 21 (3.2%) isolates from the treated slices showed reduced susceptibility to this phage.

In the PT scenario, 720 and 631 isolates were recovered from the ceca of untreated and treated broilers, respectively (Colom et al., 2017) (Table 3). Most of them were sensitive to the UAB_Phi78 phage, but 70 (9.7%) of the isolates from the untreated group and 21 (3.3%) from the group treated with the cocktail showed reduced susceptibility to this phage (Table 3).

3.2 Molecular basis of reduced phage-susceptibility of *S.* Typhimurium ATCC 14028 Rif^R variants isolated from LAB and FOOD

All variants with reduced UAB_Phi78-susceptibility isolated from LAB and FOOD scenarios were insensitive to UAB_Phi78 infection and their efficiency of plating (EOP) was zero. Data from the spot test analysis to the two other phages of the cocktail showed that the 96 variants isolated from treated LAB samples (Table 1) were also insensitive to infection by the other phages of the cocktail. In the case of the 21 variants isolated from treated FOOD samples (Table 2), 12 were also insensitive to UAB_Phi20 and 9 were insensitive to the three phages of the cocktail. Our initial hypothesis was that these variants were resistant to phage infection due to changes in their phage receptors, which are located in the LPS of the outer membrane. To study this, eight of these variants were selected (Table 4), and their LPS electrophoretic profile was assessed and compared with those of the parental strain *S.* Typhimurium ATCC 14028Rif^R and the *S.* Typhimurium LT2 LPS mutants (Supplementary Table S1). Results showed that the LPS electrophoretic profile of five variants isolated from both LAB (CI1, CI2 and CI3) and FOOD (HT3 and HT5) was similar to those of the *rfaL-*, *rfaK-*, *rfaJ-*, and *rfaI-* rough mutants (Figure 2). On the other hand, the HT1, HT2 and HT4 variants from FOOD showed a LPS electrophoretic profile resembling that of the *rfc-* rough mutant (Figure 2).

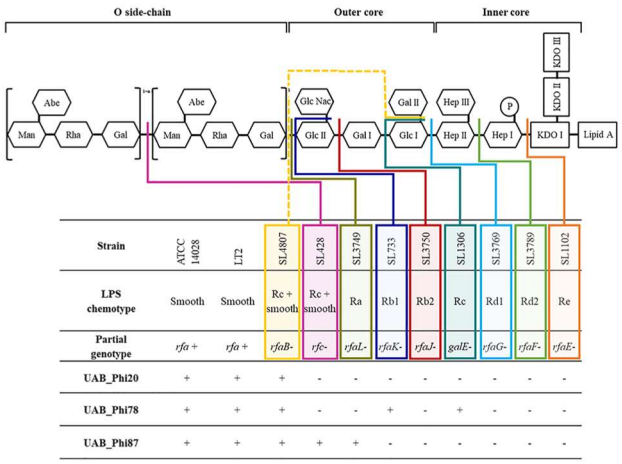


FIGURE 1
Scheme of *S.* Typhimurium LPS and detail of the infective capacity of bacteriophages UAB_Phi20, UAB_Phi78 and UAB_Phi87 against different LPS mutants of *S.* Typhimurium LT2 (based on Hitchcock et al., 1986). The different colored lines (solid and dashed) indicate the level of LPS impairment structure in the mutant strains +, lytic spot; -, no infection.

10.3389/fcimb.2023.1266685

TABLE 1 *S.* Typhimurium ATCC 14028 Rif^R variants with reduced UAB_Phi78-susceptibility isolated from uninfected and phage infected bacterial cultures (LAB).

Time (h)[a]	Uninfected		Infected	
	No. tested isolates	No. variants (%)	No. tested isolates	No. variants (%)
0	50	0 (0)	50	0 (0)
4	50	0 (0)	49	24 (49)
6.5	50	0 (0)	49	27 (55)
24	50	0 (0)	49	45 (92)
Total	200	0	197	96

[a]Time after infection of bacterial cultures (MOI=1) with the phage cocktail.

TABLE 2 *S.* Typhimurium ATCC 14028 Rif^R variants with reduced UAB_Phi78-susceptibility isolated from untreated, and phage treated cooked ham slices (FOOD).

Time (days)[a]	Sample number	Untreated		Treated	
		No. tested isolates	No. variants (%)	No. tested isolates	No. variants (%)
0	1	48	0	48	0
	2	48	0	48	2
	3	48	0	43	0
	4	48	0	48	2
	5	48	0	48	1
Subtotal		240	0 (0)	235	5 (2.1)
3	1	47	0	48	1
	2	46	0	17	0
	3	46	0	43	2
	4	48	0	48	3
	5	45	0	42	0
Subtotal		232	0 (0)	198	6 (3.0)
7	1	48	0	46	0
	2	48	0	45	6
	3	30	0	48	2
	4	42	0	46	1
	5	46	0	47	1
Subtotal		214	0 (0)	232	10 (4.3)
Total		686	0 (0)	665	21 (3.2)

[a]Time after treatment of cooked ham slices with the phage cocktail (MOI=100).

To further explore the hypothesis that the observed resistance was due to changes in phage receptors, we sequenced the genomes of the variants indicated in Table 4 and that of the parental strain ATCC 14028 Rif^R, and we mapped their sequencing reads to the reference ATCC 14028s genome (GenBank CP001363.1). Results revealed several point mutations in the genomes of all variants and the parental strain when compared to the NCBI reference genome (Supplementary Table S3). To test our hypothesis, we focused on identifying mutations in genes involved in LPS biosynthesis present in the variants but absent in the parental strain genome. In this regard, we found that the genomes of the CI2 and CI3 variants from LAB and the HT5 variant from FOOD, which display an identical phage sensitivity phenotype, contained point mutations in the *rfaJ* gene. Specifically, the CI2 and CI3 variants displayed a G→T transversion at position 910 of this gene, while the genome of the HT5 variant had an adenine deletion at position 742 of the *rfaJ* gene (Table 5). Furthermore, after PCR amplification and sequencing of the *rfaJ* gene, we found that the CI1 variant had the same G→T transversion identified in CI2 and CI3, while an adenine deletion at position 715 was detected in the HT3 variant (Table 5). All these

10.3389/fcimb.2023.1266685

TABLE 3 *S.* Typhimurium ATCC 14028 Rif^R variants with reduced UAB_Phi78-susceptibility isolated from untreated, and phage treated broiler chickens (PT).

Time (days)[a]	Animal number	Untreated group		Treated group	
		No. tested isolates	No. variants (%)	No. tested isolates	No. variants (%)
1	1	30	0	29	0
	2	30	0	30	0
	3	30	0	15	0
	4	30	0	30	0
	5	30	0	28	0
	6	30	0	26	0
	7	30	0	3	2
	8	30	0	5	0
Subtotal		240	0 (0)	166	2 (1.2)
8	1	30	0	15	0
	2	30	9	30	0
	3	30	1	30	1
	4	30	26	30	0
	5	30	9	30	0
	6	30	0	30	0
	7	30	0	30	0
	8	30	0	30	0
Subtotal		240	45 (18.7)	225	1 (0.4)
15	1	30	1	30	0
	2	30	6	30	0
	3	30	9	30	18
	4	30	0	30	0
	5	30	5	30	0
	6	30	0	30	0
	7	30	1	30	0
	8	30	3	30	0
Subtotal		240	25 (10.4)	240	18 (7.5)
Total		720	70 (9.7)	631	21 (3.3)

[a]An ATCC 14028 Rif^R strain suspension (10^7 CFU/animal) was orally administered to animals at day 0. The three-phage cocktail (10^{10} PFU/animal) was orally administrated once daily from day -1 to day 7 of the infection (Colom et al., 2017). Time indicates the day of the ceca sampling for the bacteria isolation.

point mutations give rise to a premature ochre stop codon (UAA) in the *rfaJ* gene.

On the other hand, the genome sequence of the HT1 variant from FOOD showed a deletion of 2,557 bp that encompassed the *rfc* gene. In the parental strain genome, this region is flanked by two direct repeats (DR) of 114 bp located upstream of the STM14_1615 gene (CP001363.1: 1,419,477–1,419,592) and downstream of the STM14_1618 gene (CP001363.1: 1,422,035–1,422,148) (Figure 3). The HT1 variant deletion involved the STM14_1615, *rfc*, STM14_1617, and STM14_1618 genes and the loss of one DR (Figure 3). Furthermore, by using PCR amplification and DNA sequencing, we searched for mutations in this DNA region in the genomes of HT2 and HT4 variants. We identified the same deletion in the HT4 variant and a C→A transversion at position 219 of the *rfc* gene of the HT2 variant giving rise to a premature ochre stop codon (UAA) (Table 5).

Finally, we demonstrated that complementation *in trans* of the *rfc* and *rfaJ* wild-type genes in the variants that presented mutations in these genes restored both the sensitivity to phages and LPS profiles seen in the parental strain.

10.3389/fcimb.2023.1266685

TABLE 4 Selected reduced UAB_Phi78-susceptibility *S.* Typhimurium ATCC 14028 Rif^R variants isolated from LAB and FOOD for further characterization.

Scenario[a]	Group	Time[b]	Variant name[c]	Phenotype[d]	
				UAB_Phi20	UAB_Phi87
LAB	Infected	4 h	CI1	–	–
		6.5 h	**CI2**	–	–
		24 h	**CI3**	–	–
FOOD	Treated	0	**HT1**	–	+
		3 d	HT2	–	+
			HT3	–	–
		7 d	HT4	–	+
			HT5	–	–

[a]LAB, laboratory cultures; FOOD, cooked ham slices.
[b]Time indicates the day (d) or hour (h) of variants isolation after phage cocktail application in FOOD and LAB, respectively.
[c]Variants selected for further genome sequencing and analysis are highlighted in bold.
[d]Determined by spot test. +, clear plaques; -, no plaques.

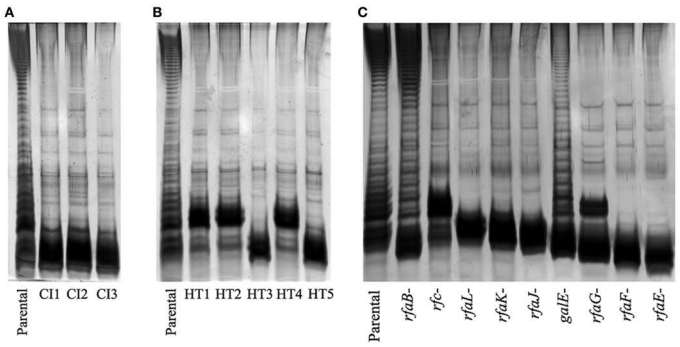


FIGURE 2
LPS electrophoretic profiles of the variants isolated from **(A)** LAB, **(B)** FOOD, and **(C)** LPS mutants of *S.* Typhimurium LT2 strain. The LPS electrophoretic profile of the ATCC 14028 Rif^R parental strain is also shown as control.

3.3 Molecular basis of reduced phage-susceptibility of *S.* Typhimurium ATCC 14028 Rif^R variants isolated from PT

In the PT scenario, the A_{550} of cultures for *S.* Typhimurium ATCC 14028 Rif^R variants with reduced UAB_Phi78-susceptibility (Table 3) remained almost constant or increased after infection with the UAB_Phi78 phage, although their absorbances were lower than that of the non-infected parental strain (Supplementary Figure S1). The number of viable cells declined, especially in one of the two variants, but to a much lesser extent than observed in the UAB_Phi78-infected parental strain. These data suggested that phage infection could cause cell death of these variants, but with limited lysis activity. Spot test analyses of the two other cocktail phages revealed that, of the 70 variants with reduced susceptibility to UAB_Phi78 isolated from the untreated group (Table 3), 62 were insensitive to the other two phages of the cocktail (UAB_Phi20 and UAB_Phi87), and 8 only to the UAB_Phi87 phage. In contrast, all 21 variants isolated from the treated group (Table 3) were insensitive to UAB_Phi87 phage, but sensitive to UAB_Phi20 phage. Sixteen variants from untreated and treated animal groups were selected according to their susceptibility profile to the cocktail phages and to the date of isolation (Table 6), and their LPS electrophoretic profiles were examined. We observed no differences between the electrophoretic profiles of these variants and that of the parental strain (Supplementary Figure S2), suggesting that they have functional phage receptors. Consequently, we hypothesized that these variants might have

10.3389/fcimb.2023.1266685

TABLE 5 Mutations identified in the *rfc* and *rfaJ* genes of selected *S.* Typhimurium ATCC 14028 Rif^R variants isolated from LAB and FOOD.

Scenario[a]	Variant name	Gene	Type of mutation[b]	Phenotype[c]		
				UAB_Phi78	UAB_Phi20	UAB_Phi87
LAB	CI1	*rfaJ*	G/C to T/A at position 910	–	–	–
	CI2		G/C to T/A at position 910	–	–	–
	CI3		G/C to T/A at position 910	–	–	–
FOOD	HT3	*rfaJ*	(- A) at position 715	–	–	–
	HT5		(- A) at position 742	–	–	–
	HT1	*rfc*	Deletion of 2,557 bp including the *rfc* gene	–	–	+
	HT2		C/G to A/T at position 219	–	–	+
	HT4		Deletion of 2,557 bp including the *rfc* gene	–	–	+

[a]LAB, laboratory cultures; FOOD, cooked ham slices.
[b]Mutations detected in variants highlighted in bold were determined by genome sequencing. Mutations in the other variants were identified by PCR amplification of *rfaJ* or *rfc* genes and DNA sequencing.
[c]Determined by spot test. +, clear plaques; -, no plaques.

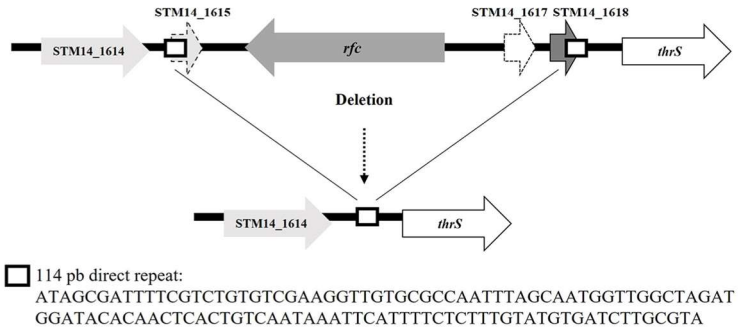


FIGURE 3
Deletion found in the *rfc* gene in variants HT1 and HT4 isolated from FOOD. The sequence of direct repeats is shown.

some mechanism of interference with the multiplicative cycle of the phages. Therefore, seven of these variants (highlighted in bold in Table 6) were chosen for an in-depth study.

Firstly, we proceeded to determine the adsorption constant (*K*) and various infection parameters [efficiency of plating (EOP), efficiency of center of infection (ECOI) and burst size] of the three phages. The data obtained revealed that all seven variants had functional receptors for both UAB_Phi78 and UAB_Phi20 phages since *K* values of both phages in the variants were like those for the parental strain (Table 7). Regarding the EOP, ECOI and burst size parameters of both phages, variants were divided into two groups. One group, encompassing the IC3, IC5 and IC10 variants, was insensitive to these phages with EOP and ECOI values of 0 (Table 7). The other group, which included IC6, IC8, IT2 and IT3 variants, displayed a medium production efficiency [EOP values between 0.1 and 0.5 (Khan Mirzaei and Nilsson, 2015)] for both phages, with the exception of the IT3 variant, considered as low production efficiency [EOP values between 0.001 and 0.1 (Khan Mirzaei and Nilsson, 2015)] for UAB_Phi78 phage, and the IC6 variant, which achieved high production [EOP values ≥ 0.5 (Khan Mirzaei and Nilsson, 2015)] for the UAB_Phi20 phage. For both phages, ECOI values of the variants in this group were < 0.5 and burst sizes were lower than those obtained in the parental strain (Table 7). On the other hand, although we could determine that the UAB_Phi87 phage adsorbs to the parental strain with a low *K* value (2.3E-9 ± 7.5E-10 mL/min), the slopes of adsorption curves in these variants were lower than that of the parental strain, and the *K* values could not be calculated as described previously (Kropinski, 2009). In addition, no plaques were observed when this phage was titered on these variants.

Altogether, the results above confirmed our hypothesis that the variants isolated from PT with reduced sensitivity to phages must have some mechanism of interference that affects processes involved in phage multiplication in bacterial cells. To elucidate this, the genomes of these seven variants were sequenced. Analysis of these genome sequences revealed no point mutations or indels

10.3389/fcimb.2023.1266685

TABLE 6 Selected reduced UAB_Phi78-susceptibility *S.* Typhimurium ATCC 14028 Rif^R variants isolated from PT.

Scenario[a]	Group	Animal[b]	Time[c] (days)	Variant name[d]	Phenotype[e]	
					UAB_Phi20	UAB_Phi87
PT	Untreated	2	8	IC1	–	–
		3		IC2	+	–
		4		**IC3**	–	–
		5		IC4	–	–
		5		**IC5**	–	–
		1	15	**IC6**	+	–
		2		IC7	+	–
		2		**IC8**	+	–
		3		IC9	–	–
		5		**IC10**	–	–
		7		IC11	–	–
		8		IC12	–	–
	Treated	7	1	IT1	+	–
		3	8	**IT2**	+	–
		3	15	**IT3**	+	–
		3		IT4	+	–

[a]PT, phage therapy.
[b]Indicates the animal number from which each variant was isolated.
[c]Time indicates the day post-infection the ceca were obtained for the bacteria isolation.
[d]Variants selected for further studies to determine the adsorption kinetic, diverse infection parameters, and genome sequencing of the phages are highlighted in bold. All variants were isolated from different broilers except the pairs of variants IC4-IC5 and IT3-IT4 obtained each from the same animal.
[e]Determined by spot test. +, clear plaques; -, no plaques.

TABLE 7 Parameters of phages UAB_Phi78 and UAB_Phi20 on reduced phage-susceptibility variants isolated from PT.

Parental strain Variant name	UAB_Phi78				UAB_Phi20			
	K[a] (ml/min)	EOP[b]	ECOI[c]	Burst size (PFU/cell)	K[a] (ml/min)	EOP[b]	ECOI[c]	Burst size (PFU/cell)
ATCC 14028 Rif^R	3.9E-8 ± 2.7E-8	1.0	1.0	98.16 ± 2.6	1.1E-8 ± 5.2E-9	1.0	1.0	189.2 ± 9.6
IC6	3.1E-8 ± 1.9E-8	0.2 ± 0.1	0.3 ± 0.1	9.48 ± 1.1	6.7E-9 ± 3.4E-9	0.6 ± 0.1	0.3 ± 0.0	142.9 ± 7.4
IC8	2.4E-8 ± 1.0E-8	0.2 ± 0.0	0.3 ± 0.0	10.2 ± 1.1	7.4E-9 ± 8.2E-9	0.4 ± 0.1	0.2 ± 0.1	26.0 ± 2.2
IT2	3.3E-8 ± 2.4E-8	0.1 ± 0.0	0.3 ± 0.1	6.4 ± 1.8	1.3E-8 ± 8.2E-9	0.4 ± 0.1	0.2 ± 0.1	83.5 ± 6.9
IT3	2.1E-8 ± 1.7E-8	0.01 ± 0.0	0.2 ± 0.1	22.4 ± 0.3	7.1E-9 ± 3.5E-9	0.4 ± 0.1	0.2 ± 0.0	34.5 ± 2.6
IC3	7.5E-9 ± 4.6E-9	0.0	0.0	ND	3.7E-9 ± 2.8E-9	0.0	0.0	ND
IC5	5.4E-7 ± 4.1E-8	0.0	0.0	ND	1.2E-8 ± 7.1E-9	0.0	0.0	ND
IC10	5.7E-9 ± 3.2E-9	0.0	0.0	ND	5.0E-9 ± 2.3E-9	0.0	0.0	ND

For all the parameters, the mean of at least two independent experiments ± standard deviation is shown.
ND, not determined due to the inefficient infection of phage.
[a]Adsorption rate constant (K).
[b]Efficiency of plating (EOP).
[c]Efficiency of centre of infection (ECOI).

involving known genes related to phage defense mechanisms when compared to the genome sequence of the parental strain (Supplementary Table S3). However, analysis of unmapped Illumina reads demonstrated that all these variants carried several plasmids in addition to the pSLT plasmid, known to be present in the serovar Typhimurium of *S. enterica* (Jones et al., 1982). Sequencing determined that all variants carried a large conjugative IncI1α plasmid (~96-110 Kb) (Table 8). IC3, IC5,

10.3389/fcimb.2023.1266685

TABLE 8 Characteristics of plasmids identified in reduced phage-susceptibility variants isolated from PT.

Variant name	Plasmid	Size (pb)	Replicon (% identity)[a]	Antibiotic resistance	Genbank accession number
IC3	pUA1135	96,685	IncI1 (100)	CTX-M-14	MW590592
	pUA1144	4,612	NF	–	MW655531
	pUA1145	3,257	Col440I (93.8)	–	MW655532
IC5	pUA1135	96,685	IncI1 (100)	CTX-M-14	MW590592
IC10	pUA1135	96,685	IncI1 (100)	CTX-M-14	MW590592
	pUA1144	4,612	NF	–	MW655531
IC6	pUA1136	104,489	IncI1 (99.3)	TEM-1	MW655523
IC8	pUA1136	104,489	IncI1 (99.3)	TEM-1	MW655523
	pUA1138	31,244	IncX4 (100)	–	MW655525
IT2	pUA1139	110,041	IncI1 (100)	–	MW655526
IT3	pUA1139	110,041	IncI1 (100)	–	MW655526
	pUA1141	38,709	IncX4 (86.1)	–	MW655528
	pUA1142	5,463	Col156 (94.8)	–	MW655529

[a]Identity obtained with PlasmidFinder 2.1 (80% of nucleotide identity threshold); NF, not found.

and IC10 variants harbored the pUA1135 plasmid, encoding a CTX-M-14 beta-lactamase. IC6 and IC8 variants carried the pUA1136 plasmid, encoding a TEM-1 beta-lactamase, and IT2 and IT3 variants contained the pUA1139 plasmid, which did not encode any known antibiotic-resistance mechanism (Table 8). Furthermore, some of these variants carried additional lower-size plasmids from different incompatibility groups (Table 8).

Since the IC5, IC6, and IT2 variants only carried, respectively, the pUA1135, pUA1136, and pUA1139 large plasmids, we hypothesized that these plasmids encode interference mechanisms. To demonstrate this, these variants were used as donors in conjugation experiments, using the phage-sensitive and streptomycin-resistant *S.* Typhimurium LB5000 strain as a recipient. Transconjugant strains receiving the pUA1135 and pUA1136 plasmids were selected on streptomycin and ampicillin plates, and streptomycin and kanamycin plates were used for transconjugants for the pUA1139 plasmid, to which a kanamycin resistance cassette had been previously introduced by one-step inactivation (Datsenko and Warner, 2000). The mating frequencies were 5.0E-3, 4.7E-3, and 9.0E-4 for the pUA1135, pUA1136, and pUA1139 plasmids, respectively. The presence of large plasmids in four transconjugants of each mating was confirmed by PCR, using specific primers for each plasmid (Supplementary Table S1). EOP and ECOI values for both UAB_Phi20 and UAB_Phi78 phages were determined for one transconjugant of each mating (Table 9). Results indicated that the acquisition by conjugation of the pUA1135 plasmid gave rise to transconjugants insensitive to both UAB_Phi20 and UAB_Phi78 phages. In addition, transconjugants that acquired the pUA1136 and pUA1139 plasmids also exhibited a reduced sensitivity to UAB_Phi20 and UAB_Phi78 phages, with EOP and ECOI values quite similar to those of the bacterial donors (Table 9). In this regard, it must be considered that the genetic backgrounds of the donor and recipient strains were different since the donor strain derived from *S.* Typhimurium ATCC 14028 Rif^R, and the recipient was *S.* Typhimurium LB5000. Concerning phage UAB_Phi87, the transconjugants exhibited a reduced sensitivity to this phage, with EOP values around 0.1-0.2 and lower size plaques compared to the ones observed on the parental strain (LB5000) (Table 9). To corroborate this, plasmids pUA1135, pUA1136, and pUA1139 were subsequently cured from IC5, IC6 and IT2 variants, respectively

TABLE 9 Values of EOP and ECOI of UAB_Phi78, UAB_Phi20 and UAB_Phi87 phages on both donor and transconjugants.

Donor							Transconjugant					
Variant name	Plasmid	UAB_Phi78		UAB_Phi20		UAB_Phi87	Plasmid[b]	UAB_Phi78		UAB_Phi20		UAB_Phi87
		EOP[a]	ECOI[a]	EOP[a]	ECOI[a]	EOP[a]		EOP[c]	ECOI[c]	EOP[c]	ECOI[c]	EOP[c]
IC5	pUA1135	0.0	0.0	0.0	0.0	0.0	pUA1135	0.0	0.0	0.0	0.0	0.2± 0.0
IC6	pUA1136	0.2 ± 0.1	0.3 ± 0.1	0.6 ± 0.1	0.3 ± 0.03	0.0	pUA1136	0.2 ± 0.1	0.3 ± 0.0	0.7 ± 0.0	0.8 ± 0.0	0.1± 0.0
IT2	pUA1139	0.1 ± 0.0	0.3 ± 0.1	0.4 ± 0.1	0.2 ± 0.1	0.0	pUA1139	0.1 ± 0.0	0.6 ± 0.1	0.2 ± 0.0	0.5 ± 0.1	0.1± 0.0

[a]The values were calculated compared to the parental strain *S.* Typhimurium ATCC14028 Rif^R.
[b]The presence of plasmid was confirmed by PCR amplification.
[c]The values were calculated compared to the *S.* Typhimurium LB5000 because it was used as the recipient strain.

10.3389/fcimb.2023.1266685

(Figure 4). Their loss entailed the recovery of sensitivity to both UAB_Phi20 and UAB_Phi78 phages, as evidenced by EOP values like those of *S.* Typhimurium ATCC 14028 Rif^R However, sensitivity to the UAB_Phi87 phage was not fully recovered, since lower EOP values (≤ 0.1) than those of the parental strains were observed.

4 Discussion

The increased interest in the application of bacteriophages as therapeutic tools raises the question of whether the emergence of bacteria with reduced phage-susceptibility could jeopardize the

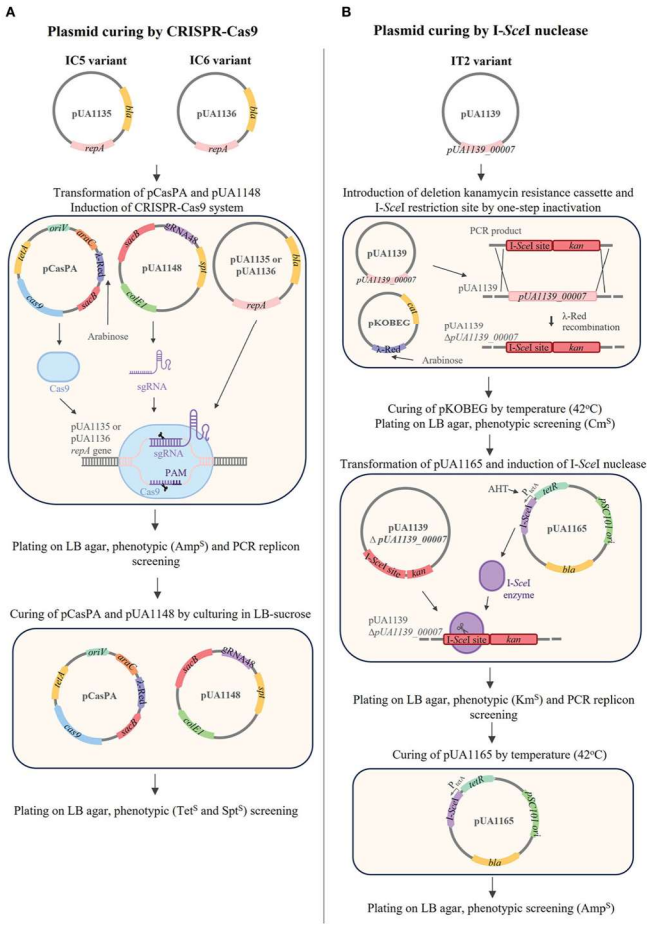


FIGURE 4
Procedures for curing plasmids pUA1135, pUA1136 and pUA1139 from IC5, IC6, and IT2 variants, respectively. **(A)** pUA1135 and pUA1136 were cured using CRISPR-Cas9 targeting *repA* gene. First, pCasPA and pUA1148 were transformed into each variant, and the CRISPR-Cas9 system was induced by arabinose. Cured clones were checked by phenotypic screening (Amp^S) and PCR amplifying the *repA* gene. Plasmids pCasPA and pUA1148 were cured in the presence of sucrose, and cured clones were checked by phenotypic screening (Tet^S and Spt^S). **(B)** pUA1139 was cured by λ-Red mutagenesis and I-*Sce*I nuclease. First, the PCR product containing I-*Sce*I restriction site and the Km^R cassette was transformed into the variant containing pKOBEG, deleting the gene *pUA1139_00007*, by one-step inactivation. pKOBEG was cured by culturing at 42°C and clones were screened for Cm^S. Then, pUA1165 was transformed into the modified cell and I-*Sce*I nuclease was induced by the addition of AHT. Cured clones were checked by phenotypic screening (Km^S) and PCR with primers specific for the *repA* gene. pUA1165 was cured by culturing at 42°C and clones were screened for Amp^S.

effectiveness of this antibacterial strategy. In certain applications, environmental conditions such as lower temperatures, variable resource availability, low phage-to-bacteria ratio and competing surrounding microbiota could influence the emergence of phage-resistant bacteria. Other aspects, such as the ability of bacteriophages to co-evolve with the host, overcoming both phage resistance and bacterial defense mechanisms, the bacterial fitness cost and compromised virulence that entails the development of resistance, and the use of bacteriophage cocktails preventing the development of resistance, are also issues that need to be addressed (Levin and Bull, 2004; Oechslin, 2018).

The present work studies the emergence of bacterial variants with reduced susceptibility to bacteriophages, using *Salmonella* and a cocktail composed by three bacteriophages (UAB_Phi20, UAB_Phi78, and UAB_Phi87) in three different environmental conditions: *in vitro* cultures (LAB), cooked ham slices (FOOD), and oral phage therapy in broilers (PT).

Our experimental approach was to first isolate *Salmonella* variants with reduced susceptibility to the UAB_Phi78 phage due to its dual adsorption ability and subsequently determine their susceptibility to the other two phages. UAB_Phi78 phage is capable of infecting both smooth bacteria and specific rough mutants (Figure 1) because it presumably has two functional receptors as previously described for the SP6 phage (Tu et al., 2017). The tail spike proteins (TSP) would interact with the O-antigen in the infection of smooth bacteria, and the phage tail itself would interact with some component of the inner LPS core when infecting some rough mutants (Tu et al., 2017). This assumption for UAB_Phi78 phage is based on results in LPS mutant strains (Figure 1) and the high sequence identity (≥ 96%) of both its TSP and tail fiber proteins to those of SP6 phage (Bardina et al., 2016). Furthermore, as UAB_Phi78 showed a faster multiplicative cycle than the other two phages of the cocktail, this could favor an earlier selection of variants with reduced sensitivity to this phage.

Our results highlight a much higher percentage of isolation of variants with reduced UAB_Phi78-susceptibility in the LAB setting than in either the FOOD or PT scenarios. Furthermore, mutagenesis seems to be the biological process involved in the emergence of LAB and FOOD resistance while, in suitable conditions, phage interference mechanisms encoded in large conjugative plasmids surface in oral PT.

Results from the LAB setting demonstrated that the percentage of isolation of variants with reduced UAB_Phi78 susceptibility increased over time, achieving 92% after 24 h of the infection of cells with the cocktail (Table 1). The EOP of UAB_Phi78 and the other two phages of the cocktail was zero in all these isolates. Bacteriophage-insensitive mutants have also been encountered by other authors in *in vitro* conditions (Pereira et al., 2016; Oechslin et al., 2017; Bai et al., 2019; Wright et al., 2019). Genome sequencing and subsequent trans-complementation assays of three (CI1, CI2 and CI3) of the LAB variants (Table 5) pointed to mutations in the receptors of the three phages. These mutations generated a premature stop codon at position 910 in the *rfaJ* gene, which encodes a UDP-glucose: (Galactosyl) LPS α-1,2-glucosyltransferase involved in the addition of α-l, 2-linked glucose II residues to the LPS core (Schnaitman and Klena, 1993) (Figure 1), resulting in insensitivity to the three phages. Consistent with this finding, the LPS electrophoretic profiles of these variants resembled that of the *S.* Typhimurium *rfaJ*- rough mutant (Figure 2) with identical phage insensitivity patterns (Figure 1). Moreover, it should be noted that CI1, CI2 and CI3 variants were isolated, respectively, at 4, 6.5 and 24 h following bacterial cultures infection. This would suggest a clonal relationship among these variants, with this higher-fitness clone being the most abundant in the cultures after 24 h of incubation.

On the other hand, the percentage of variants showing reduced UAB_Phi78-susceptibility in cooked ham slices treated with the cocktail and maintained at 4°C (FOOD) increased only slightly over time, with values of 2.1%, 3.0%, and 4.3% at 0, 3 and 7 days, respectively (Table 2). The low percentages obtained agree with those observed in different biocontrol studies applying individual or phage cocktails on meat where reduced phage-susceptibility was rarely detected (Abuladze et al., 2008; Hong et al., 2016; Tomat et al., 2018). The low percentages of variants with reduced phage-susceptibility obtained in this scenario compared to LAB could be attributed to a low initial bacterial concentration in FOOD, the solid surface of meat inhibiting bacterial motility, limiting phage selective pressure and the spread of resistant variants, as well as the incubation temperature (4° C), which significantly decreases the *Salmonella* metabolic activity and bacteriophage multiplication. It should be noted that zero-day time (Table 2) corresponds to the initial day of storing cooked ham slices at 4°C after phage treatment. Therefore, the identification of variants with reduced UAB_Phi78-susceptibility on treated samples at this time suggested that they were possibly present in the *Salmonella* culture used to contaminate the cooked ham slices and were selected by phage predation pressure during treatment and storage (15 min), because no such variants were identified in control samples after the same period (Table 2). Not all variants with reduced UAB_Phi78-susceptibility displayed reduced susceptibility to the other two phages. Twelve of them were only insensitive to the UAB_Phi20 phage, while nine were insensitive to the other two phages. Genome analysis and trans-complementation determined that point mutations producing a truncated RfaJ protein were responsible for the insensitivity to the three phages in some variants (HT3 and HT5) (Table 5). In contrast, the loss of the O-antigen ligase, encoded by the *rfc* gene and required for polymerization of multiunit O-antigen molecules (Schnaitman and Klena, 1993) (Figure 1), prevented the infection of the variants HT1, HT2 and HT4 by both UAB_Phi78 and UAB_Phi20 phages, but not by UAB_Phi87 phage (Table 5). This can be due to the *rfc* mutants displaying the N-acetylglucosamine residue of the terminal glucose II of the LPS core, necessary for UAB_Phi87 adsorption, but losing the multiunit O-antigen that allows UAB_Phi20 and UAB_Phi78 phage adsorption to the Rc+ smooth strains, as it occurred in *S.* Typhimurium SLA28 strain (Figure 1). These results were in agreement with the infection profiles of the three bacteriophages for different LPS mutants of *S.* Typhimurium LT2 (Figure 1) and with the LPS electrophoretic profile of these variants (Figure 2). In contrast to LAB, no clonal relationship can be inferred among the analyzed variants of FOOD, except for HT1 and HT4 (Table 5), which present the same mutation in the *rfc* gene. Since the mutational events that gave rise to RfaJ and Rfc truncated proteins were found in different cooked ham slices, we believe these could be the most frequent mutational events or those that conferred the highest fitness to

10.3389/fcimb.2023.1266685

Salmonella cells selected by the phage treatment. It should be noted that the involvement of LPS or other external structures in *Salmonella* phage susceptibility in laboratory cultures has been investigated by other authors (Adler et al., 2021; Barron-Montenegro et al., 2022). To our knowledge, however, this is the first study that characterizes the emergence of mechanisms involved in reduced phage-susceptibility in food biocontrol.

In the PT scenario, a low frequency of variants with reduced UAB_Phi78-susceptibility was detected. Contrary to the two previous scenarios, these variants emerged in both the untreated and the phage-treated groups but with higher frequency in the former (9.7%) than in the latter (3.3%) (Table 3). This low frequency of emergence of reduced phage-susceptibility variants, might be due to the synergistic effect of a significant decrease of the *Salmonella* population caused mainly by the phage cocktail and the concomitant control exerted by the host immune system as has been suggested (Salazar et al., 2021; Gaborieau and Debarbieux, 2023). Furthermore, these variants were detected in 10 (41.7%) and 3 (12.5%) of the 24 broilers of the untreated and treated groups, respectively, but with different isolation frequencies per animal. These results differ from other studies in which the reduced phage-susceptibility variants were collected mainly from treated animals (Maura and Debarbieux, 2012; Oechslin, 2018; McCallin and Oechslin, 2019; Salazar et al., 2021; Gaborieau and Debarbieux, 2023). Our findings indicated that the processes involved in the emergence of these variants in our PT experiments could be different from those taking place in previous studies and in the above described in LAB and FOOD scenarios, in which insensitive variants were identified only in treated samples.

Most of the variants with reduced UAB_Phi78-susceptibility belonging to control animals (n=62/70) also showed reduced susceptibility to the other two phages of the cocktail, while the remainder (n=8/70) displayed reduced-susceptibility to UAB_Phi87 but were susceptible to UAB_Phi20. This last pattern was also detected in all the variants (n=21) with reduced UAB_Phi78-susceptibility isolated from the treated group. The LPS electrophoretic profiles of the sixteen variants selected for analysis (Table 6) were not significantly different from that of the parental strain, suggesting that the observed reduced phage susceptibility might be caused by interference mechanisms with the lytic cycle of the phages and not by changes in the phage receptors. In agreement with this, the *K* values of UAB_Phi78 and UAB_Phi20 phages determined for seven of these variants (Table 7) confirmed the receptors' functionality. In this regard, EOP and ECOI values were zero for UAB_Phi20 and UAB_Phi78 phages in IC3, IC5, and IC10 variants (Table 7), and the slight decrease of their viability without complete lysis (Supplementary Figure S1) suggested an abortive infection behavior (Hyman and Abedon, 2010). Likewise, the low EOP and ECOI values (lower than 1) and a high decrease of burst size exhibited by UAB_Phi20 and UAB_Phi78 phages when infecting IC6, IC8, IT2, and IT3 variants (Table 7) also point to this mechanism. Results for EOP and ECOI of UAB_Phi20 phage when infecting these last variants indicated that, although the infection was inefficient, it was enough to detect plaques in spot test assays (Table 6), which suggest that this type of assay should only be considered as a first screening tool for phage host-range and that its results must be corroborated by other methods.

The variants with reduced susceptibility to UAB_Phi87 phage deserve special mention since the phage showed inefficient adsorption and EOP values of 0. We speculate that this is caused by the involvement of phage interference in adsorption and perhaps in other processes of the phage multiplicative cycle, because no mutations were found in genes involved in LPS biosynthesis.

The comparison of whole-genome sequencing data from these variants (Table 6) and ATCC14028 Rif^R parental strain did not reveal changes in chromosomal and pSLT plasmid genes linked to previously described phage interference mechanisms. However, the detailed study of unmapped Illumina reads revealed the presence of large IncI1α plasmids in all variants and of other smaller plasmids from different incompatibility groups in some of these variants (Table 8). We believe that some of the ATCC14028 Rif^R parental bacterial cells, used to colonize the digestive tract of broilers, acquired these plasmids by lateral transfer from the broilers' commensal gut microbiota. We suspected that the pUA1135, pUA1136, and pUA1139 plasmids contained in, respectively, IC5, IC6, and IT2 variants must encode the interference mechanisms against UAB_Phi78, UAB_Phi20 and UAB_Phi87 phages because no other exogenous plasmids were detected in these three variants. We confirmed this hypothesis through conjugation experiments, detection of plasmids on transconjugants by PCR, and curing the plasmids. EOP and ECOI values of UAB_Phi78 and UAB_Phi20 phages in transconjugants were very similar to those in donor variants (Table 9). Again, the data from these studies for UAB_Phi87 were inconclusive, displaying EOP values close to 0.1 (Table 9) and plaques with a smaller size than recipient strain *S.* Typhimurium LB5000. In this case, an EOP equal to zero would be expected since UAB_Phi87 does not present variations of adsorption on *S.* Typhimurium LB5000 and this strain is sensitive to this phage. Removing the plasmids further confirmed their implication in UAB_Phi20 and UAB_Phi78 interference, with cured strains recovering susceptibility to both phages. However, plasmid removal did not give rise to UAB_Phi87-sensitive variants like the parental strain because EOP values around 0.1 were obtained and plaque size was smaller (data not shown). Plasmid conjugation and removal results for UAB_Phi87 indicate that both a lower adsorption and interference in the multiplicative cycle of the phage could be involved in the reduced susceptibility of the variants to this phage, as discussed above. Although the role of the IncI1α plasmids in the reduced UAB_Phi87-susceptibility is clear, more studies will be required to elucidate in depth what specific processes are involved.

IncI1α plasmids are common in *Enterobacteriaceae*, and their conjugative transfer in *S.* Typhimurium causes a change of phage type to the recipient strain that has been documented *in vitro* (Hughes and Meynell, 1977; Hiley et al., 2021) and that is attributed to plasmid regions encoding phage growth inhibition systems (Furuichi et al., 1984; Sampei et al., 2010; Hiley et al., 2021). Our results indicate that this biological phenomenon could be taking place in the intestinal tract of broilers and, under certain conditions, could be the main cause of the emergence of bacterial variants with reduced susceptibility to phages in PT due to interference mechanisms encoded in the acquired plasmids. Furthermore, although receptor mutation could happen, the lateral transfer frequency in this case is most likely higher than the mutation

events involved in phage resistance, because we did not detect any variants with mutations in phage receptors in PT. For the observed phenomenon to occur, the target bacterium must be at high concentration, and some of the bacteria from the environmental microbiota must harbor plasmids encoding genes involved in phage interference mechanisms and with high mating frequencies. Moreover, it is not necessary to have the phage cocktail's selective pressure for these plasmids to be transmitted, because we isolated variants with plasmid-mediated reduced susceptibility from the untreated group of broilers.

In conclusion, and contrary to what has been previously proposed (Salazar et al., 2021; Gaborieau and Debarbieux, 2023), our findings highlight how *in vitro* assays might not anticipate the dynamics of *in vivo* reduced phage-susceptibility. This puts into question the exclusive use of *in vitro* studies to foresee bacterial phage interference mechanisms aimed for use in some kinds of therapy. Moreover, they reveal how the acquisition of plasmids in an *in vivo* scenario with a high and diverse microbiota content, such as the digestive tract, compared to FOOD and LAB scenarios resulted in bacterial reduced phage susceptibility, which to our knowledge is the first study that described this. Furthermore, this plasmid acquisition could have a larger impact than the emergence of resistance through receptor mutations. However, it is very important to highlight that the likelihood of these events does not hinder the efficacy of oral phage therapy, and our results underscore the potential of its application by using phage cocktails containing bacteriophages that recognize different receptors in the target host. Further studies are necessary to determine the plasmid regions responsible for the observed phage interference and which processes of the multiplicative cycle of the phages are affected. Finally, additional studies will be required to ascertain if the selective pressure caused by antibiotics could also play a role in the spread of anti-phage defense mechanisms and how this can influence the success of phage therapy.

Data availability statement

The datasets presented in this study can be found in online repositories. The names of the repository/repositories and accession number(s) can be found below: https://www.ncbi.nlm.nih.gov/bioproject/PRJNA746119, https://www.ncbi.nlm.nih.gov/nuccore/MW590592, https://www.ncbi.nlm.nih.gov/nuccore/MW655523, https://www.ncbi.nlm.nih.gov/nuccore/MW65552, https://www.ncbi.nlm.nih.gov/nuccore/MW655526, https://www.ncbi.nlm.nih.gov/nuccore/MW655528, https://www.ncbi.nlm.nih.gov/nuccore/MW655529, https://www.ncbi.nlm.nih.gov/nuccore/MW655531, https://www.ncbi.nlm.nih.gov/nuccore/MW655532.

Author contributions

JL-P: Investigation, Writing – review & editing. JO: Investigation, Writing – review & editing. MS-O: Formal Analysis, Investigation, Writing – review & editing. IE: Formal Analysis, Writing – review & editing. PC: Project administration, Supervision, Writing – original draft, Writing – review & editing. ML: Conceptualization, Project administration, Supervision, Writing – original draft, Writing – review & editing.

Funding

This work has received funding from the Ministerio de Ciencia e Innovación de España PID2020-117708GB-I00, and from AGAUR-Generalitat de Catalunya (2021 SGR 00646). Furthermore, M. S-O and J. L-P received a predoctoral fellowship from the Ministerio de Educación y Formación Profesional de España. The funders had no role in study design, data collection and interpretation, or the decision to submit the work for publication.

Acknowledgments

We are grateful to late Dr. J. Casadesus (Universidad de Sevilla) for providing us the experimental protocol for extracting the LPS, to Dr T. Sekizaki (National Institute of Animal Health, Ibaraki, Japan) for providing the pSET4s plasmid and to Dr. Quanjiang Ji (ShanghaiTech University, Shanghai, China) for supplying the pACRISPR and pCasPA plasmids used in this work. We thank J. Colom for his assistance in carrying out the *in vivo* phage therapy experiments, and Susana Escribano and Joan Ruiz for their excellent technical assistance.

Conflict of interest

PC, and ML are the inventors in patent application EP2750519. JO is currently working at SK8 Biotech, which is exploiting patent EP2750519 for the use in food biocontrol.

The remaining authors declare that the research was conducted in the absence of any commercial or financial relationships that could be construed as a potential conflict of interest.

Publisher's note

All claims expressed in this article are solely those of the authors and do not necessarily represent those of their affiliated organizations, or those of the publisher, the editors and the reviewers. Any product that may be evaluated in this article, or claim that may be made by its manufacturer, is not guaranteed or endorsed by the publisher.

Supplementary material

The Supplementary Material for this article can be found online at: https://www.frontiersin.org/articles/10.3389/fcimb.2023.1266685/full#supplementary-material

References

Abuladze, T., Li, M., Menetrez, M. Y., Dean, T., Senecal, A., and Sulakvelidze, A. (2008). Bacteriophages reduce experimental contamination of hard surfaces, tomato, spinach, broccoli, and ground beef by *Escherichia coli* O157:H7. *Appl. Environ. Microbiol.* 74 (20), 6230–6238. doi: 10.1128/AEM.01465-08

Adler, B. A., Kazako, A. E., Zhong, C., Liu, H., Kutter, E., Lui, L. M., et al. (2021). The genetic basis of phage susceptibility, cross-resistance and host-range in *Salmonella*. *Microbiology* 167 (12), 1126. doi: 10.1099/mic.0.001126

Altschul, S. F., Madden, T. L., Schäffer, A. A., Zhang, J., Zhang, Z., Miller, W., et al. (1997). Gapped BLAST and PSI-BLAST: a new generation of protein database search programs. *Nucleic Acids Res.* 25 (17), 3389–3402. doi: 10.1093/nar/25.17.3389

Bai, J., Jeon, B., and Ryu, S. (2019). Effective inhibition of *Salmonella* Typhimurium in fresh produce by a phage cocktail targeting multiple host receptors. *Food Microbiol.* 77, 52–60. doi: 10.1016/j.fm.2018.08.011

Bankevich, A., Nurk, S., Antipov, D., Gurevich, A. A., Dvorkin, M., Kulikov, A. S., et al. (2012). SPAdes: a new genome assembly algorithm and its applications to single-cell sequencing. *J. Comput. Biol.* 19 (5), 455–477. doi: 10.1089/cmb.2012.0021

Bardina, C., Spricigo, D. A., Cortés, P., and Llagostera, M. (2012). Significance of the bacteriophage treatment schedule in reducing *Salmonella* colonization of poultry. *Appl. Environ. Microbiol.* 78, 6600–6607. doi: 10.1128/AEM.01257-12

Bardina, C., Colom, J., Spricigo, D. A., Otero, J., Sánchez-Osuna, M., Cortés, P., et al. (2016). Genomics of three new bacteriophages useful in the biocontrol of *Salmonella*. Front. *Microbiol* 7. doi: 10.3389/fmicb.2016.00545

Barron-Montenegro, R., Rivera, D., Serrano, M. J., García, R., Álvarez, D. M., and Benavides, J. (2022). Long-term interactions of *Salmonella* Enteritidis with a lytic phage for 21 days in high nutrients media. *Front. Cell. Infect. Microbiol.* 12. doi: 10.3389/fcimb.2022.897171

Bertozzi Silva, J., Storms, Z., and Sauvageau, D. (2016). Host receptors for bacteriophage adsorption. *FEMS Microbiol. Lett.* 363 (4), fnw002. doi: 10.1093/femsle/fnw002

Bondy-Denomy, J., Qian, J., Westra, E. R., Buckling, A., Guttman, D. S., Davidson, A. R., et al. (2016). Prophages mediate defense against phage infection through diverse mechanisms. *ISME J.* 10 (12), 2854–2866. doi: 10.1038/ismej.2016.79

Buendía-Clavería, A., Moussaid, A., Ollero, F., Vinardell, J., Torres, A., Moreno, J., et al. (2003). A *purL* mutant of *Sinorhizobium fredii* HH103 is symbiotically defective and altered in its lipopolysaccharide. *Microbiology* 149, 1807–1818. doi: 10.1099/mic.0.26099-0

Carattoli, A., Zankari, E., García-Fernández, A., Voldby Larsen, M., Lund, O., Villa, L., et al. (2014). *In silico* detection and typing of plasmids using PlasmidFinder and plasmid multilocus sequence typing. *Antimicrob. Agents Chemother.* 58 (7), 3895–3903. doi: 10.1128/AAC.02412-14

Chan, R. K., Botstein, D., Watanabe, T., and Ogata, Y. (1972). Specialized transduction of tetracycline resistance by phage P22 in *Salmonella* Typhimurium. II. Properties of a high-frequency-transducing lysate. *Virology* 50, 883–898. doi: 10.1016/0042-6822(72)90442-4

Chaveroche, M. K., Ghigo, J. M., and d'Enfert, C. (2000). A rapid method for efficient gene replacement in the filamentous fungus *Aspergillus nidulans*. *Nucleic Acids Res.* 28 (22), E97. doi: 10.1093/nar/28.22.e97

Chen, W., Zhang, Y., Zhang, Y., Pi, Y., Gu, T., Song, L., et al. (2018). CRISPR/Cas9-based genome editing in *Pseudomonas aeruginosa* and cytidine deaminase-mediated base editing in *Pseudomonas* species. *iScience* 6, 222–231. doi: 10.1016/j.isci.2018.07.024

Colom, J., Cano-Sarabia, M., Otero, J., Cortés, P., Maspoch, D., and Llagostera, M. (2015). Liposome-encapsulated bacteriophages for enhanced oral phage therapy against Salmonella spp. *Appl. Environ. Microbiol.* 81 (14), 4841–4849. doi: 10.1128/AEM.00812-15

Colom, J., Cano-Sarabia, M., Otero, J., Aríñez-Soriano, J., Cortés, P., Maspoch, D., et al. (2017). Microencapsulation with alginate/$CaCO_3$: A strategy for improved phage therapy. *Sci. Rep.* 7, 41441. doi: 10.1038/srep41441

Darling, A. E., Mau, B., and Perna, N. T. (2010). Progressive Mauve: multiple genome alignment with gene gain, loss and rearrangement. *PloS One* 5 (6), e11147. doi: 10.1371/journal.pone.0011147

Datsenko, K. A., and Wanner, B. L. (2000). One-step inactivation of chromosomal genes in *Escherichia coli* K-12 using PCR products. *Proc. Natl. Acad. Sci. U.S.A.* 97 (12), 6640–6645. doi: 10.1073/pnas.120163297

de Jonge, P. A., Nobrega, F. L., Brouns, S. J. J., and Dutilh, B. E. (2019). Molecular and evolutionary determinants of bacteriophage host range. *Trends Microbiol.* 27 (1), 51–63. doi: 10.1016/j.tim.2018.08.006

de Moraes, M. H., and Teplitski, M. (2015). Fast and efficient three-step target-specific curing of a virulence plasmid in *Salmonella enterica*. *AMB Express* 5 (1), 139. doi: 10.1186/s13568-015-0139-y

De Sordi, L., Lourenço, M., and Debarbieux, L. (2019). "I will survive": A tale of bacteriophage-bacteria coevolution in the gut. *Gut Microbes* 10 (1), 92–99. doi: 10.1080/19490976.2018.1474322

Doron, S., Melamed, S., Ofir, G., Leavitt, A., Lopatina, A., Keren, M., et al. (2018). Systematic discovery of antiphage defense systems in the microbial pangenome. *Science* 359 (6379), eaar4120. doi: 10.1126/science.aar4120

Dy, R. L., Przybilski, R., Semeijn, K., Salmond, G. P. C., and Fineran, P. C. A. (2014). Widespread bacteriophage abortive infection system functions through a type IV toxin–antitoxin mechanism. *Nucleic Acids Res.* 42, 4590–4605. doi: 10.1093/nar/gkt1419

Egido, J. E., Costa, A. R., Aparicio-Maldonado, C., Haas, P. J., and Brouns, S. J. J. (2022). Mechanisms and clinical importance of bacteriophage resistance. *FEMS Microbiol. Rev.* 46 (1), fuab048. doi: 10.1093/femsre/fuab048

European Antimicrobial Resistance Collaborators (2022). The burden of bacterial antimicrobial resistance in the WHO European region in 2019: a cross-country systematic analysis. *Lancet Public Health* 7 (11), e897–e913. doi: 10.1016/S2468-2667(22)00225-0

Finn, R. D., Coggill, P., Eberhardt, R. Y., Eddy, S. R., Mistry, J., Mitchell, A. L., et al. (2016). The Pfam protein families database: towards a more sustainable future. *Nucleic Acids Res.* 44 (D1), D279–D285. doi: 10.1093/nar/gkv1344

Furuichi, T., Komano, T., and Nisioka, T. (1984). Physical and genetic analyses of the Inc-I alpha plasmid R64. *J. Bacteriol.* 158 (3), 997–1004. doi: 10.1128/jb.158.3.997-1004.1984

Gaborieau, B., and Debarbieux, L. (2023). The role of the animal host in the management of bacteriophage resistance during phage therapy. *Curr. Opin. Virol.* 58, 101290. doi: 10.1016/j.coviro.2022.101290

García-Quintanilla, M., Ramos-Morales, F., and Casadesús, J. (2008). Conjugal transfer of the *Salmonella enterica* virulence plasmid in the mouse intestine. *J. Bacteriol.* 190 (6), 1922–1927. doi: 10.1128/JB.01626-07

Goldfarb, T., Sberro, H., Weinstock, E., Cohen, O., Doron, S., Charpak-Amikam, Y., et al. (2015). BREX is a novel phage resistance system widespread in microbial genomes. *EMBO J.* 34 (2), 169–183. doi: 10.15252/embj.201489455

Gordillo Altamirano, F., and Barr, J. (2019). Phage therapy in the postantibiotic era. *Clin. Microbiol. Rev.* 32 (2), e00066–e00018. doi: 10.1128/CMR.00066-18

Górski, A., Międzybrodzki, R., Łobocka, M., Głowacka-Rutkowska, A., Bednarek, A., Borysowski, J., et al. (2018). Phage therapy: what have we learned? *Viruses* 10 (6), 288. doi: 10.3390/v10060288

Guttman, B., Raya, R., and Kutter, E. (2005). "Basic phage biology," in *Bacteriophages: Biology and Application*. Eds. E. Kutter and A. Sulakvelidze (Boca Raton, FL: CRC Press), 29–66.

Hernandez, C. A., and Koskella, B. (2019). Phage resistance evolution in *vitro* is not reflective of in *vivo* outcome in a plant-bacteria-phage system. *Evolution* 73 (12), 2461–2475. doi: 10.1111/evo.13833

Hiley, L., Graham, R. M. A., and Jennison, A. V. (2021). Characterisation of IncI1 plasmids associated with change of phage type in isolates of *Salmonella enterica* serovar Typhimurium. *BMC Microbiol.* 21 (1), 92. doi: 10.1186/s12866-021-02151-z

Hille, F., Richter, H., Wong, S. P., Bratovič, M., Ressel, S., and Charpentier, E. (2018). The biology of CRISPR-Cas: backward and forward. *Cell* 172 (6), 1239–1259. doi: 10.1016/j.cell.2017.11.032

Hitchcock, P. J., Leivem, L., Mäkeläm, P. H., Rietschel, E. T., Strittmatter, W., and Morrison, D. C. (1986). Lipopolysaccharide nomenclature-past, present, and future. *J. Bacteriol.* 166 (3), 699–705. doi: 10.1128/jb.166.3.699-705.1986

Hong, Y., Schmidt, K., Marks, D., Hatter, S., Marshall, A., Albino, L., et al. (2016). Treatment of *Salmonella* -contaminated eggs and pork with a broad-spectrum, single bacteriophage: Assessment of efficacy and resistance development. *Foodborne Pathog. Dis.* 13 (12), 679–688. doi: 10.1089/fpd.2016.2172

Hughes, V., and Meynell, G. G. (1977). The contribution of plasmid and host genes to plasmid-mediated interference with phage growth. *Genet. Res.* 30 (2), 179–185. doi: 10.1017/s0016672300017572

Hyman, P., and Abedon, S. T. (2010). Bacteriophage host range and bacterial resistance. *Adv. Appl. Microbiol.* 70, 217–248. doi: 10.1016/S0065-2164(10)70007-1

Isaev, A. B., Musharova, O. S., and Severinov, K. V. (2021a). Microbial arsenal of antiviral defenses. Part I. *Biochem. (Mosc)* 86 (3), 319–337. doi: 10.1134/S0006297921030081

Isaev, A. B., Musharova, O. S., and Severinov, K. V. (2021b). Microbial arsenal of antiviral defenses. Part II. *Biochem. (Mosc)* 86 (4), 449–470. doi: 10.1134/S0006297921040064

Jones, G. W., Rabert, D. K., Svinarich, D. M., and Whitfield, H. J. (1982). Association of adhesive, invasive, and virulent phenotypes of *Salmonella* Typhimurium with autonomous 60-megadalton plasmids. *Infect. Immun.* 38 (2), 476–486. doi: 10.1128/iai.38.2.476-486.1982

Khan Mirzaei, M., and Nilsson, A. S. (2015). Isolation of phages for phage therapy: a comparison of spot tests and efficiency of plating analyses for determination of host range and efficacy. *PloS One* 10 (3), e0118557. doi: 10.1371/journal.pone.0118557

Kropinski, A. M. (2009). Measurement of the rate of attachment of bacteriophage to cells. *Methods Mol. Biol.* 501, 151–155. doi: 10.1007/978-1-60327-164-6_15

Kropinski, A. M. (2018). Practical advice on the one-step growth curve. *Methods Mol. Biol.* 1681, 41–47. doi: 10.1007/978-1-4939-7343-9_3

Kutter, E. (2009). Phage host range and efficiency of plating. *Methods Mol. Biol.* 501, 141–149. doi: 10.1007/978-1-60327-164-6_14

Levin, B. R., and Bull, J. J. (2004). Population and evolutionary dynamics of phage therapy. *Nat. Rev. Microbiol.* 2 (2), 166–173. doi: 10.1038/nrmicro822

Lopatina, A., Tal, N., and Sorek, R. (2020). Abortive infection: bacterial suicide as an antiviral immune strategy. *Annu. Rev. Virol.* 7 (1), 371–384. doi: 10.1146/annurev-virology-011620-040628

Makarova, K. S., Wolf, Y. I., van der Oost, J., and Koonin, E. V. (2009). Prokaryotic homologs of Argonaute proteins are predicted to function as key components of a novel system of defense against mobile genetic elements. *Biol. Direct.* 25 (4), 29. doi: 10.1186/1745-6150-4-29

Maura, D., and Debarbieux, L. (2012). On the interactions between virulent bacteriophages and bacteria in the gut. *Bacteriophage. 1;2* 4), 229–233. doi: 10.4161/bact.23557

Mayola, A., Irazoki, O., Martínez, I. A., Petrov, D., Menolascina, F., Stocker, R., et al. (2014). RecA protein plays a role in the chemotactic response and chemoreceptor clustering of *Salmonella enterica*. *PloS One* 9 (8), e105578. doi: 10.1371/journal.pone.0105578

McCallin, S., and Oechslin, F. (2019). "Bacterial resistance to phage and its impact on clinical therapy," in *Phage Therapy: A Practical Approach*. Eds. A. Górski, R. Międzybrodzki and J. Borysowski (© Springer Nature Switzerland AG 2019), 59–91.

Millman, A., Bernheim, A., Stokar-Avihail, A., Fedorenko, T., Voichek, M., Leavitt, A., et al. (2020). Bacterial retrons function in anti-phage defense. *Cell* 183 (6), 1551–1561.e12. doi: 10.1016/j.cell.2020.09.065

Millman, A., Melamed, S., Leavitt, A., Doron, S., Bernheim, A., Hör, J., et al. (2022). An expanding arsenal of immune systems that protect bacteria from phages. *Cell Host Microbe* 30 (11), 1556–1569.e5. doi: 10.1016/j.chom.2022.09.017

Moineau, S., Durmaz, E., Pandian, S., and Klaenhammer, T. R. (1993). Differentiation of two abortive mechanisms by using monoclonal antibodies directed toward lactococcal bacteriophage capsid proteins. *Appl. Environ. Microbiol.* 59 (1), 208–212. doi: 10.1128/aem.59.1.208-212.1993

Oechslin, F., Piccardi, P., Mancini, S., Gabard, J., Moreillon, P., Entenza, J. M., et al. (2017). Synergistic interaction between phage therapy and antibiotics clears *Pseudomonas aeruginosa* infection in endocarditis and reduces virulence. *J. Infect. Dis.* 215 (5), 703–712. doi: 10.1093/infdis/jiw632

Oechslin, F. (2018). Resistance development to bacteriophages occurring during bacteriophage therapy. *Viruses* 10 (7), 351. doi: 10.3390/v10070351

Ofir, G., Melamed, S., Sberro, H., Mukamel, Z., Silverman, S., Yaakov, G., et al. (2018). DISARM is a widespread bacterial defence system with broad anti-phage activities. *Nat. Microbiol.* 3 (1), 90–98. doi: 10.1038/s41564-017-0051-0

Pedruzzi, I., Rivoire, C., Auchincloss, A. H., Coudert, E., Keller, G., de Castro, E., et al. (2015). HAMAP in 2015: updates to the protein family classification and annotation system. *Nucleic Acids Res.* 43, D1064–D1070. doi: 10.1093/nar/gku1002

Pereira, C., Moreirinha, C., Lewicka, M., Almeida, P., Clemente, C., Cunha, Â., et al. (2016). Bacteriophages with potential to inactivate *Salmonella* Typhimurium: use of single phage suspensions and phage cocktails. *Virus Res.* 220, 179–192. doi: 10.1016/j.virusres.2016.04.020

Rousset, F., Depardieu, F., Miele, S., Dowding, J., Laval, A. L., Lieberman, E., et al. (2022). Phages and their satellites encode hotspots of antiviral systems. *Cell. Host. Microbe* 30 (5), 740–753.e5. doi: 10.1016/j.chom.2022.02.018

Salazar, K. C., Ma, L., Green, S. I., Zulk, J. J., Trautner, B. W., Ramig, R. F., et al. (2021). Antiviral resistance and phage counter adaptation to antibiotic-resistant extraintestinal pathogenic *Escherichia coli*. *mBio* 12 (2), e00211–e00221. doi: 10.1128/mBio.00211-21

Sampei, G., Furuya, N., Tachibana, K., Saitou, Y., Suzuki, T., Mizobuchi, K., et al. (2010). Complete genome sequence of the incompatibility group I1 plasmid R64. *Plasmid* 64 (2), 92–103. doi: 10.1016/j.plasmid.2010.05.005

Sánchez-Osuna, M., Cortés, P., Barbé, J., and Erill, I. (2019). Origin of the mobile dihydro-pteroate synthase gene determining sulfonamide resistance in clinical isolates. *Front. Microbiol.* 9. doi: 10.3389/fmicb.2018.03332

Schnaitman, C. A., and Klena, J. D. (1993). Genetics of lipopolysaccharide biosynthesis in enteric bacteria. *Microbiol. Rev.* 57 (3), 655–682. doi: 10.1128/mr.57.3.655-682.1993

Schooley, R. T., Biswas, B., Gill, J. J., Hernandez-Morales, A., Lancaster, J., Lessor, L., et al. (2017). Development and use of personalized bacteriophage-based therapeutic cocktails to treat a patient with a disseminated resistant *Acinetobacter baumannii* infection. *Antimicrob. Agents Chemother.* 61 (10), e00954–e00917. doi: 10.1128/AAC.00954-17

Seemann, T. (2014). Prokka: rapid prokaryotic genome annotation. *Bioinformatics* 30 (14), 2068–2069. doi: 10.1093/bioinformatics/btu153

Takamatsu, D., Osaki, M., and Sekizaki, T. (2001). Thermosensitive suicide vectors for gene replacement in *Streptococcus suis*. *Plasmid* 46 (2), 140–148. doi: 10.1006/plas.2001.1532

Tatusov, R. L., Galperin, M. Y., Natale, D. A., and Koonin, E. V. (2000). The COG database: a tool for genome-scale analysis of protein functions and evolution. *Nucleic Acids Res.* 28 (1), 33–36. doi: 10.1093/nar/28.1.33

Tock, M. R., and Dryden, D. T. F. (2005). The biology of restriction and anti-restriction. *Curr. Opin. Microbiol.* 8, 466–472. doi: 10.1016/j.mib.2005.06.003

Tomat, D., Casabonne, C., Aquili, V., Balagué, C., and Quiberoni, A. (2018). Evaluation of a novel cocktail of six lytic bacteriophages against Shiga toxin-producing *Escherichia coli* in broth, milk and meat. *Food Microbiol.* 76, 434–442. doi: 10.1016/j.fm.2018.07.006

Tu, J., Park, T., Morado, D. R., Hughes, K. T., Molineux, I. J., and Liu, J. (2017). Dual host specificity of phage SP6 is facilitated by tailspike rotation. *Virology* 507, 206–215. doi: 10.1016/j.virol.2017.04.017

Vielva, L., de Toro, M., Lanza, V. F., and de la Cruz, F. (2017). PLACNETw: a web-based tool for plasmid reconstruction from bacterial genomes. *Bioinformatics* 33 (23), 3796–3798. doi: 10.1093/bioinformatics/btx462

von Wintersdorff, C. J., Penders, J., van Niekerk, J. M., Mills, N. D., Majumder., S., van Alphen, L. B., et al. (2016). Dissemination of antimicrobial resistance in microbial ecosystems through horizontal gene transfer. *Front. Microbiol.* 7. doi: 10.3389/fmicb.2016.00173

Wright, R. C. T., Friman, V. P., Smith, M. C. M., and Brockhurst, M. A. (2019). Resistance evolution against phage combinations depends on the timing and order of exposure. *mBio* 10 (5), e01652–e01619. doi: 10.1128/mBio.01652-19

Zerbino, D. R. (2010). Using the Velvet *de novo* assembler for short-read sequencing technologies. *Curr. Protoc. Bioinf.* 31 (11.5), 1-12. doi: 10.1002/0471250953.bi1105s31

Supplementary material

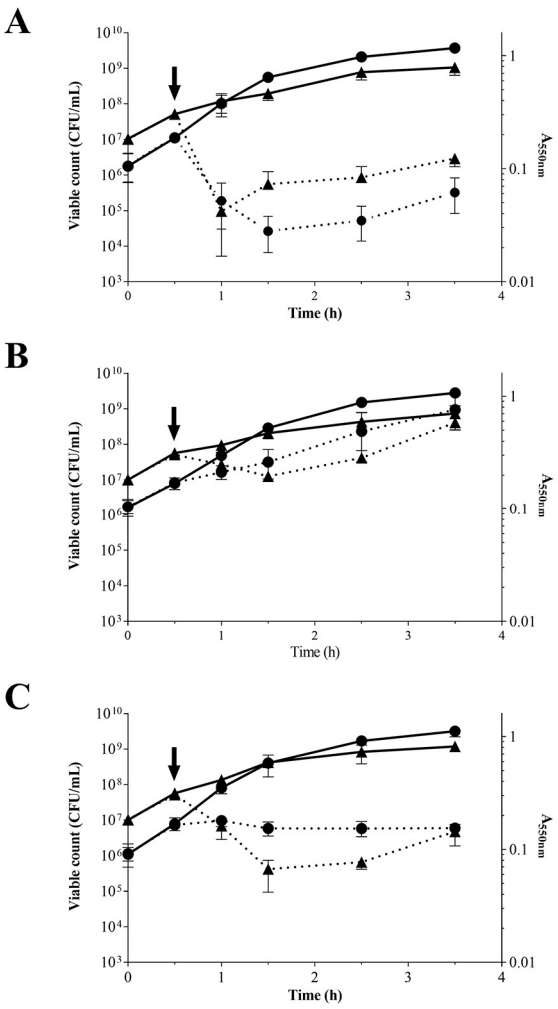


Figure S3.1 Growth kinetics, measured as absorbance (A_{550} nm) (●) and viable count (▲) of cultures of the parental strain ATCC14028 Rif^R (A) and the variants IC10 (B) and IT2 (C) as examples of those isolated from PT, non-infected (solid line) and infected (dot line) with UAB_Phi78 bacteriophage. Arrow indicates the time of phage infection of cultures. The standard deviation of at least three experiments is shown.

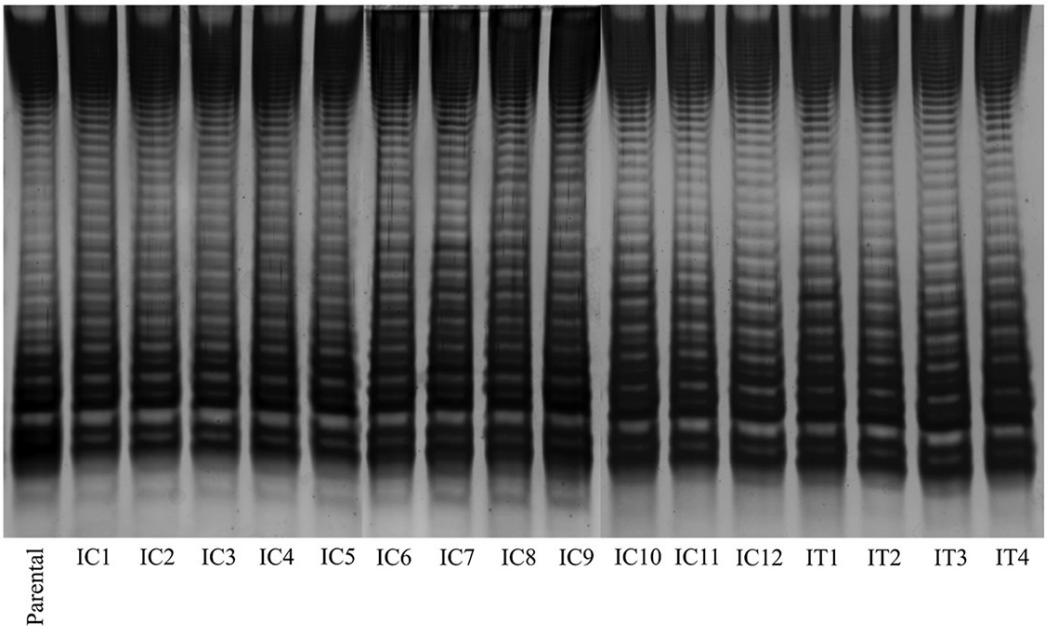


Figure S3.2 LPS electrophoretic profiles of the sixteen ATCC14028 Rif^R variants isolated from PT. The LPS electrophoretic profile of the ATCC14028 Rif^R parental strain is also shown as control.

Table S3.1 Strains and plasmids used in this study.

	Relevant characteristics	Source or reference
Strains		
ATCC 14028 Rif^R	*S.* Typhimurium *rfa* (+); smooth LPS*;* Rif^R	Universitat Autònoma de Barcelona
LB5000	*S.* Typhimurium *metA22 metE551 trpC2 ilv-452 H1-b metA22 metE551 trpC2 ilv-452 H1-b H2-e,n,x* (cured of Fels 2) *fla-66 rpsL120 xyl-404 leu hsdL6 hsdSA29 hsdSB*	University of Calgary
DH5α	*E. coli supE4 ΔlacU169* (φ80 Δ*lacZ* Δ*M15*) *hsdR17, recA1, endA1, gyrA96, thi-1, relA1*	Clontech
TA1537	*S.* Typhimurium *hisC3076 rfa uvrB*; deep rough LPS	Dr. Bruce Ames (University of California, Berkeley)
SL3770	*S.* Typhimurium *rfa* (+); smooth LPS	
SL4807	*S.* Typhimurium rfaB707; mixture of Rc and smooth	
SL428	*S.* Typhimurium *rfc*-458; Ra with 1 side chain unit	*Salmonella* Genectic Stock Center (University of Calgary)
SL3749	*S.* Typhimurium *rfaL446;* Ra	
SL733	*S.* Typhimurium *rfaK953;* Rb1	
SL3750	*S.* Typhimurium *rfaJ417;* Rb2	
SL1306	*S.* Typhimurium *galE503;* Rc	
SL3769	*S.* Typhimurium *rfaG471;* Rd1	
SL3789	*S.* Typhimurium *rfaF511;* Rd2	
SL1102	*S.* Typhimurium *rfaE543;* Re	
Plasmids		
pKD4	Amp^R Km^R	
pKD46	Vector containing the λ-Red recombinase system, Amp^R, thermosensitive	Datsenko and Warner, 2000
pCP20	Vector carrying FLP system, OriV, thermosensitive, Amp^R	
pKOBEG	Vector containing the λ-Red recombinase system, Cm^R, thermosensitive	Generous gift of Prof. I. Lasa; Chaveroche *et al*., 2000
pUA1108	pGEX 4T-1 derivative plasmid carrying the *Ptac* promoter and the *lacIq* gene; Amp^R	Mayolla *et al*., 2014
pCasPA	Vector codifying Cas9 nuclease and λ-Red recombination system, Tet^R, sucrose counter-selectable, Amp^R	Generous gift of Prof. Quanjiang Ji (ShanghaiTech). Chen *et al*., 2018.
pACRISPR	Vector codifying sgRNA for targeting a specific sequence, Amp^R	
pSET4s	Replication function of pG + host3 and pUC19, *lacZ*' Spt^R	Generous gift of Dr. T. Sekizaki. Takamatsu *et a*l., 2001
pUA1148	pACRISPR derivative; Spt^R	This study
pUA1148+gRNA 48	pUA1148 derivative for pUA1135 and pUA1136 elimination	
pUA1165	pKD46 plasmid without λ-Red system genes and with I-*Sce*I endonuclease under control of tetracycline inducible promoter (P_{tetA}), thermosensitive, Amp^R	

* Ra, Rb1, Rb2, Rb3, Rc, Rd1, and Rd2 are rough chemotypes. Re is a deep rough chemotype (Hitchcock *et al*., 1986). LPS, lipopolysaccharide. Amp, ampicillin; Cm, chloramphenicol; Km, kanamycin; Rif, rifampicin; Spt, spectinomycin; Tet, tetracycline. ^{R} resistant.

Table S3.2 Oligonucleotides used in this work.

Name	Sequence (5'-3')	Application	Reference
rfc_F	GTTGGTAATGATGGCTCA	PCR and sequencing of *rfc*	This study
rfc_rv	CACCTTATTTGCCTGATG		
rfc_int_F	GACTGCTATAACAGCAAAC	Sequencing of *rfc*	
rfc_int_rv	GTTTGCTGTTATAGCAGTC		
HiFirfc_F	TTCACACAGGAAACAGTACAATGCTTATAATTTCATACATTGC	PCR of *rfc* for HIFI cloning on pUA1108	
HiFirfc_Rv	TCGACCCGGGGAATTCCGGGTTATTTATTGTTTCTTAGTAAAACGAATC		
HIFIrfaJ_F	TTCACACAGGAAACAGTACAATGGATTCATTTCCTGAGATAGAAATAG	PCR of *rfaJ* for HIFI cloning on pUA1108	
HIFIrfaJ_R	TCGACCCGGGGAATTCCGGGTTATTTGTGGAAAAGTTTACGATAAAG		
Rep1_fw	CTCCTGTTCCTGCCTTTC	Detection of plasmid pUA1144	
Rep1_rv	CTTTCCGGGTTGGACTC		
Rep2_fw	GTGAGCACTCCACCAAAC	Detection of plasmids pUA1135, pUA1136, and pUA1139	
Rep2_rv	GACGCCCAGCATCTG		
Abi5_fw	GCAGATATTATTCGGATGCAAC	Detection of plasmid pUA1141	
Abi5_rv	CTGTTAAATAATCGGGTGTGG		
kikA_fw	GTGGTTTTACCAGCCTTG	Detection of plasmid pUA1138	
kikA_rv	CTTTAACCTTGCCGAACTTAC		
Rep3_fw	GCTGCGATTGACTGGAG	Detection of plasmid pUA1142	
Rep3_rv	CAATAGCCCGACATTCAG		
Rep4_fw	CTGCGCTGAATATGGCG	Detection of plasmid pUA1145	
Rep4_rv	CCTGTTTCACTTTCGGTC		

Table S3.2 (continued)

Name	Sequence (5'-3')	Application	Reference
P4_Km_P1[a]	GGAAACCGCCCGTTTCTTTTCCGACAAAGGATGTC GCCGTGCTCCTCTTTTT*gtgtaggctggagctgcttc*	PCR of Km gene from pKD4 plasmid with homology regions of the intergenic region of the plasmid pUA1139 of the strains IT2 and IT3	This study
P4_Km_P2[a]	GCCGGACGCGGGACACTGACCACAGGCAGCGTTTA TGCCGCGCCGCGTCAGC*atgggaattagccatggtcc*		
P4km_extf	CATTATGGCGGATGAAGTATG	PCR and sequencing to check the Km insertion into the intergenic region of the strains IT2 and IT3	
P4km_extr	CTGGCGTACACTGTCAC		
pACRISPR_fwd	CTGTCAGACCAAGTTTAC	Inverse PCR to amplify pACRISPR plasmid (without *bla* gene) for HIFI cloning	
pACRISPR_rev	ACTCTTCCTTTTTCAATATTATTG		
Spc_fwd	AATATTGAAAAAGGAAGAGTGTGAGGAGGATATAT TTGAATAC	PCR to amplify *spt* gene from pSET4s for HIFI cloning	
Spc_rev	GAGTAAACTTGGTCTGACAGTTATAATTTTTTTAAT CTGTTATTTAAATAGTTTATAG		
Spc_int_fw	GAGGAATTACTACCTGATATTC	PCR to check the pUA1148 plasmid construction	
pACRISPR_rv2	CTGGTAACAGGATTAGCAG		
gRNA48_fw[b]	GTGGGTGTTTCAGAGGAAACCCTG	Phosphorylated primers to anneal the gRNA48 spacer through Golden Gate assembly	
gRNA48_rv[b]	AAACCAGGGTTTCCTCTGAAACAC		
pACRISPR2622_rv	CATGGGTATGGACAGATC	PCR and sequencing of cloned gRNA48 spacer in pUA1148	
pACRISPR2431_fw	GTGCCAATACCAGTAGAAAC		
*Sce*I_sec_rv	TCGATGTTCAGTTCGATCAG		
pUA1139_00007_km_p1.2[a,c]	TACAGATGCACCGATGCGCTTGCGTGGCTTTTCAGG GAGATAAAGTTATGAGTTACGCTAGGGATAACAGG GTAATATAG*taggaacttcaagatcccct*	PCR of Km gene from pKD4 plasmid with homology regions of the *pUA1139_00007* gene of the plasmid pUA1139	
pUA1139_00007_km_p2.1[a]	TTCCGGCACAGGTGAGGCCGGAATTCGGACTAAAA CGTAAACCGCGGGCC*atgggaattagccatggtcc*		
pUA1139_00007_ext_fw	GCTGAGTGAAAACACCCTT	PCR and sequencing to check the Km insertion into the *pUA1139_00007* gene	
pUA1139_00007_ext_rv_2	GGCTGAAGGCCTTTATAGT		

Table S3.2 (continued)

Name	Sequence (5'-3')	Application	Reference
pKD46_inv_fw	CGAAATCCACTGAAAGCACA	Inverse PCR to amplify pKD46 plasmid without λ-Red system genes	de Moraes and Teplitski, 2015
pKD46_inv_rv	AAGCTGCTTTTGAGCACCAC		
*Sce*I_pKD46_fw	TACCAGTAGAAACAGACGAAGAATCGACCAATTCGGGTCGACTTATTATTTC	Amplification of I-*Sce*I synthetic gene and tetracycline inducible promoter	This study
*Sce*I_pKD46_rv	TATCAAAGGGAAAACTGTCCATACCGGAAAAAGGTTATGCTGCTTTTAAG		
pKD46_mod_comp_fw	GACAACTTGACGGCTACA	PCR and sequencing to check the pUA1165 plasmid construction.	
pKD46_mod_comp_rv	GAACAACTGTTCACCGTTACA		
*Sce*I_sec_fw	CTGATCGAACTGAACATCGA		
*Sce*I_sec_rv	TCGATGTTCAGTTCGATCAG		

[a] P1 and P2 sequences, homologues to the pKD4 plasmid, are represented in lower case italics; [b] Regions of homology with pUA1148 are represented underlined; [c] I-*Sce*I restriction site is represented underlined.

Table S3.3 Point mutations identified in the genomes of all the *Salmonella* variants and the parental strain sequenced with respect to the genome of the NCBI reference strain ATCC14028s (GenBank CP001363.1).

					Mutation Frequency (%)											
Locus tag	**Gene**	**Function[a]**	**CDS Position**	**Codon change**	**Parental**	**CI2**	**CI3**	**HT1**	**HT5**	**IC3**	**IC5**	**IC6**	**IC8**	**IC10**	**IT2**	**IT3**
STM14_3335		Transposase IS3/IS911 family	228	CAA/CA**G**	0	0	0	0	0	0	0	0	0	0	28.0	27.6
			246	GA**G**/GA**A**	0	0	0	0	0	0	0	0	0	0	52.1	56.2
			249	GA**A**/GA**G**	0	0	0	0	0	0	0	0	0	0	52.6	56.9
			255	GC**C**/GC**T**	0	0	0	0	0	0	0	0	0	0	54.0	58.7
			258	AT**T**/AT**C**	0	0	0	0	0	0	0	0	0	0	54.5	59.6
			264	CA**G**/CA**A**	0	0	0	0	0	0	0	0	0	0	57.7	63.2
STM14_3336		Putative transposase	15	TT**C**/TT**T**	0	0	0	0	0	0	0	0	0	0	63.8	66.1
			18	AT**C**/AT**T**	0	0	0	0	0	0	0	0	0	0	63.6	66.8
			41	A**AT**/A**GC**	0	0	0	0	0	0	0	0	0	0	59.3	60.8
			51	GC**C**/GC**A**	0	0	0	0	0	0	0	0	0	0	57.8	58.9
			378	AG**C**/AG**T**	0	0	0	0	0	0	0	0	0	0	0	40.8
			387	AA**T**/AA**C**	0	0	0	0	0	0	0	0	0	0	0	38.1
			398	G**TG**/G**CA**	0	0	0	0	0	0	0	0	0	0	0	29.8
			402	GG**T**/GG**A**	0	0	0	0	0	0	0	0	0	0	0	30.4
STM14_4210	*yrfH*	Heat shock protein Hsp15	287	**ATG**/-TG	0	0	0	0	0	0	0	0	0	0	0	91.4
STM14_4478	*rfaJ*	Glycosyl transferase	742	AT**A**/AT-	0	99.5	99.5	0	0	0	0	0	0	0	0	0
			910	**G**AA/**T**AA	0	0	0	0	99.8	0	0	0	0	0	0	0
STM14_4904	*yneC*	AI-2-degrading protein LsrG	114	CG**T**/CG**C**	99.7	99.4	99.7	99.8	99.7	99.7	99.5	99.7	99.7	99.4	99.5	100.0
STM14_4922	*cytR*	Transcriptional regulator, LacI family	656	G**A**A/G**T**A	99.7	99.7	99.7	99.7	99.7	99.7	99.7	99.3	99.6	99.5	99.7	100.0
STM14_5121		Putative inner membrane protein	7206	GT**G**/GT**C**	99.7	99.7	99.7	99.7	99.7	99.7	99.7	99.3	99.7	99.7	99.8	100.0
			7243	**TTG**/**C**TG	99.7	99.8	99.5	99.8	99.7	99.7	99.5	99.3	99.7	99.8	99.8	100.0
STM14_5349	*mgtA*	Magnesium-translocating P-type ATPase	2234	CA**G**/CT**G**	0	0	0	0	0	99.7	0	0	0	0	0	0

Table S3.3 (continued)

Locus tag	Gene	Function[a]	CDS Position	Codon change	Mutation Frequency (%)											
					Parental	CI2	CI3	HT1	HT5	IC3	IC5	IC6	IC8	IC10	IT2	IT3
STM14_3335		Transposase IS3/IS911 family	228	CA**A**/CA**G**	0	0	0	0	0	0	0	0	0	0	28.0	27.6
			246	GA**G**/GA**A**	0	0	0	0	0	0	0	0	0	0	52.1	56.2
			249	GA**A**/GA**G**	0	0	0	0	0	0	0	0	0	0	52.6	56.9
			255	GC**C**/GC**T**	0	0	0	0	0	0	0	0	0	0	54.0	58.7
			258	AT**T**/AT**C**	0	0	0	0	0	0	0	0	0	0	54.5	59.6
			264	CA**G**/CA**A**	0	0	0	0	0	0	0	0	0	0	57.7	63.2
STM14_3336		Putative transposase	15	TT**C**/TT**T**	0	0	0	0	0	0	0	0	0	0	63.8	66.1
			18	AT**C**/AT**T**	0	0	0	0	0	0	0	0	0	0	63.6	66.8
			41	A**A**T/A**G**C	0	0	0	0	0	0	0	0	0	0	59.3	60.8
			51	GC**C**/GC**A**	0	0	0	0	0	0	0	0	0	0	57.8	58.9
			378	AG**C**/AG**T**	0	0	0	0	0	0	0	0	0	0	0	40.8
			387	AA**T**/AA**C**	0	0	0	0	0	0	0	0	0	0	0	38.1
			398	G**TG**/G**CA**	0	0	0	0	0	0	0	0	0	0	0	29.8
			402	GG**T**/GG**A**	0	0	0	0	0	0	0	0	0	0	0	30.4
STM14_4210	*yrfH*	Heat shock protein Hsp15	287	**A**TG/-TG	0	0	0	0	0	0	0	0	0	0	0	91.4
STM14_4478	*rfaJ*	Glycosyl transferase	742	AT**A**/AT-	0	99.5	99.5	0	0	0	0	0	0	0	0	0
			910	**G**AA/**T**AA	0	0	0	0	99.8	0	0	0	0	0	0	0
STM14_4904	*yneC*	AI-2-degrading protein LsrG	114	CG**T**/CG**C**	99.7	99.4	99.7	99.8	99.7	99.7	99.5	99.7	99.7	99.4	99.5	100.0
STM14_4922	*cytR*	Transcriptional regulator, LacI family	656	G**A**A/G**T**A	99.7	99.7	99.7	99.7	99.7	99.7	99.7	99.3	99.6	99.5	99.7	100.0
STM14_5121		Putative inner membrane protein	7206	GT**G**/GT**C**	99.7	99.7	99.7	99.7	99.7	99.7	99.7	99.3	99.7	99.7	99.8	100.0
			7243	**T**TG/**C**TG	99.7	99.8	99.5	99.8	99.7	99.7	99.5	99.3	99.7	99.8	99.8	100.0
STM14_5349	*mgtA*	Magnesium-translocating P-type ATPase	2234	CA**G**/CT**G**	0	0	0	0	0	99.7	0	0	0	0	0	0

[a], Data extracted from EggNOG. In all cases, P-values were around 0.0.

4. CHAPTER II

Summary

In this second chapter we address the third objective of this thesis:

- Identify the gene involved in interference of the UAB_Phi20 phage cycle and characterize this mechanism at the molecular level.

A bioinformatic analysis yielded the identification of the gene *ibfA*, located in a hypervariable region of the plasmid pUA1135, harboured by the *Salmonella* IC5 variant strain, and previously related to interfere with several phages. To demonstrate the implication of the gene *ibfA* in the interference against UAB_Phi20 phage, an *ibfA* mutant strain and subsequent complementation of *ibfA* were performed. A more in-depth study of basic parameters of phage infection (EOP, ECOI, adsorption constant, and burst size) was also conducted in an ATCC14028 Rif^R strain carrying the *ibfA* gene with its own promoter cloned in the pBAD33 vector. Furthermore, we investigated the potential molecular mechanism underlying this interference by evaluating several steps of phage infection, such as injection and replication of phage DNA, transcription of basic phage genes, use of cellular ATP, and assembly of virion particles inside the bacterial cells by TEM.

The results showed that IbfA exerts an interference by reducing the expression of UAB_Phi20 late proteins, thereby hindering the assembly of virion particles as observed through TEM. Finally, based on these findings, we detailed the possible mechanism by which IbfA could interfere with the multiplicative cycle of the UAB_Phi20 bacteriophage.

Deciphering the causes of IbfA-mediated abortive infection in the P22-like phage UAB_Phi20

Júlia López-Pérez[1], Ivan Erill[2,3], Pilar Cortés[1], Montserrat Llagostera[1]

[1]Departament de Genètica i Microbiologia, Universitat Autònoma de Barcelona, Cerdanyola del Vallès, Spain, [2]Department of Biological Sciences, University of Maryland, Baltimore, MD, United States, [3]Departament Enginyeria de la Informació i de les Comunicacions, Universitat Autònoma de Barcelona, Cerdanyola del Vallès, Spain.

Abstract

The study of bacterial defence mechanisms against phage infection is gaining significance due to their potential to hinder the efficacy of phage therapy in combating bacterial infections. This work delves into a phage defence mechanism targeting the virulent phage UAB_Phi20, a P22-like phage, encoded in the large IncI1α conjugative plasmid pUA1135, which was acquired by *Salmonella* Typhimurium after oral phage therapy in broilers. Employing a multifaceted approach combining bioinformatics, molecular microbiology, transmission electron microscopy, and conventional microbiology techniques, we identify the *ibfA* gene as a new defence mechanism against UAB_Phi20. IbfA, a two-domain protein comprising an ATPase and a TOPRIM domain, clustered with other plasmid-encoded IbfA homologues in *Enterobacteriaceae* species. This protein significantly impacts UAB_Phi20 productivity, as evidenced by a reduced EOP, ECOI, and a diminished burst size, potentially leading to decreased cellular viability without observable cell lysis, evoking an abortive infection behaviour. The underlying molecular mechanism of IbfA does not involve cellular ATP depletion or inhibition of phage genome replication. Instead, IbfA, either directly or indirectly, enhances the transcription of early genes, including the antirepressor *ant*, which inhibits the C2 repressor of the lytic cycle, resulting in an imbalance in Cro/C2 concentration. This leads to a reduction in the transcription of late genes encoding structural and cellular lysis proteins, ultimately causing the abortion of UAB_Phi20 infection.

Keywords: *Salmonella*, phage therapy, bacterial defence mechanism, IncI1α conjugative plasmid, *ibfA*, abortive infection.

4.1 Introduction

The increase in infections caused by multi-drug resistant bacteria is of great concern nowadays. This has accelerated the search for alternative therapies, and bacteriophages (or phages) are one of the most promising. Phages are viruses that infect bacteria, and they are genetically the most diverse biological entities on Earth (Comeau *et al*., 2008), greatly outnumbering their hosts in nature (Parikka *et al*., 2017). Bacteriophages have many advantages that make them a highly capable solution for the treatment of bacterial infections, such as their ability to self-replicate inside their hosts and their ability to infect specific bacteria, without affecting the surrounding microbiota. However, the evolutionary arms race between phages and bacteria has resulted in the development of a wide range of bacterial strategies to combat phage infection, posing an important challenge for the extensive application of phage therapy in human and animal health. The study of these defence strategies is crucial for the safe employment of phages in phage therapy.

The number of described phage defence strategies has grown exponentially the last few years. These strategies are very diverse, and they block the phage life cycle at different stages (Georjon and Bernheim, 2023). The first line of defence against phages is the prevention of adsorption to their receptors, either through the mutation or deletion of the receptor genes, masking the receptor with extracellular polymeric substances or using outer membrane vesicles as a decoy (Bertozzi Silva *et al*., 2016). DNA injection is prevented by mechanisms such as superinfection exclusion (Sie) (Bondy-Denomy *et al*., 2016). Once phage DNA has been injected, restriction-modification (RM) (Tock and Dryden, 2005), phage growth limitation (PgI) (Chinenova *et al*., 1982), bacteriophage exclusion (BREX) (Goldfarb *et al*., 2015), defence island associated with RM (DISARM) (Ofir *et al*., 2018), prokaryotic argonautes (pAgos) (Makarova *et al*., 2009), restriction by an adenosine deaminase acting on RNA (RADAR) (Gao *et al*., 2020; Gao *et al*., 2023) or clustered regularly interspaced short palindromic repeats and associated proteins (CRISPR-Cas) (Hille *et al*., 2018) act through different mechanisms to inhibit phage genome replication. Transcription of phage genes can also be the target of bacterial defences. For example, prokaryotic viperins (pVips) (Bernheim *et al*., 2021) produce several modified ribonucleotides that inhibit phage transcription by acting as RNA chain terminators. On the other hand, abortive infection (Abi) systems cause cell death before phages have completed their life cycle, avoiding the spread of the infection in the population. These systems typically target replication, transcription, or translation, and they are mechanistically very diverse. One of the classical Abi mechanisms are toxin-antitoxin (TA) systems (Dy *et al*., 2014; Lopatina *et al*., 2020). Other more recently described Abi systems are cyclic-oligonucleotide-based antiphage signalling systems (CBASS) (Cohen *et al*., 2019), Thoeris (Doron *et al*., 2018; Ofir *et al*., 2021), bacterial gasdermins (Johnson *et al*., 2022), and retrons (Millman *et al*., 2020). In addition to these well-characterized phage

defence systems, there is a growing list of systems with unknown mechanisms that are known to interfere with the phage cycle (Doron *et al*., 2018; Millman *et al*., 2022).

In previous work by our group, Colom *et al*., 2017 used bacteriophage UAB_Phi20 (a P22-like bacteriophage) in combination with two other phages (UAB_Phi78 and UAB_Phi87) in a phage therapy study performed on broiler chickens experimentally contaminated with *Salmonella enterica* serovar Typhimurium ATCC14028 resistant to rifampicin (Rif^R). This study achieved a reduction in *Salmonella* concentration in the ceca of broilers of 2.8-log_{10} at 6 days after a daily phage treatment of animals. In that study, several *Salmonella* variants with reduced phage susceptibility were isolated from the broilers' ceca, in which interference with the phage multiplicative cycle was related to IncI1α large conjugative plasmids acquired by lateral transfer from the broilers' gut microbiota (López-Pérez *et al*., 2023). One of the variants, named IC5, harboured one large conjugative plasmid pUA1135 (96,685 bp) and exhibited reduced susceptibility to phage UAB_Phi20 and the other two phages of the cocktail. *Salmonella* phage UAB_Phi20 is a virulent phage belonging to the *Lederbergvirus* genus. It has an icosahedral head of about 60 nm and a noncontractile short tail (13 ± 0.7 nm) (Bardina *et al*., 2012). Its genome is a linear double-stranded DNA (dsDNA) molecule of 41,809 base pairs (bp) in length with circularly permuted direct terminal repeats (Bardina *et al*., 2016). UAB_Phi20 genome is highly similar to *Salmonella* phage P22 (Bardina *et al*., 2016), and although it encodes all components necessary for a lysogenic cycle, it was shown to be a virulent phage (Bardina *et al*., 2016).

Here, we identify the *ibfA* gene encoded in plasmid pUA1135 as the agent responsible for UAB_Phi20 interference. This gene is homologous to the *ibfA* gene found in plasmid R64, which has been related to changes in phage type (Hiley *et al*., 2021) and interference of coliphages PhiI and λ, and *S*. Typhimurium phages P22 and St (Anderson and Lewis, 1965; Hughes and Meynell, 1977). However, its mechanism of action has not been elucidated. In this paper, we also characterize the molecular mechanism by which the IbfA protein interferes with the lytic cycle of UAB_Phi20.

4.2 Materials and methods

Bacterial strains, phage, and growth conditions

The parental strain used to determine the efficiency of plating (EOP) and study phage defence mechanisms was a spontaneous mutant of *Salmonella enterica* serovar Typhimurium ATCC14028 Rif^R, obtained by us. The *S*. Typhimurium IC5 variant (López-Pérez *et al*., 2023) was used in the deletion and complementation experiments of genes involved in phage defence mechanisms. Finally, the strain *Escherichia coli* DH5α was used for cloning phage defence genes into pBAD33 plasmid (Table S4.1).

ATCC14028 Rif^R, IC5, and the derived strains were cultured on Luria-Bertani (LB) liquid or agar media supplemented with rifampicin (75 µg/mL). Strains containing pBAD33 plasmids were grown in media supplemented with 34 µg/mL of chloramphenicol. All bacterial culture plates were incubated for 18 h at 37ºC. Phage infection experiments were performed with the phage UAB_Phi20 (NCBI accession number: NC_031019; Bardina *et al*., 2012; Bardina *et al*., 2016).

Phage lysate production

Phage lysates were obtained following a previously described protocol (Colom *et al*., 2015) and filtered through 0.45 µm pore size polyether sulfone (PES) membranes (Millex®-HP). Phage titration was performed by plating ten-fold serial dilutions onto LB plates using the double agar layer method (Kutter, 2009).

Bacterial growth kinetics

Salmonella liquid LB cultures were grown for 18 h at 37ºC with agitation. Afterwards, cultures were diluted (1:100) and incubated at 37ºC monitoring the absorbance at 550 nm ($A_{550\ nm}$) using the spectrophotometer Genesys 10S UV-Vis (Thermo Fisher Scientific, Massachusetts, USA) at 30-min or 1-h intervals. In addition, the concentration of viable cells as colony-forming units per mL (cfu/mL) was determined at each interval. At least two independent experiments were performed to obtain the standard deviations.

EOP, phage adsorption constant, efficiency of centre of infection (ECOI), and burst size determination

For EOP determination, bacterial cultures were incubated at 37ºC for 18 h in LB medium until they reached the stationary phase. One hundred µL of the bacterial culture (1 x 10^8 cfu/mL) were mixed with 100 µL of ten-fold serial dilutions of UAB_Phi20 lysate in 0.7% LB molten agar. The mixture was plated in LB agar by the double agar layer method (Kutter, 2009). The number of plaque-forming units (pfu) was counted after 18 h incubation at 37ºC and the EOP was calculated as described previously (Khan Mirzaei and Nilsson, 2015). Three replicates were performed, and the standard deviations were calculated.

Measurement of the adsorption rate constant of UAB_Phi20 was done as described previously (Kropinski, 2009). Both the centre of infection (COI) and the burst size were determined as described in Moineau *et al*., 1993 and Kropinski, 2018 with some modifications. Briefly, *Salmonella* cultures incubated at 37ºC for 18 h were diluted 1/100 and incubated at 37ºC until they reached mid-log phase. Cultures were then adjusted to $A_{550\ nm} = 0.4$ and incubated for 5 min at 37ºC with shaking at 60 revolutions per minute (r.p.m). Infection was performed at a multiplicity of infection (MOI) of 0.1 pfu/cfu, and the phage was allowed to adsorb for 15 min at 37ºC without shaking. Two serial 1/100 dilutions were done and 100 µL of the 10^{-4} dilution were

plated onto a lawn of ATCC14028 Rif^R (parental sensitive strain) by the double agar layer method (Kutter, 2009). The number of plaques determined the COI formed on the test strain. The ECOI was calculated by dividing the number of COI from the test strain by the number of COI from the parental strain ATCC14028 Rif^R (sensitive strain). A control of correct adsorption of the phage was performed by mixing 1 mL of the 10^{-4} dilution to 100 µL of ice-cold chloroform. The mixture was centrifuged for 1 min at 6,797 x *g*, and 100 µL of the supernatant were plated by the double layer method using the ATCC14028 Rif^R parental strain (Kutter, 2009). To determine the burst size, the 10^{-4} dilution was serially diluted up to a 10^{-7} dilution. One hundred µL samples were collected from the appropriate dilution every 10 min up to 125 min of phage infection, mixed in 0.7% LB molten agar containing 100 µL of ATCC14028 Rif^R and plated in LB agar by the double layer method (Kutter, 2009). Burst size on a test strain was calculated by dividing the final concentration of phage to the resulting number of the subtraction of the adsorption control to the initial concentration of phage (Moineau *et al*., 1993, Kropinski, 2018). Experiments were performed at least three times, and the standard deviations were calculated.

One-step growth

Experiments of one-step growth were performed as described in Doermann, 1952 with some modifications. The desired *Salmonella* cultures were grown in LB medium for 18 h at 37ºC. Afterwards, cultures were diluted and incubated at 37ºC until an $A_{550\ nm}$ of 0.4 was reached. Cultures were synchronized with potassium cyanide (KCN) 10 mM (Merck Life Science S.L.U.) for 10 min at 37ºC without shaking. Afterwards, they were infected with UAB_Phi20 bacteriophage at a MOI of 1 pfu/cfu and left at 37ºC without shaking for the 15 min required for UAB_Phi20 adsorption. Then, the cultures were centrifuged at 12,880 x *g* for 10 min and the pellet resuspended in the same volume of fresh LB. Cultures were serially diluted up to 10^{-8} in the case of ATCC14028 Rif^R pBAD33 and 10^{-7} for ATCC14028 Rif^R pBAD33::*ibfA* and incubated at 37ºC with shaking at 150 r.p.m. One hundred µL samples were taken every 10 min until 80 min after phage adsorption, and titration was done by double agar layer method (Kutter, 2009) using ATCC14028 Rif^R as host strain to determine the released phages (latent period). Furthermore, 100 µL of samples were mixed with 800 µL LB and 100 µL chloroform, vortexed and centrifuged at 6,797 x *g* for 1 minute, and the titration of the supernatant was done to determine the total phage (eclipse period). Three replicates were performed, and standard deviations were determined.

Phage infection kinetics

Salmonella bacterial cultures infected with UAB_Phi20 were prepared as explained above. Following the 15 min of phage adsorption and subsequent removal of KCN, 1mL samples were withdrawn at specified intervals and centrifuged at 6,797 x *g* for 2 min. The titration of the

supernatant was done by the double agar layer method (Kutter, 2009) to quantify the produced phage. The pellet was washed with 1mL of cold NaCl (0.9%) and centrifuged at 6,797 x *g* for 2 min. The resulting pellet was then resuspended in 1mL cold NaCl (0.9%) and serially diluted to plate the viable cells on LB agar plates. Simultaneously, at the same time points, 800 µL aliquots were collected from the cultures and directly mixed with 200 µL of 10% formaldehyde, and at the end of the assay the $A_{550\ nm}$ was determined. Three replicates were performed, and standard deviations were determined.

Total ATP determination

Salmonella bacterial cultures infected with UAB_Phi20 were prepared as explained above. Uninfected cultures were similarly prepared and used as control. After the 15 min of phage adsorption and removal of KCN, 1 mL samples were collected for ATP extraction every 20 min until 80 min. ATP extraction was performed as described in Lee and Groisman, 2012. All samples were kept in ice until measure, carried out using the ATP determination Kit (Invitrogen) in a Spark luminometer (Tecan) according to the manufacturer's instructions, in a final volume of 200 µL per well (Laboratori de Luminiscència i Espectroscòpia de Biomolècules, UAB). Each sample was measured twice, the experiment was performed at least three times, and the standard deviations were calculated.

Deletion of *ibfA* through one-step inactivation

A λ-Red recombinase strategy (Datsenko and Wanner, 2000) was performed to delete *ibfA* or the *ibfA*-containing transcriptional unit from pUA1135 (NCBI accession number: MW590592.1) in the IC5 variant. Briefly, *Salmonella* cells were made electrocompetent and the pKOBEG plasmid (Table S4.1) was electroporated and selected on LB agar plates containing chloramphenicol (34 µg/mL). Simultaneously, the kanamycin resistance cassette from pKD4 plasmid (Table S4.1) was obtained by polymerase chain reaction (PCR) using Phusion™ High-fidelity DNA polymerase (Thermo Scientific™) and using primers with homology tails matching the desired region in the pUA1135 plasmid (Table S4.2). The resulting linear product was purified with NzyGelpure kit (NZYTech, Lisboa, Portugal) and introduced by electroporation in target pKOBEG-containing cells. Transformant cells were selected in LB agar plates containing 50 µg/mL kanamycin and 34 µg/mL chloramphenicol and incubated at 30ºC overnight. The kanamycin cassette insertion was confirmed by PCR and sequencing (Macrogen) using the appropriate primers (Table S4.2). The pKOBEG plasmid was cured by incubating at 42ºC and clones that were kanamycin resistant and chloramphenicol susceptible were selected.

Transcriptional analysis of *ibfA* operon

RNA extraction was done from *Salmonella* cultures using the RNeasy Mini kit (Qiagen) following manufacturer's instructions with a previous lysis step with lysozyme (50 mg/mL) in TE buffer (10 mM Tris-HCl, pH 7.5, 1 mM EDTA, pH 8.0), at 37ºC vortexing every 2 min for 10 min. DNA removal was accomplished with the TURBO DNA-free kit (Invitrogen) as described by the manufacturer with modifications. Briefly, 90 µL samples were incubated with 1X TURBO DNase™ Buffer and 8 units of TURBO DNase™ Enzyme for 45 min at 37ºC. This treatment was performed twice. Enzyme inactivation was done according to manufacturers' instructions. RNA sample cleanup was done using the RNeasy Mini kit (Qiagen).

Reverse transcription of DNase-treated RNAs (1 µg) was carried out with NZY First-Strand cDNA Synthesis Kit (NZYTech, Lisboa, Portugal) following the manufacturer's conditions and using appropriate primers (Table S4.2). cDNA amplification was performed by conventional PCR using Invitrogen™ Taq DNA Polymerase and the same primers as detailed before. The resulting PCR products were visualized by agarose (2%) gel electrophoresis and stained in RedSafe™ Nucleic Acid Staining Solution (iNtRON). DNA molecular weight marker NZYDNA Ladder V marker (NZYTech) was used as standard.

Cloning of *ibfA* onto the vector pBAD33

The genomic DNA was purified from *S.* Typhimurium IC5, which contains the pUA1135 plasmid, by using the Easy-DNA™ kit (Invitrogen), following the manufacturer's instructions. Gene *ibfA* or the *ibfA*-containing transcriptional unit were PCR amplified from pUA1135 with their own promoter using primers listed in Table S4.2. The PCR product was purified using NzyGelpure kit (NZYTech, Lisboa, Portugal) and inserted onto the vector pBAD33, previously linearized with KpnI restriction enzyme (New England Biolabs, Inc), using NEBuilder® HiFi DNA Assembly Master Mix (New England Biolabs, Inc). This construction was then transformed into DH5α competent cells by electroporation and selected on LB agar plates supplemented with chloramphenicol (34 µg/mL). The correct cloning of *ibfA* or the transcriptional unit was checked by PCR and sequencing (Macrogen) using the appropriate primers (Table S4.2).

Replication of UAB_Phi20 genome

The quantification of *Salmonella* DNA, and intracellular and extracellular UAB_Phi20 DNA was performed by quantitative real-time PCR (qPCR). Bacterial cultures were prepared as explained above and infected with UAB_Phi20 at a MOI of 1 pfu/cfu. One mL aliquots were withdrawn just after phage adsorption (t: 0 min) and at 15, 30, 50, 70 and 90 min, and centrifuged at 6,797 x *g* for 2 min. The supernatants were kept at 4ºC and used to quantify extracellular bacteriophage DNA. The pellets were washed once with NaCl (0.9%) and frozen at -80ºC. Once all samples

were collected, pellets were defrosted and resuspended in 100 µL TE buffer (10 mM Tris-HCl, pH 7.5, 1 mM EDTA, pH 8.0). Cell lysis was accomplished by temperature treatment (100ºC) for 10 min. Samples were then centrifuged at 6,797 x *g* for 2 min and the supernatants were kept at -20ºC for quantification of *Salmonella* DNA and intracellular bacteriophage DNA.

qPCR was prepared using 2 µl of template DNA from cell pellets or 2 µl of supernatants, appropriate primers (0.5 µM final concentration) (Table S4.2), Milli-Q water and 1X LightCycler® 480 SYBR Green I Master kit buffer (Roche) for a final volume of 20 µl. qPCR assays were performed on a Lightcycler 480® Instrument II (LC480, Roche) with the following cycle conditions: preincubation at 95ºC for 30 s followed by 45 amplification cycles of 3 s at 95ºC, 15 s at 57ºC and 18 s at 72ºC, and a final melting curve up to 95ºC. All qPCR reactions were made in technical duplicates and non-infected samples were included as negative controls. Total DNA extracted from *S.* Typhimurium ATCC14028 Rif^R using the Easy-DNA™ kit (Invitrogen) and UAB_Phi20 DNA purified by the phenol-chloroform protocol (Sambrook and Russel, 2001) were used to generate the respective standard curves. For this, 10-fold gradient dilutions of each DNA were prepared representing 10^0 to 10^9 genome copies/µL of templates and tested in triplicate to obtain the copy number per µL from the target genes *gyrB* (*Salmonella*) and helicase (*gp3*, UAB_Phi20) (Table S4.2). The determination of gene copies according to the size of the bacteria or phage genome, and the concentration of DNA used, was obtained as previously described (Ritalahti *et al*., 2006). The final results in copies/mL of intracellular and extracellular phage DNA and *Salmonella* cells were obtained from imported standard curves as described (Ritalahti *et al*., 2006), taking into account the dilution factor of each sample when necessary. Biological triplicates were prepared, and qPCR experiments were performed from two technical replicates to calculate the average copy number per mL, and the standard deviations.

Gene expression quantification

To assess the expression of some UAB_Phi20 phage genes and the bacterial gene *ibfA*, reverse transcription-quantitative polymerase chain reaction (RT-qPCR) was performed. Bacterial cultures were prepared as explained above. Uninfected cultures were treated similarly to the infected ones, but without the addition of the phage.

Two samples of 5 mL were collected at 0, 10, 20, 30 and 40 min after phage adsorption and mixed with 1/10 stop solution (1:10 buffered phenol, 9:10 absolute ethanol) as described previously (Brandão *et al*., 2021), vortexed and placed on ice for total RNA extraction. When all samples were collected, they were centrifuged at 12,857 x *g* for 10 min and the supernatant was removed. Pellets were stored at -80ºC until RNA extraction, that was performed using the RNeasy Mini kit (Qiagen) as described above, except for an additional DNase treatment consisting of the addition

of 5 µL of 10X TURBO DNase™ Buffer and 4 units of TURBO DNase™ Enzyme that was incubated for 1 h at 37ºC.

One-step RT-qPCR was done on a Lightcycler 480® Instrument II (LC480, Roche) using the LightCycler® RNA Master SYBR Green I kit (Roche). qPCR reactions (20 µL) contained the primers (Table S4.2) of the target genes at a final concentration of 0.3 µM, 3.25 mM of $Mn(OAc)_2$, 1X LightCycler® RNA Master SYBR Green I buffer, and two µL of RNA samples. RNA samples were prepared by adjusting at the same concentration, and further diluting 1:10 for the phage genes and 1:100 for the 16S rRNA gene of *Salmonella*, which served as the reference gene. RT-qPCR conditions were the same as detailed previously for qPCR but with an initial RT step at 61ºC for 20 min prior to the qPCR reaction. The quantification of mRNA transcripts for target genes was performed using the E-Method, which considers the efficiency of the target genes as well as that of the reference gene (16S rRNA) (Tellmann, 2006; Roche, 2019) and time 0 as the calibrator. Three independent infection experiments were carried out, and each RNA sample was studied twice in each RT-qPCR experiment.

Transmission electron microscopy (TEM) of infected *Salmonella* cells

The visualization of the formation of viral capsids inside cells was carried out using TEM. Bacterial cultures were prepared as explained above and infected with UAB_Phi20 at MOI of 1 pfu/cfu. Samples of 10 mL were taken from the cultures at 0, 20, 30, 40, 60 and 80 min after phage adsorption and centrifuged at 12,857 x *g* for 10 min. The pellets were suspended in 2 mL fixative solution [2% paraformaldehyde, 2.5% glutaraldehyde in phosphate buffer (0.1M NaH_2PO_4, pH 7.4)] and incubated for at least 2 h at 4ºC. After fixation, the samples were washed four times with phosphate buffer for 10 min. Post-fixation was performed using 1% OsO_4 overnight at 4ºC. Then, the samples were washed four times with water for 5 min, and 1% uranyl acetate was added to the samples and kept overnight at 4ºC. Finally, the washing step was repeated as previously described. Dehydration was carried out using a series of acetone solutions at increasing concentrations of 50%, 70%, 90%, 96%, and 100%. The samples were then embedded in Epon-815 Resin (Electron Microscopy Sciences) using a series of resin:acetone mixtures at ratios 1:3, 2:2, 3:1 and 4:0, respectively, at room temperature for 2 h each, and finally left overnight with resin. The following day, another change of resin was done, and the samples left for 2 h at room temperature. Polymerization was performed at 70ºC for 48 h. Subsequently, 70 nm sections were obtained using a Reichert-Jung Ultracut E ultramicrotome and placed on PELCO® copper-coated 200-mesh grids (Ted Pella, Inc.). The stained sections were examined in a Hitachi H-7000 transmission electron microscope at 100 kV at instrumental magnifications of 0.5 or 1 µm (Servei de Microscòpia i Difracció de Raig X UAB).

Bioinformatic studies

Several bioinformatics analyses were carried out to characterize the plasmid pUA1135 genome. A functional category enrichment of plasmid pUA1135 was performed using eggNOG-mapper v2 (Huerta-Cepas *et al*., 2019). PADLOC (Payne *et al*., 2022) and DefenseFinder (Abby *et al*., 2014; Tesson *et al*., 2022) were used to determine the presence of known defence systems in plasmid pUA1135. To assess the presence of unknown mechanisms of phage interference, we used tBLASTN against the PLSDB database to identify thirty homologous plasmids, prioritizing query coverage. Plasmid sequences were aligned using Mauve (Darling *et al*., 2010) and inspected for regions of high variability. To quantify the variability of the region comprised between the *repA* and *parA* genes, we used hmmscan against the clusters of orthologous groups (COG) database to assign COG identifiers to each protein-coding gene in all plasmid sequences (Tatusov *et al*., 1997; Galperin *et al*., 2015). Plasmids were then compared pairwise and variability in a given region was assessed as the ratio between the sum of shared COGs and the total sum of COGs for that region in both plasmids.

To construct the phylogeny of IbfA, a BLASTP search was conducted using the IbfA protein sequence against the *clustered nr* database of bacterial (taxid:2) and archaeal (taxid:2157) protein sequences. Results were filtered to include only hits with >85% query coverage, and only those from complete chromosomal or plasmid sequences were kept. Alignments were performed using ClustalX (Larkin *et al*., 2007) and T-Coffee (Notredame *et al*., 2000) with default parameters, and integrated with T-Coffee. Phylogenetic inference was performed using iqtree (Minh *et al*., 2020) with default parameters and annotation of the resulting tree was performed with iTOL (Letunic *et al*., 2021).

Promoter prediction for *ibfA* and its transcriptional unit was done using BPROM (Solovyev and Salamov, 2011) and SAPHHIRE.CNN (Coppens *et al*., 2022) using default parameters. The study of the protein functional domains of IbfA was performed using HHpred (Söding, 2005) against the PDB, PFAM and COG databases and the *E. coli* proteome, with otherwise default parameters. Furthermore, a sequence-based search against Alphafold DB (Jumper *et al*., 2021; Varadi *et al*., 2022) was used to find similar proteins with an experimentally-obtained function or structure.

Statistical analysis

Differences between means were assessed using the t-Test with Prism 8.0.2 (GraphPad, La Jolla, CA, USA). Data are depicted as the mean and standard deviation, or as the geometric mean and standard deviation of the mean in the case of gene expression studies. Differences were considered as statistically significant when $p < 0.05$.

4.3 Results

Unravelling the plasmid region that disrupts the UAB_Phi20 multiplicative cycle

Phage defence systems are known to often localize to high-variability regions of plasmid and chromosome sequences (Chevallereau and Westra, 2022; Rousset *et al*., 2022; Hochhauser *et al*., 2023). A detailed analysis of the pUA1135 plasmid carried by the *S.* Typhimurium IC5 strain revealed a region, comprised between nucleotides 2,000 (*repA* gene) and 18,500 (*parA* gene), that shows considerably more variation than the rest of the plasmid sequence when compared to homologous plasmid sequences. Homologues of pUA1135 exhibited numerous rearrangements, insertions, and deletions within this region in comparison to pUA1135. To quantify this variability, we performed a study of the frequency of distribution of shared COGs through pairwise comparisons between the variable region and the rest of the plasmid (Figure 4.1). A COG inventory of the variable region of these homologous plasmids revealed a preponderance of transposases, underscoring the inherent variability of this region (Table S4.3).

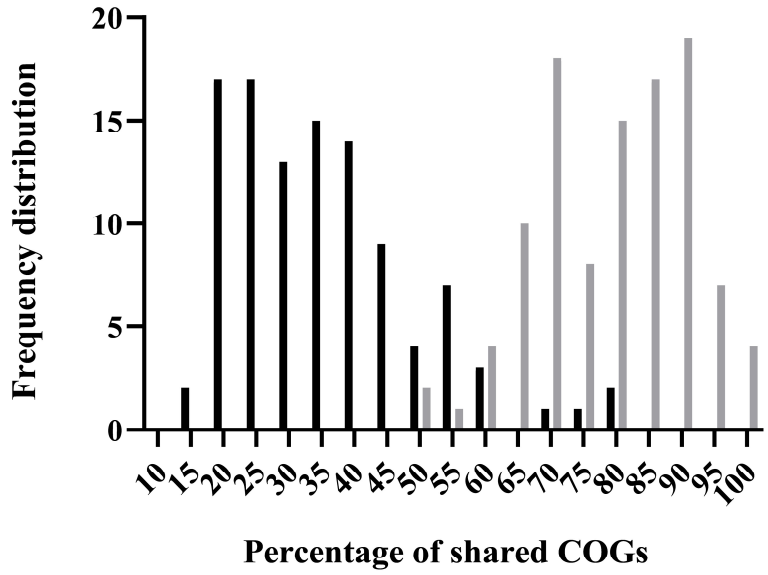


Figure 4.1 Frequency distribution of the fraction of shared COGs in pairwise comparisons of the variable region (black) and the rest of pUA1135 plasmid sequence (grey).

The variable region of pUA1135 plasmid comprises mainly genes encoding hypothetical proteins, alongside an RNA chaperone, a putative nucleotide-binding protein, a β-lactamase flanked by transposases, two *korC* genes, and homologues of the *ibfA*, *ydeA*, and *ydfA* genes (Figure 4.2). We found that the DNA region located between positions 3,805 bp and 5,361 bp in this plasmid is homologous to the HEC-04 defence system (Payne *et al*., 2024), which displays antiviral activity against T4, T5 and several other coliphages, and exhibits a 97.11% and 97.50% sequence identity at the gene and protein levels, respectively, with the *ibfA* gene encoded by the R64 plasmid (Sampei *et al*., 2010), which was previously reported to interfere with the multiplication

of several unrelated phages, including λ, P22 and T7 (Hughes and Meynell, 1977). Considering the high sequence similarity between the UAB_Phi20 and P22 phages (Bardina *et al*., 2016), we hypothesized that the *ibfA* gene encoded in pUA1135 plasmid may be involved in UAB_Phi20 interference. This gene is 1,557 bp in length and is located between the *pUA1135_00003*, encoding the RNA chaperone ProQ, and the *ydeA* genes (Figure 4.3A).

Given their identical orientation, it was possible that the genes *pUA1135_00003*, *ibfA*, *ydeA* and *ydfA* comprised a transcriptional unit. Using BProm, we identified a putative promoter sequence for this transcriptional unit, located 103 bp upstream of the *ydfA* gene, with the transcription start site being at 69 bp from the translation start site (TLS). Furthermore, our bioinformatic analysis revealed the presence of a putative promoter for the *ibfA* gene, located 156 bp upstream of its TLS, with a transcription start site at 121 bp from the start of the gene. To confirm that *ibfA* is part of a transcriptional unit, we conducted a RT-PCR analysis on total RNA from the *S.* Typhimurium IC5 variant containing pUA1135. Figure 4.3B shows the positive amplification of the intergenic regions of the cluster of genes through RT-PCR. This suggested that all genes in the cluster constituted an operon transcribed in a polycistronic manner.

The *ibfA* gene encodes for a protein consisting of 518 amino acids. A HHpred analysis revealed two distinct regions within IbfA. The first region comprised amino acids 1 to approximately 300. This region corresponds to an ATP-binding domain present in several types of nuclease proteins, including endonucleases from the overcoming lysogenization defect family (Akritidou and Thurtle-Schmidt, 2023; Dot *et al*., 2023), the chromosome partitioning protein SMC (Strunnikov, 2006), and other proteins with ATPase components. This would suggest that IbfA possessed an ATPase or ATP-binding domain. The second region (from approximately amino acid 300 to the end of the sequence) shows similarity to the TOPRIM (topoisomerase-primase) domain, which is usually involved in DNA or RNA binding. Furthermore, a sequence-based search with the entire IbfA sequence against the Alphafold database yielded six proteins annotated as members of the AAA-family ATPases or ATP-binding cassette domain-containing proteins, showing a 100% identity match (data not shown). However, none of these proteins have an experimentally-determined function or structure.

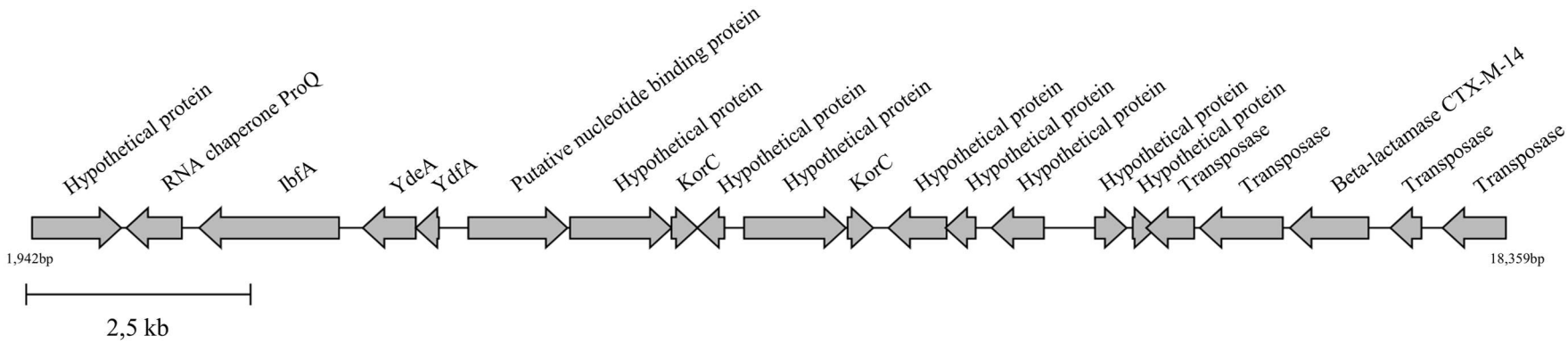


Figure 4.2 Schematic representation of the variable region of pUA1135 plasmid. Annotations of each gene correspond to their predicted protein product.

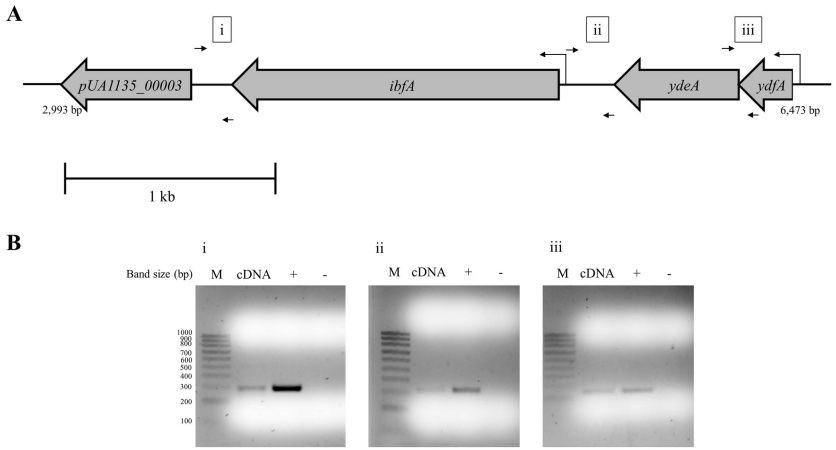


Figure 4.3 (A) Schematic representation of the transcriptional unit containing *pUA1135_00003*, *ibfA*, *ydeA* and *ydfA* genes. The small arrows indicate the primers used for RT-PCR while the large arrows signify the predicted promoters from the transcriptional unit. (B) RT-PCR analysis was conducted on the intergenic regions between (i) *pUA1135_00003* and *ibfA*, (ii) *ibfA* and *ydeA*, and (iii) *ydeA* and *ydfA* and resolved by agarose gel electrophoresis of the products. M represents the NZYDNA Ladder V marker (NZYTech), cDNA corresponds to the cDNA sample obtained through RT-PCR of the intergenic regions, + indicates a PCR positive control with genomic DNA, and – the PCR negative control.

To validate the hypothesis of *ibfA* gene interference with the UAB_Phi20 bacteriophage multiplication cycle, the region encompassing the *pUA1135_00003*, *ibfA*, *ydeA* and *ydfA* operon, as well as the individual *ibfA* gene, were deleted from the pUA1135 plasmid. Subsequently, we examined the infection of each deletion mutant by the UAB_Phi20 bacteriophage. The results revealed that both deletions restored the high efficiency of UAB_Phi20 infection for IC5, with EOP values exceeding 0.5 (Khan Mirzaei and Nilsson, 2015) in both mutants (Table 4.1). To further corroborate this finding, the *ibfA* gene was cloned, along with its own promoter, into the low-copy-number pBAD33 vector, positioning it opposite to the arabinose promoter. The construction was then introduced into the previous deletion mutants, and the EOP of the UAB_Phi20 bacteriophage was determined for the resulting strains. Our data revealed that cloning the *ibfA* gene into this vector resulted in a low efficiency of phage infection, with an EOP value of 0.05 (Table 4.2). Similarly, the entire operon was cloned into the pBAD33 vector and introduced into the IC5 Δ *pUA1135_00003, ibfA, ydeA, ydfA* mutant, yielding results consistent with those mentioned above (Table 4.2).

Table 4.1 EOP values of the UAB_Phi20 bacteriophage for deletion mutants of the IC5 strain.

Strain	**EOP[b]**
ATCC14028 Rif^R	1
IC5[a]	0
IC5 Δ *ibfA*	0.94 ± 0.13
IC5 Δ *pUA1135_00003, ibfA, ydeA, ydfA*	0.65 ± 0.07

[a] This strain contains the pUA1135 plasmid.
[b] Calculated with respect to the parental strain ATCC14028 Rif^R. Standard deviation was obtained from three independent replicates.

Table 4.2 EOP values of the UAB_Phi20 bacteriophage for complementation of deletion mutants of the IC5 strain.

Strain	**EOP[a]**
IC5 Δ *ibfA* / pBAD33	1
IC5 Δ *ibfA* / pBAD33::*ibfA*	0.05 ± 0.00
IC5 Δ *pUA1135_00003, ibfA, ydeA, ydfA* / pBAD33::*pUA1135_00003, ibfA, ydeA, ydfA*	0.01 ± 0.00

[a] Calculated with respect to the strain IC5Δ*ibfA*/pBAD33. Standard deviation was obtained from three independent replicates.

To investigate the process or processes of the phage multiplicative cycle in which the *ibfA* gene interferes, we obtained the ATCC14028 Rif^R/pBAD33::*ibfA* strain (*ibfA*$^+$) by introducing the plasmid pBAD33::*ibfA* into the parental strain ATCC14028 Rif^R. As expected, the infection of this strain by the UAB_Phi20 phage exhibited low efficiency, with an EOP value of 0.05 ± 0.01. However, neither the bacterial growth kinetics (Figure 4.4) nor the adsorption constant of UAB_Phi20 phage in this strain, with a value of 1.2E-8 ± 5.0E-9 ml/min, showed significant

variations compared to its parental strain (1.3E-8 ± 1.7E-9 ml/min). Once the suitability of the *ibfA*$^{+}$ strain was verified, we proceeded to investigate the role of *ibfA* in phage interference using this strain.

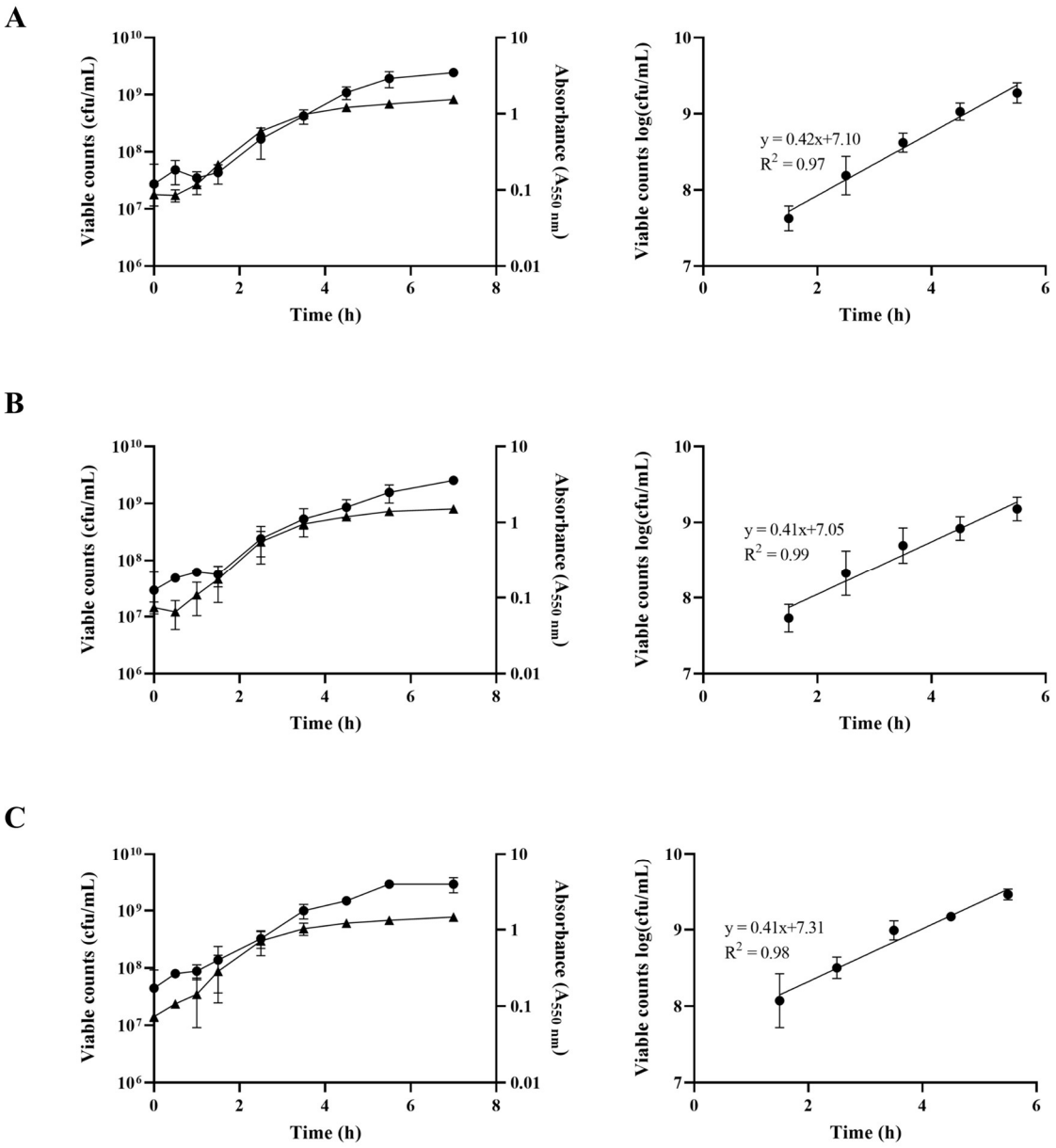


Figure 4.4 Growth kinetics of ATCC14028 Rif^{R}/pBAD33 (A), and ATCC14028 Rif^{R}/pBAD33::*ibfA* (B) strains. Viables (cfu/mL) (●); absorbance ($A_{550\ nm}$) (▲). The growth kinetics of ATCC14028 Rif^{R} (C) are also shown. Error bars indicate standard deviation calculated from two independent experiments.

Effect of the *ibfA* gene on the infection of *Salmonella* by UAB_Phi20

Doermann and one-step growth curves showed that both *ibfA*$^-$ and *ibfA*$^+$ strains exhibited similar eclipse and latent periods of 20 and 30 minutes, respectively, for UAB_Phi20 infection (Figure 4.5). However, in the presence of *ibfA*, the phage's burst size was significantly reduced (44.7 ± 7.8 pfu/cell *vs*. 230 ± 12.1 pfu/cell), coinciding with the smaller plaque size observed in *ibfA*$^+$ (data not shown). Furthermore, the infection kinetics of UAB_Phi20 in *ibfA*$^+$ liquid cultures (Figure 4.6), showed an altered pattern compared to *ibfA*$^-$. The absorbance of cultures remained stable throughout the course of infection in presence of *ibfA*, but decreased in its absence. Besides, the presence of the *ibfA* gene gave rise to a reduction of approximately 1.5-$\log_{10}$ in phage production (Figure 4.6). Finally, the ECOI values of UAB_Phi20 in presence and absence of this gene were 0.16 and 1, respectively.

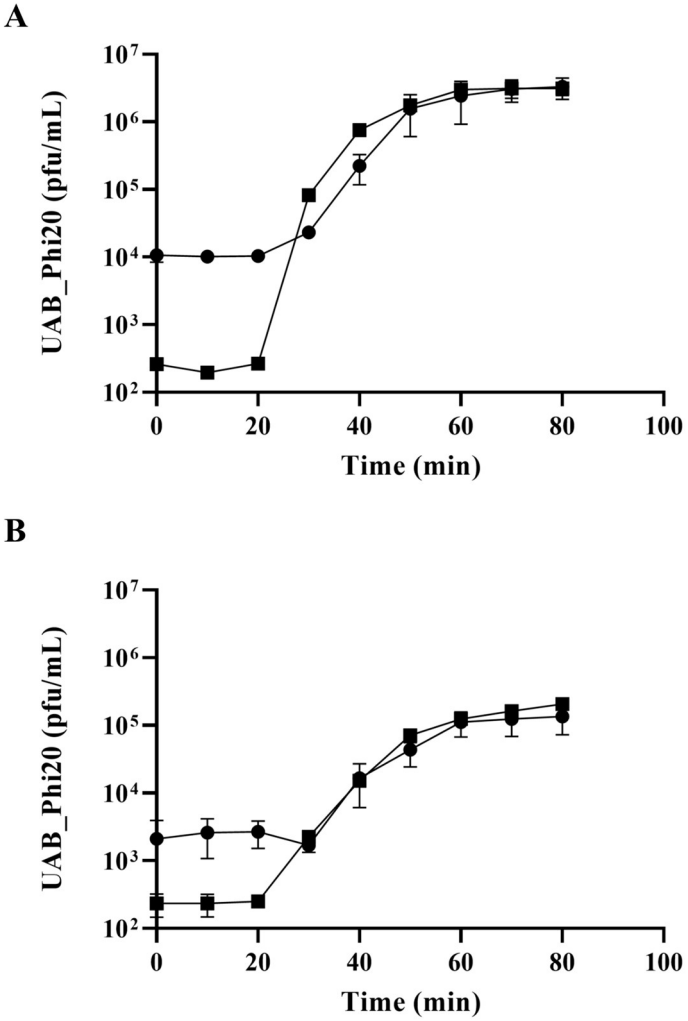


Figure 4.5 Doermann and one-step growth curves of UAB_Phi20 when infecting the ATCC14028 Rif^R/pBAD33 (A) and ATCC14028 Rif^R/pBAD33::*ibfA* (B) strains. Free phage (●); total phage (■). Error bars indicate standard deviation calculated from three independent experiments.

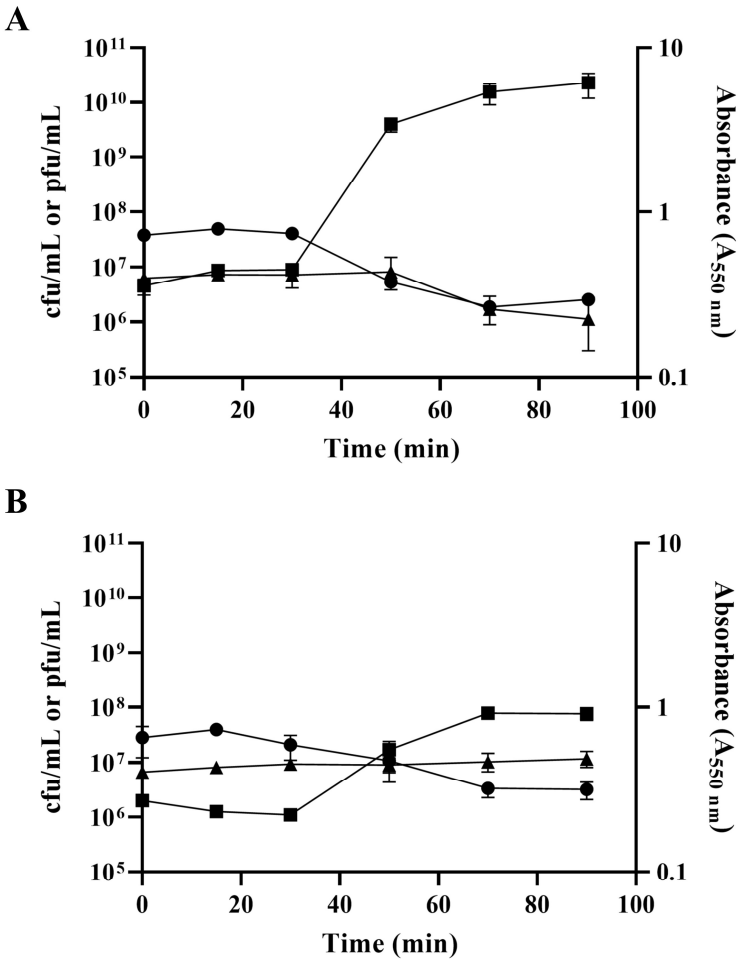


Figure 4.6 Infection kinetics of ATCC14028 Rif^{R}/pBAD33 (A) and ATCC14028 Rif^{R}/pBAD33::*ibfA* (B) strains by the UAB_Phi20 bacteriophage. Bacterial viable count (cfu/mL) (●); absorbance ($A_{550\ nm}$) (▲); UAB_Phi20 concentration (pfu/mL) (■). Error bars represent standard deviation calculated from three independent replicates.

Expression of *ibfA* in UAB_Phi20 infected *Salmonella* cells

To ascertain whether the infection of *Salmonella* by the UAB_Phi20 phage affected the expression of the *ibfA* gene, we measured mRNA levels by RT-qPCR in *ibfA*$^{+}$ cultures, both uninfected and infected with UAB_Phi20 (Figure 4.7). The results revealed a significant decrease in *ibfA* expression from 10 min after adsorption of UAB_Phi20, compared to the uninfected strain.

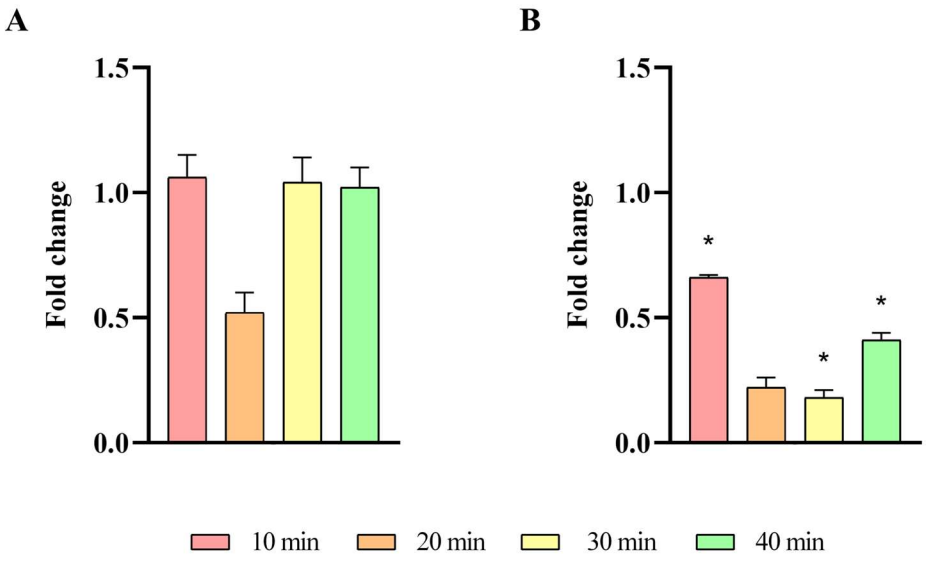


Figure 4.7 Expression of the *ibfA* gene in uninfected (A) and UAB_Phi20-infected (B) cultures of the ATCC14028 Rif^{R}/pBAD33::*ibfA* strain at different times after phage adsorption. Quantification was performed using the E-method, with time 0 as a calibrator and 16S rRNA as the reference gene. The values represent the geometric mean and the standard deviation of the mean of three independent experiments performed in duplicate. * $p < 0.05$.

Impact of the *ibfA* gene on ATP concentration in UAB_Phi20-infected *Salmonella* cells

Our bioinformatic analyses suggested the presence an ATPase domain within the IbfA protein. To explore the potential involvement of this domain in the interference with the multiplicative cycle of the UAB_Phi20 phage, we conducted a luciferin/luciferase assay to measure ATP concentration in both uninfected and UAB_Phi20-infected cultures of *ibfA*$^{-}$ and *ibfA*$^{+}$ strains. The results revealed that, as in parental cells, there was no apparent change in ATP concentration in the uninfected culture of the *ibfA*-containing strain relative to growth rate (Figure 4.8). However, upon infection, ATP consumption was observed in the control strain, but not in the *ibfA*-containing strain.

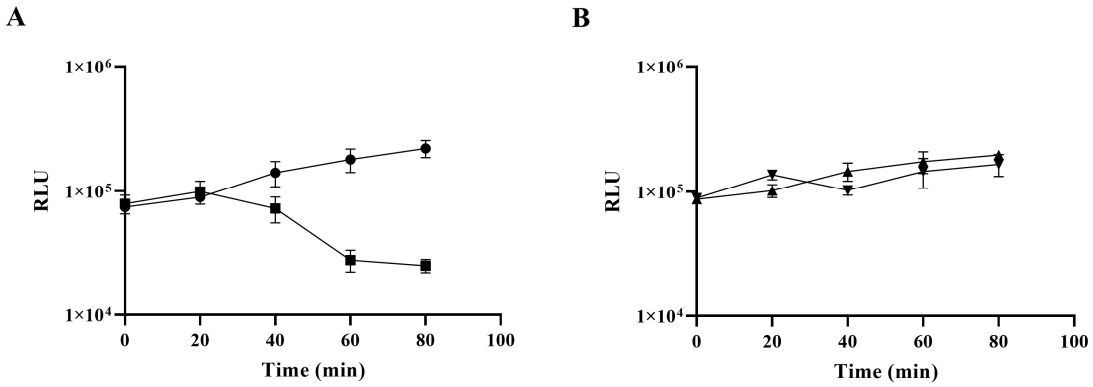


Figure 4.8 ATP concentration in ATCC14028 Rif^{R}/pBAD33 (A) and ATCC14028 Rif^{R}/pBAD33:*ibfA* (B) strains, uninfected (●,▲) and infected (■,▼) with the bacteriophage UAB_Phi20. RLU indicates the real light units measured by the luminometer. Error bars indicate standard deviation obtained from three biological replicates.

Impact of the *ibfA* gene on the multiplicative cycle of UAB_Phi20 bacteriophage

The subsequent experiments sought to elucidate which phase of the phage multiplicative cycle after injection of DNA was affected by the presence of the *ibfA* gene.

First, the replication of the phage genome was studied after infection of synchronic cultures of bacterial cells. The results shown in Figure 4.9 indicated that the number of UAB_Phi20 DNA copies inside cells increased by 1-$\log_{10}$ 30 min after phage adsorption to the cell, and that this increase was independent of the *ibfA* gene. The number of UAB_Phi20 DNA copies inside cells thereafter stabilized in the absence of the *ibfA* gene, but decreased non-significantly in the presence of this gene 50 min after phage adsorption. In contrast, the number of UAB_Phi20 DNA copies outside the cells remained constant until 30 min after adsorption of the phage to the cell, at which time a high increase of extracellular phage DNA copies was observed. However, this increase was higher (around 2-$\log_{10}$) in the absence of the *ibfA* gene than in its presence (about 1-$\log_{10}$) (Figure 4.9).

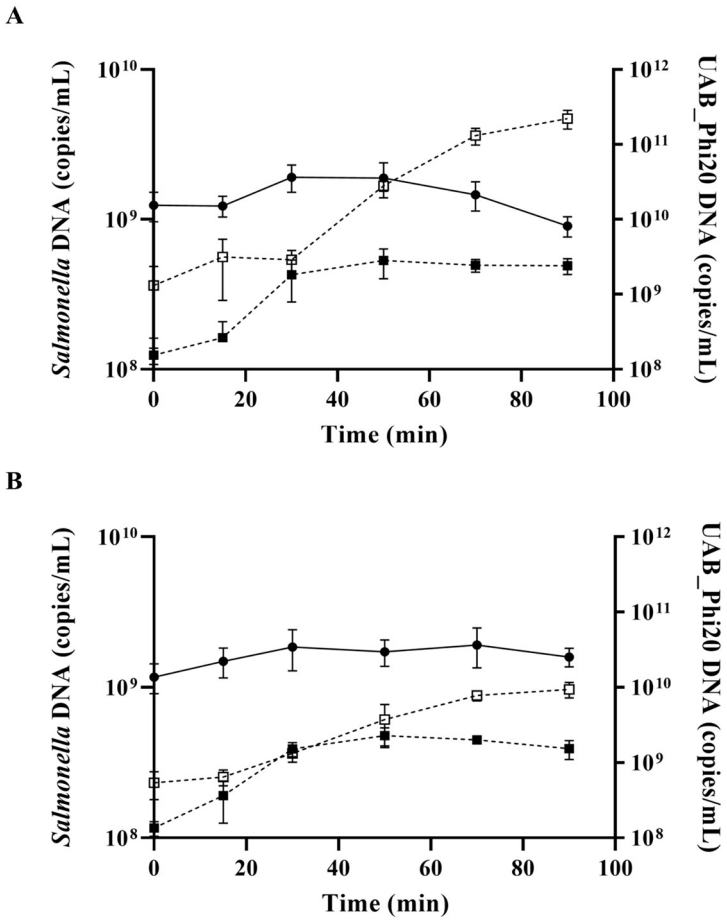


Figure 4.9 Genome replication of the UAB_Phi20 phage in ATCC14028 Rif^R/pBAD33 (A) and ATCC14028 Rif^R/pBAD33::*ibfA* (B) strains. Bacterial genome copies/mL (●); bacteriophage genome copies/mL inside (■) and outside (□) of *Salmonella* cells. Time 0 was defined as 15 min after phage adsorption of synchronized cultures. Data correspond to three biological replicates with error bars showing standard deviation.

Next, the gene expression of early genes from the UAB_Phi20 bacteriophage was studied in the presence and absence of the *ibfA* gene, after infection of synchronic bacterial cultures. Specifically, the early genes studied were *gp74*, *int*, *gp14,* and *gp3*, which encode the early antitermination, integrase, late antitermination, and replicative DNA helicase proteins, respectively, and whose expression is regulated from P_R or P_L (Figure S4.1). Results revealed that expression of three out of four early genes was significantly higher at 30 min and 40 min in the presence of the *ibfA* gene, except for the *gp14* gene, whose expression was significantly lower (Figure 4.10). Also, the expression of *cro*, *c2* and *c1* early genes of the *immC* region was examined (Figure S4.2B). These genes encode the Cro repressor, C2 repressor, and protein C1 involved in lysogeny establishment in temperate bacteriophages such as P22. Results also demonstrated an increase in the expression of these genes in the presence of *ibfA* gene, similar to the trend observed for the other early genes (Figure 4.11). Given that transcription of the *c2* gene was not initially expected due to the absence of a C1 protein binding site in the P_{RE} promoter of UAB_Phi20 bacteriophage (Bardina *et al*, 2016), the genome sequence of this bacteriophage was reanalysed, and a recognition site for the C1 protein was identified on the P_{RE} promoter, albeit with a single nucleotide change (TT**G**CN_6TTGT), compared to the corresponding site (TT**T**CN_6TTGT) in the P22 bacteriophage.

A sizeable proportion of P22-like phages harbour a genomic region known as *immI*, which includes the *arc*, *ant* and *sar* early genes. These genes encode the Arc repressor, responsible for regulating the expression from the P_{ANT} promoter, the Ant antirepressor of the C2 repressor, and the small antisense RNA (Sar), respectively (Figure S4.2C). In line with the observations made for the early genes, an increase in the expression levels of these genes was observed in the presence of *ibfA* (Figure 4.12).

Finally, the expression of the late genes *gp30, gp17, gp18,* and *gp45*, which encode the coat, holin, lysozyme, and tailspike proteins, respectively, was also studied (Figure S4.3). The results indicated a significant decrease in the expression of these four genes at 30 and 40 min in the presence of the *ibfA* gene (Figure 4.13).

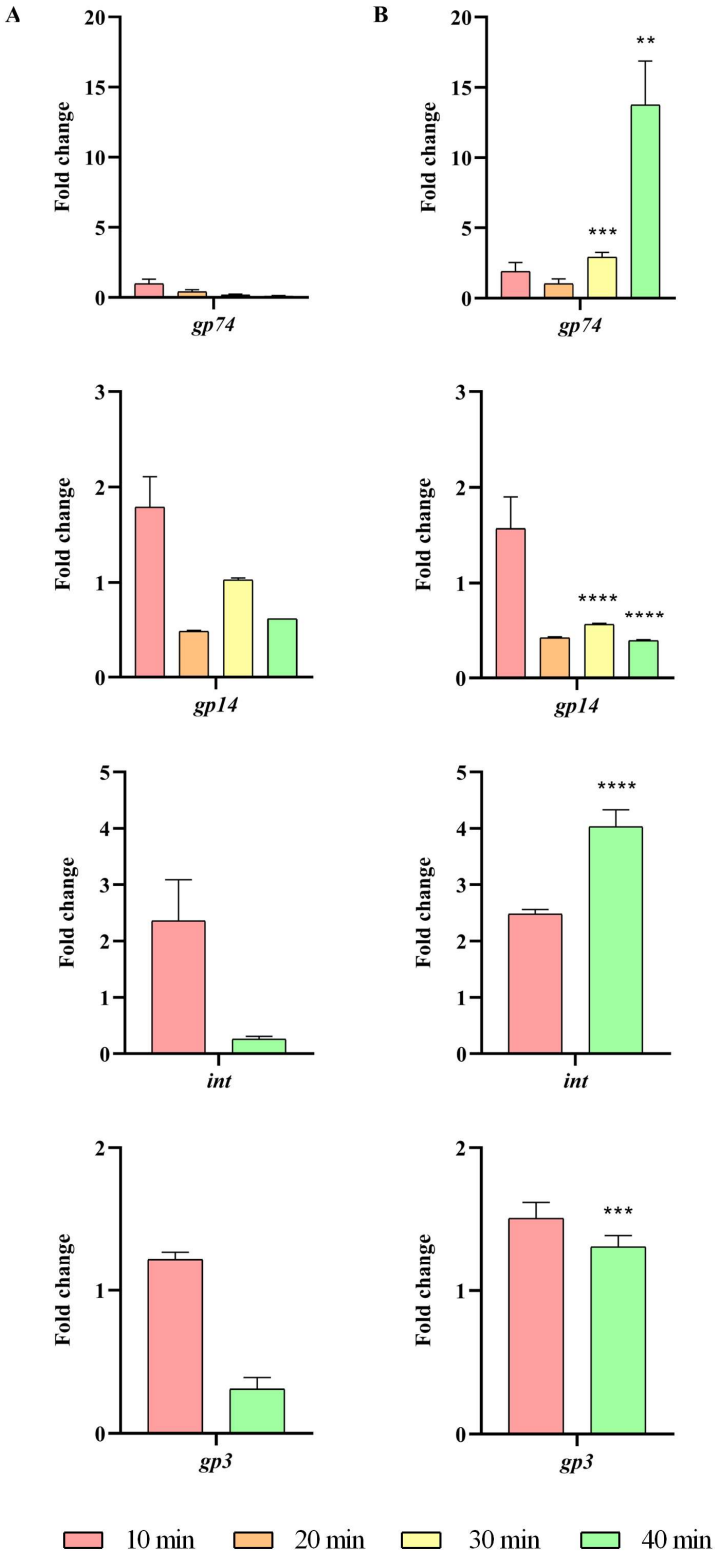


Figure 4.10 Expression levels of early UAB_Phi20 genes in the absence of *ibfA* (A) and in the presence of this gene (B) after phage adsorption. RT-qPCR quantification was performed using the E-method, with time 0 as a calibrator and 16S rRNA as the reference gene. The values represent the geometric mean and the standard deviation of the mean of three independent experiments performed in duplicate. ** $p < 0.01$, *** $p < 0.001$ and **** $p < 0.0001$.

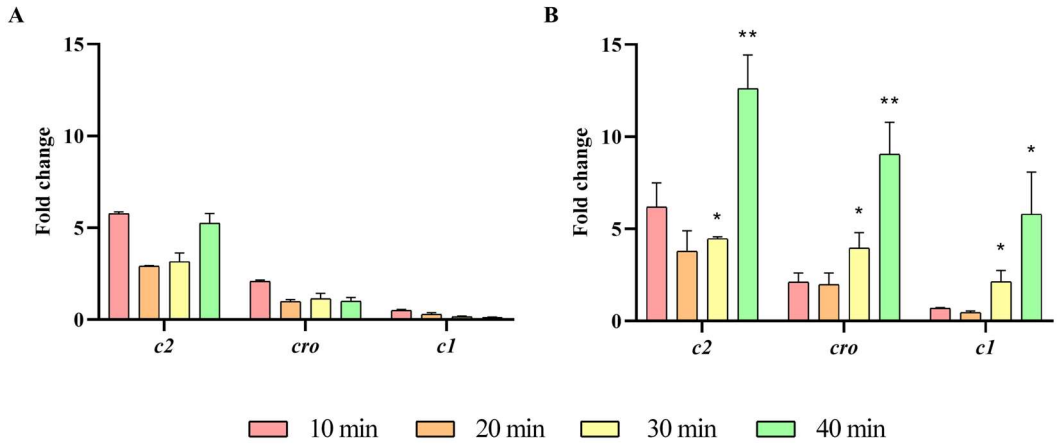


Figure 4.11 Expression of UAB_Phi20 *immC* region genes in absence of *ibfA* (A) and in the presence of this gene (B) after phage adsorption. RT-qPCR quantification was performed using the E-method, with time 0 as a calibrator and 16S rRNA as the reference gene. The values represent the geometric mean and the standard deviation of the mean of three independent experiments performed in duplicate. * $p < 0.05$ and ** $p < 0.01$.

Visualization of UAB_Phi20 virions by electron microscopy

The assembly of UAB_Phi20 virions in the presence and absence of *ibfA* gene was examined at an ultrastructural level using cellular thin sections observed through TEM. This was done after infection of synchronic cultures over time, as depicted in Figure 4.14. Initially, only a few bacteriophages were observed attached to both types of bacterial cells after phage adsorption (time 0). Intracellular virions were first detected in the absence of *ibfA* gene at 30 min. By 40 min, fully formed capsids were distinguishable inside the infected cells, albeit with a notable difference in the number of viral particles between the $ibfA^+$ and $ibfA^-$ strains (Table 4.3). Similarly, the percentage of sections containing virions relative to the total number of recorded sections was significantly lower in the presence of the *ibfA* gene (Table 4.3). These differences became more pronounced at 60 min, with the 88.8% of sections showing virions when the *ibfA* gene was absent, while the percentage remained low (3.6%) in its presence (Table 4.3). Furthermore, by 80 min, complete lysis of cells lacking the *ibfA* gene was evident, whereas barely any lysis could be observed in cells containing this gene (Figure 4.14).

Table 4.3 Mean of virions per cell section and percentage of cell sections with virions in the presence and absence of the *ibfA* gene.

	***ibfA* gene**	**40 min**	**60 min**	**80 min**
Mean of virions / cell section ± SD	-	31 ± 3.6	27 ± 3.7	28 ± 4.3
	+	16 ± 3.7	7 ± 3.5	7 ± 2.9
Percentage of cell sections with virions *vs.* total of recorded sections	-	32.9	88.8	8.5
	+	2.3	3.6	7.5

The values represent the mean and the standard deviation of 16 fields of 70 nm sections.

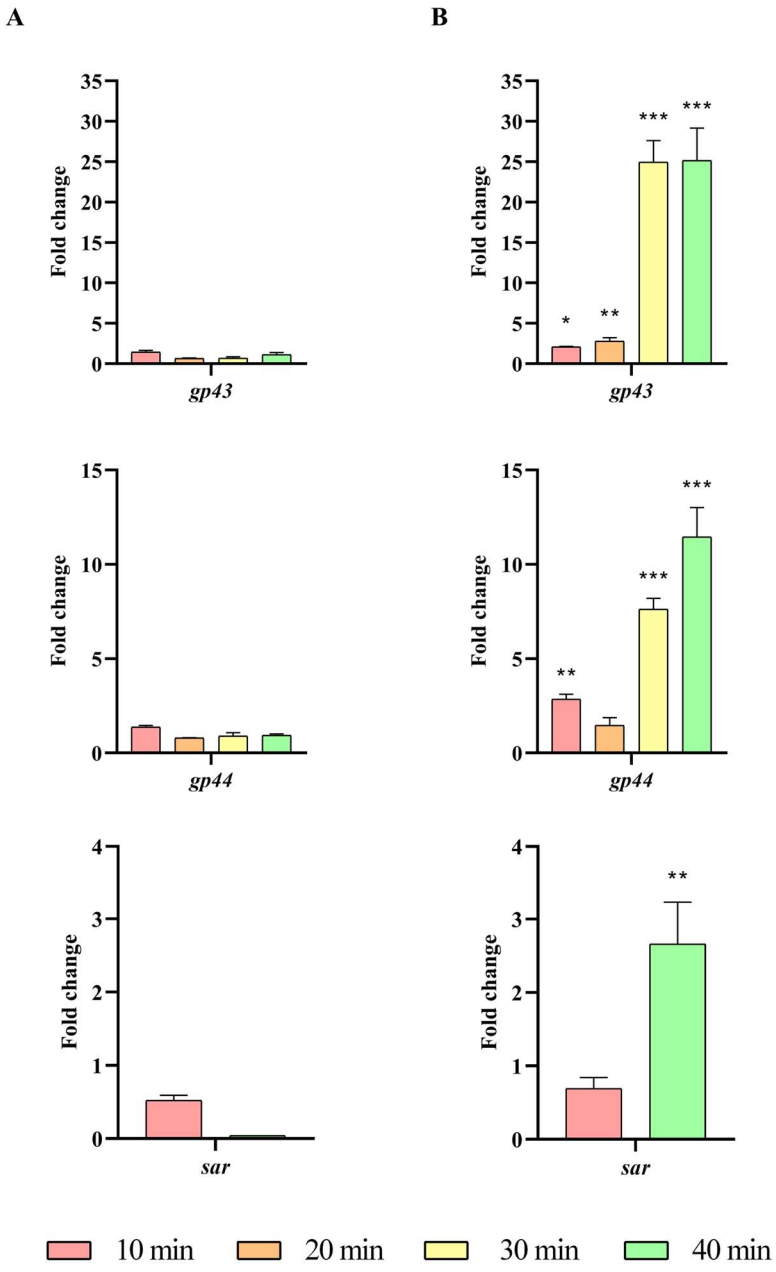


Figure 4.12 Expression of UAB_Phi20 *immI* region genes in absence of *ibfA* (A) and in presence of this gene (B) after phage adsorption. RT-qPCR quantification was performed using the E-method, with time 0 as a calibrator and 16S rRNA as the reference gene. The values represent the geometric mean and the standard deviation of the mean of three independent experiments performed in duplicate. * $p < 0.05$, ** $p < 0.01$ and *** $p < 0.001$.

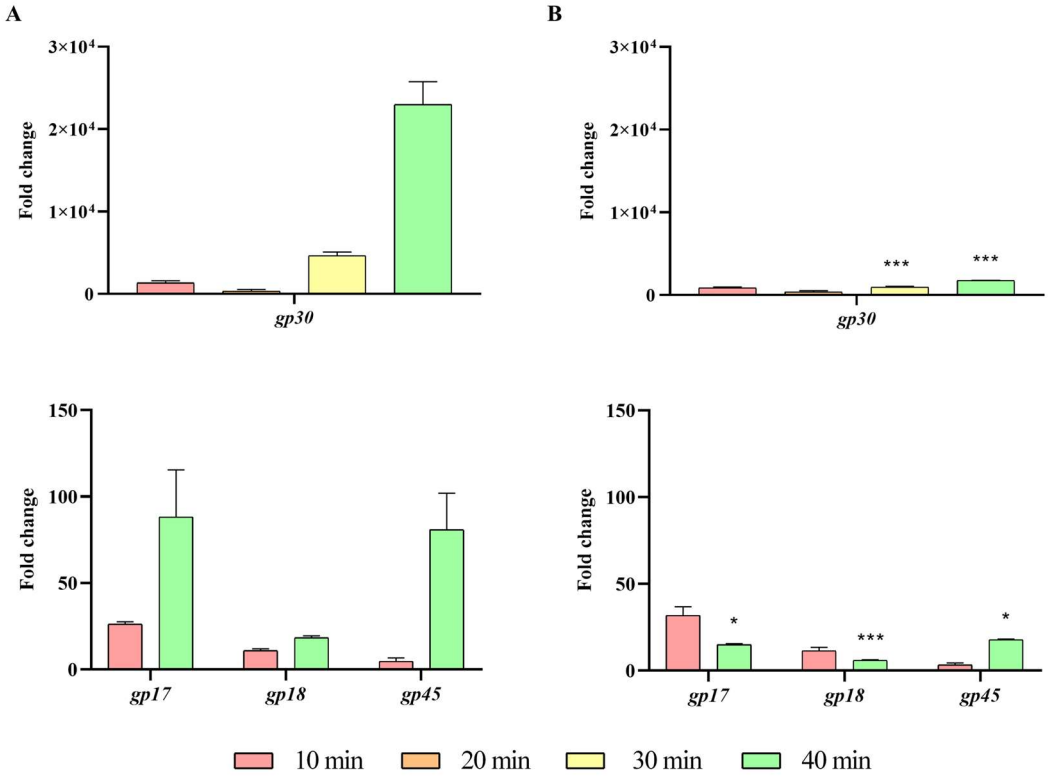


Figure 4.13 Expression levels of late UAB_Phi20 genes in absence of *ibfA* (A) and in the presence of this gene (B) after phage adsorption. RT-qPCR quantification was performed using the E-method, with time 0 as a calibrator and 16S rRNA as the reference gene. The values represent the geometric mean and the standard deviation of the mean of three independent experiments performed in duplicate. * $p < 0.05$ and *** $p < 0.001$.

Distribution of *ibfA*-related genes in prokaryotic genomes

The dissemination of *ibfA* among prokaryotic genomes was investigated through a BLASTP search of IbfA against the *nr* database, filtering results for an 85% query coverage, which yielded 2,416 hits. The identified proteins belonged exclusively to the *Enterobacteriaceae* family, with the majority originating from *Salmonella enterica* (1,388/2,416; 57.5%) and *Escherichia* (933/2,416; 38.6%). To ascertain whether IbfA homologues were also present outside *Enterobacteriaceae*, another BLASTP search was conducted against the *clustered nr* database, filtering results for 85% query coverage. This search yielded 214 hits that exhibited a much broader distribution across bacterial and archaeal phylogeny. Among these proteins, those identified in complete chromosome or plasmid sequences were selected (Figure 4.15). The analysis revealed that IbfA from pUA1135 clustered with IbfA from other *Enterobacteriaceae* species and was predominantly found amongst other plasmid-encoded IbfA homologues. Conversely, the majority of the IbfA homologues from other phylogenetic lineages were located within chromosomes.

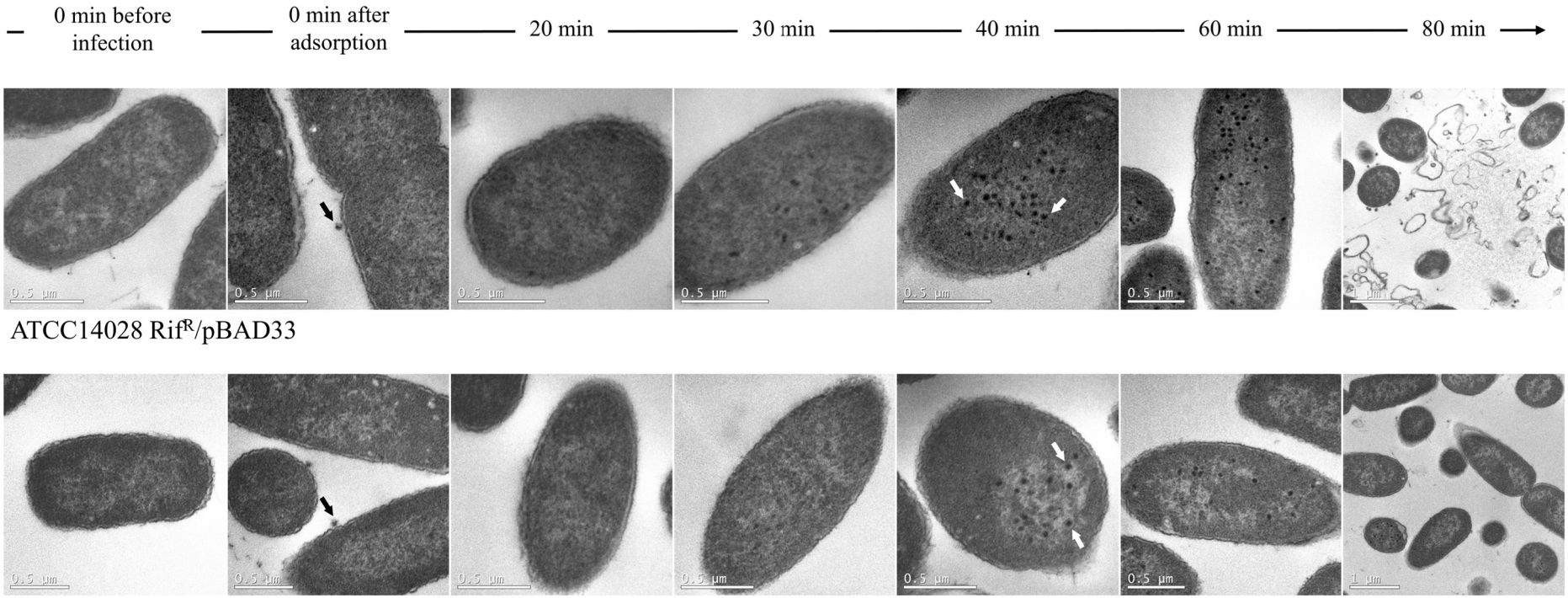


Figure 4.14 Transmission electron micrographs of ultrathin sections from ATCC14028 Rif^R/pBAD33 and ATCC14028 Rif^R/pBAD33::*ibfA* cells after infection with UAB_Phi20 phage at different times. Black and white arrows indicate adsorbed phages at time 0 min after adsorption, and fully formed capsids at 40 min, respectively. All image scales are 0.5 µm except at 80 min, where they are 1 µm.

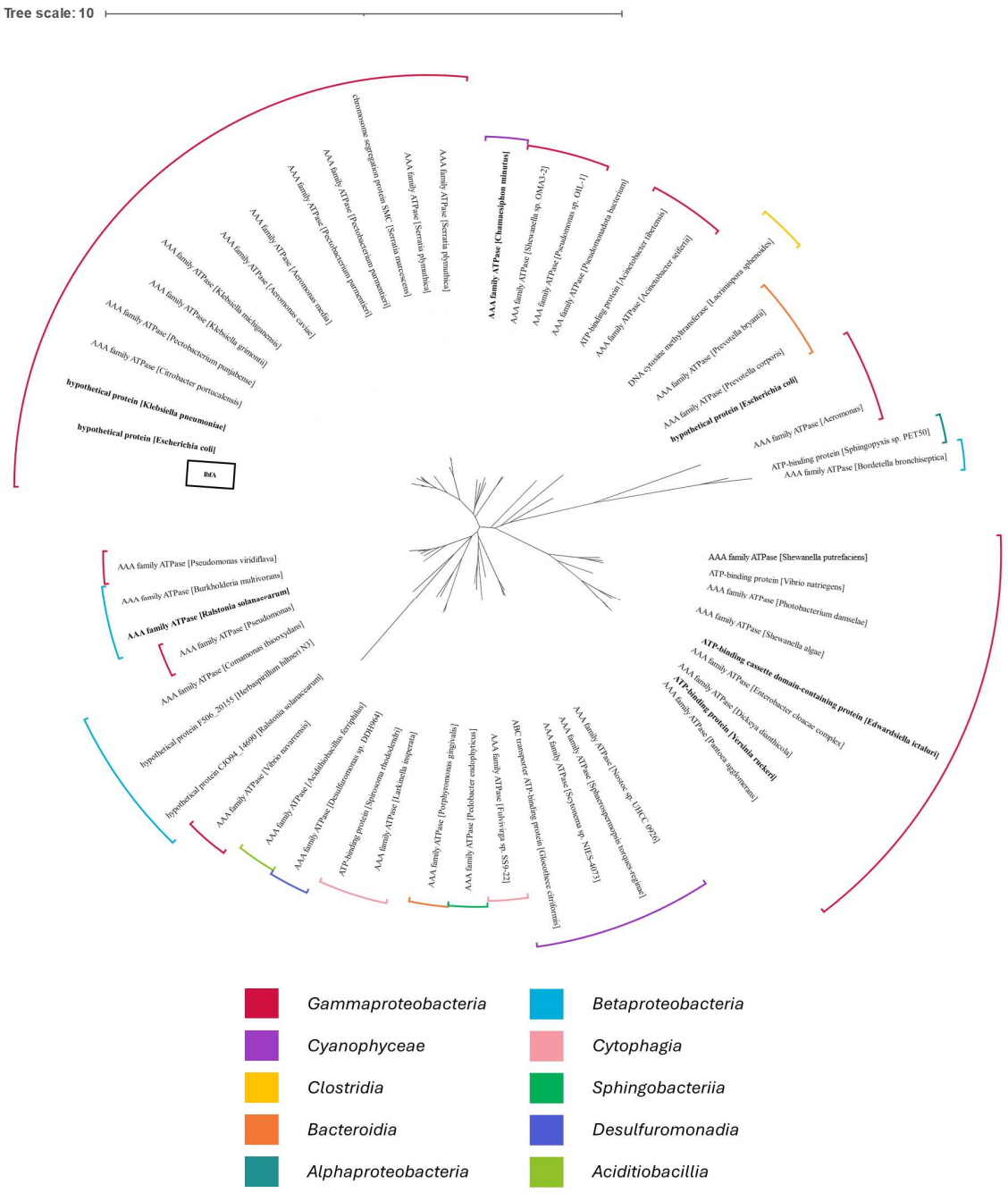


Figure 4.15 Phylogenetic tree of IbfA homologues in bacterial and archaeal complete plasmids (highlighted in bold) or chromosomes. IbfA protein is marked in a black square. Fifty-five different proteins were included in the tree. Tree scale indicates branch length.

4.4 Discussion

In our previous manuscript (López-Pérez *et al*., 2023), we identified large conjugative plasmids mediating bacteriophage interference mechanisms. These plasmids were found in *S.* Typhimurium ATCC14028 Rif^R variants isolated from a phage therapy study performed on broiler chickens experimentally contaminated and treated with a three-phage cocktail containing the UAB_Phi20, UAB_Phi78 and UAB_Phi87 phages. Among those variants was IC5, harbouring the IncI1α plasmid pUA1135, which was responsible for interference of the P22-like UAB_Phi20 bacteriophage. This prompted us to determine the gene or genes responsible for UAB_Phi20 interference and to elucidate the potential novel molecular mechanism behind it. In this study, we demonstrate that the *ibfA* gene, located on plasmid pUA1135, is accountable for interference of UAB_Phi20 and we describe the mechanism through which IbfA leads to this defence.

Defence systems are commonly encountered within mobile genetic elements, including conjugative plasmids (Koonin *et al*., 2020; Rocha and Bikard, 2022), and often within regions of high variability (Hochhauser *et al*., 2023). Our initial analysis of the pUA1135 sequence revealed the presence of a hypervariable region situated between *repA* and *parA* genes (Figure 4.2). Given its variability, we hypothesized that the segment of pUA1135 spanning from 2,000 bp to 18,500 bp positions could contain the gene or genes responsible for the mechanism of defence against UAB_Phi20. Indeed, deletion of a full transcriptional unit, comprising the *pUA1135_00003, ibfA*, *ydeA,* and *ydfA* genes (Figure 4.3) or solely the *ibfA* gene, led to the restoration of susceptibility to UAB_Phi20 in the IC5 variant (Table 4.3), underscoring the essential role of *ibfA* in UAB_Phi20 interference. It is notable that complementation of this gene did not fully reverse the interference with UAB_Phi20 (Table 4.4). We speculate that perhaps other gene(s) encoded in the pUA1135 plasmid, and located outside the *ibfA* transcriptional unit, could be necessary for the full function of *ibfA* in the interference phenotype of UAB_Phi20 or that the *ibfA* copy number is critical for achieving effective interference.

The *ibfA* gene identified in pUA1135 is homologous to the *ibfA* gene encoded in the R64 plasmid, an IncI1 incompatibility group plasmid that hinders infection by coliphages BF23, PhiI and λ, as well as *S*. Typhimurium phages P22 and St (Anderson and Lewis, 1965; Hughes and Meynell, 1977; Furuichi *et al*., 1984), and has more recently been associated to changes in phage type (Hiley *et al*., 2021). It must be noted that, although the ColIb plasmid harbours a gene annotated as *ibfA* (Uemura and Mizobuchi, 1982), this gene shares no sequence identity, neither at the gene nor at protein level, with *ibfA* from pUA1135. Furthermore, we found that *ibfA* is also homologous to the recently described HEC-04 defence system (Payne *et al*., 2024). The HEC systems, referred as Hma (Helicase, Methylase, ATPase)-embedded-candidate systems, are genes found between

Hma system genes, confirmed to confer phage resistance (Payne *et al*., 2021). More precisely, HEC-04 is an ABC ATPase protein fused to a TOPRIM domain that confers defence against *Escherichia coli* phages T4 and T5, albeit not against T7 or λ. Our bioinformatic analysis of the functional domains of the IbfA protein encoded in the pUA1135 plasmid showed that this protein contains both ATPase and TOPRIM domains. Several phage defence systems are known to operate through the association of ATPase and TOPRIM domains, as exemplified by the two-protein PARIS (Deep *et al*., 2024) and Gabija (Antine *et al*., 2024) systems. Furthermore, phage interference attributed to cellular ATP depletion has also been described (Rousset *et al*. 2023). In attention to this, we studied the effect of the *ibfA* gene on the ATP concentration in infected and non-infected cultures (Figure 4.8). Results showed that when infecting the parental strain culture with UAB_Phi20, the ATP concentration decreased due to the ATP-dependent processes involved in phage formation (Shim *et al*., 2021). However, this ATP consumption was not observed when infecting the *ibfA*$^{+}$ strain. This result indicated that IbfA did not function as an ATPase depleting cellular ATP. Furthermore, it suggested that phage particle formation processes were disrupted, as evidenced by the lower burst size of UAB_Phi20 when infecting cells carrying the *ibfA* gene (Figure 4.6).

IbfA clearly impacts the productivity of UAB_Phi20 infection, as evidenced by the reduced EOP, ECOI and plaque size, a behaviour also observed for the infection of P22 phage (data not shown). Lower productivity could result from an extended latent period or a decrease in burst size (Hyman and Abedon, 2010). Our results clearly showed that the latent and eclipse periods were not altered by the presence of *ibfA* gene (Figure 4.5). Instead, we observed a significant reduction in UAB_Phi20 burst size when infecting bacterial cells harbouring the *ibfA* gene (Figure 4.6). TEM imaging on cellular cross sections of infected cells corroborated that the number of observed infected cells and the number of viral particles assembled inside *ibfA*$^{+}$ cells was significantly lower than in the absence of this gene (Figure 4.14 and Table 4.3). In addition to the EOP, ECOI and burst size values, the infection kinetics of the UAB_Phi20 phage also pointed to an *ibfA*-mediated interference mechanism reminiscent of an abortive infection, because cellular viability decreased without observable cell lysis (Figure 4.6). In any case, interference with the UAB_Phi20 multiplicative cycle mediated by IbfA did not imply an increase in the transcription of *ibfA* due to phage infection. In fact, *ibfA* expression decreased significantly as early as 10 min in infected cells (Figure 4.7B) due to the effect of phage infection on the bacterial genome transcription (Shim *et al*., 2021). Despite this decrease, our results indicate that the intracellular concentration of IbfA protein must be sufficient to interfere with the UAB_Phi20 bacteriophage.

We also analysed if the *ibfA*-mediated interference affected replication or transcription of the phage genome in synchronic bacterial cultures. The quantification by qPCR of the UAB_Phi20 DNA inside and outside *Salmonella* cells, as well as *Salmonella* intracellular DNA, showed that

phage genome replication was evident during the initial 30 min after bacteriophage adsorption in cells that did not contain the *ibfA* gene (Figure 4.9A). After this, UAB_Phi20 DNA began to increase outside the cell (Figure 4.9A), coinciding with the observed latent period of the phage (Figure 4.5). In the presence of *ibfA*, UAB_Phi20 DNA inside *Salmonella* mirrored the pattern observed in the parental strain (Figure 4.9B), suggesting successful DNA injection and unaffected replication of UAB_Phi20 genome. However, extracellular phage DNA levels were approximately 1.5-$\log_{10}$ lower, agreeing with the reduced burst size of the phage in presence of *ibfA*, above commented.

The subsequent pivotal phase in the phage life cycle involves the transcription of its genes to orchestrate its cycle and facilitate the production of essential structural proteins for the assembly of new virions as well as proteins involved in cell lysis. The quantification by RT-qPCR of the expression of early (*gp74*, *int*, and *gp3*) genes, those that are in the *immC* region (*cro*, *c2* and *c1*), and those of the *immI* region (*gp43*, *gp44* and *sar*) demonstrated that their expression increases significantly at 30 min and 40 min in the presence of *ibfA* (Figure 4.10, 4.11 and 4.12), except for the *gp14* early gene, whose expression was significantly lower (Figure 4.10). This gene encodes for the late antitermination protein, which facilitates antitermination of the transcript generated from the P_{LATE} promoter (Susskind and Botstein, 1978) and is located at the end of the P_R transcript (Figure S4.1). Furthermore, it is negatively regulated by a small antisense RNA expressed from the P_{A23} promoter (Figure S4.1), which is in turn positively regulated by C1 (Ho *et al*., 1992). Consequently, the increased expression of the early gene *c1* at 30 and 40 min leads to a decreased expression of the late antiterminator. Additionally, the diminished expression of *gp14* will give rise to a reduced expression of the genes controlled by P_{LATE} (*gp30*, *gp17*, *gp18* and *gp45*; Figure S4.3) encoding phage structural and cellular lysis proteins, at 30 and 40 min as it was detected (Figure 4.13). These results correlate with the decreased burst size, the infection kinetics (Figure 4.6) and the almost inexistent lysis observed through TEM in *ibfA*$^+$ cells (Figure 4.14).

On the other hand, considering what has been described for phage P22 about the *immI* region (Botstein *et al*., 1975; Levine *et al*., 1975; Susskind and Botstein, 1975), we hypothesize that the significantly increased expression of the early genes in the presence of *ibfA* at 30 and 40 min post-adsorption must be related to the increase in the expression of the *ant* gene, which encodes the Ant antirepressor that inhibits C2, repressor of the lytic cycle (Susskind and Botstein, 1978). Regarding this, the genes of the *immI* region (*arc*, *ant* and *sar*) are all early genes. Both *arc* and *ant* genes are transcribed from the P_{ANT} promoter (Figure S4.2C), which is self-repressed by the Arc protein during the lytic cycle (Wu *et al*., 1987). Besides, both genes are also transcribed from the P_{LATE} promoter (Figure S4.2), but this transcription would be low in the presence of *ibfA* as it occurs for the other late genes. On the other hand, the *sar* gene encodes a small antisense RNA

transcribed from P_{sar} and inhibits *arc* translation from the P_{LATE} promoter (Susskind and Youderian, 1982; Wu *et al*., 1987). Therefore, we hypothesize that *ibfA* could be directly or indirectly hampering the function of the Arc protein. As a result, an intracellular increase of the antirepressor Ant would be expected and the equilibrium of C2 and Cro concentration, responsible for the control of lysis/lysogeny decision, would be disrupted, causing an increase in early gene expression from P_R and P_L. In fact, a similar phenotype has been previously described by the P22 phage (Susskind, 1980), where an Arc^- mutant underproduced late proteins and overproduced early proteins, though the author did not offer a definitive explanation for the observed phenotype. Obviously, the underexpression of the late proteins agrees with the characteristics commented in this work about the *ibfA*-mediated interference with the multiplicative cycle of the UAB_Phi20.

We have demonstrated that *ibfA* encodes a defence mechanism that interferes with UAB_Phi20 phage genome transcription, decreasing the expression of genes encoding virion structural proteins and those involved in cell lysis, giving rise to an abortive infection. This mechanism would be extensive to P22-type phages. Moreover, despite its unclear origin, we have found a widespread distribution of this gene among prokaryotic genomes, including chromosomes and plasmids (Figure 4.15). Therefore, we suggest that *ibfA* might possess additional functions unrelated to phage defence that would be beneficial for bacterial cells. Furthermore, its presence across a non-standard bacterial phylogeny suggests that *ibfA* may disseminate through bacterial populations via plasmids and has been integrated into bacterial chromosomes through diverse events of bacterial evolution.

References

1. Abby SS, Néron B, Ménager H, Touchon M, Rocha EPC. MacSyFinder: A program to mine genomes for molecular systems with an application to CRISPR-Cas systems. PLoS One. 2014;9(10):e110726.
2. Akritidou K, Thurtle-Schmidt BH. OLD family nuclease function across diverse anti-phage defense systems. Front Microbiol. 2023;14:1268820.
3. Anderson ES, Lewis MJ. Characterization of a transfer factor associated with drug resistance in *Salmonella* Typhimurium. Nature. 1965;208(5013):843–9.
4. Antine SP, Johnson AG, Mooney SE, Leavitt A, Mayer ML, Yirmiya E, *et al*. Structural basis of Gabija anti-phage defence and viral immune evasion. Nature. 2024;625(7994):360–5.
5. Bardina C, Spricigo DA, Cortés P, Llagostera M. Significance of the bacteriophage treatment schedule in reducing *Salmonella* colonization of poultry. Appl Environ Microbiol. 2012;78(18):6600–7.
6. Bardina C, Colom J, Spricigo DA, Otero J, Sánchez-Osuna M, Cortés P, *et al*. Genomics of three new bacteriophages useful in the biocontrol of *Salmonella*. Front Microbiol. 2016;7:545.
7. Bernheim A, Millman A, Ofir G, Meitav G, Avraham C, Shomar H, *et al*. Prokaryotic viperins produce diverse antiviral molecules. Nature. 2021;589(7840):120–4.
8. Bertozzi Silva J, Storms Z, Sauvageau D. Host receptors for bacteriophage adsorption. FEMS Microbiol Lett. 2016;363(4):fnw002.
9. Bondy-Denomy J, Qian J, Westra ER, Buckling A, Guttman DS, Davidson AR, *et al*. Prophages mediate defense against phage infection through diverse mechanisms. ISME J. 2016;10(12):2854–66.
10. Botstein D, Lew KK, Jarvik V, Swanson CA. Role of Antirepressor in the bipartite control of repression and immunity by bacteriophage P22. J Mol Biol. 1975;91(4):439–62.
11. Brandão A, Pires DP, Coppens L, Voet M, Lavigne R, Azeredo J. Differential transcription profiling of the phage LUZ19 infection process in different growth media. RNA Biol. 2021;18(11):1778–90.
12. Chevallereau A, Westra ER. Bacterial immunity: mobile genetic elements are hotspots for defence systems. Curr Biol. 2022;32(17):R923–6.
13. Chinenova TA, Mkrtumian NM, Lomovskaia ND. Genetic characteristics of a new phage resistance trait in *Streptomyces coelicolor* A3(2). Genetika. 1982;18(12):1945–52.
14. Cohen D, Melamed S, Millman A, Shulman G, Oppenheimer-Shaanan Y, Kacen A, *et al*. Cyclic GMP–AMP signalling protects bacteria against viral infection. Nature. 2019;574(7780):691–5.

15. Colom J, Cano-Sarabia M, Otero J, Cortés P, Maspoch D, Llagostera M. Liposome-encapsulated bacteriophages for enhanced oral phage therapy against *Salmonella* spp. Appl Environ Microbiol. 2015;81(14):4841–9.
16. Colom J, Cano-Sarabia M, Otero J, Aríñez-Soriano J, Cortés P, Maspoch D, *et al*. Microencapsulation with alginate/$CaCO_3$: A strategy for improved phage therapy. Sci Rep. 2017;7:41441.
17. Comeau AM, Hatfull GF, Krisch HM, Lindell D, Mann NH, Prangishvili D. Exploring the prokaryotic virosphere. Res Microbiol. 2008;159(5):306–13.
18. Coppens L, Wicke L, Lavigne R. SAPPHIRE.CNN: Implementation of dRNA-seq-driven, species-specific promoter prediction using convolutional neural networks. Comput Struct Biotechnol J. 2022;20:4969–74.
19. Darling AE, Mau B, Perna NT. ProgressiveMauve: Multiple genome alignment with gene gain, loss and rearrangement. PLoS One. 2010;5(6):e11147.
20. Datsenko KA, Wanner BL. One-step inactivation of chromosomal genes in *Escherichia coli* K-12 using PCR products. Proc Natl Acad Sci U S A. 2000;97(12):6640–5.
21. Deep A, Liang Q, Enustun E, Pogliano J, Corbett KD. Architecture and infection-sensing mechanism of the bacterial PARIS defense system. bioRxiv. 2024.
22. Doermann AH. The intracellular growth of bacteriophages. I. Liberation of intracellular bacteriophage T4 by premature lysis with another phage or with cyanide. J Gen Physiol. 1952;35(4):645–56.
23. Doron S, Melamed S, Ofir G, Leavitt A, Lopatina A, Keren M, *et al*. Systematic discovery of antiphage defense systems in the microbial pangenome. Science. 2018;359(6379):eaar4120.
24. Dot EW, Thomason LC, Chappie JS. Everything OLD is new again: How structural, functional, and bioinformatic advances have redefined a neglected nuclease family. Mol Microbiol. 2023;120(2):122–40.
25. Dy RL, Przybilski R, Semeijn K, Salmond GPC, Fineran PC. A widespread bacteriophage abortive infection system functions through a Type IV toxin-antitoxin mechanism. Nucleic Acids Res. 2014;42(7):4590–605.
26. Furuichi T, Komano T, Nisioka T. Physical and genetic analyses of the Inc-I alpha plasmid R64. J Bacteriol. 1984;158(3):997–1004.
27. Galperin MY, Makarova KS, Wolf YI, Koonin EV. Expanded microbial genome coverage and improved protein family annotation in the COG database. Nucleic Acids Res. 2015;43(Database issue):D261–9.
28. Gao L, Altae-Tran H, Böhning F, Makarova KS, Segel M, Schmid-Burgk JL, *et al*. Diverse enzymatic activities mediate antiviral immunity in prokaryotes. Science. 2020;369(6507):1077–84.

29. Gao Y, Luo X, Li P, Li Z, Ye F, Liu S, *et al*. Molecular basis of RADAR anti-phage supramolecular assemblies. Cell. 2023;186(5):999-1012.e20.
30. Georjon H, Bernheim A. The highly diverse antiphage defence systems of bacteria. Nat Rev Microbiol. 2023;21(10):686–700.
31. Goldfarb T, Sberro H, Weinstock E, Cohen O, Doron S, Charpak-Amikam Y, *et al*. BREX is a novel phage resistance system widespread in microbial genomes. EMBO J. 2015;34(2):169–83.
32. Hiley L, Graham RMA, Jennison AV. Characterisation of IncI1 plasmids associated with change of phage type in isolates of *Salmonella enterica* serovar Typhimurium. BMC Microbiol. 2021;21(1):92.
33. Hille F, Richter H, Wong SP, Bratovič M, Ressel S, Charpentier E. The biology of CRISPR-Cas: backward and forward. Cell. 2018;172(6):1239–59.
34. Ho YS, Pfarr D, Strickler J, Rosenberg M. Characterization of the transcription activator protein C1 of bacteriophage P22. J Biol Chem. 1992;267(20):14388–97.
35. Hochhauser D, Millman A, Sorek R. The defense island repertoire of the *Escherichia coli* pan-genome. PLoS Genet. 2023;19(4):e1010694.
36. Huerta-Cepas J, Szklarczyk D, Heller D, Hernández-Plaza A, Forslund SK, Cook H, *et al*. EggNOG 5.0: a hierarchical, functionally and phylogenetically annotated orthology resource based on 5090 organisms and 2502 viruses. Nucleic Acids Res. 2019;47(D1):D309–14.
37. Hughes V, Meynell GG. The contribution of plasmid and host genes to plasmid-mediated interference with phage growth. Genet Res. 1977;30(2):179–85.
38. Hyman P, Abedon ST. Bacteriophage Host Range and Bacterial Resistance. Adv Appl Microbiol. 2010:70:217–48.
39. Johnson AG, Wein T, Mayer ML, Duncan-Lowey B, Yirmiya E, Oppenheimer-Shaanan Y, *et al*. Bacterial gasdermins reveal an ancient mechanism of cell death. Science. 2022;375(6577):221–5.
40. Jumper J, Evans R, Pritzel A, Green T, Figurnov M, Ronneberger O, *et al*. Highly accurate protein structure prediction with AlphaFold. Nature. 2021;596(7873):583–9.
41. Khan Mirzaei M, Nilsson AS. Isolation of phages for phage therapy: a comparison of spot tests and efficiency of plating analyses for determination of host range and efficacy. PLoS One. 2015;10(3):e0118557.
42. Koonin EV, Makarova KS, Wolf YI, Krupovic M. Evolutionary entanglement of mobile genetic elements and host defence systems: guns for hire. Nat Rev Genet. 2020;21(2):119–31.
43. Kropinski AM. Measurement of the rate of attachment of bacteriophage to cells. Methods Mol Biol. 2009;501:151–5.

44. Kropinski AM. Practical advice on the one-step growth curve. Methods Mol Biol. 2018;1681:41–7.
45. Kutter E. Phage host range and efficiency of plating. Methods Mol Biol. 2009;501:141–9.
46. Larkin MA, Blackshields G, Brown NP, Chenna R, Mcgettigan PA, McWilliam H, *et al*. Clustal W and Clustal X version 2.0. Bioinformatics. 2007;23(21):2947–8.
47. Lee EJ, Groisman EA. Control of a *Salmonella* virulence locus by an ATP-sensing leader messenger RNA. Nature. 2012;486(7402):271–5.
48. Letunic I, Bork P. Interactive tree of life (iTOL) v5: An online tool for phylogenetic tree display and annotation. Nucleic Acids Res. 2021;49(W1):W293–6.
49. Levine M, Truesdell S, Ramakrishnan T, Bronson MJ. Dual Control of Lysogeny by Bacteriophage P22: An antirepressor locus and its controlling elements. J Mol Biol. 1975;91(4):421–38.
50. Lopatina A, Tal N, Sorek R. Abortive infection: bacterial suicide as an antiviral immune strategy. Annu Rev Virol. 2020;7(1):371–84.
51. López-Pérez J, Otero J, Sánchez-Osuna M, Erill I, Cortés P, Llagostera M. Impact of mutagenesis and lateral gene transfer processes in bacterial susceptibility to phage in food biocontrol and phage therapy. Front Cell Infect Microbiol. 2023;13:1266685.
52. Makarova KS, Wolf YI, van der Oost J, Koonin EV. Prokaryotic homologs of Argonaute proteins are predicted to function as key components of a novel system of defense against mobile genetic elements. Biol Direct. 2009;4:29.
53. Millman A, Bernheim A, Stokar-Avihail A, Fedorenko T, Voichek M, Leavitt A, *et al*. Bacterial retrons function in anti-phage defense. Cell. 2020;183(6):1551-1561.e12.
54. Millman A, Melamed S, Leavitt A, Doron S, Bernheim A, Hör J, *et al*. An expanded arsenal of immune systems that protect bacteria from phages. Cell Host Microbe. 2022;30(11):1556-1569.e5.
55. Minh BQ, Schmidt HA, Chernomor O, Schrempf D, Woodhams MD, Von Haeseler A, *et al*. IQ-TREE 2: new models and efficient methods for phylogenetic inference in the genomic era. Mol Biol Evol. 2020;37(5):1530–4.
56. Moineau S, Durmaz E, Pandian S, Klaenhammerl TR. Differentiation of two abortive mechanisms by using monoclonal antibodies directed toward lactococcal bacteriophage capsid proteins. Appl Environ Microbiol. 1993;59(1):208–12.
57. Notredame C, Higgins DG, Heringa J. T-coffee: a novel method for fast and accurate multiple sequence alignment. J Mol Biol. 2000;302(1):205–17.
58. Ofir G, Melamed S, Sberro H, Mukamel Z, Silverman S, Yaakov G, *et al*. DISARM is a widespread bacterial defence system with broad anti-phage activities. Nat Microbiol. 2018;3(1):90–8.

59. Ofir G, Herbst E, Baroz M, Cohen D, Millman A, Doron S, *et al*. Antiviral activity of bacterial TIR domains via immune signalling molecules. Nature. 2021;600(7887):116–20.
60. Parikka KJ, Le Romancer M, Wauters N, Jacquet S. Deciphering the virus-to-prokaryote ratio (VPR): insights into virus–host relationships in a variety of ecosystems. Biol Rev Camb Philos Soc. 2017;92(2):1081–100.
61. Payne LJ, Todeschini TC, Wu Y, Perry BJ, Ronson CW, Fineran PC, *et al*. Identification and classification of antiviral defence systems in bacteria and archaea with PADLOC reveals new system types. Nucleic Acids Res. 2021;49(19):10868–78.
62. Payne LJ, Meaden S, Mestre MR, Palmer C, Toro N, Fineran PC, *et al*. PADLOC: a web server for the identification of antiviral defence systems in microbial genomes. Nucleic Acids Res. 2022;50(W1):W541–50.
63. Payne LJ, Hughes TCD, Fineran PC, Jackson SA. New antiviral defences are genetically embedded within prokaryotic immune systems. bioRxiv. 2024.
64. Ritalahti KM, Amos BK, Sung Y, Wu Q, Koenigsberg SS, Löffler FE. Quantitative PCR targeting 16S rRNA and reductive dehalogenase genes simultaneously monitors multiple *Dehalococcoides* strains. Appl Environ Microbiol. 2006;72(4):2765–74.
65. Rocha EPC, Bikard D. Microbial defenses against mobile genetic elements and viruses: Who defends whom from what? PLoS Biol. 2022;20(1):e3001514.
66. Roche. LightCycler® 480 Instrument Operator's Manual. 2019.
67. Rousset F, Depardieu F, Miele S, Dowding J, Laval AL, Lieberman E, *et al*. Phages and their satellites encode hotspots of antiviral systems. Cell Host Microbe. 2022;30(5):740-753.e5.
68. Rousset F, Yirmiya E, Nesher S, Brandis A, Mehlman T, Itkin M, *et al*. A conserved family of immune effectors cleaves cellular ATP upon viral infection. Cell. 2023;186(17):3619-3631.e13.
69. Sambrook J, Russell D. Molecular Cloning: A Laboratory Manual. Cold Spring Harbor Protocols; 2001.
70. Sampei GI, Furuya N, Tachibana K, Saitou Y, Suzuki T, Mizobuchi K, *et al*. Complete genome sequence of the incompatibility group I1 plasmid R64. Plasmid. 2010;64(2):92–103.
71. Shim H, Shivram H, Lei S, Doudna JA, Banfield JF. Diverse ATPase proteins in mobilomes constitute a large potential sink for prokaryotic host ATP. Front Microbiol. 2021;12:691847.
72. Söding J. Protein homology detection by HMM-HMM comparison. Bioinformatics. 2005;21(7):951–60.
73. Solovyev V, Salamov A. Automatic annotation of microbial genomes and metagenomic sequences. In: Li RW (eds) Metagenomics and its applications in agriculture, biomedicine, and environmental studies. 2011.

74. Strunnikov AV. SMC complexes in bacterial chromosome condensation and segregation. Plasmid. 2006;55(2):135–44.
75. Susskind MM, Botstein D. Mechanism of action of *Salmonella* phage P22 Antirepressor. J Mol Biol. 1975;98(2):413–24.
76. Susskind MM, Botstein D. Molecular genetics of bacteriophage P22. Microbiol Rev. 1978;42(2):385–413.
77. Susskind MM. A new gene of bacteriophage P22 which regulates synthesis of antirepressor. J Mol Biol. 1980;138(4):685–713.
78. Susskind MM, Youderian P. Transcription *in vitro* of the bacteriophage P22 antirepressor gene. J Mol Biol. 1982;154(3):427–47.
79. Tatusov RL, Koonin EV, Lipman DJ. A genomic perspective on protein families. Science. 1997;278(5338):631–7.
80. Tellmann G. The E-Method: a highly accurate technique for gene-expression analysis. Nat Methods. 2006;3:i–ii.
81. Tesson F, Hervé A, Mordret E, Touchon M, D'Humières C, Cury J, *et al*. Systematic and quantitative view of the antiviral arsenal of prokaryotes. Nat Commun. 2022;13(1):2561.
82. Tock MR, Dryden DTF. The biology of restriction and anti-restriction. Curr Opin Microbiol. 2005;8(4):466–72.
83. Uemura H, Mizobuchi K. Inhibition of growth of bacteriophage BF23 by the ColIb plasmid: identification of the *ibfA* and *ibfB* genes of the ColIb plasmid. Molec Gen Genet. 1982;185:13–20.
84. Varadi M, Anyango S, Deshpande M, Nair S, Natassia C, Yordanova G, *et al*. AlphaFold protein structure database: massively expanding the structural coverage of protein-sequence space with high-accuracy models. Nucleic Acids Res. 2022;50(D1):D439–44.
85. Wu TH, Liao SM, McClure WR, Susskind MM. Control of gene expression in bacteriophage P22 by a small antisense RNA. II. Characterization of mutants defective in repression. Genes Dev. 1987;1(2):204–12.

Supplementary materials

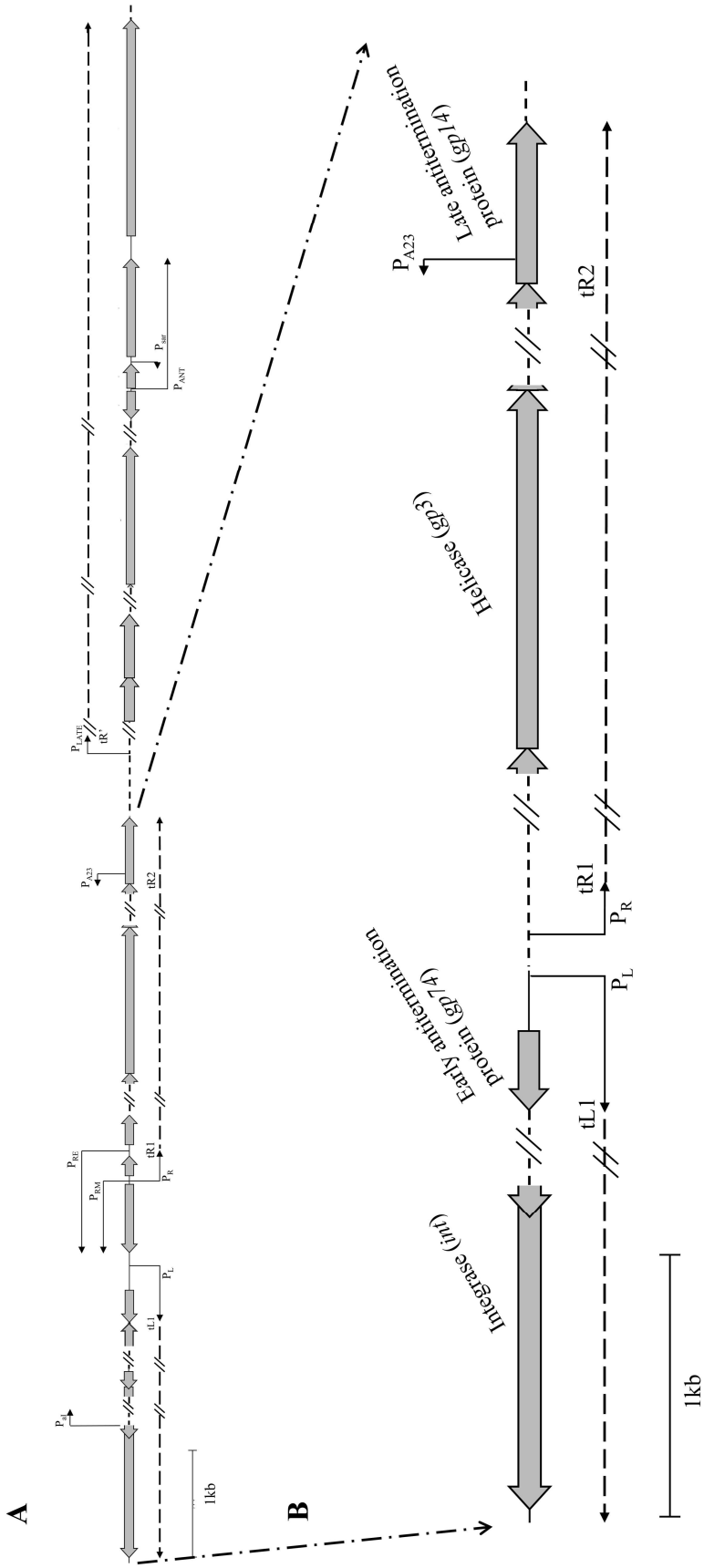


Figure S4.1 (A) Schematic representation of the genome of UAB_Phi20 phage. (B) Enlargement of the early genes controlled by P_L and P_R, whose transcription was studied through RT-qPCR.

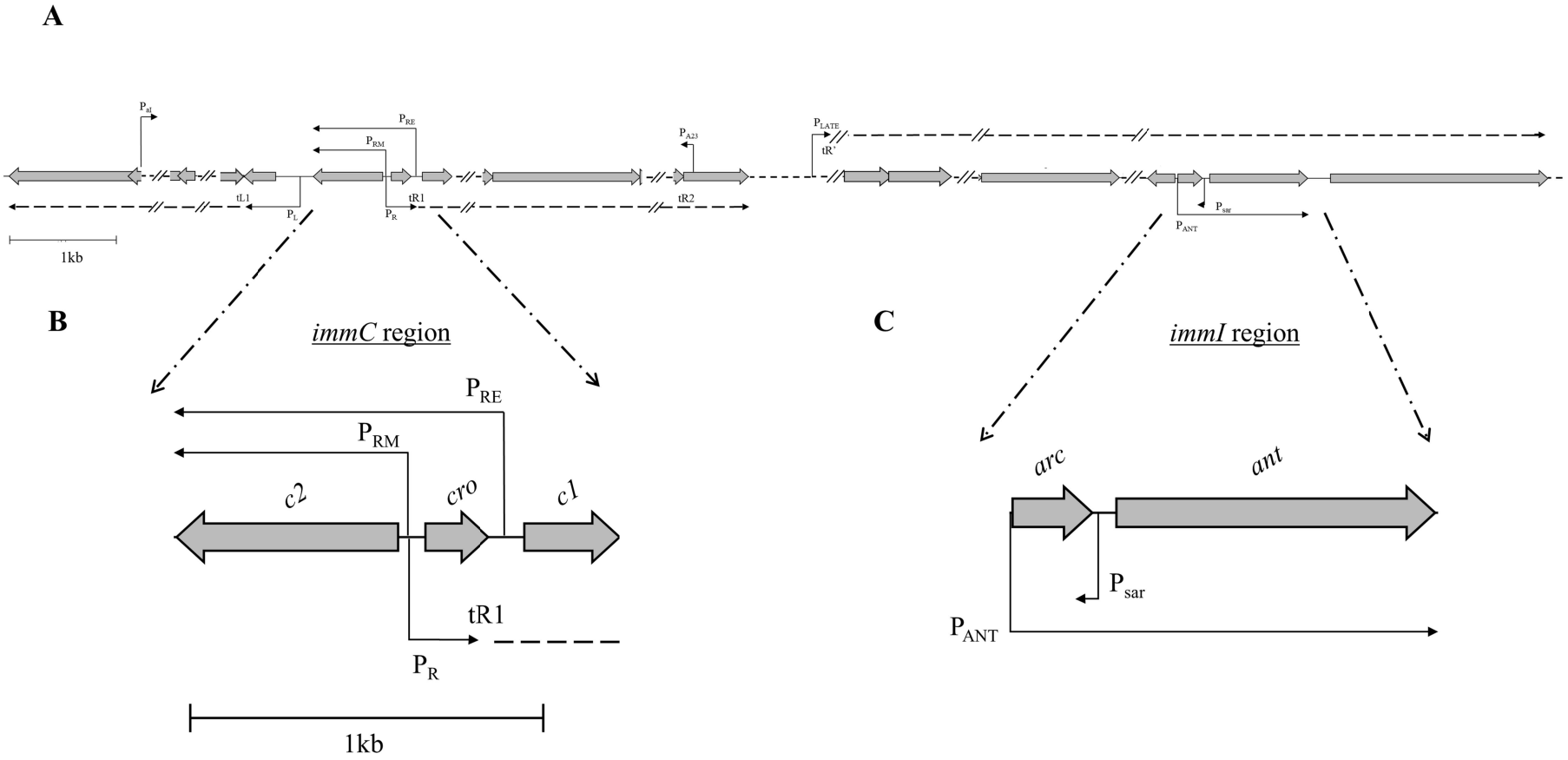


Figure S4.2 (A) Schematic representation of the genome of UAB_Phi20 phage. Enlargement of the *immC* (B) and of the *immI* (C) regions, whose transcription was studied through RT-qPCR.

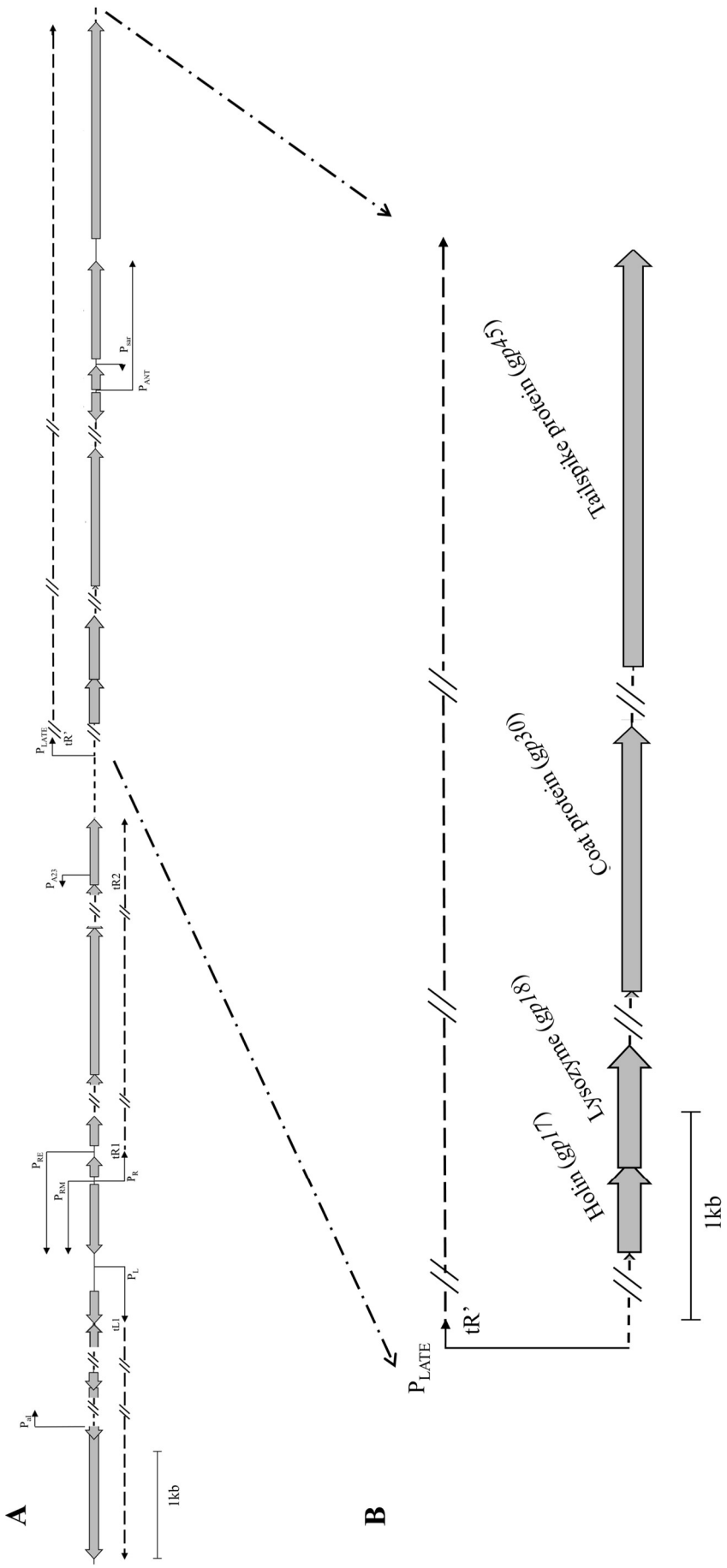


Figure S4.3 (A) Schematic representation of the genome of UAB_Phi20 phage. (B) Enlargement of the late genes controlled by P_{LATE}, whose transcription was studied through RT-qPCR.

Table S4.1 Strains and plasmids used in this study.

Strain	**Relevant characteristics**	**Source or reference**
ATCC14028 Rif^R	*S.* Typhimurium; Rif^R	This research group
DH5α	*E. coli supE4 ΔlacU169* (φ80 Δ*lacZ* Δ*M15*) *hsdR17, recA1, endA1, gyrA96, thi-1, relA1*	Clontech
IC5	ATCC14028 Rif^R variant; Amp^R	López-Pérez *et al*., 2023
ATCC14028 Rif^R pBAD33	*S.* Typhimurium with pBAD33 vector; Rif^R, Cm^R	This work
ATCC14028 Rif^R pBAD33::*ibfA*	*S.* Typhimurium with pBAD33 vector containing *ibfA* gene cloned with its own promoter; Rif^R, Cm^R	This work
Plasmid	**Relevant characteristics**	**Source or reference**
pKD4	Amp^R Km^R	Datsenko and Warner, 2000
pKOBEG	Vector containing the λ-Red recombinase system, Cm^R, thermosensitive	Generous gift of Prof. I. Lasa; Chaveroche *et al*., 2000
pBAD33	Low copy number vector containing the arabinose inducible pBAD promoter, Cm^R	Guzman *et al*., 1995
pBAD33::*ibfA*	pBAD33 derivative containing the *ibfA* gene cloned under the control of its own promoter, Cm^R	This work
pBAD33::*pUA1135_00003, ibfA, ydeA, ydfA*	pBAD33 derivative containing the *ibfA*-containing transcriptional unit cloned under the control of its own promoter, Cm^R	

Amp, ampicillin; Cm, chloramphenicol; Km, kanamycin; Rif, rifampicin; R, resistant.

Table S4.2 Primers used in this work.

Name	Sequence (5'-3')	Application
ibfA_km_p1.2[a]	TTTCTGAATTACATGGTGAATTCCCCCAACATAATGCTAGG ATTTAAAAATG*gtgtaggctggagctgcttc*	PCR of Km gene from pKD4 plasmid with homology regions of the *ibfA* gene
ibfA_km_p2[a]	TATTTGCTCATTCGGGATGGTTGGATATTTTAAGTTATATCT ACTGTATC*atgggaattagccatggtcc*	
ibfA_ext_fw2	GAGGTTCGCGTACAGATAA	PCR and sequencing to check the Km insertion into the *ibfA* gene.
ibfA_ext_rv2	CCATCTTTACCGTCTCTGAA	
UT_km_p1[a]	CTTCACAATGAATATCATTGTGTTGGTAACCTGCTGTTATCG TGATGAAA*gtgtaggctggagctgcttc*	PCR of Km gene from pKD4 plasmid with homology regions of the *ibfA*-containing transcriptional unit.
UT_km_p2[a]	ACATGATATGATTTTTACCTGTCAGAACATTATCAGATGGA GCGTGCAGG*atgggaattagccatggtcc*	
UT_ext_fw	GTACTTGCCACAGCAGGT	PCR and sequencing to check the Km insertion into the *ibfA*-containing transcriptional unit.
UT_ext_rv	TGTGCTAACGGCATGTATTAC	
00003_ibfA_fw	ATAATGATGGGTGTTTTCTTTTCT	Primers used in RT-PCR to determine the formation of a transcriptional unit.
00003_ibfA_rv	AGCCCGTAGTTTCTGATTT	
ibfA_ydeA_fw	CTTGACCAGTAATAGTTTTT	
ibfA_ydeA_rv	CGCGTACAGATAAATGAAA	
ydeA_ydfA_fw	GGCATCCTCCAGACGAC	
ydeA_ydfA_rv	TGAATGCCATAAAGAGACAG	
ibfA_P1_pBAD33_fw[b]	*agcgaattcgagctcggtac*TTAAGTTATATCTACTGTATCATTCTCAG GTAATCGTTC	PCR of *ibfA* gene from pUA1135 plasmid used to clone this gene into pBAD33 vector under the control of its own promoter.
ibfA_P1_pBAD33_rv[b]	*tctagaggatccccgggtac*GAACACGCCTGTGCACGG	
pUA1135-Big4_pBAD33_f[b]	*gctcggtacccggggatcctctagagtcgacctg*GAAAGGAATACTTCACAAT GAATATCATTG	PCR of *ibfA*-containing transcriptional unit from pUA1135 plasmid used to clone into pBAD33 vector under the control of its own promoter.
pUA1135-Big4_pBAD33_r[b]	*cttctctcatccgccaaaacagccaagcttgcatgcctg*CCTATTATCTCCGTGTT AGCCG	

Table S4.2 (continued).

Name	Sequence (5'-3')	Application
pBAD_F	ATGCCATAGCATTTTTATCC	PCR and sequencing to check the introduction of *ibfA* or the *ibfA*-containing transcriptional unit in pBAD33 vector
pBAD_R	CCTGATACAGATTAAATCAG	
sec_ibfA_P1_1	GCAGCTTCAAACGCATTCA	
sec_ibfA_P1_2	CACGAATAAGTGTACTGGCA	
sec_ibfA_P1_3	CGGCAGTGACTTCATTGT	
sec_ibfA_P1_4	CTCGAACATCAGCTTTTCCA	
gyrBupRT	GTTTTTGCGACAGAGCGTTGAC	Quantification of ATCC14028 Rif^R *gyrB* through qPCR
gyrBdwRT	ACATGGTATTCGAGGTGGTAGA	
16SRNAupSa	CACATGCAAGTCGAACGGTAAC	Quantification of ATCC14028 Rif^R 16S rRNA through RT-qPCR
16SRNAdwSa	AGTGTGGCTGGTCATCCTCTCA	
ibfA_P1_RT_fw	TCACCGGCACAGAATCAC	Quantification of ATCC14028 Rif^R pBAD33::*ibfA* *ibfA* gene through RT-qPCR
ibfA_P1_RT_rv	TCCACCCAATCCGTCCAGT	
Phi20_gp03_RT_fw	CCGGCGCAGGAATGATGTC	Quantification of UAB_Phi20 helicase through qPCR and RT-qPCR
Phi20_gp03_RT_rv	CGTTCCGCTTTTGGTTTCTC	
Phi20_gp17_RT_fw	CATGATGGCGGCAAAGGAAC	Quantification of UAB_Phi20 holin expression through RT-qPCR
Phi20_gp17_RT_rv	TCTGTGCCGATGTAGCCGATAAAC	
Phi20_gp18_RT_fw	AGCAGGGGGATACCAACCAT	Quantification of UAB_Phi20 lysozyme expression through RT-qPCR
Phi20_gp18_RT_rv	CGGGACGCGAACAAGACTAC	
Phi20_gp30_RT_fw2	GAAACCATCTCCGCAATCAC	Quantification of UAB_Phi20 coat protein expression through RT-qPCR
Phi20_gp30_RT_rv2	GCAGTCTCGTCTCGCAAGTC	
Phi20_gp45_RT_fw	CAGCGGTCGTTGCCACTTT	Quantification of UAB_Phi20 tailspike protein expression through RT-qPCR
Phi20_gp45_RT_rv	GACCGCTAGCCCGATGAACT	
Phi20_gp14_RT_fw	GGGAATGGCGCAATCACAAG	Quantification of UAB_Phi20 late transcription antitermination protein expression through RT-qPCR
Phi20_gp14_RT_rv	CGCGGCACTACGGCAATAAT	
Phi20_gp74_RT_fw	CCATAGAGCGCGACACCATC	Quantification of UAB_Phi20 early transcription antitermination protein expression through RT-qPCR
Phi20_gp74_RT_rv	CCTCCTTCAACTTCCTTCTG	
Phi20_gp43_RT_fw	CCACGGTGGACCTGTATTGT	Quantification of UAB_Phi20 *arc* expression through RT-qPCR
Phi20_gp43_RT_rv	CAATGCGCCCTTCCTTCTTA	

Table S4.2 (continued).

Name	Sequence (5'-3')	Application
Phi20_gp44_RT_fw	ACCGCTGGCCGTAGAGTA	Quantification of UAB_Phi20 antirepressor *ant* expression through RT-qPCR
Phi20_gp44_RT_rv	GAATTCATGGCCGTAGTCGT	
Phi20_sar_RT_fw	GTGTTAACTGCTTCTAAAATTGCTA	Quantification of UAB_Phi20 *sar* expression through RT-qPCR
Phi20_sar_RT_rv	GAAGCCCCAACTGCGGTAAC	
Phi20_gp77_RT_fw	ATTAGCGATGCAGCGGTCTC	Quantification of UAB_Phi20 *cro* expression through RT-qPCR
Phi20_gp77_RT_rv	CTTGGCGATAAGCGTTTTCTTG	
Phi20_gp51_RT_fw	CCGGCTTAGGCTTGAATACC	Quantification of UAB_Phi20 integrase expression through RT-qPCR
Phi20_gp51_RT_rv	AGAAGGCGCATAAGAAGTCG	
Phi20_C1_RT_fw	ACGCAATTACCAGCAGCATC	Quantification of UAB_Phi20 *c1* expression through RT-qPCR
Phi20_C1_RT_rv	ATCCTCGACACCCCACTC	
Phi20_C2_RT_fw	GAATGTGGCCTCGTTTTCAC	Quantification of UAB_Phi20 *c2* expression through RT-qPCR
Phi20_C2_RT_rv	TAAGCGCAGGGCAATGGAT	

[a]P1 and P2 sequences, homologues to the pKD4 plasmid, are represented in lower case italics; [b]Homology sequences to pBAD33 are represented in lower case italics.

Table S4.3 List of COGs from the variable region of homologues of the pUA1135 plasmid.

COG	COG annotation	Number of plasmids that contain this COG in their variable region*
COG3316	Transposase (or an inactivated derivative)	44
COG4974	Site-specific recombinase XerD	22
COG3109	sRNA-binding protein	15
COG1192	Cellulose biosynthesis protein BcsQ	14
COG4637	Predicted ATPase	14
COG4271	Predicted nucleotide-binding protein containing TIR -like domain	12
COG2367	Beta-lactamase class A	10
COG2814	Predicted arabinose efflux permease, MFS family	7
COG0030	16S rRNA A1518 and A1519 N6-dimethyltransferase RsmA/KsgA/DIM1 (may also have DNA glycosylase/AP lyase activity)	6
COG3039	Transposase and inactivated derivatives, IS5 family	6
COG0294	Dihydropteroate synthase	5
COG0459	Chaperonin GroEL (HSP60 family)	5
COG1662	Transposase and inactivated derivatives, IS1 family	5
COG0262	Dihydrofolate reductase	4
COG0270	Site-specific DNA-cytosine methylase	4
COG0645	Predicted kinase	4
COG0840	Methyl-accepting chemotaxis protein	4
COG1309	DNA-binding transcriptional regulator, AcrR family	4
COG2076	Multidrug transporter EmrE and related cation transporters	4
COG2746	Aminoglycoside N3'-acetyltransferase	4
COG3385	IS4 transposase	4
COG4644	Transposase and inactivated derivatives, TnpA family	4
COG0399	dTDP-4-amino-4,6-dideoxygalactose transaminase	3
COG1961	Site-specific DNA recombinase related to the DNA invertase Pin	3
COG3173	Predicted kinase, aminoglycoside phosphotransferase (APT) family	3
COG3843	Type IV secretory pathway, VirD2 components (relaxase)	3
COG0480	Translation elongation factor EF-G, a GTPase	2
COG0583	DNA-binding transcriptional regulator, LysR family	2
COG1357	Uncharacterized protein YjbI, contains pentapeptide repeats	2
COG1670	Protein N-acetyltransferase, RimJ/RimL family	2
COG2801	Transposase InsO and inactivated derivatives	2
COG3231	Aminoglycoside phosphotransferase	2
COG3547	Transposase	2

Table S4.3 (continued)

COG	COG annotation	Number of plasmids that contain this COG in their variable region*
COG3570	Streptomycin 6-kinase	2
COG4584	Transposase	2
COG0110	Acetyltransferase (isoleucine patch superfamily)	1
COG0491	Glyoxylase or a related metal-dependent hydrolase, beta-lactamase superfamily II	1
COG0491	Glyoxylase or a related metal-dependent hydrolase, beta-lactamase superfamily II	1
COG0640	DNA-binding transcriptional regulator, ArsR family	1
COG0768	Cell division protein FtsI/penicillin-binding protein 2	1
COG0786	Na+/glutamate symporter	1
COG1476	DNA-binding transcriptional regulator, XRE-family HTH domain	1
COG1484	DNA replication protein DnaC	1
COG1695	DNA-binding transcriptional regulator, PadR family	1
COG1708	Predicted nucleotidyltransferase	1
COG1715	Restriction endonuclease Mrr	1
COG2059	Chromate transport protein ChrA	1
COG2329	Heme-degrading monooxygenase HmoA and related ABM domain proteins	1
COG4747	Uncharacterized conserved protein, contains tandem ACT domains	1
COG4875	Uncharacterized protein	1
COG4977	Transcriptional regulator GlxA family, contains an amidase domain and an AraC-type DNA-binding HTH domain	1

*, only hits with an e-value of less than 1E-5 were considered.

5. DISCUSSION

One of the most critical public health challenges of the 21st century is the emergence of antimicrobial resistance (AMR) and its rapid dissemination, driven largely by the abuse and misuse of antibiotics in human and veterinary medicine, as well as in agriculture. In fact, it is predicted that antimicrobial resistance could cause around 10 million deaths worldwide by 2050 (Sugden *et al*., 2016). Hence, combating antibiotic resistance is a global concern and the development of novel strategies to combat bacterial infections is a pressing matter. While the emergence of AMR is a natural phenomenon that cannot be fully eradicated, there are several actions that can be undertaken to mitigate its rapid proliferation. These include promoting the judicious use of antibiotics, implementing better waste management practices in drug manufacturing to minimize environmental contamination, raising awareness among the worldwide population, improving regulatory policies to curb the overuse of antibiotics, and exploring alternative treatment options against bacterial infections. Several non-antibiotic strategies have been proposed as alternatives to combat antimicrobial-resistant pathogens (Ghosh *et al*., 2019), including bacteriocins, antimicrobial peptides, faecal microbiota transplants, CRISPR/Cas9 techniques, and, most notably, phage therapy. Bacteriophages have been used in both human and veterinary medicine, as well as in the food industry. In fact, the number of studies related to phage therapy in these fields has increased exponentially in recent years (Loponte *et al*., 2021; Pirnay *et al*., 2022; Imran *et al*., 2023), with promising outcomes.

Regarding the animal husbandry industry, phage therapy serves not only to safeguard animal health and productivity, but also to mitigate the prevalence of foodborne pathogens, as farm animals often serve as significant reservoirs for bacterial pathogens such as *Salmonella*, *Campylobacter* or *E. coli* (Ali and Alsayeqh, 2022). Numerous *in vitro* and *in vivo* animal studies have evaluated the efficacy of phages against these pathogens, among others, yielding promising results (Ferriol-González and Domingo-Calap, 2021; Loponte *et al*., 2021). In the case of *Salmonella* in poultry, which is the subject of this thesis, several studies have evaluated the efficacy of phages and phage cocktails against this pathogen (Loponte *et al*., 2021; Thanki *et al*., 2021; Imran *et al*., 2023; Khan and Rahman, 2022). All this research demonstrates that phages are a highly capable solution for *Salmonella* treatment in poultry.

The properties of bacteriophages make phage therapy a promising alternative to antibiotics. Phages exhibit host-specificity, thereby not affecting the surrounding microbiota (Gordillo Altamirano and Barr, 2019; de Jonge *et al*., 2019). Furthermore, low dosages of phages are needed to treat bacterial infection due to their capacity to auto-replicate inside their host. While phages are still commonly used to treat human bacterial infections in ex-Soviet countries such as Russia and Georgia, their use in Western medicine as a routine therapeutic approach raises numerous inquiries within regulatory agencies and in society at large. Nonetheless, there have been several instances of phage therapy use in compassionate cases (Dedrick *et al*., 2023; Onallah *et al*., 2023)

and both the European Medicines Agency (EMA) and the European Pharmacopoeia have recently released guidelines for the use of phages in human and veterinary medicine (© Council of Europe, 2024; European Medicines Agency, 2023a; European Medicines Agency, 2023b). Several crucial aspects regarding the biology of phages and phage therapy need to be addressed to ensure the safe therapeutic application of phages (Górski *et al*., 2018). These include the selection of appropriate bacteriophages and delivery routes for specific types of bacterial infections, their innocuousness to human health and the environment, and the emergence of resistance against the bacteriophages used in therapy. The latter aspect is particularly significant to avert repeating history and to prevent future problems like those encountered with antibiotics, underscoring the importance of investigating the molecular mechanisms underlying this resistance (Levin and Bull, 2004; Oechslin, 2018). In fact, phage resistance and interference have been documented at virtually every step of a phage's lytic life cycle. Among the most commonly cited causes of resistance *in vitro* is the mutation or loss of the phage receptor (Pereira *et al*., 2016; Oechslin *et al*., 2017; Bai *et al*., 2019; Wright *et al*., 2019), resulting in the inability of the phage to adsorb to the bacterial surface. Phage resistance has also been observed in numerous *in vivo* studies (Maura and Debarbieux, 2012; Schooley *et al*., 2017; Oechslin, 2018; De Sordi *et al*., 2019; Hernandez and Koskella, 2019; McCallin and Oechslin, 2019; Salazar *et al*., 2021), although the cause of resistance is only occasionally investigated and is typically attributed to changes in the phage receptor (Schooley *et al*., 2017). Apart from phage resistance due to inability of the phage to infect its host, an increasing number of studies describe mechanisms of interference with the multiplicative cycle of the phage (Georjon and Bernheim, 2023), wherein phage DNA injection or replication, protein production, virion assembly, or even cell lysis can be affected. In these cases, phage infection may initiate, but these mechanisms interfere with the phage multiplicative cycle, impeding or decreasing the production of new viable phage progeny.

Considering the importance of phages as an imminent therapeutic option against bacterial infections, this thesis aimed to identify the phage resistance or interference mechanisms that emerge during oral phage therapy in the model *Salmonella* / phage cocktail / broilers.

The present work first investigated a collection of seven *Salmonella* variants obtained in a prior study by our research group (Otero J, 2019), which demonstrated reduced susceptibility to either two or all three phages from a cocktail (UAB_Phi20, UAB_Phi78, and UAB_Phi87) used in an oral phage therapy experiment to treat *Salmonella*-infected broilers (Table 3.6). The LPS electrophoretic profiles of these variants revealed no significant differences from the parental sensitive strain, and no mutations associated with known bacterial resistance mechanisms to phages, including genes linked to LPS biosynthesis, were detected in their genomes (Otero J, 2019). These data indicated that the reduced susceptibility to the phages did not stem from an LPS alteration, which is the receptor of the three phages, suggesting that the phages infected the

Salmonella variants but encountered some interference mechanism with the phage lytic cycle. Furthermore, in agreement with these findings, data on the adsorption of UAB_Phi78 and UAB_Phi20 phages onto bacterial surfaces (Table 3.7) confirmed their ability to adsorb, with observed *K* values similar to the parental sensitive strain. However, phage UAB_Phi87 exhibited inefficient adsorption onto these variants, suggesting potential phage interference in adsorption mechanisms independent of LPS.

To delve deeper into the interference phenotype of the three bacteriophages, the EOP, ECOI, and burst size parameters for UAB_Phi20, UAB_Phi78 and UAB_Phi87 were determined across all seven variants. These parameters serve as crucial metrics for studying specific phage characteristics. EOP calculations compare phage titres on the experimental bacterial host versus fully susceptible hosts, with EOP values indicating production levels. EOP $\geqslant 0.5$ indicates a high production, $0.1 \leqslant \text{EOP} < 0.5$ a medium production, $0.001 \leqslant \text{EOP} < 0.1$ a low production and an EOP $\leqslant 0.001$ no production (Khan Mirzaei and Nilsson, 2015). In an ECOI assay (Moineau *et al*., 1993; Abedon, 2018), the phage is pre-adsorbed onto the test strain and plated onto a sensitive strain (where the phage demonstrates high EOP). Therefore, if the phage effectively infects the test strain, plaques will form and be readily observable on the sensitive strain. Finally, burst size indicates de number of phage particles produced by a single infected cell. The EOP and ECOI values of 0 for UAB_Phi20 and UAB_Phi78 obtained on IC3, IC5 and IC10 indicated no phage production and hindered burst size determination (Table 3.7). On the other hand, IC6, IC8, IT2 and IT3 variants displayed significantly low EOP and ECOI values for both phages, accompanied by a marked decrease in burst size, suggesting reduced viability of these phages in these strains (Abedon, 2018). For UAB_Phi87, EOP values of 0 were observed in these variants; however, ECOI and burst size determinations were unfeasible due to inefficient adsorption, as previously mentioned. These parameters require a phage adsorption of 95% for their determination (Kropinski, 2018), a threshold never attained before UAB_Phi87 production started. One may speculate that some phage interference mechanism, potentially involving adsorption and other lytic cycle processes of UAB_Phi87, was at play. Furthermore, the infection kinetics of any of the three phages on the seven *Salmonella* variants, displayed a slight decrease in cell viability without complete lysis (Otero J, 2019), which would denote an abortive infection process (Hyman and Abedon, 2010).

As previously mentioned, the comparison of whole-genome sequencing data from these variants and the parental strain did not reveal changes in either the chromosome or the pSLT plasmid that could be associated with phage interference mechanisms. However, a detailed analysis of unmapped Illumina reads from the seven variants revealed the presence of at least one large IncI1α plasmid in each variant, with some harbouring either one or two additional smaller plasmids from

other incompatibility groups (Table 3.8). The consistent presence of IncI1α plasmids across all seven variants suggested that they could be responsible for the observed interference with the cocktail phages. Plasmids are extrachromosomal genetic elements that can be transferred by conjugation to other bacteria if they encode the genetic elements necessary for their own transfer. They often carry accessory genes that confer a selective advantage to their host bacteria, such as antibiotic resistance or substrate utilization genes for growth. In addition, plasmids may also encode phage defence systems, such as TA systems which were initially described as mechanisms for plasmid stabilization by postsegregational killing (Gerdes and Rasmussen, 1986) or addiction (Yarmolinsky, 1995), or the lactococcal abortive infection (Abi) system, predominantly encoded on plasmids (Chopin *et al*., 2005). IncI1 group plasmids are low copy number plasmids widely distributed among *Enterobacteriaceae*, often carrying antimicrobial resistance genes, including those conferring resistance to β-lactam, chloramphenicol, tetracycline, sulfonamides, trimethoprim, or aminoglycosides, as well as virulence-associated genes such as those for bacteriocin production, plasmid maintenance and addiction genes like TA systems (Foley *et al*., 2021). Furthermore, several studies have shown that these plasmids impose minimal fitness costs (Johnson *et al*., 2015; Freire Martín *et al*., 2016). IncI1 plasmid-mediated phage interference was first reported in 1965 by Anderson and Lewis (Anderson and Lewis, 1965), where the transfer of a plasmid named Delta resulted in a change in phage type from a PT36 strain to a PT6 strain, characterized by a reduction in phage sensibility. Since then, numerous other IncI1 plasmids have been implicated in altering phage type through *in vitro* conjugation, leading to changes in phage type in recipient strains (Hughes and Meynell, 1977; Hiley *et al*., 2021). This phenomenon has been attributed to plasmid regions encoding phage growth inhibition systems (Furuichi *et al*., 1984; Sampei *et al*., 2010; Hiley *et al*., 2021).

The presence of large IncI1α plasmids pUA1135, pUA1136 and pUA1139 in variants IC5, IC6 and IT2, respectively, raised suspicions that these plasmids might encode interference mechanisms against phages UAB_Phi20, UAB_Phi78, and UAB_Phi87, as no additional plasmids were detected in these variants. This was confirmed through conjugation experiments and PCR-based detection of these plasmids in transconjugant strains. Additionally, EOP and ECOI values of UAB_Phi20 and UAB_Phi78 in the transconjugants closely resembled those in donor strains (Table 3.9). Furthermore, plasmid curing of pUA1135, pUA1136 and pUA1139 in IC5, IC6 and IT2, respectively, further supported their involvement in interfering UAB_Phi20 and UAB_Phi78, as cured strains regained susceptibility to both phages (data not shown). However, data pertaining to UAB_Phi87 following conjugation experiments and plasmid curing were inconclusive. In conjugation experiments, an EOP of 0 was expected, given that UAB_Phi87 showed adsorption on *S.* Typhimurium LB5000, a strain sensitive to this phage. Nevertheless, transconjugants exhibited EOP values close to 0.1 and formed plaques smaller than those of the

recipient strain *S*. Typhimurium LB5000 (data not shown). Moreover, plasmid curing did not result in the expected EOP of 1 exhibited by the parental strain; instead, strains with EOP values around 0.1 and smaller plaque sizes were obtained (data not shown). Again, these results suggest that, in the case of UAB_Phi87, various mechanisms involving lower adsorption and other interference mechanisms in the phage multiplicative cycle encoded in the IncI1α plasmids may be the cause of the observed reduced susceptibility in the studied strains.

The acquisition of these large IncI1α conjugative plasmids by the ATCC14028 Rif^R strain bacterial cells, used to colonize the broilers' digestive tract, can only occur through lateral transfer from the commensal gut microbiota of the broilers. This microbiota was confirmed to be *Salmonella*-free at the beginning of the experiment. For lateral gene transfer to occur in the intestinal track, both donor and recipient bacteria must be present at high concentrations. In fact, it is known that intestinal inflammatory processes, which can be triggered by bacterial infection, prompt commensal microbial blooms, thereby increasing bacterial densities (Lupp *et al*., 2007; Stecher *et al*., 2012), and facilitating conjugation events. Furthermore, bacteria from the environmental microbiota may harbour plasmids encoding genes involved in phage interference mechanisms and exhibit high mating frequencies. If these conditions were met, plasmid acquisition through lateral transfer would occur more frequently than mutation events in genes encoding phage receptors.

Annotation and alignment of plasmids pUA1135, pUA1136 and pUA1139 were conducted to investigate the phage defence-associated genes they carried. Results revealed a hypervariable region located between the *repA* and *parA* genes in all three plasmids, housing the ampicillin resistance gene in pUA1135 and pUA1136, alongside numerous hypothetical proteins and other diverse genes. It is known that variable regions within the bacterial genome or MGEs often harbour defence systems against phages and other MGEs (Chevallereau and Westra, 2022; Rousset *et al*., 2022; Hochhauser *et al*., 2023), prompting our focus on studying the genes within this region. Our exploration identified genes with similarities to several TA systems, known to be involved in phage interference functions, and proteins related to abortive infection mechanisms (data not shown). While most of these were situated within the previously described variable regions, some were also found outside (data not shown). One of the identified genes was *ibfA*, situated within the variable region of plasmid pUA1135. By deletion and complementation of this gene we demonstrated that it interfered with the multiplicative cycle of the UAB_Phi20 virulent phage, which is similar to the temperate P22 phage (Bardina *et al*., 2016). Specifically, the *ibfA* gene did not affect UAB_Phi20 adsorption kinetics, but a substantial reduction in EOP, ECOI and the burst size (Figure 4.6) was observed, along with altered infection kinetics of UAB_Phi20, characterized by a decrease in cellular viability without cell lysis (Figure 4.6). TEM images of cross sections of infected bacterial cells further corroborated these results (Figure 4.14). All these

data indicated that *ibfA* gene hampered with UAB_Phi20 viability through an abortive infection mechanism.

The *ibfA* gene from pUA1135 is similar to the R64 plasmid-like *ibfA* gene, previously associated with interference against several *E. coli* and *Salmonella* phages (Anderson and Lewis, 1965; Hughes and Meynell, 1977), although the underlying mechanism for this interference has not been elucidated. Additionally, the defence system against coliphages associated with Hma-embeded-candidate 04 (HEC-04), which shares significant homology with the *ibfA* gene here studied, is also unknown (Payne *et al*., 2024). In this regard, the studies performed in this thesis have led us to propose a model explaining the molecular mechanism involved in the interference of the phage lytic cycle by the *ibfA* gene, outlined in Figure 5.1. This model is inferred from the data obtained on the replication and transcription of the phage genome and from the fact that the IbfA protein did not function as an ATPase depleting cellular ATP (Figure 4.8). Specifically, replication of the phage genome was unaffected by the *ibfA* gene (Figure 4.9), but its presence resulted in significant changes in the transcription of the phage genes studied here (Figures 4.10 to 4.13). The observed dysregulation involved an increase in early gene expression in the presence of *ibfA*, as well as in genes from the *immC* and *immI* regions, except for the gene encoding the late antiterminator, which along with late genes, was underexpressed. We propose that the IbfA protein directly or indirectly disrupts the function of the Arc repressor found within the *immI* region of UAB_Phi20 phage. The inability to repress its own promoter, P_{ANT}, leads to an increase in the expression of the two genes controlled from this promoter, *arc* itself, and *ant*. The *ant* gene encodes the antirepressor of the repressor of the lytic cycle C2; the interaction of Ant with C2 at the protein level inhibits C2. The elevated levels of *ant* in the presence of IbfA result in the sequestering of the C2 protein present in the cell. The concentration of C2 protein is crucial in the regulation of the lysis/lysogeny decision of the phage, which depends on the Cro/C2 balance. The alteration in this balance, due to a decrease in the available C2 protein, results in an increase in the expression of early genes controlled by promoters P_R and P_L, as these promoters are regulated by both Cro and C2. One of these early genes is C1, which acts as the positive regulator of several promoters, including P_{A23}. P_{A23} controls the expression of a small RNA that inhibits the late antiterminator, which is responsible for the antitermination of the transcript generated from P_{LATE}. Therefore, the increase in C1 results in a decrease of the late antiterminator, causing reduced expression of genes under the control of P_{LATE}. These genes mostly encode virion structural proteins and cellular lysis proteins. The lower amount of available structural proteins results in decreased virion production, and the low concentration of proteins for lysis severely impairs cellular lysis.

Lastly, it must be noted that IbfA is widely distributed amongst the prokaryotic phylogeny (Figure 4.15), and it is found in both chromosomes and plasmids of several bacterial classes. This extensive distribution is characteristic of phage defence systems (Goldfarb *et al*., 2015; Ofir *et*

al., 2018; Millman *et al*., 2022), and indicates that its presence is likely beneficial for the cell. However, it could also imply that *ibfA* may have other functions beyond phage defence.

In summary, this thesis is the first report of horizontal transfer of phage defence from the intestinal microbiota of broilers to *Salmonella* in an *in vivo* phage therapy study. We have been able to describe that the transferred plasmids encoded defence mechanisms to UAB_Phi20, UAB_Phi78 and UAB_Phi87 phages. Furthermore, we were able to identify a variable region within the plasmids that most likely contains some of the genes involved in these interference mechanisms. In fact, we located one of these genes, *ibfA*, within the variable region of plasmid pUA1135, which interferes with the multiplicative cycle of the phage UAB_Phi20. We have also detailed the previously undescribed mechanism by which IbfA exerts phage interference. Specifically, we discovered that the product of the phylogenetically-widespread *ibfA* gene causes a decrease in structural virion proteins and in those related to cellular lysis by prompting a dysregulation of phage gene transcription, ultimately causing abortive infection. To our knowledge, this is the first instance of a defence mechanism that causes a general alteration in gene transcription to deplete virion production.

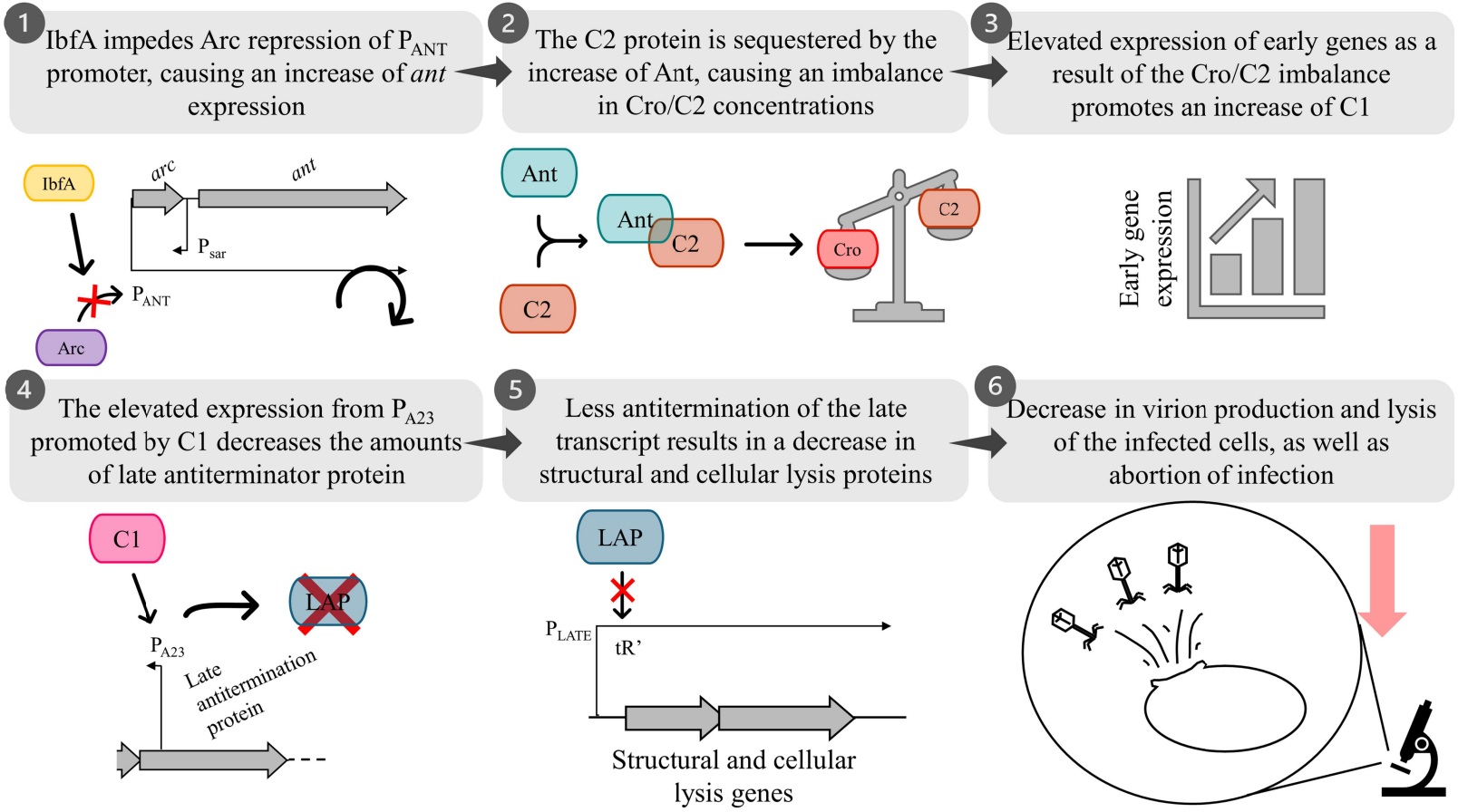


Figure 5.1. Graphic representation of the model on the molecular mechanism of *ibfA*-mediated interference in the phage lytic cycle.

6. CONCLUSIONS

The main conclusions from this work are:

1. This study demonstrates for the first time the transfer of large conjugative plasmids encoding phage defence mechanisms from the commensal microbiota in broilers' digestive tracts to the bacterial cells of a target *Salmonella* strain used in *in vivo* oral phage therapy experiments with a phage cocktail, composed of the virulent bacteriophages UAB_Phi20, UAB_Phi78, and UAB_Phi87.

2. The reduced susceptibility to UAB_Phi20 and UAB_Phi78 phages, observed in seven *Salmonella* variants from broilers' ceca, was associated with large IncI1α conjugative plasmids, and did not impact phage adsorption. This was confirmed by bioinformatic analysis, conjugation, and curing experiments. However, results for the UAB_Phi87 phage were inconclusive, suggesting the potential involvement of interference mechanisms encoded in the plasmids, in addition to other factors affecting adsorption.

3. Among the *Salmonella* variants displaying notably diminished EOP, ECOI, ECOI, and burst size in response to phages UAB_Phi20 and/or UAB_Phi78, phage interference stemmed from an abortive infection mechanism. While conclusive evidence was lacking, it is probable that interference with phage UAB_Phi87 in the seven variants was similarly linked to an abortive mechanism.

4. This study has identified a novel phage defence mechanism targeted against UAB_Phi20, a P22-like phage, encoded within the large conjugative plasmid pUA1135 in *Salmonella* variant IC5. This defence mechanism is orchestrated by the *ibfA* gene, which encodes a two-domain protein homologous to an uncharacterized HEC-04 defence protein. IbfA is composed of an ABC ATPase domain and a topoisomerase-primase (TOPRIM) domain and located within a hypervariable region of the plasmid.

5. IbfA is responsible for the abortive infection of UAB_Phi20 observed in the IC5 strain, as evidenced by the substantial reduction in EOP, ECOI, and burst size in an *ibfA*$^{+}$ strain compared to the parental strain, coupled with the decreased cell viability but without a noticeable cellular lysis.

6. Phage infection by UAB_Phi20 does not induce transcription of the *ibfA* defence gene. On the contrary, transcription of this gene is reduced due to the effects of phage infection on bacterial transcription. However, the concentration of IbfA protein prior to phage infection is sufficient to promote phage defence.

7. The molecular mechanism behind the interference carried out by *ibfA* is not associated to cellular ATP depletion or the impairment of UAB_Phi20 genome replication.

8. Analysis of the transcriptional patterns of UAB_Phi20 genes showed dysregulation in phage gene transcription. On the one hand, results showed an increase in the expression of early genes, except the late antiterminator, as well as those in the *immC* and *immI* regions of the phage. On the other hand, the expression of late genes, including genes encoding both cellular lysis-related and structural proteins, was significantly decreased.

9. Based on the gene transcription results obtained, a model is proposed to elucidate the mechanism through which IbfA induces interference with UAB_Phi20. Specifically, IbfA disrupts the phage cycle by directly or indirectly influencing Arc regulation, leading to an overproduction of the Ant antirepressor. This dysregulation ultimately triggers a significant decline in the transcription of genes encoding phage structural proteins and those required for cell lysis. Consequently, virion assembly and/or cell lysis are impaired, as confirmed by TEM microscopy of cellular cross-sections, leading to the abortion of the infection.

10. The widespread distribution of *ibfA* among bacterial and archaeal plasmids and chromosomes suggests that it has potential cellular functions beyond phage defence, and highlights its importance at an evolutionary level.

REFERENCES

1. Abby SS, Néron B, Ménager H, Touchon M, Rocha EPC. MacSyFinder: A program to mine genomes for molecular systems with an application to CRISPR-Cas systems. PLoS One. 2014;9(10):e110726.
2. Abedon ST. Detection of bacteriophages: phage plaques. In: Harper, DR, Abedon, ST, Burrowes, BH, McConville, ML (eds) Bacteriophages. 2018.
3. Abedon ST. Evolution of bacteriophage latent period length. In: Dickins TE, Dickins BJ (eds) Evolutionary Biology: Contemporary and Historical Reflections Upon Core Theory. 2023.
4. Abuladze T, Li M, Menetrez MY, Dean T, Senecal A, Sulakvelidze A. Bacteriophages reduce experimental contamination of hard surfaces, tomato, spinach, broccoli, and ground beef by *Escherichia coli* O157:H7. Appl Environ Microbiol. 2008;74(20):6230–8.
5. Adler BA, Kazakov AE, Zhong C, Liu H, Kutter E, Lui LM, *et al*. The genetic basis of phage susceptibility, cross-resistance and host-range in *Salmonella*. Microbiology (Reading). 2021;167(12):001126.
6. Akritidou K, Thurtle-Schmidt BH. OLD family nuclease function across diverse anti-phage defense systems. Front Microbiol. 2023;14:1268820.
7. Ali S, Alsayeqh AF. Review of major meat-borne zoonotic bacterial pathogens. Front Public Heal. 2022;10:1045599.
8. Altschul SF, Madden TL, Schäffer AA, Zhang J, Zhang Z, Miller W, *et al*. Gapped BLAST and PSI-BLAST: a new generation of protein database search programs. Nucleic Acids Res. 1997;25(17):3389–402.
9. Anderson ES, Lewis MJ. Characterization of a transfer factor associated with drug resistance in *Salmonella* Typhimurium. Nature. 1965;208(5013):843–9.
10. Antine SP, Johnson AG, Mooney SE, Leavitt A, Mayer ML, Yirmiya E, *et al*. Structural basis of Gabija anti-phage defence and viral immune evasion. Nature. 2024;625(7994):360–5.
11. Bai J, Jeon B, Ryu S. Effective inhibition of *Salmonella* Typhimurium in fresh produce by a phage cocktail targeting multiple host receptors. Food Microbiol. 2019;77:52–60.
12. Bankevich A, Nurk S, Antipov D, Gurevich AA, Dvorkin M, Kulikov AS, *et al*. SPAdes: A new genome assembly algorithm and its applications to single-cell sequencing. J Comput Biol. 2012;19(5):455–77.
13. Bardina C, Spricigo DA, Cortés P, Llagostera M. Significance of the bacteriophage treatment schedule in reducing *Salmonella* colonization of poultry. Appl Environ Microbiol. 2012;78(18):6600–7.

14. Bardina C, Colom J, Spricigo DA, Otero J, Sánchez-Osuna M, Cortés P, *et al*. Genomics of three new bacteriophages useful in the biocontrol of *Salmonella*. Front Microbiol. 2016;7:545.
15. Barrangou R, Horvath P. Lactic acid bacteria defenses against phages. In: Tsakalidou, E, Papadimitriou, K (eds) Stress Responses of Lactic Acid bacteria. 2011.
16. Barron-Montenegro R, Rivera D, Serrano MJ, García R, Álvarez DM, Benavides J, *et al*. Long-Term interactions of *Salmonella* Enteritidis with a lytic phage for 21 days in high nutrients media. Front Cell Infect Microbiol. 2022;12:897171.
17. Bernheim A, Millman A, Ofir G, Meitav G, Avraham C, Shomar H, *et al*. Prokaryotic viperins produce diverse antiviral molecules. Nature. 2021;589(7840):120–4.
18. Bertozzi Silva J, Storms Z, Sauvageau D. Host receptors for bacteriophage adsorption. FEMS Microbiol Lett. 2016;363(4):fnw002.
19. Blank K, Hensel M, Gerlach RG. Rapid and highly efficient method for scarless mutagenesis within the *Salmonella enterica* chromosome. PLoS One. 2011;6(1):e15763.
20. Bondy-Denomy J, Qian J, Westra ER, Buckling A, Guttman DS, Davidson AR, *et al*. Prophages mediate defense against phage infection through diverse mechanisms. ISME J. 2016;10(12):2854–66.
21. Botstein D, Lew KK, Jarvik V, Swanson CA. Role of Antirepressor in the bipartite control of repression and immunity by bacteriophage P22. J Mol Biol. 1975;91(4):439–62.
22. Bouchard JD, Dion E, Bissonnette F, Moineau S. Characterization of the two-component abortive phage infection mechanism AbiT from *Lactococcus lactis*. J Bacteriol. 2002;184(22):6325–32.
23. Brandão A, Pires DP, Coppens L, Voet M, Lavigne R, Azeredo J. Differential transcription profiling of the phage LUZ19 infection process in different growth media. RNA Biol. 2021;18(11):1778–90.
24. Buendía-Clavería AM, Moussaid A, Ollero FJ, Vinardell JM, Torres A, Moreno J, *et al*. A purL mutant of *Sinorhizobium fredii* HH103 is symbiotically defective and altered in its lipopolysaccharide. Microbiology (Reading). 2003;149(Pt 7):1807–18.
25. Carattoli A, Zankari E, Garciá-Fernández A, Larsen MV, Lund O, Villa L, *et al*. *In silico* detection and typing of plasmids using plasmidfinder and plasmid multilocus sequence typing. Antimicrob Agents Chemother. 2014;58(7):3895–903.
26. Chan RK, Botstein D, Watanabe T, Ogata Y. Specialized transduction of tetracycline resistance by phage P22 in *Salmonella* typhimurium. II. Properties of a high-frequency-transducing lysate. Virology. 1972;50(3):883–98.
27. Chanishvili N. Phage therapy - History from Twort and d'Herelle through Soviet experience to current approaches. Adv Virus Res. 2012;83:3–40.

28. Chaveroche MK, Ghigo JM, D'Enfert C. A rapid method for efficient gene replacement in the filamentous fungus *Aspergillus nidulans*. Nucleic Acids Res. 2000;28(22):E97.
29. Chen W, Zhang Y, Zhang Y, Pi Y, Gu T, Song L, *et al*. CRISPR/Cas9-based genome editing in *Pseudomonas aeruginosa* and cytidine deaminase-mediated base editing in *Pseudomonas* species. iScience. 2018;6:222–31.
30. Chevallereau A, Westra ER. Bacterial immunity: mobile genetic elements are hotspots for defence systems. Curr Biol. 2022;32(17):R923–6.
31. Chinenova TA, Mkrtumian NM, Lomovskaia ND. Genetic characteristics of a new phage resistance trait in *Streptomyces coelicolor* A3(2). Genetika. 1982;18(12):1945–52.
32. Chopin MC, Chopin A, Bidnenko E. Phage abortive infection in lactococci: variations on a theme. Curr Opin Microbiol. 2005;8(4):473–9.
33. Cohen D, Melamed S, Millman A, Shulman G, Oppenheimer-Shaanan Y, Kacen A, *et al*. Cyclic GMP–AMP signalling protects bacteria against viral infection. Nature. 2019;574(7780):691–5.
34. Colom J, Cano-Sarabia M, Otero J, Cortés P, Maspoch D, Llagostera M. Liposome-encapsulated bacteriophages for enhanced oral phage therapy against *Salmonella* spp. Appl Environ Microbiol. 2015;81(14):4841–9.
35. Colom J, Cano-Sarabia M, Otero J, Aríñez-Soriano J, Cortés P, Maspoch D, *et al*. Microencapsulation with alginate/$CaCO_3$: A strategy for improved phage therapy. Sci Rep. 2017;7:41441.
36. Comeau AM, Hatfull GF, Krisch HM, Lindell D, Mann NH, Prangishvili D. Exploring the prokaryotic virosphere. Res Microbiol. 2008;159(5):306–13.
37. Cooley W, Sirotkin K, Green R, Snyder L. A new gene of *Escherichia coli* K-12 whose product participates in T4 bacteriophage late gene expression: Interaction of lit with the T4-induced polynucleotide 5'-kinase 3'-phosphatase. J Bacteriol. 1979;140(1):83–91.
38. Coppens L, Wicke L, Lavigne R. SAPPHIRE.CNN: Implementation of dRNA-seq-driven, species-specific promoter prediction using convolutional neural networks. Comput Struct Biotechnol J. 2022;20:4969–74.
39. © Council of Europe. Phage therapy medicinal products. In: European pharmacopoeia 11.6. 2024.
40. Darling AE, Mau B, Perna NT. ProgressiveMauve: Multiple genome alignment with gene gain, loss and rearrangement. PLoS One. 2010;5(6):e11147.
41. Datsenko KA, Wanner BL. One-step inactivation of chromosomal genes in *Escherichia coli* K-12 using PCR products. Proc Natl Acad Sci U S A. 2000;97(12):6640–5.
42. de Jonge PA, Nobrega FL, Brouns SJJ, Dutilh BE. Molecular and evolutionary determinants of bacteriophage host range. Trends Microbiol. 2019;27(1):51–63.

43. de Moraes MH, Teplitski M. Fast and efficient three-step target-specific curing of a virulence plasmid in *Salmonella enterica*. AMB Express. 2015;5(1):139.
44. De Sordi L, Lourenço M, Debarbieux L. “I will survive”: a tale of bacteriophage-bacteria coevolution in the gut. Gut Microbes. 2019;10(1):92–9.
45. Dedrick RM, Smith BE, Cristinziano M, Freeman KG, Jacobs-Sera D, Belessis Y, *et al*. Phage therapy of *Mycobacterium* infections: compassionate use of phages in 20 patients with drug-resistant mycobacterial disease. Clin Infect Dis. 2023;76(1):103–12.
46. Deep A, Liang Q, Enustun E, Pogliano J, Corbett KD. Architecture and infection-sensing mechanism of the bacterial PARIS defense system. bioRxiv. 2024.
47. D’Hérelle F. Sur un microbe invisible antagoniste des bacilles dysentérique. 1917.
48. Doermann AH. The intracellular growth of bacteriophages. I. Liberation of intracellular bacteriophage T4 by premature lysis with another phage or with cyanide. J Gen Physiol. 1952;35(4):645–56.
49. Doron S, Melamed S, Ofir G, Leavitt A, Lopatina A, Keren M, *et al*. Systematic discovery of antiphage defense systems in the microbial pangenome. Science. 2018;359(6379):eaar4120.
50. dos Santos AMP, Ferrari RG, Conte-Junior CA. Virulence factors in *Salmonella* Typhimurium: the sagacity of a bacterium. Curr Microbiol. 2018;76(6):762–73.
51. Dot EW, Thomason LC, Chappie JS. Everything OLD is new again: how structural, functional, and bioinformatic advances have redefined a neglected nuclease family. Mol Microbiol. 2023;120(2):122–40.
52. Dy RL, Przybilski R, Semeijn K, Salmond GPC, Fineran PC. A widespread bacteriophage abortive infection system functions through a Type IV toxin-antitoxin mechanism. Nucleic Acids Res. 2014;42(7):4590–605.
53. EFSA, ECDC. The European Union One Health 2022 Zoonoses Report. Vol. 21, EFSA Journal. 2023.
54. EFSA, ECDC. The European Union summary report on antimicrobial resistance in zoonotic and indicator bacteria from humans, animals and food in 2021–2022. Vol. 22, EFSA Journal. 2024.
55. Egido JE, Costa AR, Aparicio-Maldonado C, Haas PJ, Brouns SJJ. Mechanisms and clinical importance of bacteriophage resistance. FEMS Microbiol Rev. 2022;46(1):fuab048.
56. Ellermeier CD, Slauch JM. The genus *Salmonella*. In: Dworkin, M, Falkow, S, Rosenberg, E, Schleifer, KH, Stackebrandt, E (eds) The Prokaryotes. 2006.
57. European Antimicrobial Resistance Collaborators. The burden of bacterial antimicrobial resistance in the WHO European region in 2019: a cross-country systematic analysis. Lancet Public Heal. 2022;7(11):e897–913.

58. European Medicines Agency. Committee for Medicinal Products for Human Use (CHMP), Concept paper on the establishment of a Guideline on the development and manufacture of human medicinal products specifically designed for phage therapy. EMA/CHMP/BWP/486838/2023; European Medicines Agency: Amsterdam, The Netherlands. 2023a.
59. European Medicines Agency. Guideline on quality, safety and efficacy of veterinary medicinal products specifically designed for phage therapy. EMA/CVMP/NTWP/32862/2022; European Medicines Agency: Amsterdam, The Netherlands. 2023b.
60. Ferriol-González C, Domingo-Calap P. Phage therapy in livestock and companion animals. Antibiotics (Basel). 2021;10(5):559.
61. Fillol-Salom A, Martínez-Rubio R, Abdulrahman RF, Chen J, Davies R, Penadés JR. Phage-inducible chromosomal islands are ubiquitous within the bacterial universe. ISME J. 2018;12(9):2114–28.
62. Fillol-Salom A, Rostøl JT, Ojiogu AD, Chen J, Douce G, Humphrey S, *et al*. Bacteriophages benefit from mobilizing pathogenicity islands encoding immune systems against competitors. Cell. 2022;185(17):3248-3262.e20.
63. Fineran PC, Blower TR, Foulds IJ, Humphreys DP, Lilley KS, Salmond GPC. The phage abortive infection system, ToxIN, functions as a protein-RNA toxin-antitoxin pair. Proc Natl Acad Sci U S A. 2009;106(3):894–9.
64. Finn RD, Coggill P, Eberhardt RY, Eddy SR, Mistry J, Mitchell AL, *et al*. The Pfam protein families database: towards a more sustainable future. Nucleic Acids Res. 2016;44(D1):D279–85.
65. Foley SL, Kaldhone PR, Ricke SC, Han J. Incompatibility Group I1 (IncI1) Plasmids: their Genetics, Biology, and Public Health Relevance. Microbiol Mol Biol Rev. 2021;85(2):e00031–20.
66. Forde A, Fitzgerald GF. Bacteriophage defence systems in lactic acid bacteria. Antonie Van Leeuwenhoek. 1999;76(1–4):89–113.
67. Freire Martín I, Thomas CM, Laing E, AbuOun M, La Ragione RM, Woodward MJ. Curing vector for IncI1 plasmids and its use to provide evidence for a metabolic burden of IncI1 CTX-M-1 plasmid pIFM3791 on *Klebsiella pneumoniae*. J Med Microbiol. 2016;65(7):611–8.
68. Furuichi T, Komano T, Nisioka T. Physical and genetic analyses of the Inc-I alpha plasmid R64. J Bacteriol. 1984;158(3):997–1004.
69. Gaborieau B, Debarbieux L. The role of the animal host in the management of bacteriophage resistance during phage therapy. Curr Opin Virol. 2023;58:101290.

70. Gal-Mor O, Boyle EC, Grassl GA. Same species, different diseases: how and why typhoidal and non-typhoidal *Salmonella enterica* serovars differ. Front Microbiol. 2014;5:391.
71. Galperin MY, Makarova KS, Wolf YI, Koonin EV. Expanded microbial genome coverage and improved protein family annotation in the COG database. Nucleic Acids Res. 2015;43(Database issue):D261–9.
72. Gao L, Altae-Tran H, Böhning F, Makarova KS, Segel M, Schmid-Burgk JL, *et al*. Diverse enzymatic activities mediate antiviral immunity in prokaryotes. Science. 2020;369(6507):1077–84.
73. Gao Y, Luo X, Li P, Li Z, Ye F, Liu S, *et al*. Molecular basis of RADAR anti-phage supramolecular assemblies. Cell. 2023;186(5):999-1012.e20.
74. García-Quintanilla M, Ramos-Morales F, Casadesús J. Conjugal transfer of the *Salmonella enterica* virulence plasmid in the mouse intestine. J Bacteriol. 2008;190(6):1922–7.
75. Garvey P, Fitzgerald GF, Hill C. Cloning and DNA sequence analysis of two abortive infection phage resistance determinants from the lactococcal plasmid pNP40. Appl Environ Microbiol. 1995;61(12):4321–8.
76. Georjon H, Bernheim A. The highly diverse antiphage defence systems of bacteria. Nat Rev Microbiol. 2023;21(10):686–700.
77. Gerdes K, Rasmussen PB, Molin S. Unique type of plasmid maintenance function: postsegregational killing of plasmid-free cells. Proc Natl Sci U S A. 1986;83(10):3116–20.
78. Ghosh C, Sarkar P, Issa R, Haldar J. Alternatives to Conventional Antibiotics in the Era of Antimicrobial Resistance. Trends Microbiol. 2019;27(4):323–38.
79. Goldfarb T, Sberro H, Weinstock E, Cohen O, Doron S, Charpak-Amikam Y, *et al*. BREX is a novel phage resistance system widespread in microbial genomes. EMBO J. 2015;34(2):169–83.
80. Gordillo Altamirano FL, Barr JJ. Phage therapy in the postantibiotic era. Clin Microbiol Rev. 2019;32(2):e00066–e00018.
81. Górski A, Międzybrodzki R, Łobocka M, Głowacka-Rutkowska A, Bednarek A, Borysowski J, *et al*. Phage therapy: what have we learned? Viruses. 2018;10(6):288.
82. Gough M. Establishment mode repressor synthesis blunts phage P22 antirepressor activity. J Mol Biol. 1977;111(1):55–64.
83. Guttman B, Raya R, Kutter E. Basic phage biology. In: Kutter E, Sulakvelidze A (eds) Bacteriophages: Biology and Application. 2005.
84. Guzman LM, Belin D, Carson MJ, Beckwith J. Tight regulation, modulation, and high-level expression by vectors containing the arabinose PBAD promoter. J Bacteriol. 1995;177(14):4121–30.
85. Haraga A, Ohlson MB, Miller SI. Salmonellae interplay with host cells. Nat Rev Microbiol. 2008;6(1):53–66.

86. Harvey AM, Hava P, Oppenheim AB, Prell HH, Soska J. Repression of ant synthesis early in the lytic cycle of phage P22. Mol Gen Genet. 1981;181(1):74–81.
87. Hernandez CA, Koskella B. Phage resistance evolution *in vitro* is not reflective of *in vivo* outcome in a plant-bacteria-phage system. Evolution. 2019;73(12):2461–75.
88. Hiley L, Graham RMA, Jennison AV. Characterisation of IncI1 plasmids associated with change of phage type in isolates of *Salmonella enterica* serovar Typhimurium. BMC Microbiol. 2021;21(1):92.
89. Hille F, Richter H, Wong SP, Bratovič M, Ressel S, Charpentier E. The biology of CRISPR-Cas: backward and forward. Cell. 2018;172(6):1239–59.
90. Hitchcock PJ, Leive L, Mäkelä PH, Rietschel ET, Strittmatter W, Morrison DC. Lipopolysaccharide momenclature-past, present, and future. J Bacteriol. 1986;166(3):699–705.
91. Ho YS, Pfarr D, Strickler J, Rosenberg M. Characterization of the transcription activator protein C1 of bacteriophage P22. J Biol Chem. 1992;267(20):14388–97.
92. Hochhauser D, Millman A, Sorek R. The defense island repertoire of the *Escherichia coli* pan-genome. PLoS Genet. 2023;19(4):e1010694.
93. Hong Y, Schmidt K, Marks D, Hatter S, Marshall A, Albino L, *et al*. Treatment of *Salmonella*-contaminated eggs and pork with a broad-spectrum, single bacteriophage: assessment of efficacy and resistance development. Foodborne Pathog Dis. 2016;13(12):679–88.
94. Huerta-Cepas J, Szklarczyk D, Heller D, Hernández-Plaza A, Forslund SK, Cook H, *et al*. eggNOG 5.0: a hierarchical, functionally and phylogenetically annotated orthology resource based on 5090 organisms and 2502 viruses. Nucleic Acids Res. 2019;47(D1):D309–14.
95. Hughes V, Meynell GG. The contribution of plasmid and host genes to plasmid-mediated interference with phage growth. Genet Res. 1977;30(2):179–85.
96. Hyman P, Abedon ST. Bacteriophage host range and bacterial resistance. Adv Appl Microbiol. 2010:70:217–48.
97. Ibarra-Chávez R, Brady A, Chen J, Penadés JR, Haag AF. Phage-inducible chromosomal islands promote genetic variability by blocking phage reproduction and protecting transductants from phage lysis. PLoS Genet. 2022;18(3):e1010146.
98. Imran A, Shehzadi U, Islam F, Afzaal M, Ali R, Ali YA, *et al*. Bacteriophages and food safety: an updated overview. Food Sci Nutr. 2023;11(7):3621–30.
99. Isaev AB, Musharova OS, Severinov KV. Microbial arsenal of antiviral defenses. Part I. Biochemistry (Mosc). 2021a;86(4):319–37.
100. Isaev AB, Musharova OS, Severinov KV. Microbial arsenal of antiviral defenses. Part II. Biochemistry (Mosc). 2021b;86(4):449–70.

101. Iwashita S, Kanegasaki S. Smooth specific phage adsorption: endorhamnosidase activity of tail parts of P22. Biochem Biophys Res Commun. 1973;55(2):403–9.
102. Johnson AG, Wein T, Mayer ML, Duncan-Lowey B, Yirmiya E, Oppenheimer-Shaanan Y, *et al*. Bacterial gasdermins reveal an ancient mechanism of cell death. Science. 2022;375(6577):221–5.
103. Johnson TJ, Singer RS, Isaacson RE, Danzeisen JL, Lang K, Kobluk K, *et al*. *In Vivo* transmission of an IncA/C plasmid in *Escherichia coli* depends on tetracycline concentration, and acquisition of the plasmid results in a variable cost of fitness. Appl Environ Microbiol. 2015;81(10):3561–70.
104. Jones GW, Rabert DK, Svinarich DM, Whitfield HJ. Association of adhesive, invasive, and virulent phenotypes of *Salmonella* typhimurium with autonomous 60-megadalton plasmids. Infect Immun. 1982;38(2):476–86.
105. Judicial Commission of the International Committee on Systematics of Prokaryotes. The type species of the genus *Salmonella* Lignieres 1900 is *Salmonella enterica* (*ex* Kauffmann and Edwards 1952) Le Minor and Popoff 1987, with the type strain $LT2^T$, and conservation of the epithet *enterica* in *Salmonella enterica* over all earlier epithets that may be applied to this species. Opinion 80. Int J Syst Evol Microbiol. 2005;55(Pt 1):519–20.
106. Jumper J, Evans R, Pritzel A, Green T, Figurnov M, Ronneberger O, *et al*. Highly accurate protein structure prediction with AlphaFold. Nature. 2021;596(7873):583–9.
107. Keen EC. A century of phage research: bacteriophages and the shaping of modern biology. BioEssays. 2014;37(1):6–9.
108. Khan Mirzaei M, Nilsson AS. Isolation of phages for phage therapy: a comparison of spot tests and efficiency of plating analyses for determination of host range and efficacy. PLoS One. 2015;10(3):e0118557.
109. Khan MAS, Rahman SR. Use of phages to treat antimicrobial-resistant *Salmonella* infections in poultry. Vet Sci. 2022;9(8):438.
110. Koonin EV, Makarova KS, Wolf YI, Krupovic M. Evolutionary entanglement of mobile genetic elements and host defence systems: guns for hire. Nat Rev Genet. 2020;21(2):119–31.
111. Koopal B, Potocnik A, Mutte SK, Aparicio-Maldonado C, Lindhoud S, Vervoort JJM, *et al*. Short prokaryotic Argonaute systems trigger cell death upon detection of invading DNA. Cell. 2022;185(9):1471–1486.e19.
112. Kropinski AM. Measurement of the rate of attachment of bacteriophage to cells. Methods Mol Biol. 2009;501:151–5.
113. Kropinski AM. Practical advice on the one-step growth curve. Methods Mol Biol. 2018;1681:41–7.
114. Kutter E. Phage host range and efficiency of plating. Methods Mol Biol. 2009;501:141–9.

115. Larkin MA, Blackshields G, Brown NP, Chenna R, Mcgettigan PA, McWilliam H, *et al*. Clustal W and Clustal X version 2.0. Bioinformatics. 2007;23(21):2947–8.
116. LaRock DL, Chaudhary A, Miller SI. Salmonellae interactions with host processes. Nat Rev Microbiol. 2015;13(4):191–205.
117. Lee EJ, Groisman EA. Control of a *Salmonella* virulence locus by an ATP-sensing leader messenger RNA. Nature. 2012;486(7402):271–5.
118. Leong JM, Nunes-Düby S, Lesser CF, Youderian P, Susskind MM, Landy A. The Φ80 and P22 attachment sites. Primary structure and interaction with *Escherichia coli* integration host factor. J Biol Chem. 1985;260(7):4468–77.
119. Letunic I, Bork P. Interactive tree of life (iTOL) v5: An online tool for phylogenetic tree display and annotation. Nucleic Acids Res. 2021;49(W1):W293–6.
120. Levin BR, Bull JJ. Population and evolutionary dynamics of phage therapy. Nat Rev Microbiol. 2004;2(2):166–73.
121. Levine M. Mutations in the temperate Phage P22 and lysogeny in *Salmonella*. Virology. 1957;3(1):22–41.
122. Levine M, Truesdell S, Ramakrishnan T, Bronson MJ. Dual control of lysogeny by bacteriophage P22: an antirepressor locus and its controlling elements. J Mol Biol. 1975;91(4):421–38.
123. Lew K, Casjens S. Identification of early proteins coded by bacteriophage P22. Virology. 1975;68(2):525–33.
124. Liao SM, Wu TH, Chiang CH, Susskind MM, McClure WR. Control of gene expression in bacteriophage P22 by a small antisense RNA. I. Characterization in vitro of the P_{sar} promoter and the sar RNA transcript. Genes Dev. 1987;1(2):197–203.
125. Loc-Carrillo C, Abedon ST. Pros and cons of phage therapy. Bacteriophage. 2011;1(2):111–4.
126. Lopatina A, Tal N, Sorek R. Abortive infection: bacterial suicide as an antiviral immune strategy. Annu Rev Virol. 2020;7(1):371–84.
127. López-Pérez J, Otero J, Sánchez-Osuna M, Erill I, Cortés P, Llagostera M. Impact of mutagenesis and lateral gene transfer processes in bacterial susceptibility to phage in food biocontrol and phage therapy. Front Cell Infect Microbiol. 2023;13:1266685.
128. Loponte R, Pagnini U, Iovane G, Pisanelli G. Phage therapy in veterinary medicine. Antibiotics (Basel). 2021;10(4):421.
129. Lupp C, Robertson ML, Wickham ME, Sekirov I, Champion OL, Gaynor EC, *et al*. Host-mediated inflammation disrupts the intestinal microbiota and promotes the overgrowth of Enterobacteriaceae. Cell Host Microbe. 2007;2(3):204.

130. Makarova KS, Wolf YI, van der Oost J, Koonin EV. Prokaryotic homologs of Argonaute proteins are predicted to function as key components of a novel system of defense against mobile genetic elements. Biol Direct. 2009;4:29.
131. Martínez-Rubio R, Quiles-Puchalt N, Martí M, Humphrey S, Ram G, Smyth D, *et al*. Phage-inducible islands in the Gram-positive cocci. ISME J. 2017;11(4):1029–42.
132. Maura D, Debarbieux L. On the interactions between virulent bacteriophages and bacteria in the gut. Bacteriophage. 2012;2(4):229–33.
133. Mayola A, Irazoki O, Martínez IA, Petrov D, Menolascina F, Stocker R, *et al*. RecA protein plays a role in the chemotactic response and chemoreceptor clustering of *Salmonella enterica*. PLoS One. 2014;9(8):e105578.
134. McCallin S, Oechslin F. Bacterial resistance to phage and its impact on clinical therapy. In: Górski A, Międzybrodzki R, Borysowski J (eds) Phage Therapy: A Practical Approach. 2019.
135. Millman A, Bernheim A, Stokar-Avihail A, Fedorenko T, Voichek M, Leavitt A, *et al*. Bacterial retrons function in anti-phage defense. Cell. 2020;183(6):1551-1561.e12.
136. Millman A, Melamed S, Leavitt A, Doron S, Bernheim A, Hör J, *et al*. An expanded arsenal of immune systems that protect bacteria from phages. Cell Host Microbe. 2022;30(11):1556-1569.e5.
137. Minh BQ, Schmidt HA, Chernomor O, Schrempf D, Woodhams MD, Von Haeseler A, *et al*. IQ-TREE 2: new models and efficient methods for phylogenetic inference in the genomic era. Mol Biol Evol. 2020;37(5):1530–4.
138. Moineau S, Durmaz E, Pandian S, Klaenhammerl TR. Differentiation of two abortive mechanisms by using monoclonal antibodies directed toward lactococcal bacteriophage capsid proteins. Appl Environ Microbiol. 1993;59(1):208–12.
139. Mueller L. 1973 The red queen hypothesis. In: Conceptual Breakthroughs in Evolutionary Ecology. 2020.
140. Naureen Z, Dautaj A, Anpilogov K, Camilleri G, Dhuli K, Tanzi B, *et al*. Bacteriophages presence in nature and their role in the natural selection of bacterial populations. Acta Biomed. 2020;91(13-S):e2020024.
141. Newman BM. The smooth slide up to life. Editorial Comment. Sci Am. 1937;156:304–6.
142. Nobrega FL, Vlot M, de Jonge PA, Dreesens LL, Beaumont HJE, Lavigne R, *et al*. Targeting mechanisms of tailed bacteriophages. Nat Rev Microbiol. 2018;16(12):760–73.
143. Notredame C, Higgins DG, Heringa J. T-coffee: A novel method for fast and accurate multiple sequence alignment. J Mol Biol. 2000;302(1):205–17.
144. Oechslin F, Piccardi P, Mancini S, Gabard J, Moreillon P, Entenza JM, *et al*. Synergistic interaction between phage therapy and antibiotics clears *Pseudomonas aeruginosa* infection in endocarditis and reduces virulence. J Infect Dis. 2017;215(5):703–12.

145. Oechslin F. Resistance development to bacteriophages occurring during bacteriophage therapy. Viruses. 2018;10(7):351.
146. Ofir G, Melamed S, Sberro H, Mukamel Z, Silverman S, Yaakov G, *et al*. DISARM is a widespread bacterial defence system with broad anti-phage activities. Nat Microbiol. 2018;3(1):90–8.
147. Ofir G, Herbst E, Baroz M, Cohen D, Millman A, Doron S, *et al*. Antiviral activity of bacterial TIR domains via immune signalling molecules. Nature. 2021;600(7887):116–20.
148. Ohl ME, Miller SI. *Salmonella*: A model for bacterial pathogenesis. Annu Rev Med. 2001;52:259–74.
149. Onallah H, Hazan R, Nir-Paz R, Israeli Phage Therapy Center (IPTC) Study Team. Compassionate use of bacteriophages for failed persistent infections during the first 5 years of the Israeli phage therapy center. Open Forum Infect Dis. 2023;10(5):ofad221.
150. Otero Carrera J. Biodistribución de bacteriófagos en mamíferos tras terapia fágica oral y emergencia de resistencia bacteriana a los fagos. Universitat Autònoma de Barcelona; 2019.
151. Parikka KJ, Le Romancer M, Wauters N, Jacquet S. Deciphering the virus-to-prokaryote ratio (VPR): insights into virus–host relationships in a variety of ecosystems. Biol Rev Camb Philos Soc. 2017;92(2):1081–100.
152. Payne LJ, Todeschini TC, Wu Y, Perry BJ, Ronson CW, Fineran PC, *et al*. Identification and classification of antiviral defence systems in bacteria and archaea with PADLOC reveals new system types. Nucleic Acids Res. 2021;49(19):10868–78.
153. Payne LJ, Meaden S, Mestre MR, Palmer C, Toro N, Fineran PC, *et al*. PADLOC: a web server for the identification of antiviral defence systems in microbial genomes. Nucleic Acids Res. 2022;50(W1):W541–50.
154. Payne LJ, Hughes TCD, Fineran PC, Jackson SA. New antiviral defences are genetically embedded within prokaryotic immune systems. bioRxiv. 2024.
155. Pecota DC, Wood TK. Exclusion of T4 phage by the *hok*/*sok* killer locus from plasmid R1. J Bacteriol. 1996;178(7):2044–50.
156. Pedruzzi I, Rivoire C, Auchincloss AH, Coudert E, Keller G, de Castro E, *et al*. HAMAP in 2015: Updates to the protein family classification and annotation system. Nucleic Acids Res. 2015;43(Database issue):D1064–70.
157. Pereira C, Moreirinha C, Lewicka M, Almeida P, Clemente C, Cunha Â, *et al*. Bacteriophages with potential to inactivate *Salmonella* Typhimurium: Use of single phage suspensions and phage cocktails. Virus Res. 2016;220:179–92.
158. Pirnay JP, Ferry T, Resch G. Recent progress toward the implementation of phage therapy in Western medicine. FEMS Microbiol Rev. 2022;46(1):fuab040.
159. Popoff MY, Bockemühl J, Brenner FW, Gheesling LL. Supplement 2000 (no. 44) to the Kauffmann-White scheme. Res Microbiol. 2001;152(10):907–9.

160. Popoff MY, Le Minor LE. *Salmonella*. In: Bergey's Manual of Systematics of Archaea and Bacteria. 2015.
161. Poteete AR, Ptashne M. Control of transcription by the bacteriophage P22 repressor. J Mol Biol. 1982;157(1):21–48.
162. Ram G, Chen J, Kumar K, Ross HF, Ubeda C, Damle PK, *et al*. Staphylococcal pathogenicity island interference with helper phage reproduction is a paradigm of molecular parasitism. Proc Natl Acad Sci U S A. 2012;109(40):16300–5.
163. Ram G, Chen J, Ross HF, Novick RP. Precisely modulated pathogenicity island interference with late phage gene transcription. Proc Natl Acad Sci U S A. 2014;111(40):14536–41.
164. Ritalahti KM, Amos BK, Sung Y, Wu Q, Koenigsberg SS, Löffler FE. Quantitative PCR targeting 16S rRNA and reductive dehalogenase genes simultaneously monitors multiple *Dehalococcoides* strains. Appl Environ Microbiol. 2006;72(4):2765–74.
165. Rocha EPC, Bikard D. Microbial defenses against mobile genetic elements and viruses: Who defends whom from what? PLoS Biol. 2022;20(1):e3001514.
166. Roche. LightCycler® 480 Instrument Operator's Manual. 2019.
167. Rodriguez-Valera F, Martin-Cuadrado AB, Rodriguez-Brito B, Pašić L, Thingstad TF, Rohwer F, *et al*. Explaining microbial population genomics through phage predation. Nat Rev Microbiol. 2009;7(11):828–36.
168. Rousset F, Depardieu F, Miele S, Dowding J, Laval AL, Lieberman E, *et al*. Phages and their satellites encode hotspots of antiviral systems. Cell Host Microbe. 2022;30(5):740-753.e5.
169. Rousset F, Yirmiya E, Nesher S, Brandis A, Mehlman T, Itkin M, *et al*. A conserved family of immune effectors cleaves cellular ATP upon viral infection. Cell. 2023;186(17):3619-3631.e13.
170. Ryan MP, O'Dwyer J, Adley CC. Evaluation of the complex nomenclature of the clinically and veterinary significant pathogen *Salmonella*. Biomed Res Int. 2017;2017:3782182.
171. Salazar KC, Ma L, Green SI, Zulk JJ, Trautner BW, Ramig RF, *et al*. Antiviral resistance and phage counter adaptation to antibiotic-resistant extraintestinal pathogenic *Escherichia coli*. mBio. 2021;12(2):e00211–21.
172. Sambrook J, Russell D. Molecular Cloning: A Laboratory Manual. Cold Spring Harbor Protocols; 2001.
173. Sampei GI, Furuya N, Tachibana K, Saitou Y, Suzuki T, Mizobuchi K, *et al*. Complete genome sequence of the incompatibility group I1 plasmid R64. Plasmid. 2010;64(2):92–103.
174. Samson JE, Bélanger M, Moineau S. Effect of the abortive infection mechanism and type III toxin/antitoxin system AbiQ on the lytic cycle of *Lactococcus lactis* phages. J Bacteriol. 2013;195(17):3947–56.

175. Sánchez-Osuna M, Cortés P, Barbé J, Erill I. Origin of the mobile di-hydro-pteroate synthase gene determining sulfonamide resistance in clinical isolates. Front Microbiol. 2019;9:3332.
176. Schaefer KL, McClure WR. Antisense RNA control of gene expression in bacteriophage P22. I. Structures of sar RNA and its target, ant mRNA. RNA. 1997;3(2):141–56.
177. Schnaitman CA, Klena JD. Genetics of lipopolysaccharide biosynthesis in enteric bacteria. Microbiol Rev. 1993;57(3):655–82.
178. Schooley RT, Biswas B, Gill JJ, Hernandez-Morales A, Lancaster J, Lessor L, *et al*. Development and use of personalized bacteriophage-based therapeutic cocktails to treat a patient with a disseminated resistant *Acinetobacter baumannii* infection. Antimicrob Agents Chemother. 2017;61(10):e00954–17.
179. Seemann T. Prokka: rapid prokaryotic genome annotation. Bioinformatics. 2014;30(14):2068–9.
180. Sharma S, Chatterjee S, Datta S, Prasad R, Dubey D, Prasad RK, *et al*. Bacteriophages and its applications: an overview. Folia Microbiol (Praha). 2017;62(1):17–55.
181. Shim H, Shivram H, Lei S, Doudna JA, Banfield JF. Diverse ATPase proteins in mobilomes constitute a large potential sink for prokaryotic host ATP. Front Microbiol. 2021;12:691847.
182. Silva C, Calva E, Maloy S. One health and food-borne disease: *Salmonella* transmission between humans, animals, and plants. Microbiol Spectr. 2014;2(1):OH-0020-2013.
183. Sing WD, Klaenhammer TR. Plasmid-induced abortive infection in lactococci: a review. J Dairy Sci. 1990;73(9):2239–51.
184. Smith HW, Huggins MB, Shaw KM. Factors influencing the survival and multiplication of bacteriophages in calves and in their environment. J Gen Microbiol. 1987;133(5):1127–35.
185. Söding J. Protein homology detection by HMM-HMM comparison. Bioinformatics. 2005;21(7):951–60.
186. Solovyev V, Salamov A. Automatic annotation of microbial genomes and metagenomic sequences. In: Li RW (eds) Metagenomics and its applications in agriculture, biomedicine, and environmental studies. 2011.
187. Spricigo DA, Bardina C, Cortés P, Llagostera M. Use of a bacteriophage cocktail to control *Salmonella* in food and the food industry. Int J Food Microbiol. 2013;165(2):169–74.
188. Stecher B, Denzler R, Maier L, Bernet F, Sanders MJ, Pickard DJ, *et al*. Gut inflammation can boost horizontal gene transfer between pathogenic and commensal *Enterobacteriaceae*. Proc Natl Acad Sci U S A. 2012;109(4):1269-74.
189. Stern A, Sorek R. The phage-host arms race: shaping the evolution of microbes. Bioessays. 2011;33(1):43–51.
190. Strunnikov AV. SMC complexes in bacterial chromosome condensation and segregation. Plasmid. 2006;55(2):135–44.

191. Sugden R, Kelly R, Davies S. Combatting antimicrobial resistance globally. Nat Microbiol. 2016;1(10):16187.
192. Summers WC. The strange history of phage therapy. Bacteriophage. 2012;2(2):130–3.
193. Susskind MM, Botstein D. Mechanism of action of *Salmonella* phage P22 Antirepressor. J Mol Biol. 1975;98(2):413–24.
194. Susskind MM, Botstein D. Molecular genetics of bacteriophage P22. Microbiol Rev. 1978;42(2):385–413.
195. Susskind MM. A new gene of bacteriophage P22 which regulates synthesis of antirepressor. J Mol Biol. 1980;138(4):685–713.
196. Susskind MM, Youderian P. Transcription *in vitro* of the bacteriophage P22 antirepressor gene. J Mol Biol. 1982;154(3):427–47.
197. Takamatsu D, Osaki M, Sekizaki T. Thermosensitive suicide vectors for gene replacement in *Streptococcus suis*. Plasmid. 2001;46(2):140–8.
198. Tatusov RL, Koonin EV, Lipman DJ. A genomic perspective on protein families. Science. 1997;278(5338):631–7.
199. Tatusov RL, Galperin MY, Natale DA, Koonin EV. The COG database: a tool for genome-scale analysis of protein functions and evolution. Nucleic Acids Res. 2000;28(1):33–6.
200. Tellmann G. The E-Method: A highly accurate technique for gene-expression analysis. Nat Methods. 2006;3:i–ii.
201. Tesson F, Hervé A, Mordret E, Touchon M, D'Humières C, Cury J, *et al*. Systematic and quantitative view of the antiviral arsenal of prokaryotes. Nat Commun. 2022;13(1):2561.
202. Thanki AM, Hooton S, Gigante AM, Atterbury RJ, Clokie MRJ. Potential roles for bacteriophages in reducing *Salmonella* from poultry and swine. In: Lamas A, Regal P, Franco CM (eds) *Salmonella* spp. - a global challenge. 2021.
203. Tindall BJ, Grimont PAD, Garrity GM, Euzéby JP. Nomenclature and taxonomy of the genus *Salmonella*. Int J Syst Evol Microbiol. 2005;55(Pt 1):521–4.
204. Tock MR, Dryden DTF. The biology of restriction and anti-restriction. Curr Opin Microbiol. 2005;8(4):466–72.
205. Tomat D, Casabonne C, Aquili V, Balagué C, Quiberoni A. Evaluation of a novel cocktail of six lytic bacteriophages against Shiga toxin-producing *Escherichia coli* in broth, milk and meat. Food Microbiol. 2018;76:434–42.
206. Tu J, Park T, Morado DR, Hughes KT, Molineux IJ, Liu J. Dual host specificity of phage SP6 is facilitated by tailspike rotation. Virology. 2017;507:206–15.
207. Turner D, Kropinski AM, Adriaenssens EM. A roadmap for genome-based phage taxonomy. Viruses. 2021;13(3):506.

208. Turner D, Shkoporov AN, Lood C, Millard AD, Dutilh BE, Alfenas-Zerbini P, *et al*. Abolishment of morphology-based taxa and change to binomial species names: 2022 taxonomy update of the ICTV bacterial viruses subcommittee. Arch Virol. 2023;168(2):74.
209. Twort FW. An investigation on the nature of ultra-microscopic viruses. The Lancet. 1915;186(4814):1241–3.
210. Tyndall C, Meister J, Bickle TA. The *Escherichia coli prr* region encodes a functional type IC DNA restriction system closely integrated with an anticodon nuclease gene. J Mol Biol. 1994;237(3):266–74.
211. Uemura H, Mizobuchi K. Inhibition of growth of bacteriophage BF23 by the ColIb plasmid: identification of the *ibfA* and *ibfB* genes of the ColIb plasmid. Molec Gen Genet. 1982;185:13–20.
212. Varadi M, Anyango S, Deshpande M, Nair S, Natassia C, Yordanova G, *et al*. AlphaFold protein structure database: massively expanding the structural coverage of protein-sequence space with high-accuracy models. Nucleic Acids Res. 2022;50(D1):D439–44.
213. Venturini C, Petrovic Fabijan A, Fajardo Lubian A, Barbirz S, Iredell J. Biological foundations of successful bacteriophage therapy. EMBO Mol Med. 2022;14(7):e12435.
214. Vielva L, de Toro M, Lanza VF, de la Cruz F. PLACNETw: A web-based tool for plasmid reconstruction from bacterial genomes. Bioinformatics. 2017;33(23):3796–8.
215. von Wintersdorff CJH, Penders J, Van Niekerk JM, Mills ND, Majumder S, Van Alphen LB, *et al*. Dissemination of antimicrobial resistance in microbial ecosystems through horizontal gene transfer. Front Microbiol. 2016;7:173.
216. Wang Y, Fan H, Tong Y. Unveil the secret of the bacteria and phage arms race. Int J Mol Sci. 2023;24(5):4363.
217. Wiedemann A, Virlogeux-Payant I, Chaussé AM, Schikora A, Velge P. Interactions of *Salmonella* with animals and plants. Front Microbiol. 2015;5:791.
218. Winfield MD, Groisman EA. Role of nonhost environments in the lifestyles of *Salmonella* and *Escherichia coli*. Appl Environ Microbiol. 2003;69(7):3687–94.
219. Winston F, Botstein D. Control of lysogenization by phage P22 I. The P22 *cro* gene. J Mol Biol. 1981;152(2):209–32.
220. Wiryaman T, MacRae IJ. Structural studies put phage defense mystery on the RADAR. Cell. 2023;186(5):903–5.
221. World Health Organization. WHO estimates of the global burden of foodborne diseases: foodborne disease burden epidemiology reference group 2007-2015. 2015.
222. Wright RCT, Friman VP, Smith MCM, Brockhurst MA. Resistance evolution against phage combinations depends on the timing and order of exposure. mBio. 2019;10(5):e01652–e01619.

223. Wu TH, Liao SM, McClure WR, Susskind MM. Control of gene expression in bacteriophage P22 by a small antisense RNA. II. Characterization of mutants defective in repression. Genes Dev. 1987;1(2):204–12.
224. Yarmolinsky MB. Programmed cell death in bacterial populations. Science. 1995;267(5199):836–7.
225. Zerbino DR. Using the Velvet *de novo* assembler for short-read sequencing technologies. Curr Protoc Bioinforma. 2010;Chapter 11:Unit 11.5.
226. Zhu Y, Shang J, Peng C, Sun Y. Phage family classification under *Caudoviricetes*: a review of current tools using the latest ICTV classification framework. Front Microbiol. 2022;13:1032186.

ANNEX

Annex 1. Materials and methods used in this work

A1. Microbial strains and culture conditions

A1.1 Bacterial strains and plasmids

The bacterial strains and plasmids are detailed in Table A.1. The studies of emergence of reduced susceptibility to bacteriophages and phage defence mechanisms were performed with a *Salmonella enterica* serovar Typhimurium ATCC14028 spontaneous mutant resistant to rifampicin (Rif^R) previously obtained by our research group. The *S. enterica* serovar Typhimurium LB5000 strain (SGSC181; University of Calgary) resistant to streptomycin (Str^R) was used for the obtention of bacteriophage lysates and as the receptor in the conjugative assays. *S*. Typhimurium ATCC14028 Rif^R variants IC5, IC6 and IT2 were used for studying the bacterial defence mechanisms against bacteriophages. The *Escherichia coli* DH5α strain was used in cloning experiments.

All strains were cultured in Luria-Bertani (LB) liquid or agar media supplemented with the antibiotics when appropriate. *S*. Typhimurium ATCC14028 Rif^R strain and its variants IC5, IC6 and IT2 were cultured in the presence of 75 µg/mL rifampicin, while *S*. Typhimurium LB5000 was cultured in media supplemented with 200 µg/mL streptomycin. Strains harbouring the pKD4 plasmid were grown in media containing kanamycin (50 µg/mL), strains with pKD46, pKOBEGA, pACRISPR or pUA1165 plasmids were grown in media containing ampicillin (100 µg/mL), strains containing pKOBEG or pBAD33 plasmids were cultured in media with chloramphenicol (34 µg/mL), strains harbouring pCasPA plasmid were grown in tetracycline (17 µg/mL), and those containing pSET4s and pUA1148 plasmids were cultured in media with spectinomycin (100 µg/mL for *E. coli* or 200 µg/mL for *Salmonella*).

A1.2 Bacteriophages

The bacteriophages UAB_Phi20, UAB_Phi78, and UAB_Phi87 belong to *Lederbergvirus, Zendervirus*, and *Felixounavirus* genera, respectively, and their genomes were sequenced and fully characterized in previous studies (Bardina *et al*., 2012; Bardina *et al*., 2016).

A2. Microbiological methods

A2.1 Bacterial growth kinetics

Salmonella liquid LB cultures were grown for 18 h at 37ºC with agitation. Afterwards, cultures were diluted (1:100) and incubated at 37ºC, while monitoring the absorbance at 550 nm ($A_{550\ nm}$) using the Genesys 10S UV-Vis spectrophotometer (Thermo Scientific™) at 30-min or 1-h intervals. In addition, 100 µL samples were serially diluted in NaCl (0.9%) and plated on LB agar plates. The following day, plates containing between 15 and 300 colonies were counted, and the

concentration of viable cells in colony forming units (cfu)/mL, was determined. At least, two independent experiments were performed to obtain the standard deviations.

A2.2 Obtention of bacteriophage lysates

An overnight culture of the host strain was diluted 1/100 and incubated at 37ºC until it reached an $A_{550\ nm}$ of 0.6. At this point, the culture was infected with the desired phage at a multiplicity of infection (MOI) of 0.1 plaque forming units (pfu)/cfu and incubated at 37ºC until it reached an $A_{550\ nm}$ of 0.0-0.1, indicating full lysis of the host strain culture. The culture was then centrifuged at 10,414 x *g* during 10 min at 4ºC to remove cellular debris. The supernatant was filtered using 0.45 µm-pore-size filters (polyethersulfone membrane, Merck Life Science S.L.U.) and the phage titre was determined.

To increase the concentration of the phage lysate and obtain a higher phage titre, the lysate was ultracentrifuged at 27,000 revolutions per minute (r.p.m) for 2 h at 15ºC for UAB_Phi20 and UAB_Phi87, and at 27,000 r.p.m for 1 h 18 min at 4ºC for UAB_Phi78, in an Optima™ XPN-100 ultracentrifuge (Beckman Coulter™ Life Sciences) using ultra-clear centrifuge tubes (Beckman Coulter™ Life Sciences). After centrifugation, the supernatant was removed, and the pellet was resuspended in 0.5 mL of 10 mM $MgSO_4$ overnight using an orbital shaker at 200 r.p.m.

A2.3 Titration of phage lysates

Phage titres were determined using the double agar layer method previously described (Kutter, 2009). Briefly, 100 µL of ten-fold serial dilutions of the phage in 10 mM $MgSO_4$ and 100 µL of a 1/10 dilution of an overnight culture of the bacterial strain were mixed with 2.5 mL of 0.7% molten agar kept at 50ºC. The mixture was then plated onto LB plates and left to solidify before incubating for 18 h at 37ºC. The following day, those plates that contained between 15 and 300 plaques were counted and the phage concentration was determined in pfu/mL.

A2.4 Efficiency of bacteriophage plating (EOP)

The EOP assessment was tested under the stationary phase of both target (ATCC14028 Rif^R variants or pBAD33 containing ATCC14028 Rif^R strains) and parental sensitive host (ATCC14028 Rif^R) strains. The procedure for phage titration was performed as described in section A2.3. After incubation, the number of plaques was counted, and the titre calculated in pfu/mL. The EOP was calculated as: titre of the phage on the test strain/titre of the phage on the sensitive strain (Khan Mirzaei and Nilsson, 2015). A minimum of three assays were performed to calculate the average and standard deviation. According to the average EOP obtained, and for a specific bacterial host, a phage was considered as having high (EOP $\geq$ 0.5), medium (EOP < 0.5

but ≥ 0.1) or low (EOP between 0.001 and 0.1) production or being inefficient (EOP < 0.0001) (Khan Mirzaei and Nilsson, 2015).

A2.5 Phage adsorption rate constant

The adsorption rate constant (*K*) of bacteriophages on bacterial strains was determined as previously described (Kropinski, 2009). Briefly, an overnight culture of the desired strain was diluted 1/100 and incubated at 37ºC until it reached an $A_{550\ nm}$ of 0.4 and then adjusted to an $A_{550\ nm}$ of 0.2 in a final volume of 10 mL. One hundred µL were stored on ice to determine the concentration of bacterial viable cells as described in section A2.1. The culture was then infected at a MOI of 0.01 and incubated at 37ºC at 60 r.p.m. in a water bath. Every min for 15 min, 50 µL were taken from the culture and mixed in ice-cold LB (950 µL) with 10% chloroform. When all samples were collected, they were centrifuged for 1 min at 6,797 x *g*, and 100 µL of the supernatant were used for titration using the ATCC14028 Rif^R (sensitive strain) as the host (section A2.3). The adsorption constant was calculated as follows (Kropinski, 2009):

$$K = [2.3/(B \cdot t)] \cdot \log (P_0/P)$$

Being: B, bacterial viable cells (cfu/mL); t, necessary time for the adsorption of the 50% of the phages, in min; P_0, initial concentration of phage (pfu/mL); P, phage concentration (pfu/mL) at the time point where 50% of the phages are adsorbed.

In all cases, the average and standard deviation were calculated for a minimum of three replicates.

A2.6 Efficiency of centres of infection (ECOI) and burst size of bacteriophages

The determination of ECOI and burst size of bacteriophages (Figure A1) was conducted as previously described (Moineau *et al*., 1993, Kropinski, 2018) with some modifications.

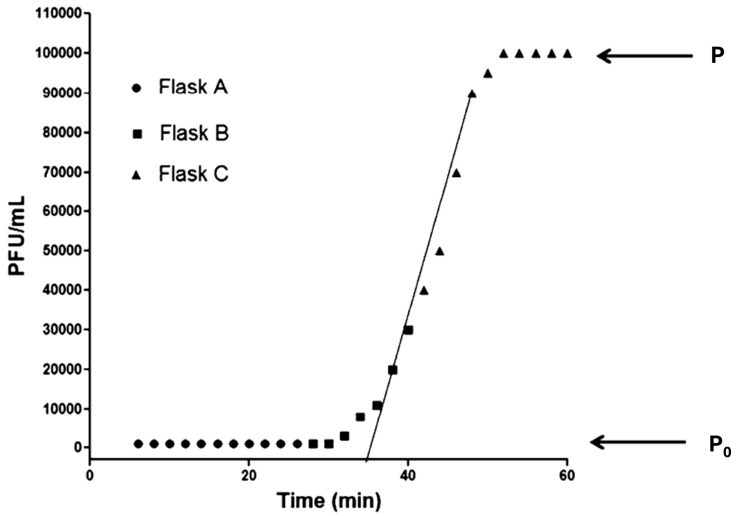


Figure A.1 Sample of plotted results of the production of phage during the time course of a single infection cycle. Obtained from Kropinski, 2018.

An overnight culture of the desired strain was diluted 1/100 and incubated at 37ºC until mid-log phase was achieved and adjusted to an $A_{550\ nm}$ of 0.4. After a 5-min incubation at 37ºC with shaking at 60 r.p.m. in a water bath, the culture was infected with the desired phage at a MOI of 0.1 pfu/cfu. The infected cultures were then kept at 37ºC without shaking (15 min for UAB_Phi20, 5 min for UAB_Phi78 and 20 min for UAB_Phi87) to facilitate phage adsorption. Following this incubation period, the 10^{-4} dilution of the culture was obtained in LB, and a 100 µL aliquot from this dilution was used for titration with the parental sensitive strain (section A2.3). The plaques counted were the value of the centre of infection (COI). From this data, the ECOI was calculated as following:

ECOI = COI of the phage on the test strain / COI of the phage on the sensitive strain

To ascertain the burst size of the phage, the 10^{-4} dilution indicated in the previous paragraph was further serially diluted in LB to the 10^{-7} dilution (in figure A1, flasks A corresponds to 10^{-5} dilution, B to 10^{-6} dilution and C to 10^{-7} dilution). For UAB_Phi20, 100 µL samples from the appropriate dilutions were withdrawn every 10 min during 2 h and the titration was performed using the parental sensitive strain as the host (section A2.3). For UAB_Phi78, samples were taken every 5 min for 50 min. Additionally, the concentration of non-adsorbed phage was determined at time zero. To do this, a 1 mL sample was taken at t_0 and mixed with 100 µL of ice-cold LB and 10% chloroform, centrifuged for 1 min at 6,797 x *g*, and 100 µL of the supernatant were used for titration (section A2.3) with the parental sensitive strain.

The burst size was calculated as following:

$$\text{Burst size} = P / (P_0\text{-Adsorption control})$$

Being: P, final phage concentration; P_0, initial phage concentration; Adsorption control, non-adsorbed phage concentration at t_0.

A2.7 One-step growth and Doermann

One-step growth experiments are classical experiments used for the determination of the eclipse and latent periods of a bacteriophage. The protocol outlined by Doermann, 1952 was followed, albeit with some modifications. An overnight culture of the desired strain was diluted 1/100 and incubated at 37ºC until achieving an $A_{550\ nm}$ of 0.4. Subsequently, potassium cyanide (KCN; Merck Life Science S.L.U.) was added at a final concentration of 10 mM, and the cultures were left at 37ºC without shaking for 10 min to synchronize the cells. The cultures were then infected with the desired phage at a MOI of 1 pfu/cfu, followed by an incubation period without shaking at 37ºC (15 min for UAB_Phi20) to facilitate phage adsorption. To remove residual KCN, the cultures were centrifuged at 12,880 x *g* for 10 min and resuspended in an equivalent volume of fresh LB medium. Serial decimal dilutions in a final volume of 10 mL (up to 8-fold dilution for

ATCC14028 Rif^R/pBAD33 and 7-fold for ATCC14028 Rif^R/pBAD33::*ibfA*) were prepared. These diluted cultures were incubated at 37ºC in a water bath at 150 r.p.m. For the determination of released phages, 100 µL of the appropriate dilution were directly used for titration (section A2.3) with the parental sensitive strain ATCC14028 Rif^R, at intervals of 10 min and up to 80 min after the phage adsorption. The total phage count (eclipse period) was also determined at the same time points. To do this, 100 µL of the corresponding dilutions were further diluted in 800 µL ice-cold LB supplemented with 10% chloroform, vigorously vortexed, and centrifuged for 1 min at 6,797 x *g*. Then, 100 µL of the resulting supernatant was used for titration (section A2.3) with the parental sensitive strain ATCC14028 Rif^R. To calculate standard deviations, the experiment was conducted in triplicate. The eclipse period was defined as the duration preceding the onset of the rise in total phage count, while the latent period was characterized as the duration preceding the rise in liberated phage count (Figure A2).

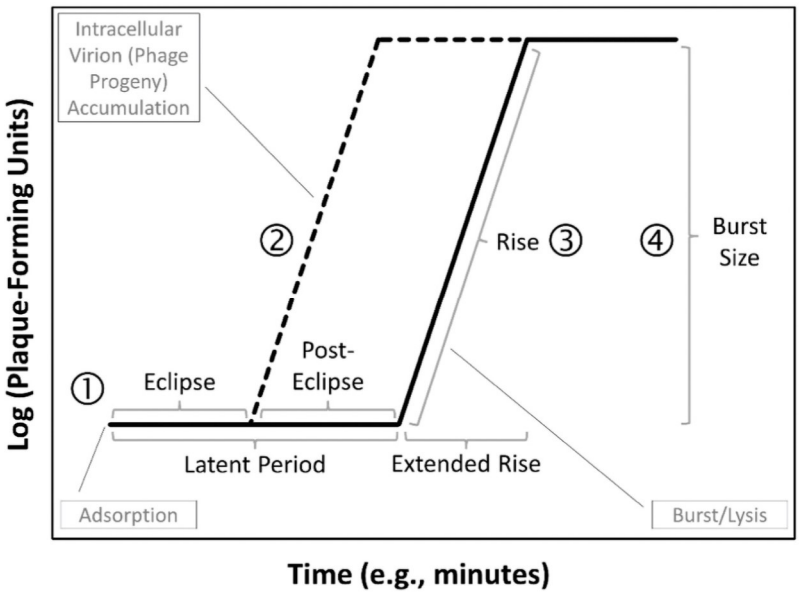


Figure A.2 Example of a one-step growth curve (Abedon, 2023). After phage adsorption, the eclipse period (1) starts, where phages replicate their genome and express their genes to start forming the necessary proteins for the generation of new phage progeny. When newly formed phages start to accumulate intracellularly (2), the eclipse period is finished, and post-eclipse starts, which will culminate in the lysis of the bacterial cell. The sum of the eclipse and post-eclipse period is known as the latent period, which corresponds to the time a bacterial cell is found infected by a phage. The burst of the cells will result in the release of viral particles (3) to the extracellular medium. The number of viral particles released by a single cell is known as the burst size (4).

A3. Biochemical methods

A3.1 Determination of adenosine triphosphate (ATP) concentration

Salmonella bacterial cultures infected with phage were prepared and synchronized as explained in section A2.7. Uninfected cultures were similarly prepared and were used as control. After the phage adsorption, 1 mL samples were collected for ATP extraction every 20 min until 80 min.

ATP extraction was carried out as described previously (Lee and Groisman, 2012). One hundred µL of perchloric acid 3M (Merck Life Science S.L.U.) were added to samples, and these were stored at -20ºC for at least 1 h. After this time, samples were defrosted in ice and 225 µL of cold buffer N (1M KOH, 0.5M Tris, 0.5M KCl) were added to each sample. These samples were then centrifuged at 6,797 x *g* for 10 min and at 4ºC, and 50 µL of the supernatant were mixed with 50 µL of buffer L (25 mM KCl, 50 mM $MgSO_4$, 100 mM HEPES pH 7.4). All samples were kept in ice until measure. Measurements were performed using the ATP determination Kit (Invitrogen), following the manufacturer's instructions in a Spark luminometer (Tecan) in a final volume of 200 µL per well (Laboratori de Luminescència i Espectroscòpia de Biomolècules, UAB). Each sample was measured twice, and the experiment was performed in triplicate to calculate the standard deviations.

A4. Genetic and molecular microbiological methods

A4.1 Conjugation assays

Assays of plasmid conjugation were performed by adapting a method previously described (García-Quintanilla *et al*., 2008). Overnight cultures of donor and recipient strains were diluted 1/100, grown to mid-log phase and adjusted to an $A_{550\ nm}$ of 0.4. Five hundred µL of each donor and recipient strains were mixed and harvested by centrifugation at 6,797 x *g* for 2 min. A major part of the supernatant was removed, and the pellet and about 100 µL of the supernatant were deposited onto a 0.45µm-pore-size membrane filter (mixed cellulose esters membrane, Merck Life Science S.L.U.) placed on an LB plate and incubated overnight at 37ºC. Afterwards, the filter was put in a tube with 1 mL NaCl 0.9% and vigorously vortexed to release the bacteria grown on the filter into the NaCl 0.9%, which were then plated on selective agar plates. As control, the same procedure was followed for the donor and recipient strains, independently. The number of colonies was recorded, and the conjugation frequencies were calculated per donor bacterium. Transfer of plasmids onto transconjugants was checked by conventional PCR (section A4.3) with appropriate primers (Table A.2).

A4.2 DNA electrotransformation

The *Salmonella* or *E. coli* DH5α electrocompetent cells were prepared according to the following general method. A 1/100 dilution of an overnight culture was grown at 37ºC without antibiotics until it reached an $A_{550\ nm}$ of 0.6. Then, two washing steps with the same volume of Milli-Q water and a third washing step with the same volume of glycerol 10% were performed by centrifuging at 12,857 x *g* for 10 min at 4ºC, and the final pellet was resuspended in 300 µL of glycerol 10%. One hundred µL aliquots were made and stored at -80ºC. However, a special protocol was applied for obtaining pKOBEGA-containing, pKOBEG-containing, or pCasPA-containing electrocompetent cells. In these cases, the overnight culture was diluted 1/100 in SOB (20 g/L

tryptone, 5g/L yeast extract, 0.5 g/L NaCl, and 0.5 mL KCl 2M, pH 7) with ampicillin (100 µg/mL), chloramphenicol (34 µg/mL) or tetracycline (17 µg/mL), depending on the plasmid, and grown at 30ºC for the thermosensitive plasmids and 37ºC for strains harbouring pCasPA, to an $A_{550\ nm}$ of 0.4-0.5. Then, L-arabinose 20 mM was added to the culture and incubated at 30ºC or 37ºC for 20 min. Cells were made electrocompetent by three washing steps with glycerol 10% at final volumes of 0.4, 0.2 and 0.1. Plasmid-containing electrocompetent cells were used the same day they were prepared.

For electroporation**,** 100 µL of electrocompetent cells and 100 ng of plasmidic DNA or 1 µg of linear DNA were mixed and left on ice for five min before electroporation. Transformation of cells was done in 2 mm gap electroporation cuvettes (Cell Projects) and performed with an electrical pulse of 2.5 kV/cm^2, 25 µF capacitance and 200 Ω resistance (Biorad Gene Pulser; Biorad, California, United States). After the electrical pulse, cells were recovered in 1 mL of cold LB, except when otherwise indicated. Recovered cells were left at 37ºC, or at 30ºC where thermosensitive plasmids were present, for 1 h with agitation at 150 r.p.m. before plating in culture media supplemented appropriately, except where it is stated otherwise.

A4.3 Polymerase chain reaction (PCR)

PCR reactions (25 µL) were performed using the Taq DNA Polymerase (Invitrogen) or the Phusion High-Fidelity DNA Polymerase (Thermo Fisher Scientific) where necessary, following manufacturer's instructions. Primers (Table A.2) were added at a final concentration of 0.5 pmols and deoxynucleotide triphosphates [dNTPs (Thermo Fisher Scientific)] at a final concentration of 0.2 mM. When the PCR was performed using DNA, 100 ng were added to the PCR reaction. If the PCR was performed from colony, this was resuspended in 100 µL of Milli-Q water and boiled for 10 min at 100ºC, and after removal of cellular debris by centrifugation, 5 µL were added to the PCR reaction. Hybridization temperature was determined according to the primer pair used for each reaction, and extension time was calculated in relation to the size of the expected PCR product. For the visualization of PCR products, these were mixed with 1:10 loading buffer (25% glycerol, 5 mM xylene cyanol, 4 mM bromophenol blue, 100 mM EDTA, pH 8.0) and loaded in 1%, 1.5% or 2% agarose (agarose E, Condalab) gels prepared in TAE 1X (40 mM Tris, 0.35% glacial acetic acid, 10 mM EDTA). 1% RedSafeTM Nucleic Acid Staining Solution (iNtRON Technology) was added into the agarose before allowing it to solidify. Gels were run in TAE 1X on a horizontal electrophoresis cell (Mini-Sub Cell GT Cell, Bio-Rad) for 30 min at 100 V. Visualization was done in a transillumination and image capture device (E-box-1000/20 M, Vilber Loumat). Molecular weight markers used were NZYDNA Ladder III, NZYDNA Ladder V or NZYDNA Ladder VII (NZYTech, Lisboa, Portugal) depending on the expected product size.

A4.4 Introduction of kanamycin resistance cassette into pUA1139

Insertion of a kanamycin resistance cassette in the pUA1139 plasmid was performed using a λ-Red recombinase strategy (Datsenko and Wanner, 2000). Briefly, the kanamycin resistance cassette from pKD4 [resistant to kanamycin and ampicillin (Km^R, Amp^R), Table A.1] was amplified by PCR (section A4.3) using Phusion™ High-fidelity DNA polymerase (Thermo Scientific™) and primers with homology with the desired regions of pUA1139 (Table A.2). The resulting linear PCR product was purified with NzyGelpure kit (NZYTech, Lisboa, Portugal), eluted in 30µL Milli-Q water and treated with DpnI enzyme (New England Biolabs, Inc) to remove any remaining pKD4 plasmid. Briefly, 57 µL MQ, 10 µL CutSmart buffer and 3 µL DpnI enzyme were added to the PCR product and incubated overnight at 37ºC. The enzyme was inactivated at 80ºC for 20 min and the product was purified using the NzyGelpure kit (NZYTech, Lisboa, Portugal).

In parallel, the pKOBEGA plasmid (Amp^R; Table A.1) was introduced by electroporation (section A4.2) into the target bacteria and selected on LB agar plates supplemented with ampicillin (100 µg/mL). The linear PCR product containing the kanamycin resistance cassette was then electroporated (section A4.2) into the pKOBEGA-containing competent cells. Cells were recovered in SOB containing 20 mM L-arabinose and incubated at 30ºC for 1 h at 150 r.p.m. Transformant clones were selected in LB agar plates supplemented with kanamycin (50µg/mL). The kanamycin cassette insertion was confirmed by PCR (section A4.3) and sequencing (Macrogen) using the appropriate primers (Table A.2).

Finally, pKOBEGA was cured by temperature by incubating an overnight culture at 42ºC, from which a 1/100 dilution was further incubated 3 h at 42ºC. Then, serial dilutions up to 10^{-6} were plated in LB plates. Replicates in LB plates containing ampicillin (100 µg/mL) and kanamycin (50 µg/mL) and LB plates containing kanamycin (50 µg/mL) were done to select for clones that were ampicillin sensitive and kanamycin resistant.

A4.5 Cloning of the *ibfA* gene or *ibfA*-containing transcriptional unit

The *ibfA* gene with its own promoter or the *ibfA*-containing transcriptional unit with its own promoter were obtained through PCR (section A4.3) using Phusion™ High-fidelity DNA polymerase (Thermo Scientific™) and appropriate primers (Table A.2) from pUA1135 plasmid (NCBI accession number: MW590592.1). Genomic DNA was obtained from *S.* Typhimurium IC5 strain using Easy-DNA™ kit (Invitrogen) following manufacturer's instructions. The PCR product was purified using NzyGelpure kit (NZYTech, Lisboa, Portugal). Simultaneously, 1µg of pBAD33 vector [resistant to chloramphenicol (Cm^R); Table A.1] was linearized with KpnI (New England Biolabs, Inc) restriction enzyme. A first round of digestion was done by adding 20 units of KpnI enzyme and 2 µL of 10X rCutSmart™ Buffer in a final volume of 20 µL and

incubating at 37ºC for 1 h. A second digestion round consisted of adding 60 units of KpnI enzyme into the previous mixture and incubating 1 more h at 37ºC. Dephosphorylation of the digested plasmid to avoid re-ligation was performed by two 30 min rounds of incubation at 37ºC where 1 unit of alkaline phosphatase (New England Biolabs, Inc) was previously added. The digested and dephosphorylated plasmid was purified using NzyGelpure kit (NZYTech, Lisboa, Portugal) from the agarose gel and treated with DpnI enzyme as previously described in section A4.4.

The PCR product was ligated onto the linearized plasmid using NEBuilder® HiFi DNA Assembly Master Mix (New England Biolabs, Inc), following manufacturer's instructions. The resulting construction was electroporated into competent *E. coli* DH5α cells and cells that had incorporated the pBAD33 plasmid were selected on LB agar plated containing chloramphenicol (34 μg/mL). PCR (section A4.3) with appropriate primers (Table A.2) was used to check the correct insertion of *ibfA* or the *ibfA*-containing transcriptional unit into the region of the pBAD33 plasmid and sequencing (Macrogen) with appropriate primers (Table A.2) verified that the resulting constructs contained no mutations.

A4.6 Deletion of the *ibfA* gene or *ibfA*-containing transcriptional unit

A λ-Red recombinase strategy (Datsenko and Wanner, 2000) was performed to delete the *ibfA* gene or the *ibfA*-containing transcriptional unit encoded in the pUA1135 plasmid of the *Salmonella* IC5 variant strain. Briefly, *Salmonella* cells were made electrocompetent and pKOBEG plasmid (Cm^R; Table A.1; Chaveroche *et al*., 2000) was electroporated (section A4.2). Cells were plated on LB agar plates containing chloramphenicol (34 μg/mL). Simultaneously, PCR (section A4.3) using Phusion™ High-fidelity DNA polymerase (Thermo Scientific™) was performed to obtain the kanamycin resistance cassette (from pKD4 plasmid; Table A.1) with homology tails with the desired region where the kanamycin cassette should be introduced in pUA1135 plasmid. The resulting linear PCR product was purified using NzyGelpure kit (NZYTech, Lisboa, Portugal), eluted in 30 μL Milli-Q water and treated with DpnI enzyme (New England Biolabs, Inc) as previously described in section A4.4 to remove all remaining pKD4 plasmid. Afterwards, it was introduced by electroporation (section A4.2) in target pKOBEG-containing cells. Transformant cells were selected on LB plates supplemented with kanamycin (50 μg/mL) and incubated overnight at 30ºC. The kanamycin cassette insertion was confirmed by PCR (section A4.3; Table A.2) and sequencing (Macrogen; Table A.2).

Curing of the pKOBEG plasmid was done by temperature treatment similarly to curing of pKOBEGA described in section A4.4. In this case, plating was done in LB plates containing kanamycin (50 μg/mL) and replicates were done in kanamycin (50 μg/mL) LB plates and kanamycin (50 μg/mL) and chloramphenicol (34 μg/mL) LB plates to select for clones that were kanamycin resistant and chloramphenicol susceptible.

A4.7 Plasmid curing methods

An adaptation of a two plasmid CRISPR-Cas9 method (Chen *et al*. 2018) was used to cure plasmids pUA1135 and pUA1136 identified in IC5 and IC6 *S.* Typhimurium Rif^R variants, respectively. This system consisted in using the pCasPA plasmid [resistant to tetracycline (Tet^R) and Amp^R; Table A.1] encoding the Cas9 protein and the λ-Red recombination system, and the pACRISPR plasmid (Amp^R; Table A.1) with the *Bsa*I site for cloning of the spacers.

Firstly, the *bla* gene that codified the β-lactamase in the pACRISPR plasmid (Table A.1) was replaced by a spectinomycin gene (*spt*). To do so, the plasmid was linearized using inverse PCR (section A4.3) with appropriate primers flanking the *bla* gene (Table A.2). The *spt* gene was obtained from plasmid pSET4s [resistant to spectinomycin (Spt^R); Table A.1; Takamatsu *et al*., 2001] by PCR amplification (section A4.3) using the Phusion™ High-fidelity DNA polymerase (Thermo Scientific™) and appropriate primers (Table A.2). Assembly was accomplished through NEBuilder® HiFi DNA Assembly Master Mix (New England Biolabs, Inc) following manufacturer's instructions. After transforming by electroporation (section A4.2) in *E. coli* DH5α competent cells, transformant clones were selected on LB agar plates supplemented with 100 µg/mL spectinomycin, and correct introduction of the *spt* gene was checked by conventional PCR (section A4.3) and sequencing (Macrogen; Table A.2). The resulting plasmid was named pUA1148 (Spt^R; Table A.1).

In parallel, a specific spacer (20 nt sequence) targeting the *repA* gene of pUA1135 and pUA1136 plasmids (gRNA48; Table A.2) was designed using the Find CRISPR Sites Tool of the Geneious Prime software, following the specified software instructions, removing all those sites that had off-targets in the *S.* Typhimurium chromosome or pSLT. The spacer with the highest activity and specificity scores was selected and the phosphorylated and annealed primers containing the spacer sequences were designed as described (Chen *et al*., 2018). Annealing of phosphorylated primers was performed by joining 2 µL of each primer at a concentration of 50 µM, 2.5 µL of NaCl 1M and 46 µL of Milli-Q water and incubating 3 min at 95ºC and slowly cooled down to room temperature using a thermocycler. The spacer sequence was cloned into the pUA1148 (Spt^R) using NEB® Golden Gate Assembly Kit (BsaI-HF®v2; New England Biolabs, Inc). Briefly, 1 µL 10X T4 DNA ligase buffer, 0.5 µL NEB Golden Gate Assembly Mix, 75 ng pUA1148 plasmid and a 2:1 molar ratio of 100 nM annealed oligos in relation to the plasmid were assembled in a thermocycler with a first incubation of 1 h at 37ºC, followed by 5 min at 60ºC and a final decrease of temperature to 10ºC. The resulting product (pUA1148+gRNA48, Spt^R; Table A.1) was transformed by electroporation (section A4.2) into *E. coli* DH5α competent cells, selected on LB agar plates supplemented with 100 µg/mL spectinomycin after 18 h of incubation at 37ºC, and

the spacer sequence was verified using PCR (section A4.3) and Sanger sequencing (Macrogen; Table A.2).

Simultaneously, a 1/100 dilution of an overnight culture of *Salmonella* IC5 (pUA1135) or IC6 (pUA1136) variants was grown until an $A_{550\ nm}$ of 0.4-0.6 and the cells were made electrocompetent. Then, 1 µg of pCasPA plasmid (Tet^R; Table A.2) was transformed by electroporation (section A4.2) and pCasPA-containing cells were selected on LB agar plates supplemented with 17 µg/mL tetracycline after 18 h of incubation at 37ºC. The presence of pCasPA was checked by PCR (section A4.3; Table A.2).

The previously obtained *Salmonella* strains containing the pCasPA plasmid were made electrocompetent (section A4.3) and 100 ng of pUA1148+gRNA48 plasmid were transformed by electroporation. The cells containing both plasmids pCasPA and pUA1148+gRNA48 were selected in plates containing 17 µg/mL tetracycline and 200 µg/mL spectinomycin. Curing of pUA1135 or pUA1136 plasmids was checked by PCR (section A4.3) using suitable primers (Table A.2). Finally, sucrose counter-selection was used to cure the pCasPA and pUA1148+gRNA48 plasmids. Briefly, a 1/100 dilution of an overnight culture of clones with cured pUA1135 or pUA1136 plasmids was grown for 3 h at 37ºC, serially diluted in 0.9% NaCl and plated on 5% v/v sucrose LB agar plates, and the absence of both plasmids was checked by PCR (section A4.3) using specific primers (Table A.2).

The elimination of plasmid pUA1139 from IT2 *Salmonella* variant strain was carried out following a method based on λ-Red mutagenesis and I-*Sce*I nuclease (de Moraes and Teplitski, 2015). One-step inactivation (section A4.4; Datsenko and Wanner, 2000) was used to introduce the kanamycin resistance cassette and the restriction site for I-*Sce*I into pUA1139 [obtained from pKD4 plasmid through PCR (section A4.3) with suitable primers (Table A.2)], deleting gene *pUA1139_00007*. To do so, the restriction site for I-*Sce*I was incorporated at the 5' end of the kanamycin resistance cassette by adding its restriction sequence into the primers used to amplify the kanamycin resistance cassette from pKD4 (section A4.4).

At the same time, the pKD46 plasmid (Amp^R; Table A.1) was amplified by inverse PCR (section A4.3; Table A.2) removing the genes related to the λ-Red system. The PCR product was purified from the agarose gel using NzyGelpure kit (NZYTech, Lisboa, Portugal) and treated with DpnI enzyme as previously described in section A4.4 to remove possibly remaining circular pKD46 plasmid. Fifty ng of the resulting PCR were ligated using T4 ligase (Thermo Scientific™) following manufacturer's instructions. One µg of the resulting plasmid was digested by the addition of 20 units of NcoI restriction enzyme (New England Biolabs, Inc) and 2 µL of 10X rCutSmart™ Buffer in a final volume of 20 µL and incubated for 1 h at 37ºC. A second round of digestion was performed by the addition of 60 units of NcoI enzyme and incubation for 1 h at

37ºC. Dephosphorylation and purification was performed as previously described in section A4.5. The I-*Sce*I nuclease controlled by the tetracycline inducible promoter (P_{tetA}; synthesized at ATG:biosynthetics GmbH, Germany; sequence obtained from Blank *et al*., 2011) was cloned into the NcoI restriction site using NEBuilder® HiFi DNA Assembly Master Mix (New England Biolabs, Inc) following manufacturer's instructions. The resulting plasmid pUA1165 (Amp^R; Table A.1) was transformed by electroporation (section A4.2) of *E. coli* DH5α competent cells. The transformants were selected on LB agar plates supplemented with ampicillin (100 μg/mL) and checked by conventional PCR as described in section A4.3 (Table A.2).

Afterwards, *Salmonella* IT2 variant containing the previously modified pUA1139 was made electrocompetent (section A4.2) and 100 ng of plasmid pUA1165 were transformed by electroporation. Induction of I-*Sce*I nuclease was done as described previously (de Moraes and Teplitski, 2015). Briefly, after 1 h of incubation at 30ºC, the transformed cells were plated onto LB plates containing 100 μg/mL ampicillin and 125 ng/mL anhydrotetracycline (Merck Life Science S.L.U.) and incubated overnight at 30ºC. Clones that were kanamycin sensitive were checked by PCR (section A4.3) with suitable primers (Table A.2).

Finally, pUA1165 was cured by temperature as described in section A4.4. Replicates in LB plates containing ampicillin (100 μg/mL) and LB plates without antibiotic were done to select for clones that were ampicillin sensitive.

A4.8 Transcriptional analysis of the *ibfA* operon

RNA extraction from *Salmonella* cultures was done using the RNeasy Mini kit (Qiagen) following manufacturer's instructions with a previous lysis step with lysozyme (50 mg/mL) in TE buffer (10 mM Tris-HCl, pH 7.5, 1 mM EDTA, pH 8.0), by incubation at 37ºC and vortexing every 2 min for 10 min. DNA removal from RNA samples was accomplished with the TURBO DNA-free kit (Invitrogen) as described by the manufacturer with modifications. Briefly, 90 μL samples were incubated with 1X TURBO DNase™ Buffer and 8 units of TURBO DNase™ Enzyme for 45 min at 37ºC. This treatment was performed twice. Enzyme inactivation was done according to manufacturer's instructions. RNA sample cleanup was done using the RNeasy Mini kit (Qiagen).

The DNase-treated RNAs (1 μg) were subjected to reverse transcription using the NZY First-Strand cDNA Synthesis Kit (NZYTech, Lisboa, Portugal) following the manufacturer's conditions and appropriate primers directed towards the genes forming the transcriptional unit (Table A.2). Afterwards, cDNA amplification was performed by conventional PCR (section A4.3) using Invitrogen™ Taq DNA Polymerase and the same primers. The resulting PCR products were visualized by agarose (2%) gel electrophoresis and stained in RedSafe™ Nucleic Acid Staining Solution (iNtRON). DNA molecular weight marker NZYDNA Ladder V marker (NZYTech) was used as standard.

A4.9 Measurement of replication of phage genome by quantitative real-time PCR

Quantitative real-time PCR (qPCR) was used to quantify *Salmonella* DNA, intracellular bacteriophage DNA, and extracellular bacteriophage DNA. Bacterial cultures were prepared and synchronized as explained above (section A2.7) and infected with the bacteriophage at a MOI of 1 pfu/cfu. Uninfected cultures were similarly prepared without the addition of the phage and used to obtain a sample at time 0 as a control. After the appropriate adsorption time and removal of the KCN, the cultures were incubated at 37ºC in an orbital shaker at 150 r.p.m. One mL aliquots were withdrawn just after phage adsorption (t=0 min) and at the times 15, 30, 50, 70 and 90 min, and then centrifuged at 6,797 x *g* for 2 min. The pellets were washed once with NaCl (0.9%) and frozen at -80ºC. The supernatants were kept at 4ºC and directly used to quantify extracellular phage DNA, following the protocol described above (section A2.3) to ensure correct phage production. Simultaneously, 100 µL samples of the culture were collected, serially diluted in 0.9% NaCl, and plated onto LB plates to determine viable cell counts (section A2.1) to control for correct infection kinetics. Once all samples were collected, pellets were defrosted in ice and resuspended in 100 µL TE buffer (10 mM Tris-HCl, pH 7.5, 1 mM EDTA, pH 8.0). To quantify intracellular *Salmonella* and phage DNA, cells lysis was carried out by temperature treatment at 100ºC for 10 min. Removal of cellular debris was done by centrifugation 6,797 x *g* for 2 min and the supernatant was kept at -20ºC for quantification of *Salmonella* DNA and intracellular bacteriophage DNA.

qPCR was conducted employing 2 µl of template DNA from cell pellets or 2 µl of supernatants. Each qPCR reaction mixture consisted of the appropriate primers (0.5 µM final concentration; Table A.2), Milli-Q water and 1X LightCycler® 480 SYBR Green I Master kit (Roche) buffer resulting in a final volume of 20 µl. The qPCR assays were executed on a Lightcycler 480® Instrument II (LC480, Roche), employing the following cycle conditions: preincubation at 95ºC for 30 s followed by 45 amplification cycles of 3 s at 95ºC, 15 s at 57ºC and 18 s at 72ºC, and a final melting curve up to 95ºC. All qPCR reactions were performed in technical duplicates, and non-infected samples were included as negative controls.

Total DNA extracted from *S.* Typhimurium ATCC14028 using the Easy DNA kit (Invitrogen) and UAB_Phi20 DNA purified as the phenol-chloroform protocol (Sambrook and Russel, 2001) were utilized to generate respective standard curves. To obtain the curves, 10-fold serial dilutions of the bacterial and phage DNA were prepared, specifically from 10^0 to 10^9 genome copies/µL of templates and tested in triplicate to determine the copy number per µL for the target *gyrB* (*Salmonella*) and *BI085_gp03* (helicase of UAB_Phi20 phage) genes (Table A.2). The determination of the number of gene copies, considering the size of bacterial or phage genome, was accomplished as previously outlined (Ritalahti *et al*., 2006). Similarly, the results of both

intracellular and extracellular phage DNA and *Salmonella* DNA expressed in number of copies/mL of the *BI085_gp03* and *gyrB* genes, respectively, proceeded from the standard curves data and were calculated as described (Ritalahti *et al*., 2006), considering the dilution factor of each sample. Three biological replicates and two technical samples in each qPCR experiments were performed, to calculate the average gene copy number per mL along with the corresponding standard deviations.

A4.10 Gene expression determination by reverse transcription-quantitative polymerase chain reaction

To study the expression of both the *ibfA* gene and several bacteriophage genes during phage infection, reverse transcription-quantitative polymerase chain reaction (RT-qPCR) was conducted. Bacterial cultures were prepared as previously explained in section A2.7. Infection was done at a MOI of 1 pfu/cfu. Uninfected cultures underwent a similar treatment to infected cultures but without the addition of the phage.

At the desired times following phage adsorption, two 5 mL samples were withdrawn from the cultures for RNA extraction. These samples were mixed with 1/10 stop solution (1:10 buffered phenol, 9:10 absolute EtOH; Brandão *et al*., 2021), vortexed and placed on ice. After collecting all the samples, they were centrifuged at 12,857 x *g* for 10 min and the supernatant was removed. Pellets were stored at -80ºC until RNA extraction. To ensure proper progression of infection kinetics, 100 µL of the cultures were withdrawn at the specified times, serially diluted in 0.9% NaCl, and plated on LB plates to determine the viable concentration, as described in section A2.1. Furthermore, another 100 µL sample was taken from the culture and the phage titre was determined, as described in section A2.3.

RNA extraction from the stored pellets followed the protocol described in section A4.8. DNA removal involved an additional step with 5 µL 10X TURBO DNase™ Buffer and 4 units TURBO DNase™ Enzyme, which was incubated at 37ºC for 1 h. Enzyme inactivation and RNA sample cleanup were carried out as detailed in section A4.8.

One-step RT-qPCR was done on a Lightcycler 480® Instrument II (LC480, Roche) using the LightCycler® RNA Master SYBR Green I kit (Roche). The qPCR reactions (20 µL) comprised the primers (Table A.2) of the target genes at a final concentration of 0.3 µM, 3.25 mM $Mn(OAc)_2$, 1X LightCycler® RNA Master SYBR Green I buffer, and 2 µL of the RNA samples. These samples were prepared by adjusting them all to the same concentration. For quantification of the phage genes, RNA samples were further diluted 1:10 and for the 16S rRNA gene of *Salmonella*, which served as the reference gene, they were diluted 1:100. RT-qPCR conditions mirrored those detailed previously for qPCR (section A4.9) but with an initial RT step at 61ºC for 20 min prior to qPCR reaction. The quantification of mRNA transcripts for target genes was determined using

the E-Method which accounts for the efficiency of target genes as well as that of reference gene (16S rRNA), with time 0 as the calibrator (Roche, 2019; Tellmann, 2006).

$$\frac{E_t^{\,CT(t)calibrator-C\ \ (t)sample}}{E_r^{\,CT(r)calibrator-\quad (r)sample}}$$

E, the qPCR efficiency of the primers; CT, the crossing point obtained by the qPCR reaction; t, the target gene; r, the reference gene; calibrator, time 0; sample, other time points.

A minimum of three independent experiments were carried out, and each RNA sample was analysed twice in each RT-qPCR experiment.

A4.11 Microscopic methods

To visualize the formation of viral capsids inside bacterial cells, transmission electron microscopy (TEM) was employed. Synchronic cultures of the *Salmonella* strains were prepared as described earlier (section A2.7), which were infected with the bacteriophage at a MOI of 1 pfu/cfu. Samples of 10 mL were collected from the cultures at 0, 20, 30, 40, 60 and 80-min after phage adsorption and centrifuged at 12,857 x *g* for 10 min. The resulting pellets were suspended in a 2 mL fixative solution [2% paraformaldehyde, 2.5% glutaraldehyde in phosphate buffer (0.1M NaH_2PO_4, pH 7.4)] and incubated for at least 2 h at 4ºC. After fixation, the samples were washed four times with phosphate buffer for 10 min each. Post-fixation was performed using 1% OsO_4 overnight at 4ºC. Then, the samples were washed four times with water for 5 min, and 1% uranyl acetate was added, and they were kept overnight at 4ºC. Finally, the washing step was repeated.

Dehydration was carried out using a series of acetone solutions with increasing concentrations of 50%, 70%, 90%, 96%, and 100%. The samples were then embedded in Epon-815 Resin (Electron Microscopy Sciences) using a series of resin:acetone mixtures with ratios 1:3, 2:2, 3:1 and 4:0, at room temperature for 2 h each, and finally left overnight with resin. The following day, another change of resin was done and left for 2 h at room temperature. Polymerization was performed at 70ºC for 48 h. Subsequently, 70 nm sections were obtained using a Reichert-Jung Ultracut E ultramicrotome and placed on PELCO® copper-coated 200-mesh grids (Ted Pella, Inc.). The stained sections were examined in a Hitachi H-7000 transmission electron microscope at 100 kV at instrumental magnifications of 0.5 µm to 1 µm. Preparation of samples for TEM and visualization were done in Servei de Microscòpia i Difracció de Raig X (UAB).

A5. Bioinformatic studies

The following procedure was followed to obtain the plasmid sequences from the unmapped Illumina reads of the genome sequences of the seven *Salmonella* variants. First, *de novo* re-assembly of trimmed paired-end reads was performed using SPAdes v3.11.1 (with ‘careful -k

21,33,55,77' settings; Bankevisch *et al*., 2012). BLASTn (coverage > 75%, e-value < 1E-10; Altschul *et al*., 1997) was used to assess those scaffolds that matched the genome or plasmid of *S*. Typhimurium 14028s, which were removed from further analyses. Combining of the retained scaffolds with PLACNETw assemblies (Vielva *et al*., 2017) was done using Velvet (Zerbino, 2010) through Geneious Prime 2020.0.4, which rendered complete plasmid sequences. These sequences were annotated using Prokka version 1.12 (Seemann, 2014) against the COG (Tatusov *et al*., 2000), HAMAP (Pedruzzi *et al*., 2015) and Pfam (Finn *et al*., 2016) databases, using the three best BLASTn complete plasmid hits as reference. Finally, PlasmidFinder 2.1 web-tool (Carattoli *et al*., 2014) was used to determine the replicon sequences of the plasmids.

The functional enrichment of plasmid pUA1135 was done using eggNOG-mapper v2 (Huerta-Cepas *et al*., 2019). A search of known defence systems in plasmid pUA1135 sequence was performed with PADLOC (Payne *et al*., 2022) and DefenseFinder (Abby *et al*., 2014; Tesson *et al*., 2022). On the other hand, the presence of unknown mechanisms of phage interference in the plasmid sequence was assessed as follows. First, a tBLASTN search against the PLSDB database was used to identify thirty homologous plasmids, prioritizing query coverage. Then, the variability of pUA1135 and its homologues was determined. To do so, plasmids were aligned using Mauve (Darling *et al*., 2010) and the variable region of each plasmid was identified as the sequence found between the *repA* and *parA* genes. Afterwards, the clusters of orthologous groups (COGs) for each gene found in all plasmids (both variable and non-variable regions) were determined by using hmmscan against the COG database (Tatusov *et al*., 1997; Galperin *et al*., 2014). Then, pairwise comparisons of COGs from the variable regions were done and the variability was calculated as the sum of shared COGs found in both plasmids divided by the sum of all COGs found in both plasmids. Finally, COGs from the non-variable regions were compared pairwise, and the variability calculated.

To construct the phylogeny of IbfA, a BLASTP search was conducted using the IbfA protein sequence against the *clustered nr* database of bacterial (taxid:2) and archaeal (taxid:2157) protein sequences. Results were filtered to include only hits with >85% query coverage and those from complete chromosomal or plasmid sequences were kept. Alignments were performed using ClustalX (Larkin *et al*., 2007) and T-Coffee (Notredame *et al*., 2000) with default parameters, and integrated with T-Coffee. iqtree (Minh *et al*., 2020) was used with default parameters to perform phylogenetic inference and annotation of the resulting tree was performed with iTOL (Letunic *et al*., 2021).

BPROM (Solovyev and Salamov 2011) and SAPHHIRE.CNN (Coppens *et al*., 2022) using default parameters were used as promoter prediction tools for *ibfA* and its transcriptional unit. The study of the protein functional domains of IbfA was done using HHpred (Söding, 2005)

selecting the PDB, PFAM and COG databases and the *E. coli* proteome, with otherwise default parameters. Furthermore, the sequence-based search against Alphafold DB (Jumper *et al*., 2021; Varadi *et al*., 2022) was used to find similar proteins with an experimentally-obtained function or structure.

A6. Statistical analysis

The t-Test using Prism 8.0.2 (GraphPad, La Jolla, CA, USA) was used to assess the differences between means of the data obtained. Data are depicted as mean and standard deviation or geometric mean and standard deviation of the mean for gene expression studies. Differences were considered as statistically significant when $p < 0.05$.

Table A.1 Strains and plasmids used in this work.

Strain	Relevant characteristics	Source or reference
ATCC14028 Rif^R	*S.* Typhimurium; Rif^R	Molecular Microbiology group (UAB)
LB5000	*S.* Typhimurium *metA22 metE551 trpC2 ilv-452 H1-b metA22 metE551 trpC2 ilv-452 H1-b H2-e,n,x* (cured of Fels 2) *fla-66 rpsL120 xyl-404 leu hsdL6 hsdSA29 hsdSB*	University of Calgary
DH5α	*E. coli supE4 ΔlacU169* (φ80 Δ*lacZ* Δ*M15*) *hsdR17, recA1, endA1, gyrA96, thi-1, relA1*	Clontech
IC5	ATCC14028 Rif^R variant; pUA1135, Amp^R	This work
IC6	ATCC14028 Rif^R variant; pUA1136, Amp^R	
IT2	ATCC14028 Rif^R variant; pUA1139, Km^R	
ATCC14028 Rif^R/ pBAD33	*S.* Typhimurium with pBAD33 vector; Rif^R, Cm^R	This work
ATCC14028 Rif^R/ pBAD33::*ibfA*	*S.* Typhimurium clone with pBAD33 vector containing *ibfA* gene with its own promoter; Rif^R, Cm^R	
Plasmid	**Relevant characteristics**	**Source or reference**
pKD4	Amp^R Km^R	Datsenko and Warner, 2000
pKD46	Vector containing the λ-Red recombinase system, Amp^R, thermosensitive	
pKOBEG	Vector containing the λ-Red recombinase system, Cm^R, thermosensitive	Generous gift of Prof. I. Lasa; Chaveroche *et al*., 2000
pKOBEGA	Vector containing the λ-Red recombinase system, Amp^R, thermosensitive	
pCasPA	Vector codifying Cas9 nuclease and λ-Red recombination system, Tet^R, sucrose counter-selectable, Amp^R	Generous gift of Prof. Quanjiang Ji (ShanghaiTech). Chen *et al*., 2018.
pACRISPR	Vector codifying sgRNA for targeting a specific sequence, Amp^R	
pSET4s	Replication function of pG + host3 and pUC19, *lacZ*' Spt^R	Generous gift of Dr. T. Sekizaki. Takamatsu *et al*., 2001
pUA1148	pACRISPR derivative; Spt^R	This work
pUA1148+gRNA48	pUA1148 derivative for pUA1135 and pUA1136 elimination; Spt^R	
pUA1165	pKD46 plasmid without λ-Red system genes and with I-*Sce*I endonuclease under control of tetracycline inducible promoter (P_{tetA}), thermosensitive, Amp^R	
pBAD33	Low copy number vector containing the arabinose inducible pBAD promoter, Cm^R	Guzman *et al*., 1995
pBAD33::*ibfA*	pBAD33 derivative containing the *ibfA* gene cloned under the control of its own promoter, Cm^R	This work
pBAD33:: *pUA1135_00003, ibfA, ydeA, ydfA*	pBAD33 derivative containing the *ibfA*-containing transcriptional unit cloned under the control of its own promoter, Cm^R	

Rif, rifampicin; Amp, ampicillin; Km, kanamycin; Cm, chloramphenicol; Tet, tetracycline; Spt, spectinomycin; R, resistant.

Table A.2 Primers used in this work.

Name	Sequence (5'-3')	Application
Rep2_fw	GTGAGCACTCCACCAAAC	Detection of plasmids pUA1135, pUA1136, and pUA1139.
Rep2_rv	GACGCCCAGCATCTG	
P4_Km_P1[a]	GGAAACCGCCCGTTTCTTTTCCGACAAAGGATGTC GCCGTGCTCCTCTTTTT*gtgtaggctggagctgcttc*	PCR of Km gene from pKD4 plasmid with homology regions of the intergenic region of the plasmid pUA1139 of the strains IT2 and IT3.
P4_Km_P2[a]	GCCGGACGCGGGACACTGACCACAGGCAGCGTTTA TGCCGCGCCGCGTCAG*Catgggaattagccatggtcc*	
P4km_extf	CATTATGGCGGATGAAGTATG	PCR and sequencing to check the Km insertion into the intergenic region of the strains IT2 and IT3.
P4km_extr	CTGGCGTACACTGTCAC	
pACRISPR_fwd	CTGTCAGACCAAGTTTAC	Inverse PCR to amplify pACRISPR plasmid (without *bla* gene) for HIFI cloning.
pACRISPR_rev	ACTCTTCCTTTTTCAATATTATTG	
Spc_fwd	AATATTGAAAAAGGAAGAGTGTGAGGAGGATATAT TTGAATAC	PCR to amplify *spt* gene from pSET4s for HIFI cloning.
Spc_rev	GAGTAAACTTGGTCTGACAGTTATAATTTTTTTAAT CTGTTATTTAAATAGTTTATAG	
Spc_int_fw	GAGGAATTACTACCTGATATTC	PCR to check the pUA1148 plasmid construction.
pACRISPR_rv2	CTGGTAACAGGATTAGCAG	
gRNA48_fw[b]	*gtgg*GTGTTTCAGAGGAAACCCTG	Phosphorylated primers to anneal the gRNA48 spacer through Golden Gate assembly.
gRNA48_rv[b]	*aaac*CAGGGTTTCCTCTGAAACAC	
pACRISPR2622_rv	CATGGGTATGGACAGATC	PCR and sequencing of cloned gRNA48 spacer in pUA1148.
pACRISPR2431_fw	GTGCCAATACCAGTAGAAAC	
*Sce*I_sec_rv	TCGATGTTCAGTTCGATCAG	

Table A.2 (continued)

Name	Sequence (5'-3')	Application
pUA1139_00007_km_p1.2 [a,d]	TACAGATGCACCGATGCGCTTGCGTGGCTTTTCAG GGAGATAAAGTTATGAGTTACGCTAGGGATAACA GGGTAATATAG*taggaacttcaagatcccct*	PCR of Km gene from pKD4 plasmid with homology regions of the *pUA1139_00007* gene of the plasmid pUA1139.
pUA1139_00007_km_p2.1 [a]	TTCCGGCACAGGTGAGGCCGGAATTCGGACTAAA ACGTAAACCGCGGGCC*atgggaattagccatggtcc*	
pUA1139_00007_ext_fw	GCTGAGTGAAAACACCCTT	PCR and sequencing to check the Km insertion into the *pUA1139_00007* gene.
pUA1139_00007_ext_rv_2	GGCTGAAGGCCTTTATAGT	
pKD46_inv_fw	CGAAATCCACTGAAAGCACA	Inverse PCR to amplify pKD46 plasmid without λ-Red system genes.
pKD46_inv_rv	AAGCTGCTTTTGAGCACCAC	
*Sce*I_pKD46_fw	TACCAGTAGAAACAGACGAAGAATCGACCAATTC GGGTCGACTTATTATTTC	Amplification of I-*Sce*I synthetic gene and tetracycline inducible promoter.
*Sce*I_pKD46_rv	TATCAAAGGGAAAACTGTCCATACCGGAAAAAGG TTATGCTGCTTTTAAG	
pKD46_mod_comp_fw	GACAACTTGACGGCTACA	PCR and sequencing to check the pUA1165 plasmid construction.
pKD46_mod_comp_rv	GAACAACTGTTCACCGTTACA	
*Sce*I_sec_fw	CTGATCGAACTGAACATCGA	
*Sce*I_sec_rv	TCGATGTTCAGTTCGATCAG	

Table A.2 (continued)

Name	Sequence (5'-3')	Application
ibfA_km_p1.2[a]	TTTCTGAATTACATGGTGAATTCCCCCAACATAATG CTAGGATTTAAAAATG*gtgtaggctggagctgcttc*	PCR of Km gene from pKD4 plasmid with homology regions of the *ibfA* gene.
ibfA_km_p2[a]	TATTTGCTCATTCGGGATGGTTGGATATTTTAAGTT ATATCTACTGTATC*atgggaattagccatggtcc*	
ibfA_ext_fw2	GAGGTTCGCGTACAGATAA	PCR and sequencing to check the Km insertion into the *ibfA* gene.
ibfA_ext_rv2	CCATCTTTACCGTCTCTGAA	
UT_km_p1[a]	CTTCACAATGAATATCATTGTGTTGGTAACCTGCTG TTATCGTGATGAAA*gtgtaggctggagctgcttc*	PCR of Km gene from pKD4 plasmid with homology regions of the *ibfA*-containing transcriptional unit.
UT_km_p2[a]	ACATGATATGATTTTTACCTGTCAGAACATTATCAG ATGGAGCGTGCAGG*atgggaattagccatggtcc*	
UT_ext_fw	GTACTTGCCACAGCAGGT	PCR and sequencing to check the Km insertion into the *ibfA*-containing transcriptional unit.
UT_ext_rv	TGTGCTAACGGCATGTATTAC	
00003_ibfA_fw	ATAATGATGGGTGTTTTCTTTTCT	Primers used in RT-PCR to determine the formation of a transcriptional unit, and to check the introduction of the *ibfA*-containing transcriptional unit in pBAD33 vector.
00003_ibfA_rv	AGCCCGTAGTTTCTGATTT	
ibfA_ydeA_fw	CTTGACCAGTAATAGTTTTT	
ibfA_ydeA_rv	CGCGTACAGATAAATGAAA	
ydeA_ydfA_fw	GGCATCCTCCAGACGAC	
ydeA_ydfA_rv	TGAATGCCATAAAGAGACAG	
ibfA_P1_pBAD33_fw[c]	*agcgaattcgagctcggtac*TTAAGTTATATCTACTGTATCAT TCTCAGGTAATCGTTC	PCR of *ibfA* gene from pUA1135 plasmid used to clone this gene into pBAD33 vector under the control of its own promoter.
ibfA_P1_pBAD33_rv[c]	*tctagaggatccccgggtac*GAACACGCCTGTGCACGG	
pUA1135-Big4_pBAD33_f[c]	*gctcggtacccggggatcctctagagtcgacctg*GAAAGGAATACTT CACAATGAATATCATTG	PCR of the *ibfA*-containing transcriptional unit from pUA1135 plasmid used to clone into pBAD33 vector under the control of its own promoter.
pUA1135-Big4_pBAD33_r[c]	*cttctctcatccgccaaaacagccaagcttgcatgcctg*CCTATTATCTC CGTGTTAGCCG	

Table A.2 (continued)

Name	Sequence (5'-3')	Application
pBAD_F	ATGCCATAGCATTTTTATCC	PCR and sequencing to check the introduction of *ibfA* or the *ibfA*-containing transcriptional unit in pBAD33 vector.
pBAD_R	CCTGATACAGATTAAATCAG	
sec_ibfA_P1_1	GCAGCTTCAAACGCATTCA	
sec_ibfA_P1_2	CACGAATAAGTGTACTGGCA	
sec_ibfA_P1_3	CGGCAGTGACTTCATTGT	
sec_ibfA_P1_4	CTCGAACATCAGCTTTTCCA	
gyrBupRT	GTTTTTGCGACAGAGCGTTGAC	Quantification of ATCC14028 Rif^R *gyrB* through qPCR.
gyrBdwRT	ACATGGTATTCGAGGTGGTAGA	
16SRNAupSa	CACATGCAAGTCGAACGGTAAC	Quantification of ATCC14028 Rif^R 16S rRNA through RT-qPCR.
16SRNAdwSa	AGTGTGGCTGGTCATCCTCTCA	
ibfA_P1_RT_fw	TCACCGGCACAGAATCAC	Quantification of ATCC14028 Rif^R pBAD33::*ibfA ibfA* gene through RT-qPCR
ibfA_P1_RT_rv	TCCACCCAATCCGTCCAGT	
Phi20_gp03_RT_fw	CCGGCGCAGGAATGATGTC	Quantification of UAB_Phi20 helicase through qPCR and RT-qPCR.
Phi20_gp03_RT_rv	CGTTCCGCTTTTGGTTTCTC	
Phi20_gp17_RT_fw	CATGATGGCGGCAAAGGAAC	Quantification of UAB_Phi20 holin expression through RT-qPCR.
Phi20_gp17_RT_rv	TCTGTGCCGATGTAGCCGATAAAC	
Phi20_gp18_RT_fw	AGCAGGGGGATACCAACCAT	Quantification of UAB_Phi20 lysozyme expression through RT-qPCR.
Phi20_gp18_RT_rv	CGGGACGCGAACAAGACTAC	
Phi20_gp30_RT_fw2	GAAACCATCTCCGCAATCAC	Quantification of UAB_Phi20 coat protein expression through RT-qPCR.
Phi20_gp30_RT_rv2	GCAGTCTCGTCTCGCAAGTC	
Phi20_gp45_RT_fw	CAGCGGTCGTTGCCACTTT	Quantification of UAB_Phi20 tailspike protein expression through RT-qPCR.
Phi20_gp45_RT_rv	GACCGCTAGCCCGATGAACT	
Phi20_gp14_RT_fw	GGGAATGGCGCAATCACAAG	Quantification of UAB_Phi20 late transcription antitermination protein expression through RT-qPCR.
Phi20_gp14_RT_rv	CGCGGCACTACGGCAATAAT	
Phi20_gp74_RT_fw	CCATAGAGCGCGACACCATC	Quantification of UAB_Phi20 early transcription antitermination protein expression through RT-qPCR.
Phi20_gp74_RT_rv	CCTCCTTCAACTTCCTTCTG	

Table A.2 (continued)

Name	Sequence (5'-3')	Application
Phi20_gp43_RT_fw	CCACGGTGGACCTGTATTGT	Quantification of UAB_Phi20 *arc* expression through RT-qPCR.
Phi20_gp43_RT_rv	CAATGCGCCCTTCCTTCTTA	
Phi20_gp44_RT_fw	ACCGCTGGCCGTAGAGTA	Quantification of UAB_Phi20 antirepressor *ant* expression through RT-qPCR.
Phi20_gp44_RT_rv	GAATTCATGGCCGTAGTCGT	
Phi20_sar_RT_fw	GTGTTAACTGCTTCTAAAATTGCTA	Quantification of UAB_Phi20 *sar* expression through RT-qPCR.
Phi20_sar_RT_rv	GAAGCCCCAACTGCGGTAAC	
Phi20_gp77_RT_fw	ATTAGCGATGCAGCGGTCTC	Quantification of UAB_Phi20 *cro* expression through RT-qPCR.
Phi20_gp77_RT_rv	CTTGGCGATAAGCGTTTTCTTG	
Phi20_gp51_RT_fw	CCGGCTTAGGCTTGAATACC	Quantification of UAB_Phi20 integrase expression through RT-qPCR.
Phi20_gp51_RT_rv	AGAAGGCGCATAAGAAGTCG	
Phi20_C1_RT_fw	ACGCAATTACCAGCAGCATC	Quantification of UAB_Phi20 *c1* expression through RT-qPCR.
Phi20_C1_RT_rv	ATCCTCGACACCCCACTC	
Phi20_C2_RT_fw	GAATGTGGCCTCGTTTTCAC	Quantification of UAB_Phi20 *c2* expression through RT-qPCR.
Phi20_C2_RT_rv	TAAGCGCAGGGCAATGGAT	

[a]P1 and P2 sequences, homologues to the pKD4 plasmid, are represented in lower case italics; [b]Homology sequences to the pUA1148 plasmid are represented in lower case italics; [c]Homology sequences to pBAD33 are represented in lower case italics; [d]I-*Sce*I sequence is underlined.

ACKNOWLEDGEMENTS

Vull expressar el meu agraïment a la Dra. Montserrat Llagostera Casas, la Dra. Maria Pilar Cortés Garmendia i el Dr. Iván Erill Sagalés per la seva orientació i el seu suport durant el desenvolupament d'aquesta tesi doctoral. Els seus consells i coneixements han estat fonamentals pel meu creixement com a investigadora. Gràcies per creure en mi i per guiar-me en aquest emocionant viatge cap a la investigació.

Montse, moltes gràcies per tot el que m'has ensenyat durant aquests quatre anys. Agraeixo molt la teva guia i l'estímul constant per anar més enllà en la meva recerca. Ha estat una gran experiència aprendre amb tu i valoro molt el teu suport i dedicació.

Pilar, han estat moltes les hores compartides, dedicades a llargs debats científics i anàlisis sobre els resultats obtinguts. Ha estat un privilegi comptar amb la teva orientació i el teu suport incondicional. Aprecio molt la teva disposició per ajudar-me sempre que he tingut dubtes o problemes durant aquesta etapa d'investigació.

Ivan, m'agradaria agrair-te tot el que m'has ensenyat de bioinformàtica, la teva ajuda en aquest àmbit ha estat fonamental pel desenvolupament inicial d'aquesta tesi. Gràcies per compartir la teva experiència.

Jordi Barbé, valoro molt l'oportunitat de formar part del Grup de Microbiologia Molecular. Moltes gràcies per la teva guia i aportacions inavaluables durant els moments en què més ho hem necessitat.

Susana Campoy, gràcies per la teva ajuda en el final d'aquesta tesi; tot i no haver aconseguit els resultats esperats, tot el que he après ha estat molt valuós.

Jesús Aranda, agraeixo sincerament la teva ajuda i consells sempre que els he necessitat.

Joan, sempre és reconfortant veure la teva porta oberta, ja sigui per fer-nos seure i escoltar les nostres cabòries, com per fer comandes enormes. Gràcies per tenir sempre un bon consell per donar.

Susana, per tots els litres de LB i pels centenars de plaques sembrades i titulades en un sol dia, crec que parlo per tots dient que la teva disposició a ajudar-nos, tot i tenir tu també molta feina, és una de les teves virtuts que més apreciem. Gràcies de tot cor per la teva ajuda, però també per tots els cafès i totes les converses durant aquests quatre anys.

Jenni, la teva mentoria als inicis d'aquesta tesi va ser crucial per tot el seu desenvolupament posterior. Tot i no estar tan present al final, els teus consells com a persona que ha passat per les mateixes circumstàncies han sigut essencials. Moltes gràcies per tot el que m'has ensenyat, com a científica i com a persona.

Maria, Jordi, Marc, Gabi, Pau, Anna i Elena (la 4a planta), però també Dani i Ivonis, que dir-vos... No hauria pogut superar aquests quatre anys sense vosaltres. Moltes gràcies per tots els meetings post-lab, les classes al SAF, les barbacoes, etc. I sobretot, moltes gràcies per tots els riures. Espero que, tot i no veure'ns tant a partir d'ara, continuem organitzant mil activitats. Us trobaré a faltar.

Nenes, sou les millors amigues que podria haver demanat. Des d'aquí o des de l'altra punta del món, moltes gràcies per sempre estar presents, per escoltar-nos, per ajudar-nos, per no jutjar-nos, i per estar sempre juntes sigui on sigui que ens porti la vida.

Mama, papa i Martí, moltes gràcies per ser el meu suport incondicional al llarg de tots els alts i baixos d'aquest procés. Per creure en mi des del moment que vaig decidir endinsar-me en una carrera científica. Per donar-me ànims quan més ho necessitava, però també per fer-me veure que no tenia raó quan no en tenia. Per consolar-me en els moments difícils i gaudir amb mi en els més feliços. Tot el que he aconseguit no ho podria haver aconseguit sense vosaltres. Gràcies per ser-hi sempre, us estimo.

Jaume, tot i aparèixer al final del procés d'aquesta tesi, el teu amor i suport m'ha donat molta força quan més l'he necessitat. Moltes gràcies per abraçar-me sempre i fer-me riure quan més ho necessito. M'encanta compartir la vida amb tu. T'estimo.

Tickles, gordita, sempre estaràs amb mi, et trobem molt a faltar. Has sigut la millor gosseta que hauríem pogut demanar. T'estimo i t'estimaré moltíssim sempre.